Vol. 113 No. 1, January 1, 1980 ISSN 0003-2670

ANALYTICA CHIMICA ACTA

International journal devoted to all branches of analytical chemistry

ELSEVIER SCIENTIFIC PUBLISHING COMPANY

ANALYTICA CHIMICA ACTA

International journal devoted to all branches of analytical chemistry
Revue internationale consacrée à tous les domaines de la chimie analytique
Internationale Zeitschrift für alle Gebiete der analytischen Chemie

PUBLICATION SCHEDULE FOR 1980 (incorporating the section on Computer Techniques and Optimization).

	J	F	M	A	M	J	J	A	S	O	N	D
Analytica Chimica Acta	113/1 113/2	114	115	116/1	116/2	117	118/1	118/2	119	120/1	120/2	121
Section on Computer Techniques and Optimization			122/1			122/2			122/3			122/4

Scope. *Analytica Chimica Acta* publishes original papers, short communications, and reviews dealing with every aspect of modern chemical analysis, both fundamental and applied. The section on *Computer Techniques and Optimization* is devoted to new developments in chemical analysis by the application of computer techniques and by interdisciplinary approaches, including statistics, systems theory and operation research. The section deals with the following topics: Computerized acquisition, processing and evaluation of data. Computerized methods for the interpretation of analytical data including chemometrics, cluster analysis, and pattern recognition. Storage and retrieval systems. Optimization procedures and their application. Automated analysis for industrial processes and quality control. Organizational problems.

Submission of Papers. Manuscripts (three copies) should be submitted as designated below for rapid and efficient handling:

Papers from the Americas to: Professor Harry L. Pardue, Department of Chemistry, Purdue University, West Lafayette, IN 47090, U.S.A.

Papers from all other countries to: Dr. A. M. G. Macdonald, Department of Chemistry, The University, P.O. Box 363, Birmingham B15 2TT, England.

For the section on *Computer Techniques and Optimization:* Dr. J. T. Clerc, Universität Bern, Pharmazeutisches Institut, Sahlistrasse 10, CH-3012 Bern, Switzerland.

American authors are recommended to send manuscripts and proofs by INTERNATIONAL AIRMAIL.

Information for Authors. Papers in English, French and German are published. There are no page charges. Manuscripts should conform in layout and style to the papers published in this Volume. Authors should consult Vol. 111, p. 343 for detailed information. Reprints of this information are available from the Editors or from: Elsevier Editorial Services Ltd., Mayfield House, 256 Banbury Road, Oxford OX2 7DE (Great Britain).

Reprints. Fifty reprints will be supplied free of charge. Additional reprints (minimum 100) can be ordered. An order form containing price quotations will be sent to the authors together with the proofs of their article.

Advertisements. Advertisement rates are available from the publisher.

Subscriptions. Subscriptions should be sent to: Elsevier Scientific Publishing Company, P.O. Box 211, 1000 AE Amsterdam, The Netherlands. The section on *Computer Techniques and Optimization* can be subscribed to separately.

Publication. *Analytica Chimica Acta* (including the section on *Computer Techniques and Optimization*) appears in 10 volumes in 1980. The subscription for 1980 (Vols. 113–122) is Dfl. 1390.00 plus Dfl. 160.00 (postage) (total approx. U.S. $756.00). The subscription for the *Computer Techniques and Optimization* section only (Vol. 122) is Dfl. 139.00 plus Dfl. 16.00 (postage) (total approx. U.S. $75.50). Journals are sent automatically by airmail to the U.S.A. and Canada at no extra cost and to Japan, Australia and New Zealand for a small additional postal charge. All earlier volumes (Vols. 1–103) except Vols. 23 and 28 are available at Dfl. 150.00 (U.S. $73.00), plus Dfl. 10.00 (U.S. $5.00) postage and handling, per volume.

Claims for issues not received should be made within three months of publication of the issue, otherwise they cannot be honoured free of charge.

Customers in the U.S.A. and Canada who wish to obtain additional bibliographic information on this and other Elsevier journals should contact Elsevier/North Holland Inc., Journal Information Center, 52 Vanderbilt Avenue, New York, NY 10017. Tel: (212) 867-9040.

ANALYTICA CHIMICA ACTA
VOL. 113 (1980)

ANALYTICA CHIMICA ACTA

International journal devoted to all branches of analytical chemistry

ELSEVIER SCIENTIFIC PUBLISHING COMPANY

Anal. Chim. Acta, Vol. 113 (1980)

Printed in The Netherlands

Analytica Chimica Acta, 113 (1980) 1

EDITORIAL

The fundamental strength of any scientific discipline ultimately resides in the quality of research in that discipline; the lifeline of any discipline is the scientific literature that supports communication among research laboratories and practitioners of the science. The Editor of the first issue of ANALYTICA CHIMICA ACTA, published in 1947, stressed the importance of periodicals to scientific endeavour and invited all those earnestly devoted to the progress of modern analytical chemistry to contribute to the journal. Since then, ACA has developed as one of the leading journals devoted to all branches of analytical chemistry; its history was outlined in the foreword to Volume 100 of ACA published in 1978.

There continues a great need for strong general analytical journals, because analytical chemistry is a diverse discipline encompassing concepts and techniques related to physical, inorganic, organic, and biological chemistry, as well as specialized areas such as environmental and clinical chemistry. In recent years there has been an increasing tendency to specialized journals and the contribution from American scientists to international journals devoted to all aspects of analytical chemistry has declined. With this issue, we resume the European—American partnership in the editorial activity of ACA that served the international analytical community well for many years. We hope that with this renewal of an international editorial team, the journal will improve still further on its already substantial service to analytical chemistry. The critical needs are for high quality research papers, timely reviews, and feature articles related to contemporary topics. If our fellow analytical chemists agree that it is important to have strong analytical journals, then we invite them to support our efforts by submitting their best manuscripts for publication in ACA. In return, we are committed to the fastest and most efficient handling of manuscripts that is consistent with a thorough review process.

A. M. G. Macdonald
Harry L. Pardue

Analytica Chimica Acta, 113 (1980) 3—12

Special Report

THE APPLICATION OF PLASMA SOURCE ATOMIC EMISSION SPECTROMETRY IN FORENSIC SCIENCE

J. LOCKE

Home Office Central Research Establishment, Aldermaston, Reading, Berkshire, RG7 4PN (Gt. Britain)

(Received 23rd August 1979)

SUMMARY

The inductively coupled plasma and direct current plasma sources are assessed for the analysis of tissue, glass and steel by emission spectrometry in forensic science applications. With steel and glass, the analysis of 0.5-mg particles provides sufficient accuracy and precision to aid the identification of glass or steel type, and may also allow discrimination within a particular material type (e.g., window glass). Successful recovery of thallium, arsenic and mercury from doped human liver tissue (representing acute toxic poisoning cases) is demonstrated.

The Home Office Central Research Establishment maintains a continuing interest in techniques for the multi-element analysis of materials of concern to forensic scientists. Typical investigations have been the application of spark-source mass spectrometry (s.s.m.s.) to glass [1] and human liver tissue [2]. Emission spectrography, with a d.c. arc, is also employed routinely for semi-quantitative glass, metal and tissue analysis. Recent developments in atomic emission spectroscopy (a.e.s.) with plasma sources led to an assessment in this laboratory of commercially available instruments to replace or augment present equipment.

Spectrometers employing either an inductively coupled plasma (i.c.p.) or a direct current plasma (d.c.p.) were considered. The investigation was not aimed at examining the components of available systems in detail but rather the overall performance was measured by submitting test solutions to manufacturers' applications laboratories. The solutions covered selected aspects of glass, steel and human liver tissue analysis and took account of the small size of individual steel and glass particles (0.05—1 mg) frequently encountered during criminal investigations. The wide general interest in the materials studied and the associated spectroscopic problems warrant publication of the results particularly as little information directly comparing i.c.p. and d.c.p. based emission spectrometers exists in the literature.

Forensic aspects of solution design

In the matrices examined a selection of elements was made to cover a spread of concentrations and to include the elements of greatest importance to forensic scientists.

The concentrations of elements in the steel and glass solutions were selected so that aspiration of the solutions into an instrument under normal operating conditions (pneumatic nebuliser) would consume a quantity of material equivalent to a 0.5-mg particle; that is, some ten-fold heavier than the smallest fragment normally examined in case-work.

To represent cases of acute elemental poisoning, samples of both normal and doped human liver tissue were examined. A homogenised ash sample was prepared from normal tissue and then doped with three toxic metals during the acid dissolution stage.

For each of the three sample types a master set of reference solutions was prepared together with three samples of known but undeclared composition (Table 1). Each manufacturer received an identical sub-set of these solutions.

EXPERIMENTAL

Materials and solution preparation

Aristar nitric acid and sulphuric acid (BDH Chemicals Ltd.) and Suprapur

TABLE 1

Composition of solutions used in trials[a]

Solution type	Tissue (0.5% ash)[b]	Steel (0.05%)	Glass (0.1%)
A. Solvent blank used for all reference solutions	5% H_2SO_4	5% HNO_3	1% H_3BO_3, 1% HNO_3, 1.6% HF
B. Reference solution with matrix elements absent	Normal levels: Mn 1, Pb 0.4, Cu 5, Cd 2, Zn 50 Typical fatal poisonings: Hg 20, As 20, Tl 20	Pb 1, Cu 1, Mn 8. Cr 8, Ni 8.	Mn 0.2, Fe 3, Mg 50, Al 15, Sr 0.2, Ti 0.62, Rb 0.05, V 0.01
C. Matrix elements only plus solvent blank	Ca 20, Mg 50, Fe 80, Na 350, K 900, P 950	0.05% pure iron	Na 100, Ca 60, Si 350, K 6
D. Three reference solutions with matrix elements present	Analytes at 0.5, 1 and 2 times concn. of type B solution	Standard steels to cover range up to: Pb 1, Cu 1, Mn 8, Cr 6, Ni 6	Analytes at 0.5, 1 and 2 times concn. of type B solution
E. Three sample solutions for each matrix	Two normal livers, one also doped with Hg, As, Tl	BCS 215/3, BCS 225/2 (Pb doped), works analysed sample	3 window glasses (Pilkington Bros. Ltd.)

[a] All concentrations in mg l^{-1}.

[b] 1 g of wet tissue gives ca. 0.014 g ash, i.e. 0.5% ash ≡ 35% tissue solution.

hydrofluoric acid solution (Merck) were used. Reagents were of analytical-reagent grade except for the following Specpure materials (Johnson Matthey Chemicals Ltd.): SiO_2, $CaCO_3$, Na_2CO_3, K_2CO_3, H_3BO_3, Fe, MgO and Al_2O_3.

The tissue solutions were prepared by using published procedures [3]. Some steel samples required heating with a little hydrochloric acid as well as nitric acid. Glass samples were dissolved by heating at 120°C with a (4 + 1) mixture of 40% hydrofluoric acid and nitric acid in PTFE pressure digestion vessels. The dissolved glass was treated with sufficient boric acid to complex the fluoride ions, thus permitting the use of glass-lined nebulisers. Synthetic solutions representing glass were prepared from the individual components and suitable acids. Thus SiO_2, Al_2O_3 and TiO_2 were heated at 120° with HF/HNO_3 under pressure and the Na_2CO_3, $CaCO_3$, K_2CO_3, Fe, MgO, $SrCO_3$, $KMnO_4$, RbCl and NH_4VO_3 were dissolved in nitric acid.

Equipment

Details of the equipment used are given in Table 2. Each laboratory was requested to carry out simultaneous multi-element analyses where suitable analytical lines were available on the direct reading spectrometers. If no line was available for a particular element then it could be determined sequentially by using either a scanning monochromator or the single variable channel of the direct-reading multi-channel system. The final analytical lines were not necessarily optimal for the materials studied, either in sensitivity or freedom from interferences, but these were chosen for work on general applications by the manufacturers. Raw intensity data (photomultiplier voltages) were requested, without any form of prior data reduction. Elemental concentrations for the samples were read from hand-plotted calibration curves. Any available computer facilities were not used.

PRECISION, DETECTION LIMITS, INTERFERENCES

In assessing the results of this study, it must be remembered that it is impossible to compare the relative merits of the two types of plasma source in isolation. What is compared are the complete systems of plasma source plus spectrometer, which in the case of the Spectrametrics system employs an Echelle grating having a much greater resolution than the other spectrometers, thereby reducing inter-element spectral interferences in several instances. The detection limits however will depend greatly on signal (plasma) stability. All three i.c.p. systems performed similarly as regards accuracy, precision and detection limits and therefore only typical results are reported here for comparison with the corresponding results for the d.c.p.

The instrumental precision (short term only was measured) was good for both plasma types, the relative standard deviation (RSD) of the analyte signal in typical samples averaging about 0.4% in the i.c.p. but typically 1—4% for the d.c.p. (Table 3). The precision of the d.c.p. was adequate for the determination of almost all of the elements studied, exceptions being vanadium in

TABLE 2

Instrumental systems

D.c.p.: Spectrametrics Instruments (marketed in U.K. by Techmation Ltd., Edgware)	
Plasma power supply	Spectrajet III (3 electrode system). Input power 230 V, 50 Hz, 8 A. Jet current 10 A at 30 V d.c.
Sample excitation	Pneumatic nebuliser plus spray chamber. Rate of sample consumption 2 ml min^{-1}. Total argon consumed 8 l min^{-1}. 10 s each for pre-integration and integration. Standard excitation region (below centre of "Y") sampled.
Spectrometer	Spectraspan III. Modified Czerny-Turner optics using an Echelle grating with 30° prism for order separation. Focal length 0.75 m, aperture f/15. Wavelength range 190—800 nm with 0.061 nm mm^{-1} dispersion at 200 nm, resolution 0.0015 nm (25 μm slit).
I.c.p.-A: Jobin-Yvon Instruments (marketed in U.K. by EDT Research, London, NW10)	
Plasma power supply	Plasmatherm model 1500—2500. Operating frequency 27.12 MHz. Power output 1.5—2.5 kW, variable.
Sample excitation	Pneumatic nebuliser plus spray chamber. Rate of sample consumption 2.5 ml min^{-1} at argon flow rate of 0.6 l min^{-1} (Total argon consumed 15 l min^{-1}). 10 s each for pre-integration and integration. Plasmatherm concentric silica torch model T1.5 and plasma sampled at 16 mm above load coil.
Spectrometers	JY38P. Czerny-Turner scanning monochromator, focal length 1 m, with holographic grating (2400 gr mm^{-1}) of ruled area 120 × 140 mm, range 180—750 nm and 0.1 nm mm^{-1} dispersion in ultraviolet. Entrance slit 20 μm, exit slit 40 μm. JY48P. Paschen-Runge polychromator, focal length 1 m, with holographic grating (2160 gr mm^{-1}), range 168—492 nm, dispersion 0.46 nm mm^{-1} in first order. Entrance slit 20 μm, exit slit varying 38—100 μm.
I.c.p.-B: Applied Research Laboratories (Wingate Road, Luton, Beds, England)	
Plasma power supply	ARL. Operating frequency 27.12 MHz (crystal controlled). Power output approx. 1.25 kW.
Sample excitation	Pneumatic nebuliser plus spray chamber. Rate of sample consumption 0.7 ml min^{-1} at argon flow rate of 1.0 l min^{-1} (Total argon consumed 12 l min^{-1}). 40 s pre-integration and 10 s integration. Concentric silica torch with 3 gas circuits and plasma sampled 14 mm above load coil.
Spectrometer	ARL 34000/ICP. Paschen Runge polychromator, focal length 1 m, with ruled grating (2160 gr mm^{-1}), blazed at 200 nm, range 175—410 nm and 0.46 nm mm^{-1} dispersion in the first order. Variable channel consisted of 1-m monochromator.

TABLE 2 (Continued)

I.c.p.-C: Philips Instruments (marketed in UK by Pye Unicam Ltd., Cambridge, England)

Plasma power supply	PV8490. Operating frequency 50 MHz (free running). Power output approx. 1.4 kW.
Sample excitation	Pneumatic cross-flow nebuliser plus spray chamber. Rate of sample consumption 2.5 ml min^{-1} at argon flow rate of 1.3 l min^{-1} (Total argon consumed 17 l min^{-1}). 15 s integration. Concentric silica torch (Boumans design) and plasma sampled 13—17 mm above load coil.
Spectrometer	PV8210. Paschen Runge polychromator, focal length 1.5 m with holographic grating (1200 gr mm^{-1}) of ruled area 78 × 40 mm, range 190—700 nm and 0.46 nm mm^{-1} dispersion in the first order. Entrance slit 20 μm, exit slit 50—80 μm, PV8280 "roving detector" as variable channel with a mirror system and detector within the spectrometer.

TABLE 3

Analytical precision and wavelengths used

		D.c.p.		I.c.p.[a]	
		nm	RSD (%)[b]	nm	RSD (%)
Tissue	Mn	257.6	1.5	257.6[d]	0.43
	Cu	213.5[c]	1.9	324.7[d]	0.30
	Zn	206.2	0.64	213.8[d]	0.69
	Cd	214.4[c]	1.5	228.8[d]	0.42
	Pb	405.7[c]	16	283.3[d]	0.34
	As	193.7	1.2	193.7[d]	0.21
	Hg	253.6	0.84	253.6[d]	0.45
	Tl	535.0[d]	2.4	535.0[d]	0.27
Steel	Cr	425.4	1.6	267.7	0.43
	Mn	257.6	0.69	257.6	0.72
	Ni	341.4[c]	1.2	231.6	0.43
	Cu	213.5[c]	2.9	327.4	0.33
	Pb	405.7[c]	3.1	220.3	0.34
Glass	Mg	280.2[d]	1.2	285.2[d]	0.48
	Al	396.1[d]	1.0	394.4[d]	0.35
	Ti	334.9[d]	0.77	334.9	0.60
	V	318.5[d]	26	309.3[d]	0.48
	Mn	257.6	3.8	257.6	0.53
	Fe	259.9	2.2	259.9	1.04
	Rb	421.5[d]	1.0	421.5[d]	0.39
	Sr	407.7[d]	3.6	407.7[d]	0.40

[a]I.c.p. system as indicated in Figs. 2—4.
[b]Average RSD calculated from the three reference samples.
[c]Not the most sensitive line.
[d]Examined by using variable single-channel; the remainder were done by simultaneous multi-element analysis.

glass and lead in tissue. For steel and glass the data can be related to particles weighing approximately 0.5 mg and, to compare the ability of the systems to cope with smaller particles, it is necessary to estimate the limits of detection (Fig. 1). The analyte concentrations in typical samples are also displayed graphically, the separation between any particular detection limit and the corresponding analyte level in samples being a measure of the ability of the system to perform practical analyses. Those systems having lowest detection limits (furthest left in the figure) should be best able to cope with more dilute sample solutions derived from particles smaller than 0.5 mg. The i.c.p.-based systems are seen to cope more effectively, which can be attributed to the higher overall precision of this plasma source.

ANALYSIS OF TISSUE

Figure 2 illustrates the accuracy of the results, which were generally satisfactory since the "true" concentration was not always known with certainty. The accuracy was sufficient in most cases for studies of the metal content of tissue from various human populations and for the detection of toxic metals in cases of poisoning. The elements Mn, Cu, Zn and Cd had detection limits more than an order of magnitude below their normal levels in human tissue.

Almost all human livers contain a trace of lead, and the typical level selected for this work approached the limit of detection for all systems accompanied by a loss in accuracy (i.c.p.-A) or of precison (d.c.p.). The addition of matrix

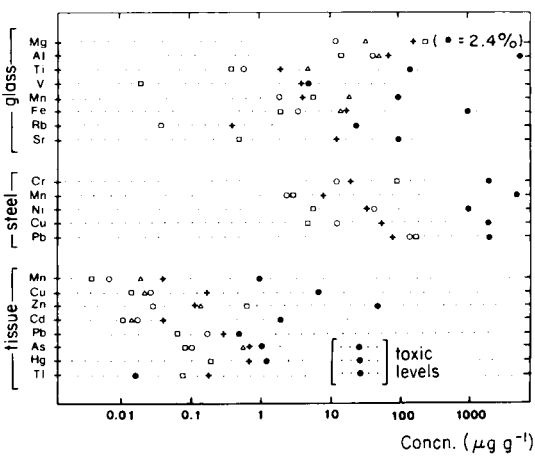

Fig. 1. Comparison of limits of detection of the four systems [(+) d.c.p.; (□) i.c.p.-A; (○) i.c.p.-B; (△) i.c.p.-C] and typical concentrations (•) in samples. The limit of detection is defined as twice the standard deviation of a matrix blank expressed as a solution concentration which is then converted to concentration in the original solid matrix. For Mg and Zn the limit of detection is not the best attainable as the necessary dilute solutions were not available. For As, Hg and Tl both maximum normal and toxic levels are indicated.

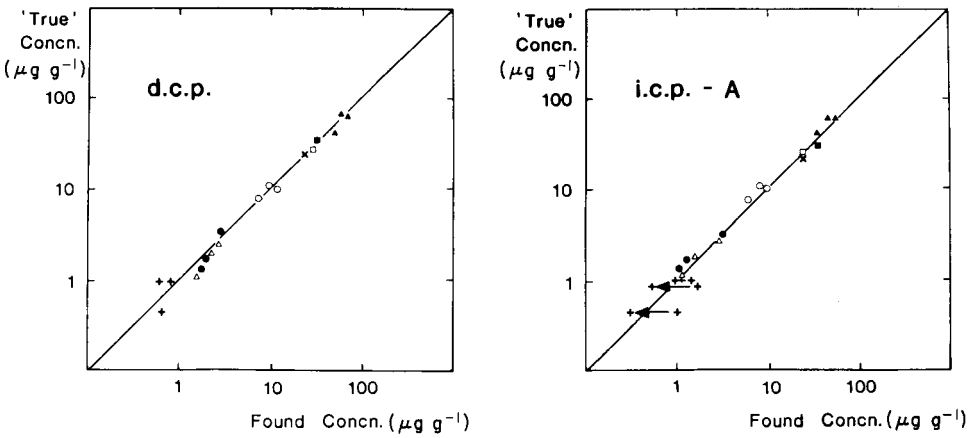

Fig. 2. Accuracy of results expressed as concentration in tissue. Simple metal solutions were used for calibration except for lead, where for best accuracy matrix-containing standards were necessary (arrow points towards corrected result). (×) As; (•) Cd; (○) Cu; (□) Hg; (△) Mn; (+) Pb; (■) Tl; (▲) Zn.

elements to the standards improved the accuracy (i.c.p.-A), the discrepancy being attributed to severe line overlap of the 283.307-nm lead and 283.310-nm iron lines combined with incompletely matched iron levels in standards and samples. Acute toxic levels of lead at ten to one hundred times greater than normal should be readily measurable, although a case of chronic poisoning with a lead concentration only several times that of normal would be less easily interpreted.

Three elements (Tl, As and Hg) were added to one of the tissue solutions at levels representing acute toxic poisoning. No difficulty was seen in the determination of thallium but arsenic and mercury gave trouble with some systems. With arsenic, i.c.p.-A gave spurious signals in the two undoped samples, corresponding to about 3 $\mu g\ g^{-1}$ in the tissue, representing a level markedly higher than that seen in normal human liver. This effect was not seen at the same wavelength (193.7 nm) in the d.c.p. or i.c.p.-B or at 234.9 nm in i.c.p.-C.

With mercury, similar spurious signals equivalent to some 5 $\mu g\ g^{-1}$ in the tissue were seen in undoped samples with i.c.p.-C at 313.1 nm. In this system a more intense line was not available but the line at 253.6 nm was satisfactory with the d.c.p. and i.c.p.-A.

The poor detection limits for arsenic and mercury relative to normal tissue concentrations (Fig. 1) when either plasma type was used may require a separate method of sample introduction (gaseous hydride/metal vapour) for some toxicological work.

ANALYSIS OF STEELS

Although the steel solutions used in this study were very dilute all five el-

ements studied had detection limits at least an order of magnitude below their concentrations in the samples. The precision of measurement was also acceptable throughout. For elements present at the highest concentrations studied (derived from low-alloy steels) the accuracy was good (Fig. 3). An exception was lead, which suffered line overlap problems at several wavelengths. As with tissue, severe overlap with iron occurred at 283.307 nm. Also the line at 405.782 nm lies close to 405.795 nm (Mn) and 405.783 nm (V) and inter-element corrections are necessary. Even in a leaded steel (0.1% Pb, 0.09% V, 1.2% Mn) line overlap was significant, the vanadium contributing several percent and the manganese 10% to the lead signal. This does not account for all of the observed interference and other lines or background effects may be involved. With the Echelle spectrometer (d.c.p.) no serious errors were observed and a simple metal solution was adequate for calibration. At the 220.3-nm lead line (i.c.p.-B), iron substantially interfered although nickel and vanadium may also be involved.

In forensic investigations, loss of accuracy caused by systematic errors is not serious where two fragments are being compared. For a leaded steel this might involve the comparison of fragments recovered from a hacksaw blade (possibly in the possession of a suspect) with a sawn-off shotgun recovered from a crime scene. Clearly under the same instrumental conditions the fragments can be expected to show the same resemblance as when accurate results are obtainable. However, for identification and classification of an unknown material, then absolute compositional data is to be preferred. To achieve the required accuracy here for steel particles, iron may be added to the standards to compensate for interferences arising from both line overlap by iron and background continuous radiation. Further improvements in accuracy can be expected by using computed inter-element corrections for the minor or residual elements but this was not attempted in the present comparison.

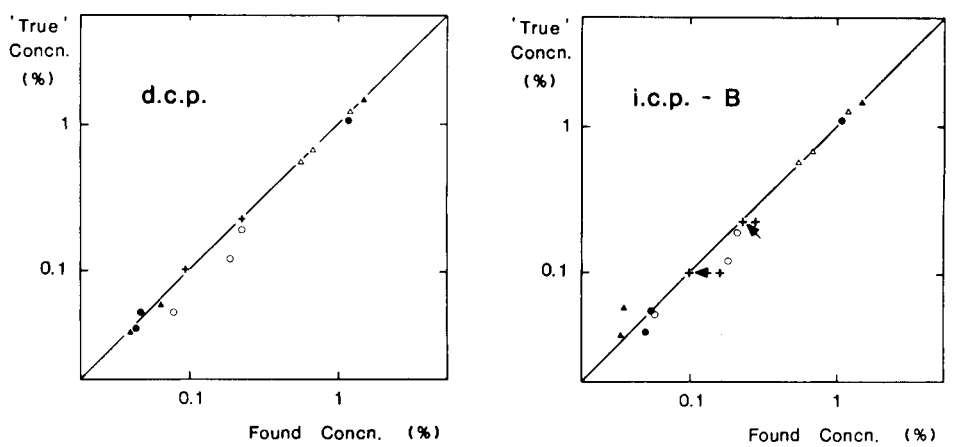

Fig. 3. Accuracy of results expressed as concentration in steel, lead corrected as for Fig. 2. (•) Cr; (○) Cu; (△) Mn; (▲) Ni; (+) Pb.

With nickel, chromium and manganese similar but smaller effects than with lead were observed. Nickel at 231.604 nm required correction attributable to nearby cobalt and manganese lines whereas the nickel line at 341.4 nm was satisfactory. Manganese at 294.9 nm suffers severe line overlap from iron (which would make a substantial contribution in low manganese steels), but this is avoidable by working at 257.6 nm.

ANALYSIS OF GLASS

The elemental concentrations for the glass samples spanned almost four orders of magnitude and illustrate the ability of plasma source spectrometers to measure trace and minor elements simultaneously. For certain elements (e.g., Ti and Sr) all systems gave similar "inaccurate" results (Fig. 4) and it is probable that the "true" results (from s.s.m.s. studies) were substantially in error. This feature would be expected to increase at trace levels. In view of the high sample dilution, brought about by limited sample size, the results were remarkably good, with generally no serious analytical problems being observed.

The identification of glass type (window, bottle, spectacle lens, vehicle headlamp, etc.) is aided by determination of the elements controlled by the manufacturer in glass production. These include Fe, Mn, Mg, Al and Ti, and the accuracy is sufficient to distinguish between typical modern window glass and container glass (milk, soft drink bottles, etc.). Modern British window glass is of fairly closely controlled composition containing 2.3% magnesium and 0.1% iron whereas most colourless containers have iron in the range 0.01—0.07% and magnesium 0.01—1.0%.

If it is necessary to distinguish between glass samples of the same type for purposes of discriminating between glasses associated with scenes of crimes,

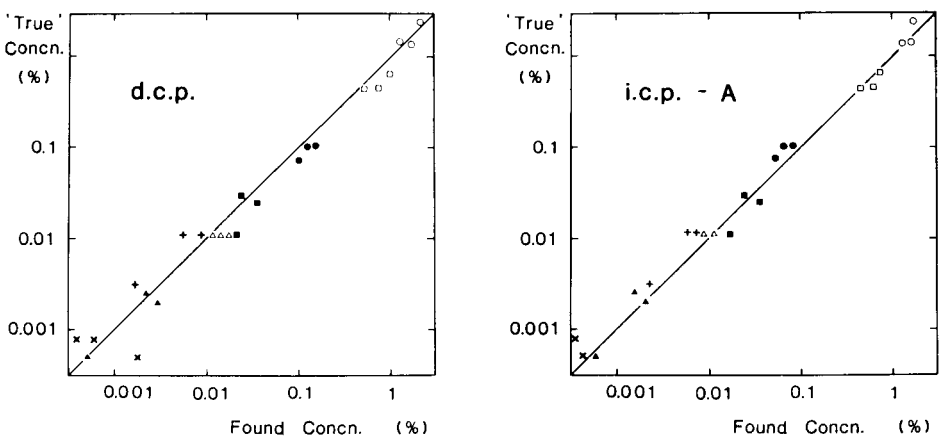

Fig. 4. Accuracy of results expressed as concentration in glass. Simple metal solutions used for calibration. (□) Al; (•) Fe; (○) Mg; (△) Mn; (▲) Rb; (+) Sr; (■) Ti; (×) V.

then one must look for characteristic batch-to-batch variations in trace elements. Window glass from break-ins is of greatest importance, with rubidium, strontium and vanadium being useful for discrimination purposes [4]. In this work, rubidium and strontium are seen to be determinable at trace levels even in small samples (Fig. 4), which demonstrates the feasibility of this approach. For vanadium, however, the results are of doubtful significance, as one is attempting to measure merely 10 ng of this element in the presence of much other accompanying material.

CONCLUSIONS

Both the i.c.p. and d.c.p. are suitable plasma sources for the elemental analysis of materials arising in forensic science applications. Where limited sample is available (glass, metal) the i.c.p. should generally be superior, with lower detection limits because of the high precision attainable with this source. The analysis of sample material of a size frequently seen in case-work is feasible, and furnishes valuable compositional data for classification and discrimination. For a particle of given size more reliable data should be obtainable if sample presentation is such as to conserve the analytical solution as, for instance, by use of ultrasonic nebulisation.

In this study very few interference effects were observed for either plasma type that seriously affected the analysis of the materials of interest. Undoubtedly the high resolution of the Echelle spectrometer resolved a number of spectral interferences where the conventional Paschen-Runge spectrometers failed. These results overall suggest that the combination of an i.c.p. source with special sample presentation methods linked to a high-resolution spectrometer such as the Echelle could provide a powerful tool for the analysis of material of interest to forensic scientists.

The author is grateful to the four manufacturers who participated both for their co-operation in supplying a wealth of experimental results and for helpful comments during the preparation of this report.

REFERENCES

1 J. Locke, D. R. Boase and K. W. Smalldon, J. Forens. Sci. Soc., 18 (1978) 123.
2 J. Locke, D. R. Boase and K. W. Smalldon, Anal. Chim. Acta, 104 (1979) 233.
3 J. Locke, Anal. Chim. Acta, 104 (1979) 225.
4 B. German and A. W. Scaplehorn, J. Forens. Sci. Soc., 12 (1972) 367.

Analytica Chimica Acta, 113 (1980) 13—20

MOLECULAR EMISSION CAVITY ANALYSIS
Part 14. Determination of Selenium Utilizing Hydrogen Selenide Generation

R. BELCHER,[a] S. L. BOGDANSKI,[b] E. HENDEN[c] and A. TOWNSHEND*

Department of Chemistry, University of Birmingham, P.O. Box 363, Birmingham B15 2TT (Gt. Britain)

(Received 26th May 1979)

SUMMARY

Selenium (0.02—2 ppm), after conversion to hydrogen selenide with sodium tetrahydroborate, can be determined by molecular emission cavity analysis. The detection limit is 7 ng of selenium. The effects of 26 ions are reported. The depressive effects of arsenic and antimony can be removed by selective volatilisation, and the enhancing effects of tellurium and sulphite by addition of tellurium to standards and by oxidation to sulphate, respectively.

The determination of selenium by atomic spectrometric techniques involving solution aspiration has several problems, especially the difficulty in atomizing selenium oxyanions and the short wavelength (<210 nm) of the main selenium atomic lines. This results in limits of detection only at the ppm level [1, 2]. The conversion of selenium oxyanions to gaseous hydrogen selenide has been found to be a convenient means of enhancing the sensitivity of such measurements [3] by facilitating atom formation, by enabling relatively cool hydrogen-based flames to be used to reduce the flame background at short wavelengths, and by separating the analyte from interfering matrices. Detection limits of 1.8 ng of selenium by atomic absorption [4] at 196.1 nm and 0.06 ng by atomic fluorescence spectrometry [5] based on such a system have been reported. Smith [6], using a sodium tetrahydroborate reduction, has shown that most transition metal ions depress the generation of hydrogen selenide. EDTA does not prevent this effect [7], as is achieved for arsenic, antimony [8] or tin [9] hydride generation, but it has been avoided by addition of tellurium(IV) or by coprecipitating selenite with lanthanum hydroxide [7].

Molecular emission cavity analysis (MECA) has also been shown to be a useful flame spectrometric procedure for the determination of selenium

[a]Department of Clinical Chemistry, Wolfson Research Labs., Q.E. Medical School, University of Birmingham, P.O. Box 363, Birmingham B15 2TT.
[b]Ronalstan Chemical Consultants, Temple House, New Street, Birmingham B2 4LH.
[c]Chemistry Department, Ege University, Bornova, Izmir, Turkey.

in inorganic and organic compounds [10]. Organic compounds were decomposed in an oxygen flask and selenium was determined by injecting the aqueous solution into a steel MECA cavity placed in an air—hydrogen—nitrogen flame. Interferences of large amounts of arsenic, antimony, sulphur and many metal ions were eliminated by reduction of selenium to the element. The red selenium was filtered onto a small, fine-porosity glass-fibre pad which was then placed in the cavity; $\geqslant 0.4$ μg of selenium could be determined.

The molecular emission obtained from selenium had a broad spectrum over the range 350—550 nm, with several maxima. The emitting species below 410 nm were identified as SeO [11] and Se_2 [12], whereas the emitting species above 410 nm was Se_2 [13] and possibly SeO_2 [14].

The determination of arsenic and antimony by MECA, by conversion to their hydrides and transport of the gases to a MECA oxy-cavity, has previously been reported [15]. This report describes the similar determination of selenium.

EXPERIMENTAL

Equipment

Emissions were measured by an Evans Electroselenium 240 flame spectrophotometer, with a maximal slit of 12 (0.91 mm $\equiv$ 3 nm), modified to accommodate a MECA cavity holding assembly [16]. A Servoscribe 1S chart recorder, having a response time of 0.5 s for f.s.d., was connected to the 10-mV output of the instrument.

The duralumin cavity used is shown in Fig. 1. Carrier gas was introduced into the cavity via stainless steel tubing (0.8 mm i.d.) through a hole in the side wall of the cavity. The cavity was positioned in the flame at 6° below the horizontal.

The volatilisation system was similar to that described earlier [15] with a few modifications. It consists of a glass reaction vessel, 13 cm long and 2 cm diameter, with a side arm. The two open ends of the reaction vessel were made with a 1/10 taper. The top of the reaction vessel was closed with a tapered (1/10) Teflon stopper with two holes for the carrier gas inlet and outlet. A glass syringe with a Teflon needle was used for injection of the sample into the reaction vessel. The needle was fixed in the hole of another tapered (1/10) Teflon stopper with four rings engraved and inserted into the side arm. Hydrogen selenide generated was collected in a 70-cm length of 2-mm bore Teflon tubing which was formed into a coil and placed in liquid nitrogen contained in a Dewar flask (cold trap for H_2Se). The trap was connected to the carrier gas introduction tube of the cavity and to the outlet of the reaction vessel. The collected hydrogen selenide was vaporised by immersing the cold trap in a water bath at 90—95°C. The tubing between the cavity and the reaction vessel was dried between experiments by sucking air with a water suction pump connected to the tip of the carrier gas outlet tube at the lower end of the top stopper.

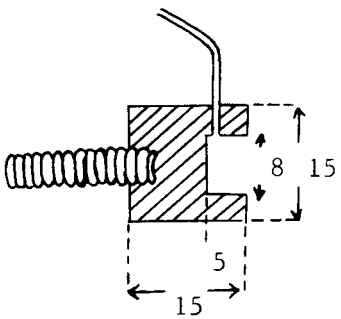

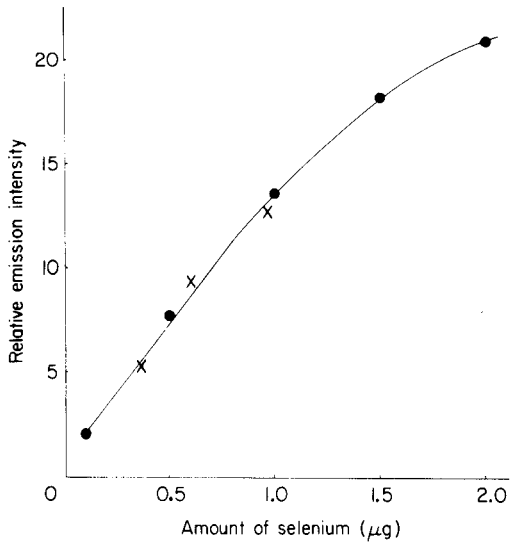

Fig. 1. Cross section of the cavity (dimensions in mm).

Fig. 2. Calibration graphs for (•) selenium(IV) and (×) selenium(VI) after hydrochloric acid reduction; low signal amplification was used.

Reagents

Selenium stock solutions (1000 ppm). Selenium powder (0.50 g, Hopkin and Williams, fine chemical grade) was dissolved in a mixture of 2.5 ml of nitric acid and 0.1 ml of hydrochloric acid. This selenium(IV) solution was diluted to 500 ml with distilled water.

Selenium(VI) stock solution was prepared by dissolving sodium selenate in distilled water.

Sodium tetrahydroborate solutions. Reagent-grade sodium tetrahydroborate pellets (5/16 in.; Alfa Inorganics) were dissolved in 0.01 M sodium hydroxide.

All reagents were analytical-reagent grade, unless otherwise stated.

Determination of selenium

Sodium tetrahydroborate solution (1 ml of 2% w/v) was pipetted into the reaction vessel; 1 ml of sample solution was taken into the syringe, which was connected to the reaction vessel and the volatilisation system was closed. Nitrogen carrier gas was turned on and the system deaerated for 30 s. The cold trap was immersed in liquid nitrogen and cooled for 15 s. The solution in the syringe was injected into the reductant and the generated hydrogen selenide was collected for 2 min. The flame was ignited and 5 s later the cold trap was taken out of the liquid nitrogen and immediately immersed in a hot water bath. Hydrogen selenide was rapidly swept to the cavity and the

emission recorded at 469 nm. The blank emission was also measured and subtracted from the emission reading of the sample.

Determination of selenium in the presence of antimony

After the system had been deaerated for 30 s with nitrogen carrier gas, 1 ml of sample solution, 0.1 M in hydrochloric acid, was injected into the reaction vessel containing about 40 mg of sodium tetrahydroborate powder. The stibine generated was swept out of the system for 2 min by nitrogen carrier gas. No cold trap was used at this stage. A syringe containing 1 ml of 2 M hydrochloric acid was connected to the reaction vessel. The system was again deaerated for 30 s and the trap cooled for 15 s in liquid nitrogen. The acid in the syringe was injected and the hydrogen selenide generated was collected for 2 min in the cold trap. The selenium emission was measured as above.

Determination of selenium in the presence of arsenic

A 0.5-ml aliquot of 0.01 M hydroxylammonium chloride was added to the reaction vessel containing 1 ml of sample solution, 0.1 M in hydrochloric acid. After 12 min, the reaction vessel and the syringe containing 1 ml of 4% sodium tetrahydroborate solution were connected to the system. After the system had been deaerated for 30 s, the reductant solution was injected and the arsine generated was swept out of the system for 2 min by the carrier gas. The syringe was rinsed with water followed by 2 M hydrochloric acid; 1 ml of 2 M hydrochloric acid was then taken into the syringe, and the procedure continued as for selenium in the presence of antimony.

Reduction of selenium(VI) to selenium(IV) [5]

Concentrated hydrochloric acid (5 ml) was added to 5 ml of selenium(VI) solution contained in a 50-ml beaker, covered with a watch glass. The mixture was boiled gently for 5 min. After cooling, the solution was transferred to a 25-ml volumetric flask and diluted with water to the mark.

Optimisation of conditions

The most sensitive position of the cavity was found to be 30 mm above the burner head in the centre of the flame. The optimal gas flows were 2.8 l H_2 min^{-1}, 5.4 l N_2 min^{-1} and, for the carrier gas, 170 ml N_2 min^{-1}.

Because a change in the cavity temperature also causes a change in the emission intensity of selenium and the temperature of the cavity increases for some time after igniting the flame, the time elapsed between igniting the flame and introducing hydrogen selenide into the cavity affects the emission intensity. The optimal time for immersing the cold trap in the hot water bath was found to be 5—6 s after igniting the flame, under the conditions used.

Acid concentration was not critical, but hydrogen selenide can be removed only from acidic solutions because of its acidic nature. The solution

in the reaction vessel, therefore, must be acidic during the entire reaction. When 1 ml of selenium solution in 1—5 M hydrochloric acid is injected into 1 ml of the 4% sodium tetrahydroborate solution, the pH after the reaction is less than 0.6. The sample solutions were prepared in 2 M hydrochloric acid. The sodium tetrahydroborate concentration also was not critical and 1 ml of a 2% solution was used, unless more was needed to reduce concomitant elements.

The emission was measured at 469 nm to decrease possible spectral interferences from volatile sulphur compounds, without markedly decreasing the selenium intensity.

During the volatilisation process, moisture from the reaction solution is carried through the tubing and a little of it condenses. In order to remove moisture, a drying tube packed with calcium chloride or Drierite was connected between the cold trap and reaction vessel. However, this led to irreproducible results. In order to prevent any build-up of condensed water, which would dissolve some hydrogen selenide, air was sucked through the tubing between experiments.

RESULTS

The calibration graph (Fig. 2) obtained by injecting 1-ml portions of solutions containing 0.1—2.0 μg of selenium(IV) was non-linear for larger amounts of selenium, but a linear graph was obtained over the range 20—130 ng. The slope of the log—log plot was 0.82. The coefficients of variation for the determination of 90 ng (7 determinations) and 0.5 μg (8 determinations) of selenium were 3.4 and 4.1%, respectively. The limit of detection (2σ) was 7 ng of selenium.

Selenium(VI) could not be reduced to hydrogen selenide by sodium tetrahydroborate, even when the concentration was increased to 4%. However, as shown in Fig. 2, selenium(VI) can be determined if it is reduced to selenium(IV) by hydrochloric acid prior to the tetrahydroborate reduction.

Interferences

The emission intensity from 0.5 μg of selenium in 2 M nitric acid was 15% lower than that in 2 M hydrochloric acid.

The effects of some cations and anions on the determination of selenium were studied. An interference was defined as significant if a change of more than two standard deviations (i.e. 8%) was observed in the measurement of 0.5 μg of selenium. Zn^{2+}, Co^{2+}, Ni^{2+}, Cd^{2+}, Fe^{3+}, Mn^{2+}, Al^{3+}, Cr^{3+}, Hg^{2+}, Ba^{2+}, silicate, phosphate, nitrate, sulphate, acetate and oxalate (all 50 μg) did not interfere. The suppression by 50 μg of Bi(III), Cu^{2+}, Ag^{+}, Sn^{2+}, Pb^{2+}, As(III), Sb(III) and Ge(IV) of the selenium emission and the maximum tolerable amounts of these ions are shown in Table 1. The effects of sulphite and tellurium are described in more detail below. On reduction, lead and copper gave black precipitates and silver formed a white precipitate (AgCl)

TABLE 1

Effect of interfering ions on the determination of selenium

Interferent	Emission suppression[a] (%)	Maximum tolerable amount (μg)	Interferent	Emission suppression[a] (%)	Maximum tolerable amou (μg)
Bi(III)	39	0.50	Pb^{2+}	39	20.00
Cu^{2+}	91	0.20	As(III)	100	0.025
Ag^{+}	89	0.20	Sb(III)	100	0.05
Sn^{2+}[b]	100	0.05	Ge(IV)	67	0.50

[a]Caused by 50 μg; [b]To eliminate the effect of spectral interference of tin emission, the same amount of tin was added to the reagent blank.

with a black tint. The black precipitates are believed to be the finely divided metal, which possibly captures hydrogen selenide by adsorption or reaction. The volatile arsenic and antimony hydrides gave rise to blue oxide emissions in the flame above the cavity (where more oxygen is available), so that their emissions were not viewed by the detector. Germanium gave a red emission, probably from GeH [17], in the flame in front of and above the cavity, but this did not cause spectral interference with the selenium emission. Tin gave a blue emission, probably from SnO [18], in the flame in front and above the cavity, and a red emission, probably from SnH [18] within the cavity; the latter emission overlapped the selenium emission at 469 nm. In addition to these spectral effects, however, the simultaneous volatilisation of these elements with selenium suppressed the selenium emission (Table 1).

Bismuth did not give any emission but deposited within the cavity and also gave a black precipitate in the reaction vessel. The emission intensity obtained from selenium was much lower in the presence of bismuth and also in any experiments following measurements of bismuth-containing solutions. It was necessary to clean the cavity after such measurements with sand-paper to restore the previous selenium emission intensity. The depression may therefore be attributed to compound formation between selenium and bismuth deposited in the cavity.

No selenium emission was observed when 0.5 μg of selenium in 0.1—0.6 M hydrochloric acid was injected onto 30—40 mg of sodium tetrahydroborate powder, but emission could be observed if the first injection was followed by a 1-ml injection of 2 M hydrochloric acid. The pH values of the solution after the first and second injections were 8.6 and 0.6, respectively. If the sample injected onto the solid reductant contained arsenic(III) or antimony-(III) in 0.1 M hydrochloric acid, the corresponding hydrides were formed, which could be detected by their blue emission above the cavity. The separation of arsenic and antimony from selenium and thus the elimination of their interference was therefore based on the selective volatilisation of the two elements from basic solution prior to the generation of hydrogen

selenide. The procedure was therefore modified as described above. The interference of antimony (10 μg) on the determination of selenium (0.5 μg) was completely eliminated by this procedure, but to eliminate completely the interference of 10 μg of arsenic it was necessary to reduce any arsenic(V) in the solution to arsenic(III) with hydroxylamine prior to the tetrahydroborate reduction. The pre-reduction was carried out in the reaction vessel in order to avoid any transfer loss of selenium that had been reduced to the element.

Because of incomplete volatilisation of tin(II), germanium(IV) and bismuth(III) in the pre-volatilisation step, the interferences of these elements could not be eliminated by the modified procedure; the colour of tin and germanium emissions could be seen after the first and second injection steps.

The emission from selenium was greater in the presence of tellurium (Table 2), although this effect mostly disappeared in the presence of large amounts of tellurium, possibly because of the formation of a black precipitate by the tetrahydroborate reduction of such amounts of tellurium. A similar enhancement of the atomic absorption signal of selenium by tellurium was reported by Smith [6], which he attributed to selenium impurities in the tellurium reagent. The present work shows that this cannot be the reason because the experiments were done at selenium concentrations in a linear part of the calibration graph, and the enhancement did not increase above 0.2 μg of tellurium. It is also interesting that no depressive effect of tellurium was noted, whereas Azad et al. [7] found a 30% depression when making non-dispersive atomic fluorescence measurements. Because the emission signal does not change significantly when the amount of tellurium in the sample solution is 0.2—10 ppm, the effect of tellurium can be eliminated by preparing sample and standard solutions containing tellurium in this range.

Sulphite formed sulphur dioxide, which was carried to the cavity and gave a blue S_2 emission [16], thus increasing the intensity measured, even at 469 nm. The effect of sulphite was eliminated by adding 1 ml of 33% (v/v) hydrogen peroxide to the sample solution (25 ml) and increasing the amount of sodium tetrahydroborate to 2 ml of 2% solution to compensate for the consumption of reductant by the hydrogen peroxide. The sulphate formed was not reduced.

TABLE 2

Effect of tellurium on the emission from 0.5 μg of selenium

Tellurium added (μg)	0.0	0.01	0.2	5	10	20
Relative emission intensity	47	48	60	60	62	63
Blank[a]	3	3	4	5	6	14
Net selenium emission	44	45	56	55	56	49

[a]Each blank contained the same amount of tellurium as the corresponding selenium solution.

CONCLUSION

MECA, when coupled with sodium tetrahydroborate reduction, is a simple and sensitive technique for the determination of selenium. The sensitivity is an order of magnitude less than that reported for atomic absorption, but instrumental development work is in progress to improve MECA sensitivities.

REFERENCES

1 R. K. Skogerboe, A. T. Heybey and G. H. Morrison, Anal. Chem., 38 (1966) 1821.
2 G. F. Kirkbright and L. Ranson, Anal. Chem., 43 (1971) 1238.
3 Y. Yamamoto, T. Kumamaru, Y. Hayashi and M. Kanke, Anal. Lett., 5 (1972) 717.
4 K. C. Thompson and D. R. Thomerson, Analyst, 99 (1974) 595.
5 K. C. Thompson, Analyst, 100 (1975) 307.
6 A. E. Smith, Analyst, 100 (1975) 300.
7 J. Azad, G. F. Kirkbright and R. D. Snook, Analyst, 104 (1979) 232.
8 R. Belcher, S. L. Bogdanski, E. Henden and A. Townshend, Analyst, 100 (1975) 522.
9 I. Z. Al-Zamil, Ph.D. Thesis, Birmingham University, 1978.
10 R. Belcher, T. Kouimtzis and A. Townshend, Anal. Chim. Acta, 68 (1974) 297.
11 R. K. Asundi, M. Jan-Khan and R. Samuel, Nature, 136 (1935) 642.
12 M. Miyanisi, Sci. Pap. Inst. Phys. Chem. Res. (Tokyo), 37 (1940) 79.
13 A. Iranpoor, unpublished work.
14 H. J. Emeléus and H. L. Riley, Proc. Roy. Soc. London, Ser. A, 140 (1933) 378.
15 R. Belcher, S. L. Bogdanski, E. Henden and A. Townshend, Anal. Chim. Acta, 92 (1977) 33.
16 R. Belcher, S. L. Bogdanski and A. Townshend, Anal. Chim. Acta, 67 (1973) 1.
17 R. W. B. Pearse and A. G. Gaydon, The Identification of Molecular Spectra, 3rd edn., Chapman and Hall, London, 1965.
18 R. M. Dagnall, K. C. Thompson and T. S. West, Analyst, 93 (1968) 518.

Analytica Chimica Acta, 113 (1980) 21—32

SPECTROSCOPIC DETERMINATION OF THE DEGREE OF ATOMIZATION IN AN ELECTROTHERMAL ATOMIZER

KUNIYUKI KITAGAWA* and YUKIO IDE

Department of Synthetic Chemistry, Faculty of Engineering, Nagoya University, Furo-cho, Chikusa-ku, Nagoya (Japan)

(the late) TSUGIO TAKEUCHI

School of Materials Science, Toyohashi University of Technology, 1-1 Hibarigaoka, Tenpaku-cho, Toyohashi, Aichi (Japan)

(Received 9th August 1979)

SUMMARY

The degree of atomization, β, is measured for an electrothermal atomizer by comparing the emission lines of copper atoms and CuCl molecules. Hydrogen increases the β value. The determined β value of CuCl is used as a standard for the determination of β values of other elements (nickel, chromium, tin and lead).

As the importance of the electrothermal atomizer becomes greater in practical analysis for trace amounts of elements by atomic absorption spectrometry, it is necessary to elucidate the mechanisms of the atomization process. Interference effects by matrices and changes in absorption with the form of the salt are often encountered in routine analysis. As well as the loss of the element as non-atomic species, these effects seem to be critical factors in causing poor accuracy and precision. The degree of atomization β is one of the indicative parameters for these effects. Many approaches for determining the β value have been reported [1—3]. These methods have been applied mainly to chemical flames. It appears to be difficult to apply them to electrothermal atomizers because they are not based on the determination of the β value in a unit reaction and there is no accepted standard for comparison.

In a previous paper [4], an alternative method was briefly described for the determination of the β value in the reaction CuCl → Cu + Cl, and was applied to the atomization of copper(II) chloride in an air—hydrogen flame. An atomic emission line of copper and a molecular emission line of CuCl (0,0) were compared. This method has the advantage that equilibrium of the chemical reactions is not required.

In this paper, an application of this method is described for the determination of the β value in the reaction CuCl → Cu + Cl in a glassy-carbon tube atomizer, and the effect of trace hydrogen mixed with the argon carrier gas on the atomization is discussed.

BASIC FORMULAE

Since the Boltzmann law applies to most atomizers, the intensity of atomic emission is given by $I_a = h\nu_a \beta N_T A_a g_a \exp(-E_a/kT_a)/Q_a(T_a)$, where h is the Planck constant, ν_a the frequency of the atomic line, β the degree of atomization, N_T the total number of atoms and molecules of interest, A_a the Einstein transition probability for spontaneous emission, g_a the statistical weight of the upper level, E_a the upper level energy, k the Boltzmann constant, T_a the excitation temperature, and $Q_a(T_a) = \Sigma_i\, g_{a,i} \exp(-E_{a,i}/kT_a)$ the partition function; the subscript a stands for an atom. The partition function for different elements has been developed by de Galan and Winefordner [11].

The intensity of molecular emission is expressed by $I_m = h\nu_m(1-\beta)N_T A_m g_m \exp(-E_m/kT_m)/Q_m$, where m indicates a molecule. Since the observed molecular line is vibrational (0,0 band) which includes much rotational fine structure, the molecular partition function can be replaced by a convolution of electronic and vibrational partition functions:

$$Q_m(T_{m,e}, T_{m,v}) = q_{m,e}(T_{m,e})\, q_{m,v}(T_{m,v})$$

where the subscripts e and v stand for electronic and vibrational, respectively. Each is given by

$$q_{m,v} = \{1 - \exp(h\nu_{m,0}/kT_{m,v})\}^{-1} \text{ and } q_{m,e} = \sum_j g_{m,j} \exp(-E_{m,j}/kT_{m,e}),$$

where $\nu_{m,0}$ is the frequency of the first fundamental vibration. The g_m value for the singlet–singlet transition is taken as unity. The A_m value is approximately estimated from $A_m = 64\pi^4 \nu_m \mu_e^2/3hc^3$, where c is the velocity of light and μ_e the dipole moment. The dipole moment of diatomic molecules is approximately expressed as those of the ground state, $\mu_e \approx eabr_e$, where e is the electronic charge, a and b the normalization factors of the wave function for the ground state. The normalization condition is given by $a^2 + b^2 = 1$. The factors a and b are related to the charge on the atoms and the charge is estimated from Pauling's electronegativity:

$$q_{Cu} \approx 2a^2 = e[1 - \exp\{-(\chi_{Cl} - \chi_{Cu})^2/4\}]$$

where q_{Cu} is the charge on the copper atom and χ is the electronegativity.

The relevant parameters for the atomic line Cu I 327.4 nm and the molecular line CuCl($^1\Sigma$–$^1\Sigma$, 0,0) 433.3 nm are listed in Table 1.

A ratio of the atomic and molecular emission intensities is given by:

$$p(\lambda)\frac{R_{Cu}}{R_{CuCl}} = \frac{\beta\lambda_{CuCl} q_{CuCl,e}(T_{CuCl,e})\, q_{CuCl,v}(T_{CuCl,v})\, g_{Cu} A_{Cu}}{(1-\beta)\lambda_{Cu} Q_{Cu}(T_{Cu}) A_{CuCl}} \exp\left(\frac{E_{CuCl}}{kT_{CuCl,e}} - \frac{E_{Cu}}{kT_{Cu}}\right)$$

where λ is the wavelength and $p(\lambda)$ the instrumental response factor which

TABLE 1

Emission lines observed for the determination of the β value

Line	Wavelength (nm)	Transition	Energy (cm^{-1})	gA value ($10^8\ s^{-1}$)
Cu I	327.4	$^2S_{1/2}$—$^2P_{1/2}$	0—30535	1.9[a]
CuCl	433.3	$^1\Sigma$—$^1\Sigma$	0—23077	0.26[b]

[a]NBS Monograph 53 (1962). [b]Calculated.

is a product of the quantum yield of the photocathode and the reflection efficiency of the grating. These factors vary with the wavelength. Except for such a case as a plasma at a reduced pressure, it can be reasonably assumed that the temperatures of different systems are approximately the same or the systems are in quasi thermal equilibrium. Therefore, with the approximation $T_{CuCl,e} \simeq T_{CuCl,v} \simeq T_{Cu}$, the degree of atomization is given by:

$$\beta = \left\{1 + \frac{R_{CuCl}\lambda_{CuCl}q_{CuCl,e}(T_{Cu})q_{CuCl,v}(T_a)g_{Cu}A_{Cu}}{p(\lambda)R_{Cu}\lambda_{Cu}Q_{Cu}(T_{Cu})A_{CuCl}} \exp\left(\frac{E_{CuCl} - E_{Cu}}{kT_{Cu}}\right)\right\}^{-1} \quad (1)$$

The excitation temperature was determined by a two-line method of atomic absorption. Although the aim was to measure the excitation temperature of copper, a suitable pair of copper lines was not available, so that other elements (Pb, Sn and Ni) were used for the temperature measurement with the assumption described above that their excitation temperatures were the same.

Browner and Winefordner [5] reported a two-line atomic absorption method based on indium, gallium and thallium for temperature measurement with a quartz iodine continuum radiation source. This method does not involve large errors in absorbance and is not greatly affected by changes in absorption line profile. However, the low sensitivity seems to restrict its application to special cases.

An alternative two-line method based on maximum atomic absorption of lead with the use of a conventional line source (hollow-cathode lamp) has already been reported [6]; the method was applied to the measurement of the excitation temperature of lead atoms above a glassy carbon strip atomizer. This method has the advantage of high sensitivity but concurrently the disadvantage that the absorption line profile is a critical factor for the precision of the temperature measurement. In the previous method [6], the Doppler broadening of the absorption line was taken into account. In the present paper, the contribution of Lorentz broadening to the error is discussed.

When Doppler and Lorentz broadening are present and the natural broadening is negligibly small, the absorption coefficient is given [7] by

$$k_\nu = k_0 \frac{a'}{\pi} P(\omega, a'),$$

where $P(\omega,a') = \int_{-\infty}^{\infty} e^{-y^2}/[a'^2 + (\omega - y)^2]\,dy$, $\omega = 2(\nu - \nu_0)\,(\ln 2)^{1/2}/\Delta\nu_D$, $y = 2\,\delta(\ln 2)^{1/2}/\nu_D$, and $a' = \Delta\nu_L(\ln 2)^{1/2}/\Delta\nu_D$. Also

$$k_0 = \frac{2}{\Delta\nu_D}\left(\frac{\ln 2}{\pi}\right)^{1/2}\frac{\pi e^2}{mc}Nf \tag{2}$$

$$\Delta\nu_D = 2\left(\frac{2R\ln 2}{c}\right)^{1/2}\nu_0\left(\frac{T'}{\mu}\right)^{1/2} \tag{3}$$

$$\Delta\nu_L = 2\left(\frac{2}{\pi}\right)^{1/2}N'\left(\frac{RT'}{\mu}\right)^{1/2}\left(\frac{\sigma + \sigma'}{2}\right) \tag{4}$$

where ν is the wavenumber, ν_0 the wavenumber at the center of the absorption line, $\Delta\nu_D$ the Doppler width, δ the variable of integration, k_0 the maximum absorption coefficient when Doppler broadening alone is present, e the charge on the electron, m the mass of the electron, c the velocity of light, N the concentration of atoms whose electron is in the lower transition level, f the oscillator strength, T' the translational temperature or gas temperature, R the gas constant, $\Delta\nu_L$ the Lorentz broadening, μ the reduced atomic or molecular weight of the colliding system, N' the concentration of the foreign species, and σ and σ' the diameters of the colliding species. The maximum absorption coefficient is given by

$$k_{\nu,\max} = k_0 a' \pi^{-1} P_{\max}(a')$$

Where the Boltzmann law applies, the concentration N can be replaced by $N = N_t\beta(1 - \chi)g_L \exp(-E_L/kT_a)/Q_a(T_a)$, where N_t is the total number of molecular, atomic and ionic species containing the element of interest, χ the degree of ionization, g_L the statistical weight of the lower level and E_L the energy level of the lower level. Letting $U_{\max}(a') = k_{\nu,\max}/k_0$ and taking a ratio of absorbance for two atomic lines with different lower level energy gives

$$\frac{A_{1,\max}}{A_{2,\max}} = \frac{k_{\nu,1,\max}}{k_{\nu,2,\max}} = \frac{k_{0,1}}{k_{0,2}}\frac{U_{\max}(a_1')}{U_{\max}(a_2')}$$

Substituting eqns. (2) and (3) gives

$$\frac{A_{1,\max}}{A_{2,\max}} = \frac{\lambda_2 f_1 g_{L,1}}{\lambda_1 f_2 g_{L,2}}\frac{U_{\max}(a_1')}{U_{\max}(a_2')}\exp\{(E_{L,2} - E_{L,1})/kT_a\}. \tag{5}$$

For small difference in a' values, the following equation can be employed:

$$U_{\max}(a_1') = U_{\max}(a_2')\left\{\left(\frac{dU_{\max}}{da'}\right)_{a' = a_2'}(a_1' - a_2') + 1\right\}.$$

Equations (3) and (4) give

$$a' = [0.5(\sigma + \sigma')]^2\lambda\pi^{-1/2}$$

Therefore, $a_1' - a_2' = a_1'(1 - a_2'/a_1') = a_1'(1 - \lambda_1/\lambda_2)$.
Consequently, eqn. (5) is replaced by

$$\frac{A_{1,\max}}{A_{2,\max}} = \frac{\lambda_2 f_1 g_{L,1}}{\lambda_1 f_2 g_{L,2}} \left\{1 + \left(\frac{dU_{\max}}{da'}\right)_{a'=a'_2} \left(1 - \frac{\lambda_1}{\lambda_2}\right)\right\} \exp\{(E_{L,2} - E_{L,1})/kT_a\} \quad (6)$$

Thus, the ratio of wavelengths is a variable yielding the variation of absorbance. The first ratio of wavelengths originates from the Doppler width and the second one (in parentheses) from the Lorentz broadening. When $A_{1,\max}/A_{2,\max}$ is found experimentally, the excitation temperature T_a can be calculated from eqn. (6).

Once the excitation temperature has been determined, the degree of atomization β can be estimated from eqn. (1) from the emission intensities of copper atoms and CuCl molecules, R_{Cu} and R_{CuCl}.

Table 1 lists the relevant physical parameters for Cu and CuCl emissions, and Table 2 for similar parameters for the two lines of the three elements lead, tin and nickel. The equations for calculating the excitation temperature do not include the term attributed to the Lorentz broadening or the term in the first bracket in eqn. (6). The effect of this term will be discussed for nickel, which was selected for the determination of the excitation temperature.

EXPERIMENTAL

Apparatus and reagents

The components used are listed in Table 3. A glassy carbon tube (2 mm i.d., 3 mm o.d. and 30 mm long; Tokai Carbon Co. Ltd.) was fitted to stainless steel electrodes through cubic graphite mounts which served as thermal

TABLE 2

Elements and equations used for the determination of excitation temperature

Element	Wavelength (nm)	Energy (cm^{-1})	*gf* value[a]	B.p. (°C)
Pb	λ_1 283.3	0—35287	0.22	
	λ_2 261.4 {261.365	7819—46069	0.19	1750
	261.418	7819—46061	2.7	
	$\exp\{-0.797A_1 \exp(-11240/T_a)\} + 14.21 \exp\{-11.32A_1 \exp(-11240/T_a)\} - 15.21 \exp(-A_2) = 0$			
Sn	λ_1 270.7	1692—38629	1.1	2275
	λ_2 284.0	3428—38629	2.5	
	$T_a = 2498.6/\{0.8692 + \ln(A_1/A_2)\}$			
Ni	λ_1 352.45	205—28569	0.85	2732
	λ_2 361.9	3410—31031	1.5	
	$T_a = 4616/\{0.595 + \ln(A_1/A_2)\}$			

[a]NBS Monograph 53 (1962).

TABLE 3

Experimental components

Atomic absorption spectrometer	Nippon Jarrell-Ash AA-1
Light source	HTV hollow-cathode lamp
Electrothermal atomizer	Glassy carbon tube located in a glass chamber
Power supply for the electrothermal atomizer	Stepwise transformers
Recorder	Sanei Sokki Co. 5L Visigraph fitted with 6L5 d.c. amplifier

insulators. The glassy carbon tube had an opening (0.8-mm diameter) on the lateral face through which sample solutions were introduced.

Argon was introduced into the atomization chamber at 1.5 l min^{-1}. In order to estimate the reduction power on atomization, hydrogen was premixed with argon.

Stock solutions of copper(II) chloride, lead nitrate, tin(II) chloride, chromium(III) chloride and nickel chloride (all analytical reagent grade) were prepared by dissolution in deionized water; the acidity was adjusted to 1 M. Working solutions were prepared by diluting the stock solution with deionized water and adjusting the acidity to 0.5 M.

Procedures

By a microsyringe (Scientific Glass Engineering Pty.), an aliquot of the sample solution was placed on the bottom of the glassy carbon tube atomizer, dried at 120°C for 2 min and atomized. The amounts introduced are listed in Table 4.

The temperature of the surface of the glassy carbon tube atomizer was measured by an optical pyrometer (Hokushin Electric Co. Ltd.). The transient temperature was determined by tracing the black-body radiation from the atomizer at 550 nm. The resulting photocurrent was calibrated by temperature measurements with the optical pyrometer.

RESULTS AND DISCUSSION

Excitation temperature

A suitable pair of copper absorption lines with different lower energies could not be found. Therefore, it was necessary to select an alternative element for the determination of the excitation temperature. The excitation temperature was estimated from the absorbances at the absorption peaks of the three elements lead, tin and nickel. Figure 1 shows the relation between the excitation temperatures and the equilibrium temperature of the atomizer surface. It can be pointed out that the excitation temperatures are in the order of the iso-vapor pressure temperature of atoms. This explains the difference in atomization temperature of the three elements.

TABLE 4

Amounts of salts introduced into the carbon tube

Salt	Wavelength (nm)	Amount (ng) of element	Salt	Wavelength (nm)	Amount (ng) of element
$CuCl_2$	Cu I 327.4	45×10^3	$SnCl_2$	Sn I 270.7	5
	CuCl 433.3			Sn I 284.0	5
$Pb(NO_3)_2$	Pb I 283.3	0.4	$CrCl_3$	Cr I 357.9	20
	Pb I 284.0	20			
$NiCl_2$	Ni I 352.5	20			
	Ni I 361.9	20			

Figure 2 shows the time correlation for the transient temperature of the atomizer surface, the appearance of the absorption peak and the excitation temperature. The excitation temperatures are in order of the peak appearance and somewhat lower than the temperature of the atomizer surface. Thermal energy may be partly distributed to the atomic system and the remainder to other processes requiring energy such as those involving latent heat or dissociation energy. In addition, the thermal energy can be distributed in the molecular energy system (translational, vibrational or rotational energy) if

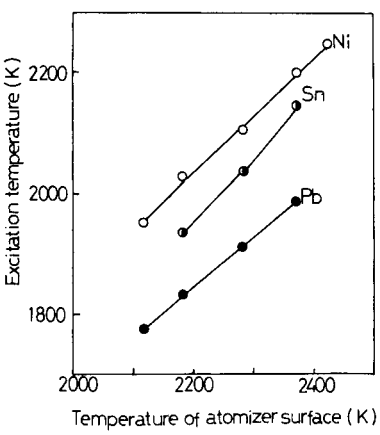

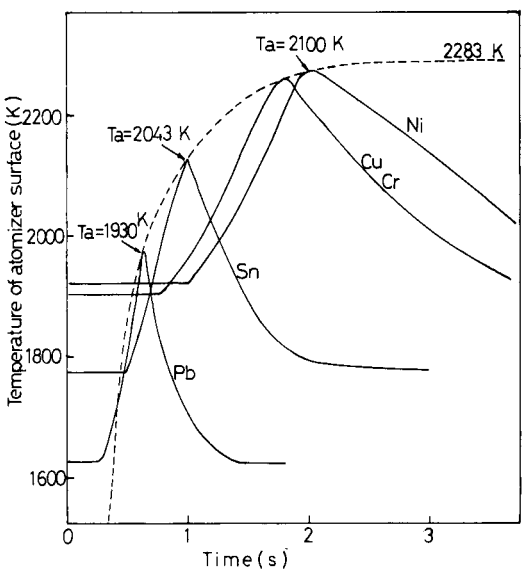

Fig. 1. Relation between the excitation temperature and temperature of the atomizer surface.

Fig. 2. Time correlation for the temperature of the atomizer surface, the appearance of the absorption peak and the excitation temperature. (---) Temperature of atomizer surface. T_a is the excitation temperature at peak maximum.

the degree of atomization is not unity. There also is a possibility that, because of the low thermal conductivity between the sample salt and the surface of the atomizer, the transient energy transfer is not enough or the temporal thermal equilibrium between them is incomplete. For these reasons, the excitation temperatures are somewhat lower than the temperature of the atomizer surface. The peak appearance time of nickel is closer to that of copper than are those of lead and tin. Consequently, nickel was chosen as the alternative element for the determination of the excitation temperature.

The error arising from Lorentz broadening is expressed as the term in the first bracket in eqn. (6). Figure 3 shows the result of numerical integration of $U_{max}(a')$ by a computer. The value of a' for various elements [8] lies in the range 1—2.5 at 2,000—3,000 K. The value of dU_{max}/da' was determined graphically and found to change from 0.2 to 0.1 over the region of a'. For the pair of nickel lines, the term in the first bracket varies from 1.00524 to 1.00655. Thus the Lorentz broadening may cause a maximum error in the absorbance ratio of 1%.

In practice, there arises the Lorentz shift in addition to Lorentz broadening.

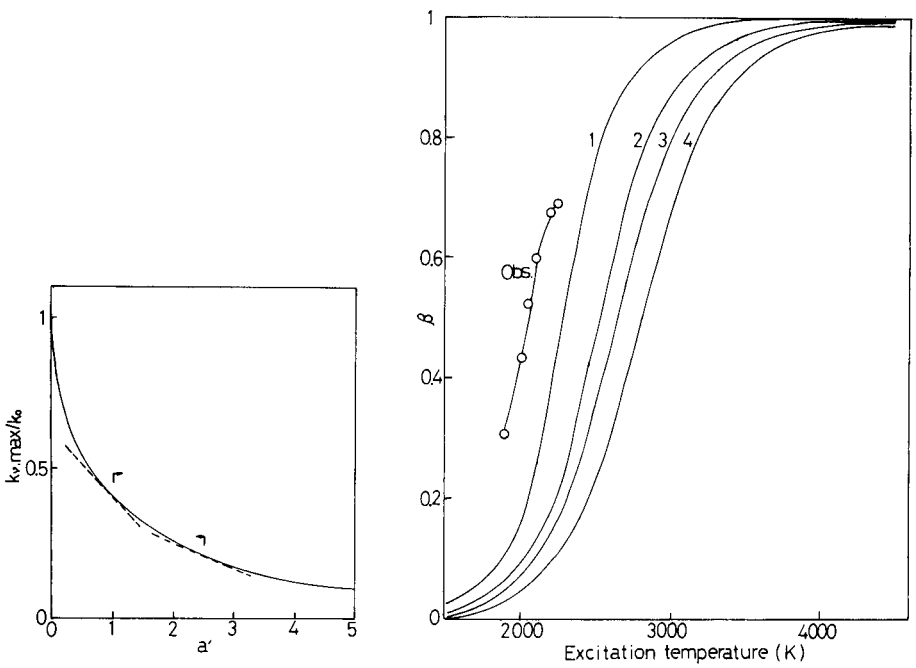

Fig. 3. Theoretical curve of the effect of Lorentz broadening on the maximum of an absorption peak. The broken line tangents and arrows indicate a typical region of a'.

Fig. 4. Dependence of the β value for CuCl on the excitation temperature. (○) The experimental curve. Also shown are the theoretical curves at a total pressure of (1) 0.1 atm.; (2) 0.5 atm.; (3) 1 atm.; (4) 2 atm.

No complete theory of a Lorentz-shifted absorption line profile has been proposed except by analogy with emission line profiles [9]. Therefore, it cannot be predicted how much the Lorentz shift contributes to the error. Lenz [9], however, concluded that the magnitude of the Lorentz shift is proportional to that of the Lorentz broadening. According to Lenz's theory, therefore, the Lorentz shift would be $\Delta\nu_S \approx -0.36\Delta\nu_L$ in an argon atmosphere. Taking this into account in the absorbance ratio, it can be suggested that the magnitude of the error does not exceed the error of measurement.

Degree of atomization β(CuCl → Cu + Cl)

It was found that there was a delay between the CuCl and Cu emission peaks of <1 s, which was dependent on the atomizer temperature; the CuCl emission preceded the Cu emission. The time required for achieving the peak copper emission was almost the same as for the nickel absorption. For this reason, the β value was estimated from the data obtained at the time of the peak copper emission. Figure 4 shows the dependence of the β value on the excitation temperature. The theoretical curves were calculated from an assumption of equilibrium in the purely thermal dissociation CuCl ⇌ Cu + Cl without other chemical reactions, which corresponds to Saha's equation of thermal ionization. There is a pronounced discrepancy between the experimental and theoretical curves over the possible total pressure range. This suggests that the molecules from the sample are partly reduced. A possible reductant is active carbon from the surface of the glassy carbon atomizer. In a previous study of the diffusion of atoms [10] the adsorption activity of glassy carbon was found to be as weak as that of quartz, compared with graphite. However, the result of the β value indicates that the surface of glassy carbon has a significant reducing power during the atomization of CuCl.

The sample was $CuCl_2$. Therefore, the degree of dissociation β' for the reaction $CuCl_2$ → CuCl + Cl should be evaluated for the determination of the overall degree of atomization $\beta'\beta$. However, it is well known that $CuCl_2$ is completely converted to CuCl above 993°C. Thus, it is fairly reasonable that $\beta = \beta'\beta$.

Effect of hydrogen on the degree of atomization

Figure 5 shows the effect of hydrogen flow rate on the excitation temperature. The temperature of the atomizer surface was 2,100°C when hydrogen was absent. As the flow rate of hydrogen increased, the excitation temperature decreased. This may be attributed to the high thermal conductivity of hydrogen.

Figure 6 shows the effect of the hydrogen flow rate on the degree of atomization. As the flow rate increases, the β value rapidly increases but does not exceed a value of ca. 0.9. This is probably due to the decrease in the temperature of the atomizer surface and partly to the rapid diffusion of CuCl in the hydrogen atmosphere or the short residence time within the hot region in the atomizer. The recommended ratio of flow rates H_2:Ar = 1:300 is enough to double the degree of atomization.

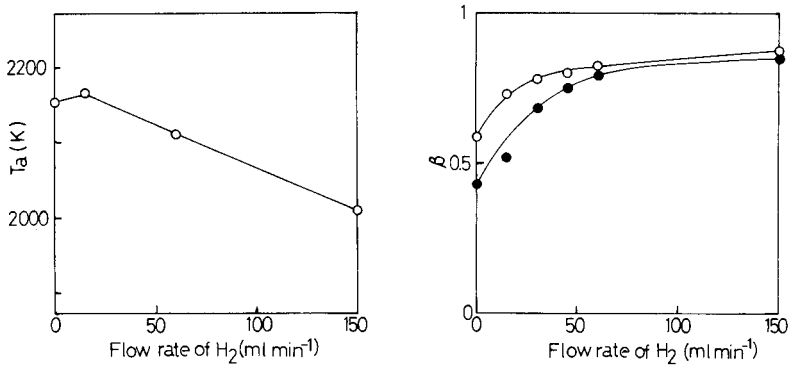

Fig. 5. Dependence of the excitation temperature on the flow rate of hydrogen. The temperature of the atomizer surface was 2373 K.

Fig. 6. Dependence of β value for CuCl on the flow rate of hydrogen at excitation temperatures of (•) 2000 K and (○) 2100 K.

The principal reaction associated with the promotion of atomization may be the abstraction of a chlorine atom by molecular or atomic hydrogen. However, since accurate reaction rates of possible reactions have not been measured, the detailed mechanism cannot be elucidated. If the reaction rates are much larger than the residence time, which is likely in radical reactions at high temperatures, chemical equilibrium applies. In this case, the difference in dissociation energy D_0 may be a means of establishing the principal reaction. Of possible diatomic molecules (CuCl, CCl, CH, H_2, HCl, etc.) HCl has the largest dissociation energy. Therefore, HCl molecules will be most stable in the high temperature environment.

Application to the determination of the β value of $CrCl_3$

The β value determined by the present method can be a standard for the determination of β values of other elements. By comparing the absorbances of copper and chromium, the relative β value was determined. As seen above, the appearance times of the nickel, copper and chromium peak almost coincide. This makes it reasonable to substitute the excitation temperature of nickel for that of copper and chromium, and to estimate the β value of chromium by comparing the copper and chromium absorbances. The relative β value is given by

$$\beta_{Cr} = \beta_{Cu} \frac{A_{Cr}}{A_{Cu}} \frac{\lambda_{Cr} f_{Cu} g_{L,Cu}}{\lambda_{Cu} f_{Cr} g_{L,Cr}} \left[\left(\frac{1}{M_{Ar}} + \frac{1}{M_{Cu}} \right) \Big/ \left(\frac{1}{M_{Ar}} + \frac{1}{M_{Cr}} \right) \right]^{1/2} \frac{Q_{Cr}(T_a)}{Q_{Cu}(T_a)} \frac{W_{Cu} M_{Cr}}{W_{Cr} M_{Cu}} \exp$$

$$\{(E_{L,Cr} - E_{L,Cu})/kT_a\},$$

where W is the sample weight and the term owing to the Lorentz broadening is neglected. For both resonance lines Cu I 327.40 and Cr I 387.87 nm, the lower term energy is zero. Therefore, the exponential term is simplified to

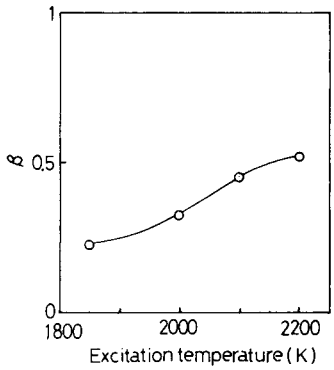

Fig. 7. Dependence of β value for $CrCl_3$ on the excitation temperature.

unity. Figure 7 shows the dependence of the β value on the excitation temperature. The β value of chromium is somewhat lower than that of copper. If the forward and backward reactions are rapid enough, the difference in β value might be attributable to the difference in dissociation energy D of CuCl and CrCl. The dissociation energy has been reported to be 3.4 and 3.0 eV for CrCl and CuCl, respectively. However, as stated above, a kinetic approach is necessary for clarification of the detailed mechanism.

Application to other elements

The standard β value of CuCl was used to attempt to determine β values for tin(II) chloride and the nitrates of lead and silver. In this application, there is a problem associated with the difference in the appearance time of the peak absorption. If the measurement is timed for the peak maximum of chromium or copper, it coincides with the tail of the silver peak, and is not superimposed upon any part of the lead or tin peaks. In practice, for example, the β value of silver nitrate was found to be ca. 100% at an excitation temperature of 2,000°C. This value seems likely for the low dissociation energy of AgO, 1.8 eV. However, this value does not coincide with a β value of silver nitrate at the moment of peak maximum of silver absorption. It might, therefore, be best to determine transient β values with the use of a more suitable partner for measuring the standard β value. This comparison method appears to be more useful for the determination of β value of samples atomized in flames where there is no absorption delay.

REFERENCES

1 L. de Galan and J. D. Winefordner, J. Quant. Spectrosc. Radiat. Transfer, 7 (1967) 251.
2 T. J. Vickers, C. R. Cottrell and D. W. Breakey, Spectrochim. Acta, Part B, 25 (1970) 437.
3 S. R. Koirtyohann and E. E. Pickett, Spectrochim. Acta, Part B, 26 (1971) 349.
4 K. Kitagawa and T. Takeuchi, Anal. Chim. Acta, 68 (1974) 212.

5 R. F. Browner and J. D. Winefordner, Anal. Chem., 44 (1972) 247.
6 Y. Ide, M. Yanagisawa, K. Kitagawa and T. Takeuchi, J. Spectrosc. Soc. Jpn. (Bunko Kenkyu), 24 (1975) 143.
7 A. C. G. Mitchell and M. W. Zemansky, Resonance Radiation and Excited Atoms, Reprinted 1961, The Syndics of the Cambridge University Press, London.
8 E. Hinnov and H. Kohn, J. Opt. Soc. Am., 47 (1957) 156.
9 W. Lenz, Z. Phys., 80 (1933) 423.
10 K. Kitagawa and T. Takeuchi, Anal. Chim. Acta, 67 (1973) 457.
11 L. de Galan, R. Smith and J. D. Winefordner, Spectrochim. Acta, Part B, 23 (1968) 521.

Analytica Chimica Acta, 113 (1980) 33—38

SAMPLE TEMPERATURE EFFECTS IN ANALYTICAL FLAME SPECTROMETRY

MALCOLM S. CRESSER** and RICHARD F. BROWNER*
School of Chemistry, Georgia Institute of Technology, Atlanta, GA 30332 (U.S.A.)
(Received 3rd August 1979)

SUMMARY

Changes in solution viscosity with temperature cause very substantial changes in nebulization rate which are not reflected by corresponding changes in analyte signals. Increased nebulization rates cause changes in droplet size distributions, resulting in decreases in nebulization efficiency. The changes in droplet size distribution are greater than would be predicted theoretically. Possible reasons for the apparent discrepancy are discussed.

It has been known from the early days of flame photometry that increases in sample temperature cause increases in analytical signals [1], although minor fluctuations in the temperatures of sample solutions around room temperature do not introduce significant errors in flame spectrometric analysis when pneumatic nebulizers and pre-mix burner systems are employed [2]. Although this stability is convenient in routine analysis, it would not be anticipated from the approaches conventionally employed for the study of nebulization phenomena. The aim of the present investigation was to consider possible causes for the insensitivity of pneumatic nebulization to sample temperature effects and to explain why the substantial fluctuations predicted from a simple theoretical approach are not encountered in practice.

EXPERIMENTAL

Apparatus and nebulization efficiency measurements

Atomic absorption measurements were made on a Baird A3400 atomic absorption spectrometer. The normal drain was replaced by a measuring cylinder for nebulization efficiency measurements. Solutions were maintained at the required temperatures in a series of thermostat tanks and transferred to the spectrometer in a water bath at the required temperature immediately prior to nebulization. The method proposed by Willis [3] was used to measure nebulization efficiencies.

**On leave from the Department of Soil Science, Aberdeen University, Meston Walk, Old Aberdeen AB9 2UE, Scotland.

Investigation of aerosol size distributions

The aerosol produced by a Perkin-Elmer nebulizer was passed via an inverted spray chamber to the pre-impactor stage of an Andersen Cascade Impactor, Model 21000. The airflow through the impactor was checked periodically using a Matheson Linear Mass Flowmeter, model 8116. The nebulization rate was controlled by a Buchler Multistaltic peristaltic pump.

RESULTS AND DISCUSSION

At moderate sample uptake rates, the nebulization rate Q is governed by the Poiseuille equation $Q = P\pi r^4(8\eta L)^{-1}$, where P is the pressure drop along the capillary, r and L are the capillary radius and length respectively, and η is the viscosity of the liquid sample. For moderate changes in sample temperature, the changes produced in r and L are negligible and P does not vary significantly. It follows that a graph of Q against the reciprocal of viscosity should be linear. If the nebulization rate is measured at any one temperature, 293 K being used in the present study, it is possible to calculate theoretical values for nebulization rates at other temperatures from literature values for viscosity [4] at those temperatures. Values calculated for water over the range 273—373 K are shown in Fig. 1. The measured values, also shown, deviate from this theoretical line, primarily because the pneumatic nebulizer acts as a heat exchanger; samples below room temperature warm up upon

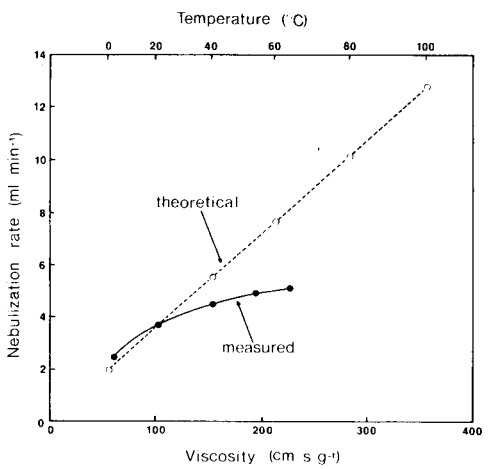

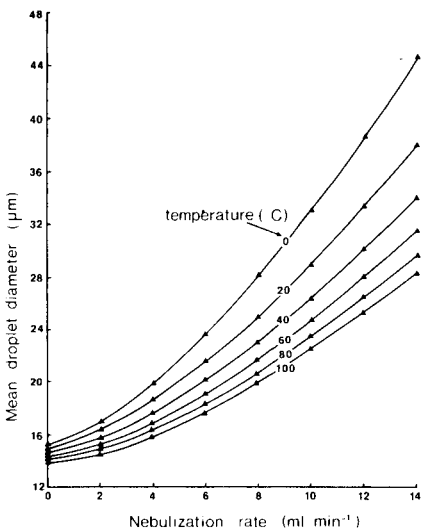

Fig. 1. Calculated and measured variations in nebulization rate with viscosity changes caused by changes in temperature.

Fig. 2. Effect of water temperature on the variation in mean droplet diameter (as predicted by the Nukiyama and Tanasawa equation) with nebulization rate.

nebulization whereas those above room temperature cool down, unless the temperature of the nebulizer is itself controlled independently.

Changes in sample density over the small temperature range 273—293 K have a negligible effect upon the amount of analyte element transported to the flame at any given nebulization rate. If nebulization rate alone, therefore, is considered as the signal controlling step in flame spectrometry, an increase in signal of 75% would be observed on raising the sample temperature from 273 to 293 K. For 1 μg ml^{-1} solutions of zinc, calcium and magnesium, increasing the sample temperature over the above range caused changes in atomic absorption signals of only 11—21%. Since these values are much less than the predicted value of 75% it must be assumed that nebulization *efficiency* decreases with increasing sample temperature. This was found to be the case in practice, the nebulization efficiency falling from 8.6% at 273 K to 6.1% at 293 K.

Increases in temperature might be expected to lead to increased solvent evaporation and hence increased efficiency of transport of sample to the flame. Both this effect and increased nebulization rate effects must therefore be countered to a significant extent either by a change in the droplet size distribution produced by the pneumatic nebulizer or by increased coalescence between droplets in the spray chamber. There is indirect evidence for assuming the latter effect to be insignificant. Thus, for example, two nebulizers have been used side by side in a single spray chamber to demonstrate the nature of interferences occurring as a result of compound formation in flames [5—7]. This approach would not have been successful if coalescence was significant in spray chambers, so that if coalescence does occur it must take place very close to the nebulizer nozzle.

The approach most commonly adopted in analytical flame spectroscopy when an indication of the droplet size produced by a pneumatic nebulizer is required is to use the Nukiyama and Tanasawa equation [8] to calculate aerosol mean droplet diameters, on a volume:surface area basis, from literature or measured values of solvent densities, surface tensions and viscosities and typical values for nebulization gas flow rate and gas and solution flow velocities [2, 9, 10]. This has been done here for aqueous solutions over the range 273—373 K. The results are shown in Fig. 2. At any given nebulization rate an increase in temperature leads to a decrease in the calculated mean droplet diameter and hence would be expected to lead to an increase in nebulization efficiency. When the increase in nebulization rate caused by increasing temperature is also considered, however, a small increase in mean droplet diameter would be expected. The overall change is very much smaller than the changes calculated when organic solvents are considered relative to water [9, 10]. It might therefore be expected to cause only a very small decrease in nebulization efficiency.

Recently a method has been developed by the authors for studying droplet size distributions over the diameter range 0.5—10 μm produced by pneumatic nebulizers [11]. The procedure is based upon the observation that evaporation effects from droplets may be reduced to a negligible level by

producing aerosols from concentrated sodium chloride solution, thus allowing droplet aerosol distributions to be measured with a conventional cascade impactor. It has been applied here to study the effect of changing the nebulization rate of a Perkin-Elmer nebulizer by using a peristaltic pump. Measurements were made with an inverted Perkin-Elmer spray chamber assembly at nebulization rates of 0.63 and 5.15 ml min^{-1}. The aerosol was sampled isokinetically at the port in which the burner head would normally be fitted. The results, shown in Fig. 3, demonstrate that a small but significant broadening of the distribution curve occurs. However, the change is small, and the mean droplet diameters are much less than the values predicted by the Nukiyama and Tanasawa equation. Moreover, the change in nebulization rate required to produce even this small change was almost one order of magnitude.

The large difference between the predicted and observed mean diameters reflects one of the major limitations of the Nukiyama and Tanasawa equation in analytical flame spectrometry, namely that it applies to the entire aerosol produced by the nebulizer, and not just to the fraction of aerosol reaching the burner head, which is the fraction studied here. The spray chamber and associated components are designed purposely to eliminate larger droplets from the air stream. The measurements were repeated after the removal of the mixer paddle from the spray chamber and the change then became very much more pronounced, as shown in Fig. 4. The difference is attributable, partly at least, to the fact that the support arm for the mixer paddle acts as an impact bead. The distribution at the higher nebulization rate became very obviously multi-modal, and the mean droplet diameter could well lie close to that predicted by the Nukiyama and Tanasawa equation, although unfortunately the measuring technique currently used does not allow measurements to be made of droplets above 10 μm in diameter.

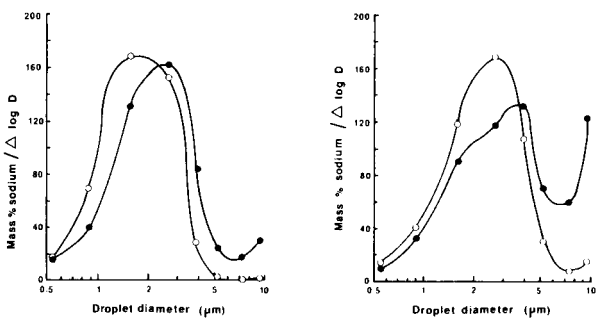

Fig. 3. Effect of nebulization rate upon droplet distribution reaching the burner head at nebulization rates of 0.63 ml min^{-1} (○) and 5.15 ml min^{-1} (●). Total air flow through spray chamber, 20 l min^{-1}. Δ log D is a normalization factor to compensate for unequal measurement ranges between adjacent mean droplet diameters, *D*.

Fig. 4. Effect of nebulization rate upon droplet distribution reaching the burner head, after removal of the mixer paddles, nebulization rates of 0.63 ml min^{-1} (○) and 5.15 ml min^{-1} (●). Total air flow through spray chamber, 20 l min^{-1}.

Figures 3 and 4 together demonstrate why, at low nebulization rates, the nebulization efficiency increases more than might be expected from consideration of the Nukiyama and Tanasawa equation alone. The efficiency of droplet removal by collision with the bead, mixer paddles and spray chamber end walls increases very rapidly once a certain initial droplet diameter, dependent on the nebulizer gas flow and velocity, is exceeded. At the low nebulization rate the contribution made by droplets above 5 μm in diameter is negligible so that very few droplets are removed by the impact bead, mixer paddles and end walls; the change in droplet diameter is slight and the nebulization efficiency is much higher.

At the higher nebulization rate studied, the multi-modal distribution with more large droplets means that far more droplets are lost via collision with the bead, paddles and walls and the nebulization efficiency is much poorer. The differences in the example studied are more pronounced than they would be for the smaller difference in nebulization rates caused by temperature change, but the trend should be similar.

The change in measured mean droplet diameter with nebulization rate is greater than that predicted from the Nukiyama and Tanasawa equation, unless at the lower nebulization rate studied a number of large droplets occur at diameters appreciably greater than 10 μm. Even if this is the case, it illustrates another serious limitation of applications of the Nukiyama and Tanasawa equation. It is possible to envisage any number of widely differing distribution curves yielding a given mean droplet diameter, although the amount of aerosol reaching the burner head could be widely different in each case.

It is possible to visualise mechanisms which explain the size distribution results obtained. The occurrence of droplet recombination to any significant extent over most of the spray chamber volume may be discounted for reasons mentioned earlier, but it is certain to occur to some extent in the immediate vicinity of the nebulizer nozzle. Smaller droplets produced by the nebulizer are more rapidly accelerated in the air stream than their larger counterparts and, if space allows, flow past larger, leading droplets, unless they have the size-velocity combination necessary to effect collision. As the nebulization rate increases, the droplet concentration, and hence the probability of collision, also increases. Such collisional processes could readily lead to the production of a multi-modal distribution of the type found. This explanation implies that the recombination process is taken into account in the Nukiyama and Tanasawa equation, and the latter does not therefore hold at very low nebulization rates when recombination is reduced to a negligible level.

A possible alternative mechanism also implies a breakdown of the Nukiyama and Tanasawa equation at low nebulization rates, but without invoking recombination as the mechanism leading to the multi-modal distribution. If temperature effects are ignored, then to a first approximation the energy dissipated during the nebulization process is primarily converted to surface energy, the magnitude of which depends upon the surface area generated and

surface tension. If the mass of droplets amongst which this energy is distributed is reduced, the same amount of new surface area is still required to dissipate the same amount of energy. At nebulization rates giving a bimodal distribution with a size peak at above 10 μm, the extra area can be readily generated by secondary fragmentation of large droplets, giving a small change in nebulization efficiency and a relatively small change in mean droplet diameter. As the nebulization rate is further reduced, a stage is eventually reached where droplets with diameters above 10 μm have all been broken up by secondary fragmentation processes and the distribution is no longer multi-modal. At this stage further decreases in nebulization rate must lead to a more significant change in mean droplet diameter and to a much greater change in nebulization efficiency.

The non-applicability of the Nukiyama and Tanasawa equation at low nebulization rates is quite conceivable because the equation was evolved from data obtained at appreciably higher nebulization rates and lower nebulizer gas velocities than those commonly employed in analytical flame spectrometry. Moreover size measurements were only made on droplets of larger diameters than those considered here.

Regardless of the reasons for the effect, decreases in nebulization rate to levels appreciably below those normally employed in analytical flame spectrometry cause marked changes in droplet size distribution which in turn lead to increased nebulization efficiency.

Conclusions

The effect on signal of a decrease in nebulization rate caused by increased viscosity on lowering the temperature of aqueous sample solutions from 298 to 273 K is offset by a change in droplet size distribution. Decrease in the aerosol mean droplet diameters at lower nebulization rates results in increased nebulization efficiency, and the combined effects mean that signal changes with temperature are kept at a level acceptable for routine analysis.

This material is based in part upon work supported by the National Science Foundation under grant No. CHE77-07618. The authors are indebted to Fiona Mitchell for assistance with some of the experimental work.

REFERENCES

1 C. T. J. Alkemade, A Contribution to the Development and Understanding of Flame Photometry, Ph.D. Thesis, University of Utrecht, 1954.
2 G. F. Kirkbright and M. Sargent, Atomic Absorption and Fluorescence Spectroscopy, Academic Press, London, 1974.
3 J. B. Willis, Spectrochim. Acta, Part A, 23 (1967) 811.
4 R. C. Weast, Ed., Handbook of Chemistry and Physics, 58th edn., C.R.C. Press, 1977.
5 C. T. J. Alkemade and M. H. Vorhuis, Fresenius Z. Anal. Chem., 163 (1958) 91.
6 S. Fukishima, Mikrochim. Acta, (1959) 596.
7 W. Schuchknecht and H. Schinkel, Fresenius Z. Anal. Chem., 162 (1958) 266.
8 S. Nukiyama and T. Tanasawa, Trans. Soc. Mech. Eng., Jpn., 5(1939) 68.
9 J. Stupar and J. B. Dawson, Appl. Opt., 7 (1968) 1351.
10 M. S. Cresser, Solvent Extraction in Flame Spectroscopic Analysis, Butterworths, London, 1978.
11 M. S. Cresser and R. F. Browner, Spectrochim. Acta, in press.

Analytica Chimica Acta, 113 (1980) 39—46

A SOLVENT EXTRACTION TECHNIQUE FOR DETERMINING NANOGRAM PER LITER CONCENTRATIONS OF CADMIUM, COPPER, NICKEL AND ZINC IN SEA WATER

RALPH G. SMITH, JR.* and HERBERT L. WINDOM

Skidaway Institute of Oceanography, P.O. Box 13687, Savannah, Georgia 31406 (U.S.A.)

(Received 17th May 1979)

SUMMARY

A dithizone—chloroform extraction technique for determining ng l^{-1} levels of Cd, Cu, Ni and Zn in sea water is described. Nickel extraction requires the addition of dimethylglyoxime. The metals are concentrated from 100 ml of sea water into 2.0 ml of dilute nitric acid and subsequently determined by electrothermal atomic absorption spectrometry. Extraction parameters, interferences and contamination considerations are discussed. The precision, based on replicate analyses, is around 10% for the four metals, and the recovery is quantitative, based on analysis of spiked samples. The application of this technique to fresh-water samples is also discussed.

The determination of trace metals in natural waters is difficult because of the low concentrations at which they occur. Most analytical methods have detection limits which require sample preconcentration and/or separation of the trace constituents from the major cations present in natural waters. Some of the more commonly used techniques include solvent extraction [1—3], ion exchange [4—6] and coprecipitation [7, 8]. Concentrations of copper, cadmium and nickel at the ng l^{-1} levels are normally below the workable range of most solvent extraction techniques. However, several workers [9—11] have reported ng l^{-1} concentrations by using solvent extraction combined with the back-extraction of the organic phase into dilute acid. Bruland et al. [11] digested the back-extracted acid phase with concentrated nitric acid prior to analysis by flameless atomic absorption spectrometry. A coprecipitation technique described by Boyle and Edmond [12, 13] has been used by others [8, 14] reporting ng l^{-1} concentrations of Cu, Ni and Cd. The major disadvantages of the technique are the quantitative transfer and digestion of the precipitate [14].

Although dithizone has been used for many years to chelate metals, its application to natural waters at ng l^{-1} levels of trace metals has not been utilized. Sandell [15] lists a number of metal dithizonates that can be formed for colorimetric determinations. The detection limits of such techniques, however, are several orders of magnitude too high for sea-water analysis. A combination of dithizone—chloroform extraction and isotope dilution techniques has been reported for determination of lead in sea water [16].

This paper describes a dithizone—chloroform extraction technique for concentrating Cu, Cd, Ni and Zn from natural waters and their subsequent determination by flameless atomic absorption spectrophotometry. The extraction of nickel requires the addition of dimethylglyoxime.

EXPERIMENTAL

Apparatus

Atomic absorption analyses were accomplished with a Perkin-Elmer model 403 atomic absorption system equipped with a deuterium background corrector and a HGA-2200 heated graphite furnace. An AS-1 automatic sampling system was used in conjunction with the heated graphite furnace. Ultrapure water ("Q" water) was made from distilled water by redistilling in a quartz subboiling still.

Reagents

A 0.040% (w/v) dithizone solution was freshly prepared from Suprapur dithizone (EM Laboratories) and high-purity chloroform (Burdick and Jackson). The dithizone reagent may be further purified as described by Patterson and Settle [17]. This purification step is only necessary when working at zinc concentrations less than 100 ng l^{-1}. An ammonium citrate buffer was made by bubbling ammonia into a 20% (w/v) ammonium citrate solution until a pH of 7.7 was reached. This solution was then purified by multiple extractions with dithizone—chloroform as described by Patterson and Settle [17]. A 1% (w/v) dimethylglyoxime solution was prepared from Suprapur dimethylglyoxime (EM Laboratories) and ethanol. High-purity nitric acid was obtained from the National Bureau of Standards. Diluted Suprapur ammonium hydroxide was used for sample pH adjustment. All reagents were prepared and stored in teflon.

Procedure

Copper was extracted from sea water at a pH of 2.0 ± 0.2 from a 100-ml sample volume. This sample aliquot was determined by weighing into a 250-ml teflon bottle to which 2.5 ml of 0.040% dithizone—chloroform and 7.5 ml of chloroform had been added. The aqueous and organic phases were equilibrated on a mechanical shaker for 20 min, and then poured into a 250-ml teflon separatory funnel. The empty teflon bottle was rinsed with "Q" water and the rinse water discarded. It is important that every drop of rinse water be removed from the bottle and from the bottle cap. After 5 min, the organic phase was withdrawn from the separatory funnel directly into the rinsed teflon bottle. Care must be exercised so that no water is drawn into the bottle with the organic phase. The organic phase was back-extracted with the addition of 200 μl of the (N.B.S.) nitric acid, using an Eppendorf pipet, and 1.8 ml of "Q" water from an Oxford pipet. The organic phase must change from bluish green to orange in color after the addition of nitric acid and prior

to the addition of "Q" water. The organic and nitric acid phases were shaken on a mechanical shaker for 5 min to ensure complete back-extraction.

The aqueous phase in the separatory funnel was discarded and the teflon separatory funnel rinsed with "Q" water to prepare it for the next separation. The rinse water was completely removed from the separatory funnel and discarded.

After the 5-min equilibration, the back-extracted sample was poured back into the teflon separatory funnel and the phases separated. The acid phase was collected in a 2.0-ml precleaned polyethylene vial and stored in a refrigerator until analyzed.

Cadmium and zinc were extracted from sea water at a pH of 7.7 ± 0.2 by using the procedure described for copper after the addition of 1.0 ml of the citrate buffer. Nickel was also extracted after the addition of 5.0 ml of 1% dimethylglyoxime—ethanol.

Standards were prepared by spiking pre-extracted water samples and re-extracting as described above. Any residual dithizone remaining in the pre-extracted sample was removed prior to the spike addition by washing the aqueous phase with two 10-ml portions of chloroform and discarding the wash; 5 min was allowed after each wash for the phases to separate.

Each of the metals was determined by flameless atomic absorption spectrometry. The manufacturer's recommended operating conditions for lamp current, wavelength, and slit width were followed. The deuterium background corrector was used for all analyses. Instrumental parameters for the heated graphite furnace are given in Table 1.

The sample injection into the heated graphite furnace was done with an automatic sampling system. Contamination did not appear to be a problem when precleaned polyethylene vials were used for sample containers. The use of the automatic sampling system enhanced the reproducibility of the sample injection and shortened the analyses time.

TABLE 1

Instrumental parameters for HGA 2200

Element	Sample volume (μl)	Gas flow ($cm^3\ min^{-1}$)	Dry cycle	Char cycle	Atomization cycle	Recorder setting[c]
Cd	10	40[a]	15 s 100°C	20 s 350°C	5 s 2000°C[b]	1.0
Cu	20	40	25 s 100°C	20 s 900°C	5 s 2300°C[b]	0.5
Ni	20	40	25 s 100°C	20 s 900°C	8 s 2300°C[b]	0.5
Zn	2.0	40	10 s 100°C	15 s 500°C	7 s 2200°C	0.5

[a]Gas interrupt mode used. [b]Temperature sensor used. [c]Full scale absorbance setting.

RESULTS AND DISCUSSION

Procedure optimization

Optimization of several parameters was of primary interest in the development of this technique. Sandell [15] reported an optimum pH of 1.0 for the dithizone extraction of copper and a neutral pH for Cd, Ni, and Zn extractions. The effect of pH on extraction efficiency was evaluated by performing extractions on aliquots of a large sea-water sample at different pH values and the results (Fig. 1) were used to determine the optimum value for the above procedure (2.0 ± 0.2 for Cu and 7.7 ± 0.2 for Cd, Ni, and Zn).

The equilibration time of dithizone—chloroform with aliquots of a large sea-water sample was varied to determine the time required for optimum extraction efficiency. Results indicated an optimum equilibration time of 20 min (Fig. 1).

The optimum solvent—water ratio was determined, by using aliquots of a large water sample, by varying the volumes of solvent and water and extracting as described above. The best recoveries for all four metals were obtained with a ratio of 1:10.

Dithizone—chloroform extraction of nickel from sea water was found to have recoveries of approximately 60%. Sandell [15] reported the use of dimethylglyoxime for chelating nickel at a slightly basic pH. The nickel dimethylglyoximate complex is soluble in the dithizone—chloroform solution and its recovery is acceptable.

Interferences

In the absence of a buffer, the extraction of Cd, Ni, and Zn was inconsistent, which was thought to be attributable to shifts in pH during extraction.

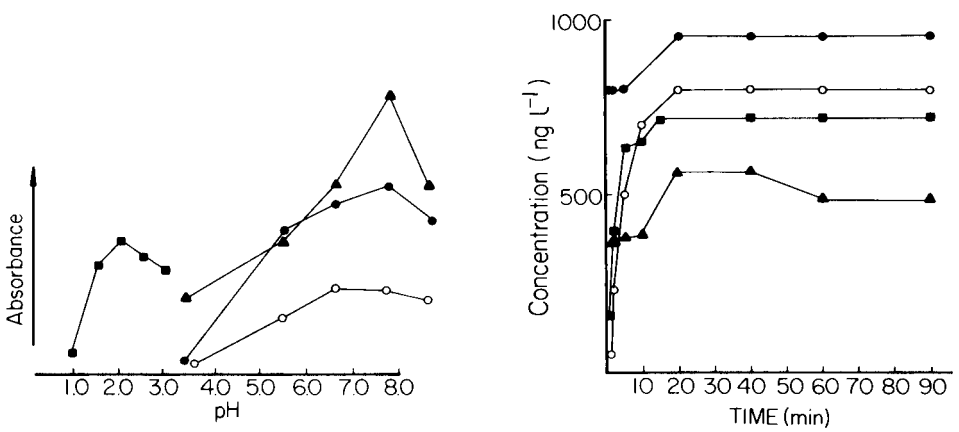

Fig. 1. Optimization of extraction parameters. For the pH study: (○) Zn, (●) Cd, (■) Cu, (▲) Ni. For the extraction time study: (○) Zn × 0.5, (●) Cd × 5, (■) Cu × 2, (▲) Ni. Note that the relative sensitivities of the curves are not comparable.

The determination of sample pH before and after extraction confirmed that pH decreases during extraction. It is obvious from Fig. 1 that a slight shift in sample pH will dramatically influence metal recovery. Maintaining the proper pH throughout extraction was, therefore, accomplished by use of the citrate buffer.

Sea salts carried over during the sample extraction could result in molecular absorption interferences. This was eliminated with the use of a deuterium background corrector. There were no detectable changes in sensitivity arising from the presence of small amounts of sea salt in the extracts.

Contamination considerations

All of the work reported here was performed in a clean-room facility. If a clean room is not available, a laminar-flow clean bench is recommended in order to obtain the lowest possible blanks. Also polyethylene gloves were worn during the sample manipulation steps. Sample exposure to the laboratory air was kept to a minimum. Plastic wrap or teflon was always placed under sample containers, reagent bottles, etc., to prevent possible contamination from the bench. The sample bottles and reagents were covered with plastic bags until used.

Initial copper extractions were done with reagent-grade chloroform. Multiple extractions of a single sea-water sample revealed a considerable amount of copper contamination. Direct furnace injection of the dithizone—chloroform solution indicated that a considerable amount of the copper was present in the chloroform. Attempts to purify the chloroform by distillation as described by Patterson and Settle [17] resulted in the formation of decomposition products such as phosgene that oxidized the dithizone. High-purity chloroform was found to be suitable for use without additional purification.

Contamination is a major concern in the extractions of Cd, Ni, and Zn because of the need for additional reagents for proper extraction. For example, the ammonia solution used to adjust sample pH from about 2.0 to 7.7 contained high concentrations of several metals. High-purity ammonium hydroxide was produced by bubbling ammonia gas into "Q" water in an all-teflon apparatus. Even under these conditions, the resulting ammonia solution occasionally contained a significant concentration of metals. To ascertain the level of contamination, each batch of ammonia solution produced was analyzed prior to use. This was done by evaporating 50 ml of the solution to dryness in a teflon beaker and dissolving the residue with 5.0 ml of 1 M nitric acid. The resulting solution was analyzed by heated graphite furnace-atomic absorption. High-purity ammonium hydroxide is commercially available but should be analyzed, as above, prior to use.

The citrate buffer was also found to be a significant source of contamination unless purified by several extractions with dithizone—chloroform as described by Patterson and Settle [17].

Leaching of metals from laboratory ware is another major contamination problem at the ng l^{-1} levels of the metals studied. Pyrex glassware could not

be adequately cleaned even after using the most rigorous procedures. Therefore, teflon was used exclusively except for the polyethylene vials and the polypropylene tips used for the micro addition of the reagents. Prior to use, all labware was acid-washed by a procedure similar to that described by Patterson and Settle [17]. All new teflon ware was initially soaked in hot concentrated reagent-grade nitric acid for three days. The teflon was then rinsed with "Q" water and filled with hot 0.05% nitric acid (N.B.S.) for three further days. After the dilute nitric acid had been discarded, the teflon was refilled with 0.05% nitric acid and stored in polyethylene bags. A one-day soak in hot concentrated nitric acid followed by three days with the dilute nitric acid was adequate after the initial cleaning. Polyethylene and polypropylene were cleaned in a similar manner.

Establishment of a reagent blank is an important part of any technique. A suitable reagent blank was prepared by re-extracting previously extracted sea water. A pre-extracted sea-water sample was washed with two 10-ml portions of chloroform and the wash discarded. All of the reagents were added to the washed, pre-extracted sample which was then extracted as described above. Replicate blanks for each metal studied were found to be 15 ± 3 ng Cu l^{-1}, <0.4 ng Cd l^{-1}, 160 ± 16 ng Ni l^{-1}, and 90 ± 8 ng Zn l^{-1}.

The method of standard additions eliminates many interferences. However, this requires additional extractions and a reagent blank must also be taken into account.

Precision, recovery, and detection limits

Replicate analyses of aliquots from a large sea-water sample gave relative standard deviations of 8%, 8%, 11%, and 12% for Cd, Cu, Ni, and Zn, respectively (Table 2), at ng l^{-1} concentrations. One sea-water aliquot was spiked to determine the recovery of the extracted metals (Table 2). The spikes were added 16 h before and just prior to extraction. No significant differences in the recoveries were found.

Analytical precision was also evaluated by replicate analysis of separate samples collected from one site. For this purpose a sea-water sample was taken off the Georgia coast (31°48'N, 80°45'W) by drawing through polyethylene tubing with a peristaltic pump. The water was pumped into a 2-l teflon bottle and then into four 250-ml teflon bottles. After return to the laboratory, aliquots from the 2-l homogenized sample were analyzed along with the individually bottled samples. The results (Table 3) demonstrate that the precision of the homogenized sample (B) is significantly better for all metals studied than in the four individually bottled samples (A). The precision of sample (B) is indicative of the analytical precision whereas sample (A) includes uncertainties arising from sample handling and/or inhomogeneity of the sea water itself.

The detection limits for Cu, Ni, and Zn are based on twice the standard deviation of the blanks; that for cadmium is limited by the instrumental detection limit. Accordingly, the detection limits are 6.0, 0.4, 32, and 16 ng l^{-1} for Cu, Cd, Ni, and Zn, respectively.

TABLE 2

Precision and recovery of Cd, Cu, Ni and Zn from sea water

Results of replicate analyses	Concentrations (ng l^{-1})			
	Cd	Cu	Ni	Zn
	18	210	117	292
	16	167	150	381
	14	199	154	378
	14	188	162	434
	14	188	162	378
	14	210	142	375
Mean	15	194	148	373
S.d.[a]	1.7	16	17	46
R.s.d. (%)	8	8	11	12
Recovery of spikes				
Amount added (ng l^{-1})	50	100	500	500
Amount found (ng l^{-1})	67	296	607	920
Recovery (%)	104	102	92	109

[a]Standard deviation and relative standard deviation.

TABLE 3

Variations in precision caused by sampling

Sample[a]	Cu	Cd	Ni	Zn
A	160	22	310	270
	160	13	310	320
	160	12	190	370
	240	12	310	230
Mean	210	15	280	300
R.s.d. (%)	22	32	16	20
B	200	15	240	320
	180	13	240	390
	240	16	190	300
	180	15	260	370
Mean	200	15	230	350
R.s.d. (%)	14	8	13	12

[a]Sample A collected in four separate teflon bottles. Sample B collected in one 2-l teflon bottle.

Fresh water

Fresh water and estuarine samples were also successfully analyzed by this technique. Because of the higher metal concentrations involved, the sample to blank ratios for fresh-water samples are more favorable than those obtained

with sea water. Recovery from spikes was comparable with that found for sea water.

Conclusions

Some of the advantages that this technique offers over others are the small sample sizes required, the absence of lengthy digestion times, and the large number of samples that may be handled per day. Approximately 35-50 samples per day may be extracted for copper by one worker. Slightly fewer analyses per day are convenient for Cd, Ni, and Zn extraction because of the additional time necessary for pH adjustment.

Further work is needed in order to lower the nickel and zinc blanks. Most of nickel and zinc found in the reagent blank can probably be attributed to the chloroform. Attempts to purify the chloroform by sub-boiling distillation resulted in decomposition products which rendered it useless. Future distillations will include the addition of 1% ethanol to preserve the chloroform.

The applicability of this technique for concentrating other metals is being studied and will be reported later.

This work was partially supported by U.S. Department of Energy Grant No. EY-76-S-09-0890.

REFERENCES

1 R. R. Brooks, B. J. Presley and I. R. Kaplan, Talanta, 14 (1967) 809.
2 D. W. Spencer, D. E. Robertson, K. K. Turekian and T. R. Folsom, J. Geophys. Res., 75 (1970) 7688.
3 J. D. Kinrade and J. C. van Loon, Anal. Chem., 46 (1974) 1894.
4 J. P. Riley and D. Taylor, Anal. Chim. Acta, 40 (1968) 479.
5 R. G. Smith, Jr., Anal. Chem., 46 (1974) 607.
6 D. E. Leyden, T. A. Patterson and J. J. Alberts, Anal. Chem., 47 (1975) 733.
7 E. Boyle and J. M. Edmond, Nature, 253 (1975) 107.
8 M. L. Bender and C. L. Gagner, J. Mar. Res., 34 (1976) 327.
9 A. Eaton, Mar. Chem., 4 (1976) 141.
10 L. G. Danielsson, B. Magnusson and S. Westerlund, Anal. Chim. Acta, 98 (1978) 47.
11 K. W. Bruland, R. P. Franks, G. A. Knauer and J. H. Martin, Anal. Chim. Acta, 105 (1979) 233.
12 E. Boyle and J. M. Edmond, Analytical Methods in Oceanography, 1st edn., American Chemical Society, 1975.
13 E. A. Boyle and J. M. Edmond, Anal. Chim. Acta, 91 (1977) 189.
14 F. R. Sclater, E. Boyle and J. M. Edmond, Earth Planet. Sci. Lett., 31 (1976) 119.
15 E. B. Sandell, Colorimetric Metal Analysis, 3rd edn., Interscience, New York, 1965.
16 Participants, Mar. Chem., 2 (1974) 69.
17 C. C. Patterson and D. M. Settle, in P. D. LaFleur (Ed.), Accuracy in Trace Analysis: Sampling, Sample Handling and Analysis, Proceedings of the 7th IMR Symposium, Natl. Bur. Stand. (U.S.) Spec. Publ. 422, 321, 1976.

Analytica Chimica Acta, 113 (1980) 47—53

DETERMINATION OF SILVER AND THALLIUM IN NICKEL-BASE ALLOYS BY ATOMIC ABSORPTION SPECTROMETRY WITH INTRODUCTION OF SOLID SAMPLES INTO AN INDUCTION FURNACE

ADRIAN A. BAKER, JAMES B. HEADRIDGE* and ROY A. NICHOLSON
Department of Chemistry, The University, Sheffield S3 7HF (Gt. Britain)
(Received 30th July 1979)

SUMMARY

Atomic absorption spectrometry with an induction furnace is used for the determination of silver (0.03—12 $\mu g\ g^{-1}$) and thallium (0.004—12 $\mu g\ g^{-1}$) in 1—40-mg samples of nickel-base alloys dropped into the furnace. Calibration graphs of peak absorbance versus mass of element were constructed by use of standardised alloys. The accuracy, precision and limits of detection of the method are described for numerous nickel-base alloys. With alloys containing more than 0.2 μg Ag g^{-1} and 0.4 μg Tl g^{-1}, relative standard deviations are usually $<15\%$ and $<12\%$, respectively. The limits of detection for silver and thallium are 0.014 $\mu g\ g^{-1}$ and 0.004 $\mu g\ g^{-1}$, respectively.

It is well known that elements that have low melting points and low solubility in nickel have deleterious effects on the properties of nickel-base alloys such as hot workability and stress-rupture life [1, 2]. These elements include thallium, tin, lead, arsenic, antimony, bismuth, sulphur, selenium, tellurium, silver, cadmium and zinc [3]. In this paper, methods will be described for the determination of silver and thallium in nickel-base alloys. Stringent specifications stating the maximum concentrations of silver, thallium and other elements in nickel-base alloys have been published [1, 2]. These concentrations are very low and can be less than 1 $\mu g\ g^{-1}$. Refined nickel is the base metal for such alloys and the specification for grade R. 99.95B (BCS 375:1977) states that the concentrations of silver and thallium should not exceed 1 $\mu g\ g^{-1}$ and 0.2 $\mu g\ g^{-1}$, respectively. Ideally, the limits of detection for the analytical methods used to determine these elements should be $\leqslant 0.1\ \mu g\ g^{-1}$ for silver and $\leqslant 0.02\ \mu g\ g^{-1}$ for thallium.

Sensitive methods that have been reported for the determination of silver and thallium in nickel-base alloys are shown in Table 1 along with their limits of detection. For silver, methods I, III, V, VI and VII have the required sensitivity for the analysis of refined nickel. However, methods III and VII are the more attractive because preconcentration steps are time-consuming and could lead to the pick-up of minute traces of silver from reagents. For thallium, only methods III and VIII have limits of detection approaching 0.02 $\mu g\ g^{-1}$ for refined nickel.

TABLE 1

Methods for the determination of silver and thallium in nickel-base alloys

Method	Limit of detection ($\mu g\ g^{-1}$)		Ref.
	Silver	Thallium	
I D.c. arc emission spectrography (preconcentration on CuS)	0.1	1	4
II D.c. arc emission spectrography (preconcentration on MoS_3)	0.2	0.2	5
III Hollow-cathode emission spectrometry	≤ 0.01	~ 0.05	6
IV Spark-source mass spectrometry	0.15	0.15	3
V A.a.s. (ion-exchange preconcentration)	~ 0.001		7
VI A.a.s. after solvent extraction	0.02		8
		0.1	9
VII A.a.s. after alloy dissolution[a]		0.1	10,11
	0.1	0.2	12
	0.005		13
VIII A.a.s. of chips[a]		0.03	14

[a]With graphite furnace atomization.

Headridge and co-workers have already used atomic absorption spectrometry for the determination of bismuth [15], silver [16], lead [17] and antimony [18] in steels and bismuth [19] in nickel-base alloys with the introduction of solid samples into an induction furnace. A similar procedure has been applied to the determination of silver and thallium in nickel-base alloys and is now described.

EXPERIMENTAL

Materials

Analysed nickel-base alloys were supplied by Henry Wiggin and Co. Ltd., the National Physical Laboratory, Rolls-Royce Ltd. (Derby and Filton) and Ross and Catherall, Ltd. Samples for analysis should preferably be millings or turnings so that no more than three pieces need be added to the furnace core at the same time. Millings and turnings should be degreased with a suitable solvent before use.

Apparatus and measurement procedure for a series of solid samples

These were identical to those previously described [15] except that the graphite core and side arms were made from AGTS-grade graphite (British Acheson Electrodes) and the flow rates of the purge and stir gas were as follows: for silver, purge gas 2 l min^{-1}, stir gas 75 ml min^{-1}; for thallium, purge gas 100 ml min^{-1}, stir gas 50 ml min^{-1}. Graphite cores and side arms were baked under vacuum for 12 h at ca. 1800°C before use. Absorbance measurements were made on a Perkin-Elmer 300S atomic absorption spectrometer using a silver (Activion) or thallium (Perkin-Elmer) hollow-cathode

lamp. The masses of samples added to the furnace were determined with a 5-place balance. The experimental conditions for the determinations of silver and thallium are shown in Table 2.

Calibration graphs

For the determination of silver in nickel-base alloys containing 0.25—11 $\mu g\ Ag\ g^{-1}$, calibration graphs of peak absorbance versus amount of silver were obtained by dropping increasing amounts of alloy R 3386 (2.2 $\mu g\ Ag\ g^{-1}$) into the graphite core under conditions capable of producing absorbances up to 1.0. For the nickel-base alloy containing $<0.25\ \mu g\ Ag\ g^{-1}$, the calibration graph was prepared in a similar way with alloy R 6287 (0.25 $\mu g\ Ag\ g^{-1}$), which was standardised against alloy R 3386.

For the determination of thallium in nickel-base alloys containing 0.4—12 $\mu g\ Tl\ g^{-1}$, calibration graphs of peak absorbance versus amount of thallium were obtained by dropping increasing amounts of alloy ST3 (2.2 $\mu g\ Tl\ g^{-1}$) into the graphite core. For the nickel-base alloys containing $<0.6\ \mu g\ Tl\ g^{-1}$, calibration graphs were prepared in a similar way with alloy R 6285 (0.71 $\mu g\ Tl\ g^{-1}$) which was standardised against alloy ST3.

Procedure for the determination of silver and thallium in nickel-base alloys

When a series of nickel-base alloys is to be analysed, suitable masses are dropped into the graphite core over a period of 2—3 h; during the same run but generally at the start of the run, various masses of R 3386 or R 6287 (for silver) or of ST3 or R 6285 (for thallium) are also added for the purpose of constructing a calibration graph. When the run has been completed, the calibration graph is drawn and the mass of silver or thallium in each sample is obtained from the graph. The concentrations of silver or thallium in the samples are then calculated.

TABLE 2

Experimental conditions for the determination of silver and thallium

Concentration range ($\mu g\ g^{-1}$)	Mass range of sample (mg)	Core temp. (°C)	Wavelength (nm)	Slit width (nm)	Scale expansion
Silver					
5—11	0.7—2.5	2300	338.1	0.2	× 1
1—5[a]	1—7	2300—2350	328.1	0.2	× 1
0.25—1	3—12	2350	328.1	0.2	× 1
<0.25	6—12	2300	328.1	0.2	× 5
Thallium					
8—12	2—5	2530	238.0	0.2	× 1
0.6—8	2—20	2400—2530	377.6	0.7	× 1
<0.6	5—40	2450—2540	276.8	0.7	× 4 to × 10

[a]When necessary, damping position 3 can be used with this range to keep the highest absorbances below 1.0. Otherwise damping position 1 is employed. Damping positions 1 and 3 are for time constants of 0.2 and 3 s, respectively.

RESULTS AND DISCUSSION

The calibration graphs for silver were straight lines through the origin over the ranges specified above. Calibration graphs for thallium were straight lines through the origin up to 15 ng of thallium but curved over slightly towards the concentration axis above this mass. From typical graphs the masses of silver producing 1% absorption were calculated as 47 pg and 80 pg at 2300°C using the 328.1 and 338.1-nm resonance lines, respectively. The masses of thallium producing 1% absorption were 41, 118 and 400 pg at 2500°C using the 276.8 377.6 and 238.0-nm resonance lines, respectively. Results for the determination of silver in 17 nickel-base alloys and thallium in 30 such alloys are shown in Tables 3 and 4.

For silver, alloy R 3386 was selected as a reliable standard because it has been stated to contain 2.2 μg Ag g^{-1} when analysed both by hollow-cathode emission spectrometry and by atomic absorption spectrometry with flame atomisation directly on a solution of the alloy [3]. For thallium, alloy ST3 was employed as a standard because it has been reported to contain 2.16 μg Tl g^{-1} when analysed by electrothermal atomic absorption spectrometry on solutions and 2.28 μg Tl g^{-1} by hollow-cathode emission spectrometry. The average value of 2.2 μg Tl g^{-1} was taken for this alloy.

The results for silver are considered to be quite good with satisfactory

TABLE 3

Results for the determination of silver in nickel-base alloys

Alloy	Silver found (μg g^{-1})	No. of samples analysed	Relative standard deviation (%)	Company result (μg g^{-1})
DTA	0.03	5	22	<1.0[a]
R 6287	0.25	6	11	<1.0[a]
ST1	1.0	6	8	0.8[b]
ST2	2.7	6	7	2.7[b]
ST3	1.3	6	10	1.0[b]
DTB	2.1	6	8	1.9[a]
DTC	3.9	5	8	3.7[a]
DTD	5.0	5	9	4.8[a]
R 3385	1.2	6	5	1.2[a]
R 6285	1.2	12	9	1.6[a]
DTE	6.8	16	19	6.7[a]
DTF	11.2	20	13	9.1[a]
R 3387	9.8	5	11	9.8[c], 10[a]
R 3388	5.7	11	17	5.0[a], 5.0[c]
R 6286	10.5	4	14	10[a]
RRF 1	6.6	6	8	7.2[b]
RRF 2	10.9	4	12	9.5[b]

[a]By direct atomic absorption with an air—acetylene flame. [b]By electrothermal atomization of solutions. [c]By hollow-cathode emission.

TABLE 4

Results for the determination of thallium in nickel-base alloys

Alloy	Thallium found ($\mu g\ g^{-1}$)	No. of samples analysed	Relative standard deviation (%)	Company result ($\mu g\ g^{-1}$)
CSA2	0.004	6	14	$<0.5^a$, $<0.2^b$
CSB2	0.008	12	28	$<0.5^a$, $<0.2^b$
CSC2	0.006	6	39	$<0.5^a$, $<0.2^b$
CSD2	0.005	5	12	$<0.5^a$, $<0.2^b$
CSE2	0.005	9	33	$<0.5^a$, $<0.2^b$
CSF2	0.005	11	23	$<0.5^a$, $<0.2^b$
CSG2	0.004	5	44	$<0.5^a$, $<0.2^b$
CSH2	0.005	6	20	$<0.5^a$, $<0.2^b$
CSJ2	0.006	6	11	$<0.5^a$, $<0.2^b$
CSK2	0.013	5	17	$<0.5^a$, $<0.2^b$
CSW2	0.45	12	8	0.6^a
CSZ2	0.037	6	14	$<0.2^a$
R 6285	0.71	12	10	1^e
R 6286	4.0	6	4	10^e
R 3385	0.71	6	3	0.7^c
R 3386	1.4	5	2	1.4^c
R 3387	6.6	6	6	6.6^c
R 3388	3.3	6	5	3.5^c
RRF2	4.5	6	7	4.1^d
TT2	3.6	12	6	5.5^b
CSL2	2.1	6	6	2.5^a, 2.5^b
CSM2	6.2	5	11	6.0^a, 6.0^b
CSN2	3.2	6	11	3.0^a, 3.0^b
CSO2	6.9	6	10	7.0^a, 7.0^b
CSX2	2.4	6	3	2.6^a
ST1	0.79	6	1	0.82^d
ST2	0.70	12	7	0.84^d
TT3	8.5	6	5	11^b
TT4	10.4	6	4	14^b
CSP2	11.8	6	3	12.5^a, 12.0^b

[a]By electrothermal atomization of solutions in a carbon tube furnace. [b]By hollow-cathode emission. [c]By flame atomic absorption after solvent extraction. [d]By electrothermal atomization of solutions in the CRA 63 cup. [e]Nominal value.

agreement between the present results and the company results except for alloy DTF. Relative standard deviations are less than 15% except for alloy DTA which contains very little silver and for alloys DTE and R 3388 which have been analysed more frequently than normal to establish results of reasonable accuracy. There may be a more inhomogeneous distribution of silver in these last two alloys.

From the results for sample DTA in Table 3 the standard deviation is calculated as 0.007 μg Ag g^{-1} and the limit of detection is therefore 0.014 μg Ag g^{-1}. An identical result was obtained when a further nine samples of this alloy were analysed in a separate run. Almost certainly this limit of detection

would have been lower if a sample containing less than 0.03 μg Ag g^{-1} had been available for analysis.

The results for thallium are very satisfactory with good agreement between the present results and the company results except for samples TT2, TT3 and TT4; these were from an early series of nickel-base alloys for whch less accurate company results were available. For thallium concentrations in excess of 0.4 μg g^{-1}, relative standard deviations are less than 12%. The limit of detection being defined as twice the standard deviation for results for alloys containing very low concentrations of thallium was estimated to be 0.004 μg g^{-1} after examination of the results for the nine alloys CSA2 to CSJ2.

These limits of detection for silver and thallium are well below the limits sought as mentioned in the introduction, namely 0.1 μg g^{-1} for silver and 0.02 μg g^{-1} for thallium. Undoubtedly this method of atomic absorption spectrometry with the introduction of solid samples to an induction furnace is among the most sensitive available for the determination of silver and thallium in nickel-base alloys.

In previous studies on the determination of bismuth [15], silver [16] and antimony [18] in steels, it was shown that there was virtually no molecular absorption nor absorbance associated with resonance-light scatter from relatively high concentrations of volatile minor elements such as manganese. Therefore there was no need for the use of a background corrector. In this study, light of band width 0.2 nm from a deuterium lamp at the wavelengths 328.1 and 338.1 nm for silver and 238.0, 276.8 and 377.6 nm for thallium (i.e. the resonance lines of silver and thallium) was used to check for background absorption when nickel-base alloys were added to the induction furnace at the appropriate temperatures. In no instance was an absorbance in excess of 0.01 detected.

We are indebted to the Science Research Council for Studentships (for A. A. B. and R. A. N.) and to Materials Quality Assurance Directorate, Woolwich, for assistance with materials; to the British Steel Corporation for the gift of the Perkin-Elmer 300S atomic absorption spectrometer; to Mr. K. Thornton of Henry Wiggin & Co. Ltd., Mr. R. A. Mostyn of M.Q.A.D., Mr. R. D. Evans of Rolls-Royce Ltd., (Derby), Mr. J. Drinkwater of Rolls-Royce Ltd. (Filton), Mr. D. J. Allan of Ross and Catherall Ltd. and Dr. E. J. McLauchlan of the National Physical Laboratory for analysed samples and very useful information.

REFERENCES

1 G. Mayer and C. A. Clark, Metall. Mater. Technol., (1974) 491.
2 R. T. Holt and W. Wallace, Int. Metals Rev., 21 (1976) 1.
3 K. M. Bills, Proceedings of the 30th Chemists' Conference, British Steel Corporation, 1977, p. 101.
4 B. E. Balfour, D. Jukes and K. Thornton, Appl. Spectrosc., 20 (1966) 168.

5 G. S. Golden and M. G. Atwell, Appl. Spectrosc., 24 (1970) 514.
6 K. Thornton, Analyst, 94 (1969) 958.
7 M. Kirk, E. G. Perry and J. M. Arnitt, Anal. Chim. Acta, 80 (1975) 163.
8 K. E. Burke, Talanta, 21 (1974) 417.
9 K. E. Burke, Appl. Spectrosc., 28 (1974) 234.
10 G. G. Welcher, O. H. Kreige and J. Y. Marks, Anal. Chem., 46 (1974) 1227.
11 J. Y. Marks, G. G. Welcher and R. J. Spellman, Progr. Anal. Chem., 8 (1976) 1.
12 T. R. Dulski and R. R. Bixler, Anal. Chim. Acta, 91 (1977) 199.
13 O. Kujirai, T. Kobayashi and E. Sudo, Trans. Jpn. Inst. Met., 19 (1978) 159.
14 J. Y. Marks, G. G. Welcher and R. J. Spellman, Appl. Spectrosc., 31 (1977) 9.
15 D. G. Andrews and J. B. Headridge, Analyst, 102 (1977) 436.
16 A. M. Aziz-Alrahman and J. B. Headridge, Talanta, 25 (1978) 413.
17 D. G. Andrews, A. M. Aziz-Alrahman and J. B. Headridge, Analyst, 103 (1978) 909.
18 A. M. Aziz-Alrahman and J. B. Headridge, Analyst, in press.
19 J. B. Headridge and R. Thompson, Anal. Chim. Acta, 102 (1978) 33.

Analytica Chimica Acta, 113 (1980) 55—66

IMPEDANCE CHARACTERIZATION OF ANODIZED SILVER/SILVER CHLORIDE ELECTRODES

RATHBUN K. RHODES and RICHARD P. BUCK*

William Rand Kenan, Jr. Laboratories of Chemistry, University of North Carolina, Chapel Hill, North Carolina 27514 (U.S.A.)

(Received 14th August 1979)

SUMMARY

Impedance measurements were made on anodized silver chloride layers on silver electrodes at 293—305 K. Thicknesses calculated from coulometry ranged from 6×10^{-5} cm to 3.6×10^{-4} cm. Results characterized the macroscopic transport properties from 56.2 kHz to 0.0178 Hz. Bulk film specific conductivities increased to a level value of 6×10^{-6} S cm^{-1} with increased thickness, and they varied with solution composition: a minimum value in 10^{-3} M $AgNO_3$ and maxima in 10^{-1} M KCl and 10^{-1} M $AgNO_3$. Activation energies indicated interstitial conduction in high contacting silver solutions and vacancy conduction in high contacting chloride solutions. For the thicker electrodes, a second process, probably grain boundary constriction impedances, is resolvable between 56.2 kHz and 316 Hz. At lower frequencies still, from 100 Hz to 0.316 Hz, effects of external solution diffusion are seen in dilute solutions of silver and chloride. Values for the absolute impedances and the frequency character are extremely close to theoretical predictions. At the lowest frequencies measured an additional impedance process occurs. For the thinnest electrodes the arc is semi-circular and may indicate a kinetic process or kinetics—diffusion coupling. For the thickest electrodes this arc appears like a semi-infinite diffusion process. The magnitude of this effect qualitatively explains the increased time responses of electrodes in the most dilute solutions.

Experimental studies of single crystal and thin film vacuum-deposited silver halides indicate the formation of diffuse space charge and surface charge layers when halides contact electronic or ionic conductors [1—3]. Diffuse space charge arises from mobile defect species, primarily interstitial Ag_i^+ and vacancies Ag_V^- already present in the crystal. Compensating charge resides on the metal electrode, or in diffuse electrolyte space charge layers near the surface and ions adsorbed on the surface. Dynamic theories of transport at these interfaces are stated in Macdonald's extensive theoretical studies [4, 5].

At zero net current with ionic solution contacts, ion-exchange processes result in uptake or loss of a sufficient number of silver interstitials or vacancies to affect experimental bulk conductances for thin (10^{-2}—10^{-3} cm) crystals of silver bromide and silver chloride [6, 7]. When layer thickness is reduced ever more (10^{-4}—10^{-5} cm), as for evaporated films, microcrystals suspended in gelatin, and anodized films on silver metal, conductivity

enhancements of 100—1000 occur [8—10]. For dislocation-free evaporated films this increase is thought to occur because a greater fraction of the total thickness is the space charge layer where interstitial accumulation occurs. However, in the case of anodized films, in which the preparation method forms less homogeneous layers, this enhancement effect may be due to preferential parallel conduction modes along grain boundaries, strains and dislocations, or channels of electrolyte [11].

This inhomogeneity may also be expected to add variability to the kinetic and diffusive impedance characteristics of these electrodes. Indeed, the electrical characterization of these electrodes is more complex than that required for thick single crystals or silver-contacted evaporated films. However, because of their relative ease of preparation and improved cost factors, anodized films on metal are more practical ion-selective halide sensors than crystals or pressed pellets and are even used for one-shot disposable applications [12].

Determination of the processes responsible for these electrodes' time responses is then important. Three-electrode rotating disk impedance measurements are among the better ways to obtain this information. They allow removal of reference electrode impedance from total impedance and reduce solution diffusion impedance to an exact form. This procedure improves resolution of the remaining electrode processes, which may be separated according to their respective time constants and equivalent resistance magnitudes [13].

EXPERIMENTAL

Chemicals and electrodes

The silver used for preparing electrodes was −100-mesh powder of 99.99% purity (Alpha Research Chemicals). The $AgNO_3$, KCl and KNO_3 (Fisher Scientific A.C.S. grade) for preparing standard solutions were used without further purification. The distilled water had a resistivity greater than 12 MΩ cm and the nitrogen was of electrochemical grade.

Silver electrodes (1.3 cm diameter, 0.15 cm thick) were prepared by pressing 1.5 g of silver powder at 75,000 psi for 10 min in a standard KBr die. The electrodes were then epoxy-sealed into precut teflon bodies and polished with 180 × sandpaper and finer materials including 1-μm diamond compound. This process gave a smooth, continuous surface across the face of the electrode and electrode body. The electrode body was threaded from the top to allow ohmic contact to the shaft of a Beckman rotating electrode. A carbon wiper on a copper contact provided electrical continuity from the shaft to the electrochemical instrumentation.

Procedures

In the rotating disk configuration (rotation rates of 0 and 36 r.p.s. using a Pt gauze counter electrode) the silver electrodes were first cathodized

in 10^{-1} M KCl at a constant current density of 3.9 mA cm^{-2} for 1 min. After open circuit for 30 s in the same solution, anodized silver chloride layers of 0.6—3.6 × 10^{-4} cm thickness were prepared by passing the reverse constant current for 1—6 min. Thicknesses were calculated from density and coulometric considerations and should be accurate to within ±5%. The cathodization pretreatment and controlled electrode rotation rate provided a visibly more even surface coverage than uncathodized electrodes or unstirred solutions.

The potentiometric responses of these electrodes versus an Orion double-junction reference electrode were verified by concentration step experiments in solutions of incremental pCl and pAg from 5 to 1. When necessary, sufficient KNO_3 was added to maintain ionic strengths of 10^{-1} M. Slopes of the electrodes ranged from 53 mV (thinnest layers) to 57 mV (thickest layers) per decade change in Cl^- and Ag^+ activities over the linear region of the response curve. Electrode reproducibility was about ±1 mV over three calibration runs, and time responses were in the range from 30 s at highest activities to 5 min at the limit of detection.

Once equilibrium potentiometric behavior of the electrodes had been established, impedance measurements were made. The bridge operated on the same principles described previously [14]. The measurements were made in the three-electrode mode at the equilibrium solution potential with a working electrode rotation rate of 36 r.p.s. The a.c. excitation was less than 5 mV peak to peak. The auxiliary electrode was a 4-cm^2 silver flag anodized to AgCl and positioned 2.5 cm below the working electrode. The reference electrode was a 0.1-cm diameter silver billet anodized to AgCl and positioned 0.2 cm below the working electrode. Solution volumes were 100 ml and temperature 20.0 ± 0.1°C unless otherwise specified.

To calculate majority carrier transport activation energies, bulk conductivities were measured in 10^{-1} M KCl and 10^{-1} M $AgNO_3$ as a function of temperature. To investigate interfacial kinetics, solution diffusion, and internal crystal diffusion effects, solution variation experiments were performed. The electrodes were initially equilibrated in 10^{-4} M solutions of KCl or $AgNO_3$ (ionic strength 0.1 M) for 30 min. After measurement of the electrode impedance, the test solution was spiked with an aliquot of the stock solution (from a syringe) which incremented the volume-corrected activity by a factor of ten. The electrode was then allowed to re-equilibrate for 30 min, the impedance remeasured and the process repeated through 10^{-1} M KCl and 10^{-1} M $AgNO_3$ test solutions for electrodes of all layer thicknesses.

Solution resistances were calculated by varying the distance of the reference electrode from the working electrode and noting the change in impedance. Instrumental contact resistances were found to be 8—10 ohms with a Keithley 160 digital multimeter. In both cases, background was subtracted to give the true electrode impedance. Nitrogen degassing was found not to change the impedance characteristics. Frequency was

systematically varied from 56.2 kHz to 0.0178 Hz at quarter-decade intervals on a log frequency scale. The admittance data obtained were converted through the usual transforms to impedances and all plotting and data regressions were done on an IBM 360 computer.

RESULTS

Bulk specific conductivities of anodized silver chloride layers

Typical impedance plane plots for anodized electrodes in 10^{-1} M KCl are shown in Fig. 1. Increase in electrode thickness is accompanied by an increase in the high-frequency intercept. This result indicates that bulk film resistances can be attributed to this intercept impedance (corrected for solution and contact resistances), although the shift is less than expected from calculations using film thickness and a thickness-independent constant, specific conductivity. Solution composition change also causes a variation in the intercept resistance for all layer thicknesses. This effect may be attributed partly to the change in solution resistance in the pores of the anodic film and partly to changing composition of charge carriers in the film. The blank-corrected specific conductivities for these electrodes as a function of layer thickness are still dependent on solution composition as shown in Table 1. From purely geometric considerations for capacitance and the

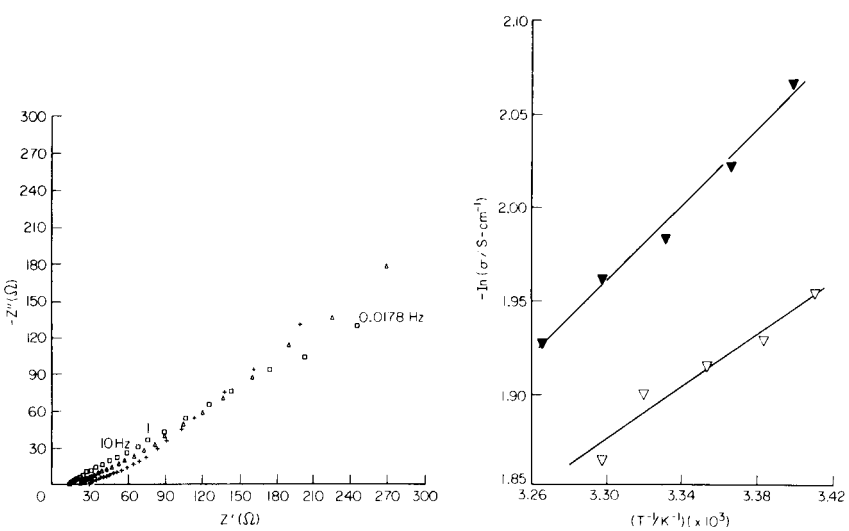

Fig. 1. Impedance plane plots of anodized silver/silver chloride electrodes in 10^{-1} M KCl. Electrode thicknesses of (□) 6×10^{-5} cm, (△) 1.2×10^{-4} cm and (+) 2.4×10^{-4} cm.

Fig. 2. Linear least-squares plot of log σ versus T^{-1} in (▼) 10^{-1} M KCl and (▽) 10^{-1} M $AgNO_3$ for electrode 3.6×10^{-4} cm thick.

TABLE 1

Bulk film specific conductances (in S cm^{-1})[a]

Solution		1u	1s	2u	2s	3s	4s
Salt	(M)	(× 10^{-6})	(× 10^{-6})	(× 10^{-6})	(× 10^{-6})	(× 10^{-6})	(× 10^{-6})
$AgNO_3$	10^{-1}	1.43	—	2.53	3.69	4.82	3.89
	10^{-2}	1.45	—	2.29	3.13	3.97	3.25
	10^{-3}	1.38	—	1.31	2.83	3.89	3.97
	10^{-4}	1.39	—	1.65	2.95	4.13	4.38
KCl	10^{-4}	0.98	1.72	1.83	3.15	4.75	5.21
	10^{-3}	1.39	1.58	1.97	3.20	4.83	5.21
	10^{-2}	1.81	1.80	2.86	3.55	5.01	5.18
	10^{-1}	2.15	2.99	3.07	4.94	6.97	5.51

[a]u, Electrode anodized in unstirred solution; s, electrode anodized in stirred solution; 1, thickness 6 × 10^{-5} cm; 2, thickness 1.2 × 10^{-4} cm; 3, thickness 2.4 × 10^{-4} cm; 4, thickness 3.6 × 10^{-4} cm.

observed specific conductances, bulk electric time constants are calculated to range from 0.4 to 1.6 μs. The peak quadrature impedance for this process then lies in the range from 580 kHz to 135 kHz which is above the high-frequency limit of the bridge used.

With increased layer thickness, the specific conductivity in 10^{-1} M KCl increases from 3 × 10^{-6} S cm^{-1} at 6 × 10^{-5} cm to a maximum value of 7 × 10^{-6} S cm^{-1} at 2.4 × 10^{-4} cm and then becomes constant at a value of 6 × 10^{-6} S cm^{-1} for thicknesses of 3.6 × 10^{-4} cm and above. Specific conductivities are also solution-dependent. They pass through a minimum in 10^{-3} M $AgNO_3$ and reach maximum end-point values in 10^{-1} M KCl and 10^{-1} M $AgNO_3$. This trend is apparent for all electrodes regardless of preparation. However values are a factor of 1.5—2 less for layers formed in unstirred solutions or on uncathodized electrodes, possibly because of less even surface coverage. This trend for solution-dependent specific conductivities is similar to that observed for very thin vacancy-doped silver halide crystals [6]. Activation energies of transport are calculated from linear least-squares plots of log σ vs. $1/T$ (Fig. 2) and are found to be 0.20 eV in KCl and 0.15 eV in $AgNO_3$. Thick crystal transport activation energies are listed as 0.16 eV for interstitials and 0.29 eV for vacancies [15]. This result suggests ionic transport mainly in the film and relatively little grain boundary or channel transport.

Impedances related to grain boundary properties

As demonstrated by impedance plane plots for thick electrodes in 10^{-3} M $AgNO_3$ (Fig. 3), a second process is sometimes resolvable in the frequency range between 56.2 and 316 Hz. The parameters attributable to this process are listed in Table 2 as a function of electrode thickness, solution composition and temperature. Measured resistances increase with thickness

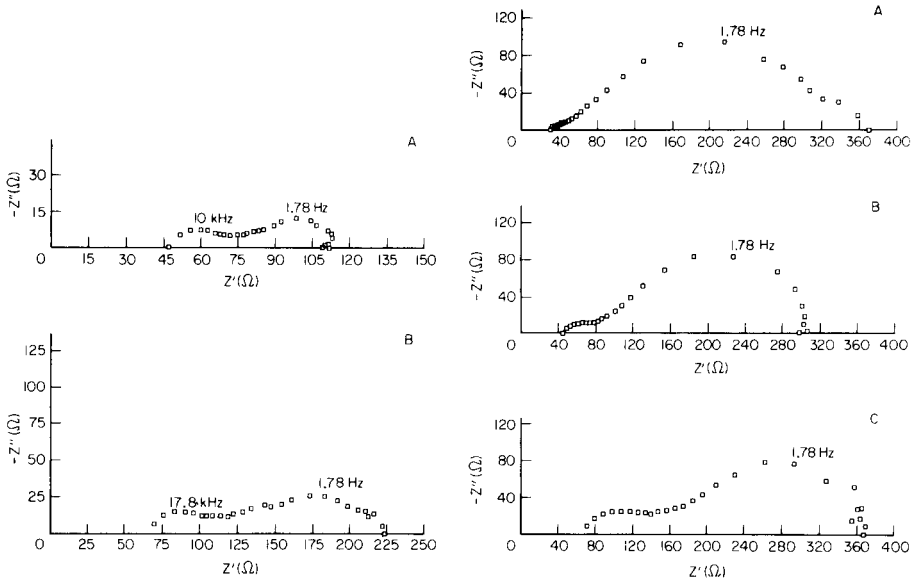

Fig. 3. Impedance plane plots demonstrating grain boundary impedances for anodized silver/silver chloride in 10^{-3} M $AgNO_3$. Lowest-frequency infinite diffusion process has been background-subtracted. (A) Thickness 2.4 × 10^{-4} cm; (B) thickness 3.6 × 10^{-4} cm.

Fig. 4. Impedance plane plots demonstrating solution diffusional impedances for anodized electrodes in 10^{-4} M $AgNO_3$. Lowest-frequency infinite diffusion process has been background-subtracted. Thicknesses: (A) 1.2 × 10^{-4} cm; (B) 2.4 × 10^{-4} cm; (C) 3.6 × 10^{-4} cm.

(although less than geometric considerations would predict) and with decrease in solution concentrations of Ag^+ and Cl^-. Resistances are lower in chloride than silver solutions while apparent capacitances are much higher. Consequently, peak quadrature impedances occur from 10 to 17 kHz in silver solution at high activity and from 1 to 5 kHz in chloride solution at high activity. This result again implies a change in the majority charge carrier as a function of solution composition. Since higher carrier concentrations result in higher capacitances, this observation implies vacancy conduction for contacting chloride solutions and interstitial conduction for contacting silver solutions. A linear least-squares plot of log R vs. $1/T$ gives an activation energy of 0.64 eV in 10^{-1} M $AgNO_3$. This quantity could not be determined in 10^{-1} M KCl because of the greater uncertainty in the small values of R. The increased activation energy over bulk transport activation energies indicates a kinetic process, most likely owing to charge/discharge at internal grain boundaries. This type of behavior has been observed before in sintered ceramics and pressed solid electrolytes [16].

TABLE 2

Grain boundary impedance characteristics

Electrode	Solution		Z_{gb} (Ω)[a]	C_{gb} (10^{-8} F)[b]	f_{max} (kHz)	α	T (°C)
	Salt	(M)					
3	KCl	10^{-1}	16.0	110.0	0.316	0.77	20.0
		10^{-2}	19.0	72.0	0.562	0.83	20.0
		10^{-3}	25.0	81.0	0.562	0.75	20.0
		10^{-4}	27.0	29.0	1.00	0.83	20.0
	$AgNO_3$	10^{-1}	15.4	1.8	10.0	0.79	20.0
		10^{-2}	17.6	1.2	17.8	0.82	20.0
		10^{-3}	25.6	2.4	10.0	0.80	20.0
		10^{-4}	42.0	9.5	3.16	0.82	20.0
4	KCl	10^{-4}	32.0	3.6	5.62	0.71	20.0
	$AgNO_3$	10^{-1}	32.8	1.5	17.8	0.85	20.0
		10^{-2}	47.3	1.3	17.8	0.82	20.0
		10^{-3}	50.0	2.5	10.0	0.88	20.0
		10^{-4}	58.0	4.5	5.62	0.89	20.0
		10^{-1}	23.4	1.1	17.8	0.85	22.3
		10^{-1}	16.2	0.9	17.8	0.85	25.0
		10^{-1}	12.5	0.8	17.8	0.83	28.0
		10^{-1}	11.8	0.7	17.8	0.83	30.0

[a] Z_{gb} = grain boundary resistance. [b] C_{gb} = grain boundary capacitance at f_{max}.

Impedances related to solution diffusional properties

From theoretical considerations, a finite Warburg diffusional impedance has the form [17]

$$Z = (\bar{\sigma}/\omega^{1/2})\ (1 - j)\ \tanh\ (\delta_N(j\omega/D_0)^{1/2}) \quad (1)$$

where j is $(-1)^{1/2}$, ω is the angular frequency of the test sine wave, $\bar{\sigma}$ is the Warburg coefficient, D_0 is the electroactive ion diffusion coefficient in $cm^2\ s^{-1}$ and δ_N is the diffusion layer thickness in cm. In rotating disk hydrodynamics, δ_N is further defined by

$$\delta_N = 1.61\ D_0^{1/3}\ \nu^{1/6}\ \bar{\Omega}^{-1/2} \quad (2)$$

where j is the kinematic viscosity in $cm^2\ s^{-1}$ and $\bar{\Omega}$ is the electrode rotation rate in rad s^{-1}. Using experimental values for $\bar{\Omega}$ and ω and literature values for ν, D_{Ag^+} and D_{Cl^-} [18, 19] eqns. (1) and (2) predict peak quadrature impedances, which are independent of solution activity, at 5 Hz in chloride solution and 4 Hz in silver solution. Experimental values for magnitudes and frequencies of this point are listed in Table 3 as a function of electrode thickness. There is a small but constant experimental shift of peak f to lower frequencies (3 Hz in chloride and 2.5 Hz in silver) which may indicate slightly lower than literature values for ν, D_{Ag^+} or D_{Cl^-}. The impedance magnitudes are higher than theory and decrease with electrode

TABLE 3

Solution diffusional impedance characteristics

Electrode	Solution		Z' (Ω)[a]	$-Z''$ (Ω)[b]	f_{max} (Hz)	Z_{DC} (Ω)
	Salt	M				
Theory	KCl	10^{-4}	66.5	55.7	5.62	137.2
2			96.0	75.6	3.16	180
3			72.0	59.4	3.16	145
Theory	$AgNO_3$	10^{-4}	109	64.7	3.16	159.9
2			160	94.9	1.78	226
3			140	82.3	1.78	202
4			147	75.1	1.78	186

[a] Z' = real impedance at f_{max}. [b] $-Z''$ = quadrature impedance at f_{max}.

thickness. This result may indicate a depletion of bulk solute by ion-exchange within the electrode. Representative examples of these solution diffusional impedances are shown in Fig. 4.

Residual low-frequency impedances corresponding to processes slower than solution diffusion

At frequencies below that where resolution of finite solution diffusion ends (~0.316 Hz), there remains an additional impedance process (Fig. 5). The exact nature of this process is undetermined. For the thickest electrodes of the most uniform coverage, the quadrature impedance at the lowest measuring frequency is less than 100 ohms and relatively independent of solution concentration. However, with thinner electrodes this magnitude increases and is much larger in chloride than silver solution. With the thinnest electrodes prepared from unstirred solutions, this residual impedance is 800—3000 ohms which is so large as to obscure resolution of all but the

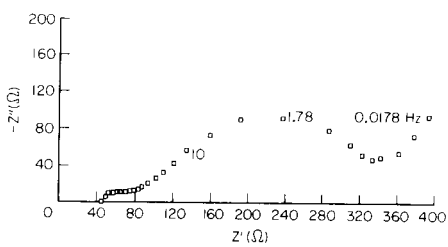

Fig. 5. Impedance plane plot of 2.4×10^{-4} cm thick anodized silver/silver chloride electrode in 10^{-4} M $AgNO_3$.

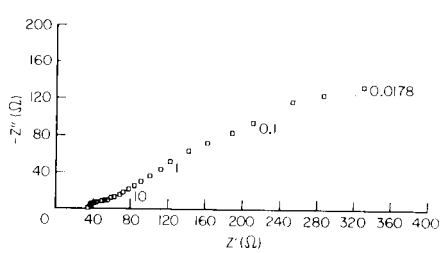

Fig. 6. Impedance plane plot of 1.2×10^{-4} cm thick anodized silver/silver chloride electrode in 10^{-1} M $AgNO_3$.

TABLE 4

Lowest-frequency impedance characterization

Electrode	Solution		ZQ_m[a]	Electrode	Solution		ZQ_m[a]
	Salt	(M)			Salt	(M)	
2u	$AgNO_3$	10^{-1}	132	3s	$AgNO_3$	10^{-1}	67
		10^{-2}	355			10^{-2}	73
		10^{-3}	391			10^{-3}	70
		10^{-4}	453			10^{-4}	87
	KCl	10^{-1}	1890		KCl	10^{-1}	128
		10^{-2}	534			10^{-2}	183
		10^{-3}	925			10^{-3}	237
		10^{-4}	407			10^{-4}	188
2s	$AgNO_3$	10^{-1}	131	4s	$AgNO_3$	10^{-1}	76
		10^{-2}	135			10^{-2}	75
		10^{-3}	142			10^{-3}	88
		10^{-4}	194			10^{-4}	81
	KCl	10^{-1}	176		KCl	10^{-1}	59
		10^{-2}	290			10^{-2}	69
		10^{-3}	459			10^{-3}	79
		10^{-4}	672			10^{-4}	119

[a] ZQ_m = quadrature impedance at 0.0178 Hz.

highest-frequency data points. Trends as a function of electrode thickness and preparation and solution composition are presented in Table 4. For the thinnest electrodes the shape of the impedance plane plots is semicircular (Fig. 6) at the lowest frequency. This result is indicative of a kinetic or kinetic—diffusional process. The plots for the thicker electrodes (Fig. 7) approach a 45° line at lowest frequencies. The process is assumed to be an infinite diffusional impedance which can be extrapolated as a function of frequency and subtracted out to provide resolution of the previously described impedances.

DISCUSSION

The conductivity of silver chloride is known to be the parallel summation of the conductivities due to the concentrations and mobilities of silver ion interstitials and vacancies. These concentrations can be varied by impurity doping, contacting solution composition and bulk size. The solution contact effect is only resolvable for very thin electrodes with thicknesses comparable to or smaller than the Debye thickness. The present results show a minimum specific conductivity at a pAg of 3 indicating that the anodized electrodes are vacancy-doped when formed, as expected by the prevalence of traces of divalent impurities (sub ppm) in salt solutions. However the value of the transport activation energy in 10^{-1} M $AgNO_3$ implies the conversion of the majority carrier to interstitials by charge injection at high silver ion activities.

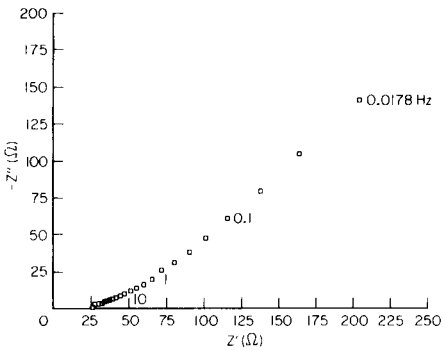

Fig. 7. Impedance plane plot of 2.4×10^{-4} cm thick anodized silver/silver chloride electrode in 10^{-1} M $AgNO_3$.

That the electrode undergoes a change in conduction mechanism as a function of solution composition explains the magnitudes and trends observed for bulk film resistances, grain boundary discharge resistances and solution diffusional impedances. These processes can be better visualized by the equivalent circuit model of Fig. 8. Essentially the measured resistances are composite resistances of the processes due to parallel interstitial and vacancy conduction. This interpretation explains why absolute impedances of all processes maximize in solutions near the p.z.c. and obtain local minima in 10^{-1} M $AgNO_3$ and 10^{-1} M KCl. Since vacancy concentrations are greater than interstitials, grain boundary impedances are lower in chloride solutions where vacancy conduction predominates.

The appearance of a process at frequencies lower than that for solution diffusion was unexpected. Since both vacancies and interstitials are unblocked at the electrode/solution interface, an internal diffusional process similar to that seen for silver sulfide should not occur [20]. In addition, a kinetic process at the Ag/AgCl interface does not seem likely and would not be dependent on thickness or solution composition. The only conclusion is that the process might be caused by diffusion/adsorption kinetics of solution with the base metal electrode. That the effect is greatest for the thinner electrodes and lowest concentrations make this qualitatively plausible. However, the complexity of this interaction makes quantitation impossible.

Conclusions

Bulk specific conductivities of anodized silver chloride electrodes are dependent on thickness and on the solution present. These values increase with thickness to a level value of 6×10^{-6} s cm^{-1} at 3.6×10^{-4} cm. Local maxima were observed in 10^{-1} M KCl and 10^{-1} $AgNO_3$ and the minimum in 10^{-3} M $AgNO_3$. Activation energies indicate interstitial conduction in

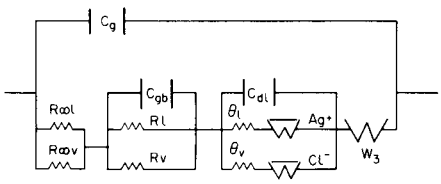

Fig. 8. Equivalent circuit model for anodized silver/silver chloride electrodes. The subscripts i and v refer to values from the interstitial and vacancy conduction, respectively. R_∞ = bulk film resistances, R = grain boundary resistances, θ = ion transfer resistances, W = solution diffusion impedances of either silver or chloride, C_g = bulk film capacitance, C_{gb} = grain boundary capacitances, C_{dl} = double layer capacitance, W_3 = unknown residual low-frequency impedance.

solutions of high silver activity and vacancy conduction in solutions of high chloride activity. At intermediate frequencies (56.2 kHz to 316 Hz) a process related to grain boundaries was discovered. Time constants of 30—150 μs in solutions of high chloride activity and 10—20 μs in those of high silver activity were found. The semicircle was also slightly sunken with a Cole—Cole alpha [21, 22] of 0.85 ± 0.04 in silver and 0.80 ± 0.05 in chloride. This result indicates a distribution of time constants for the process.

At lower frequencies still, finite solution-diffusional properties were resolved for either silver or chloride ions in dilute solutions. Since these are parallel processes the more concentrated solution species dominates the magnitude of this process. At the lowest frequency range measured, a residual impedance process was found which is believed to be associated with diffusion/adsorption kinetics of electrolyte in channels with the silver electrode.

This work was supported by National Science Foundation Grant CHE 77-20491.

REFERENCES

1 S. Danyluk and J. M. Blakely, Surf. Sci., 41 (1974) 359.
2 R. C. Baetzold and J. F. Hamilton, Surf. Sci., 33 (1972) 461.
3 E. P. Honig and J. H. Th. Hengst, J. Colloid Interface Sci., 31 (1969) 545.
4 J. R. Macdonald, J. Chem. Phys., 61 (1974) 3977.
5 J. R. Macdonald, J. Appl. Phys., 45 (1974) 73.
6 R. Matejec, Photogr. Sci. Eng., 7 (1963) 123.
7 C. A. Steidel, H. A. Hoyen, Jr. and Che-Yu Li, Materials Sci. Res., 4 (1969) 475.
8 R. C. Baetzold, J. Phys. Chem. Solids, 35 (1974) 89.
9 H. A. Hoyen, Jr., J. Appl. Phys., 47 (1976) 3784.
10 H. Lal, H. R. Thirsk and W. F. K. Wynne-Jones, Trans. Faraday Soc., 47 (1951) 70.
11 T. Katan, S. Szpak and D. N. Bennion, J. Electrochem. Soc., 120 (1973) 883.
12 H. G. Curme, Abstract 262, Clin. Chem., 25 (1979) 1115.
13 R. P. Buck, Electroanalytical Chemistry of Membranes, CRC Review 5, CRC Press, 1975, p. 323.

14 D. E. Mathis and R. P. Buck, Anal. Chem., 48 (1976) 2033.
15 J. Corish and P. W. M. Jacobs, J. Phys. Chem. Solids, 33 (1972) 1799.
16 M. L. Bayard and G. G. Barna, J. Electroanal. Chem., 91 (1978) 201.
17 R. D. Armstrong, T. Dickinson and M. Reid, Electrochim. Acta, 21 (1976) 935.
18 CRC Handbook of Chemistry and Physics, 49th edn., CRC Press, Cleveland, 1969.
19 R. N. Adams, Electrochemistry at Solid Electrodes, M. Dekker, New York, 1969, p. 219.
20 R. K. Rhodes and R. P. Buck, Anal. Chim. Acta, 110 (1979) 185.
21 K. S. Cole and R. H. Cole, J. Chem. Phys., 9 (1941) 341.
22 R. Fuoss and J. G. Kirkwood, J. Am. Chem. Soc., 63 (1941) 385.

Analytica Chimica, Acta, 113 (1980) 67—78

COMPETITIVE ION-EXCHANGE EVALUATION OF THE BROMIDE INTERFERENCE ON ANODIZED SILVER/SILVER CHLORIDE ELECTRODES

RATHBUN K. RHODES and RICHARD P. BUCK*

William Rand Kenan, Jr. Laboratories of Chemistry, University of North Carolina, Chapel Hill, North Carolina 27514 (U.S.A.)

(Received 14th August 1979)

SUMMARY

The bromide interference on rotating anodized silver/silver chloride electrodes of different thicknesses is investigated by potentiometric monitoring of mixed bromide/chloride solution activity steps. Potential—time transients consist of four distinct regions which are related to different stages in the process of surface coverage by silver bromide. The bromide depletion in solution is monitored so that chloride activity, and the total amounts of AgCl and AgBr can be calculated by assuming the stoichiometric metathesis reaction $AgCl + Br^- \rightleftharpoons AgBr + Cl^-$. Selectivity coefficients vary with surface coverage and time. Thin electrodes quickly reach the upper limiting value of 450, the approximate ratio of the solubility products, while thick electrodes with mixed precipitates retain a selectivity coefficient of about 10 in bromide activities less than 10^{-3} M. Bromide surface coverage of the anodized electrodes is best modeled by a mixed rather than a constant surface potential. The resultant "rate constant" of the forward reaction in the plateau region averages $5.18 \pm 0.80 \times 10^{-4}$ s^{-1}. The reverse reaction is at least 200 times slower. Impedance measurements verify the ion-exchange mechanism and the degree of electrode interconversion.

Ion-selective electrodes are well known to be imperfectly selective in their response to primary ions. In general, the Nicolsky equation

$$E = E^0 + (RT\,F^{-1}) \ln [a_i^{1/z_i} + (\Sigma\, K_{i,j}^{pot}\, a_j^{1/z_j})] \quad (1)$$

may be used empirically to express the steady-state potential response of the electrode to a primary ion and any number of interfering ions [1—3]. For precipitate-based electrodes, early theoretical models for interpreting these interference effects were based on the assumption that the interfering ions are not mobile in the membrane phase and that the selectivity coefficients, K_{ij}^{pot}, are defined by the ratio of the equilibrium solubility products of the salts [4]. However, variability in the selectivity coefficients for bromide on silver iodide [5], bromide on silver chloride [6—8], and hydroxide on lanthanum fluoride [7, 8] have been reported. These differences have been attributed to non-equilibrium diffusional processes of the solution in the vicinity of the membrane, to variability of electrode standard potential with porous surface coverings, and to differing surface coverages of tightly bound primary and interfering salts [5—8].

To obtain a better experimental description of these phenomena, anodized electrodes of limited ion-exchange capacity were used in potentiometric monitoring of dilute bromide/chloride solutions to observe and deduce properties of the ion-exchange kinetics for the metathesis reaction

$$AgCl + Br^- \rightleftharpoons AgBr + Cl^- \quad (2)$$

Questions related to mixed salt surface coverages, degree of electrode conversion, and kinetic parameters as a function of halide activities and electrode thickness are discussed.

EXPERIMENTAL

Chemicals and electrodes

The silver used for preparing electrodes was −100 mesh powder of 99.99% purity (Alpha Research Chemicals). The KNO_3, KCl and KBr (Fisher Scientific A.C.S. grade) for preparing standard solutions were used without further purification. Water was doubly distilled and passed through ion-exchange columns and its purity was verified by obtaining a resistivity of 12 MΩ cm or greater. Halide concentrations were monitored potentiometrically using standard Orion Ag_2S/AgCl and Ag_2S/AgBr electrodes versus an Orion double-junction reference with a Beckman expanded-scale pH meter.

Silver electrodes were prepared by pressing 1.5 g of silver powder at 75,000 psi for 10 min in a standard KBr die. These were then epoxy-sealed into precut teflon bodies and polished with 1-μm diamond compound to give a smooth continuous surface across the face of the electrode body. The body was threaded from the top to allow electrical contact to the shaft of a Beckman rotating electrode. These electrodes were cathodized in 10^{-1} M KCl for 1 min at a constant current density of 3.9 mA cm^{-2} and a constant electrode rotation rate of 36 r.p.s. After open circuit for 30 s in the same solution, anodized silver chloride layers 0.6, 1.2 and 2.4 × 10^{-4} cm thick were prepared by passing the reverse constant current for 1, 2 and 4 min. These thicknesses were calculated from density and coulometric considerations and should be accurate to within ±5%.

The cell for the ion-exchange/interference studies consisted of a thermostatted jacketed beaker; 50 ml of solution was used at 20.0 ± 0.1°C. A rubber stopper held in fixed geometry (1) the Orion double-junction electrode, (2) the Orion bromide electrode and (3) the principal Ag/AgCl disk electrode rotated at 36 r.p.s. Potential—time transients were monitored with an Orion electrode switch attached to the expanded-scale pH meter which was connected to a Beckman 10-in. recorder.

Procedures

For studies in chloride solutions of low activity, an initial solution ca. 10^{-5} M in chloride and 10^{-6} M in bromide was allowed to equilibrate with the electrodes and the potentials were monitored. Then at 15 min a mixed

bromide/chloride solution (0.25, 0.50 or 1.00 ml volume) was added to the initial solution with a calibrated syringe. Bromide activity levels were "spiked" from 7.4×10^{-5} M to 2.9×10^{-3} M and chloride from 2.2×10^{-5} M to 2.9×10^{-3} M. For all electrode thicknesses, the bromide level was at least twice the amount needed to convert completely the silver chloride to silver bromide. Potential—time transients were then monitored for both electrodes until they reached similar steady-state values.

For studies in 10^{-2} M or greater chloride activity, the standard bromide electrode was omitted since it suffers a chloride interference when bromide activity is below 10^{-3} M. This limitation effectively makes it impossible to follow the ion-exchange kinetics of the system and only allows checking of trends for potential—time transients of the metathesized electrodes. As a result, this high-chloride, low-bromide region was not extensively studied.

For selected solution combinations in both high and low chloride activities, the standard Orion chloride electrode was substituted for the thin anodized test electrode. This allowed monitoring of the interference effect for an electrode of essentially infinite thickness and bromide scavenging capacity (for initial bromide activity less than 10^{-3} M) and served as a limit for comparison with finite thickness electrodes.

Further information was obtained on the change in response mechanism by use of impedance measurements. An electrode 1.2×10^{-4} cm thick was equilibrated in 10^{-4} M KCl for 30 min and a three-probe rotating disk impedance measurement was made. The electrode was then equilibrated at open circuit with initial bromide levels of 1×10^{-4} M, 2×10^{-4} M, and 1×10^{-3} M and the impedance remeasured (closed circuit equilibration results in passage of large currents and resultant stripping of the electrode). The impedance method, bridge electronics and cell setup have been described previously [9, 10]. Silver/silver bromide counter and reference electrodes were substituted for those used in the previous work.

RESULTS

For anodized silver chloride electrodes, activity steps in chloride result in monotonic potential—time transients. However, when the baseline solution is "spiked" with a mixed bromide/chloride interferent solution, an unusual non-monotonic transient occurs. Representative examples are shown in Fig. 1. The potential transient consists of four identifiable regions. At short times (region 1) (not seen in Fig. 1) there is a negative-going potential overshoot which readjusts to a still negative potential plateau (region 2). This potential persists for a few seconds at highest bromide activity and for 10 min at lowest bromide activities for thickest electrodes. The potential then moves negatively fairly quickly and begins to level off toward the breakdown point (region 3) where the potential falls off abruptly negatively to that potential expected for a normal AgBr electrode (region 4). Table 1 lists experimental conditions and time-response parameters for these regions.

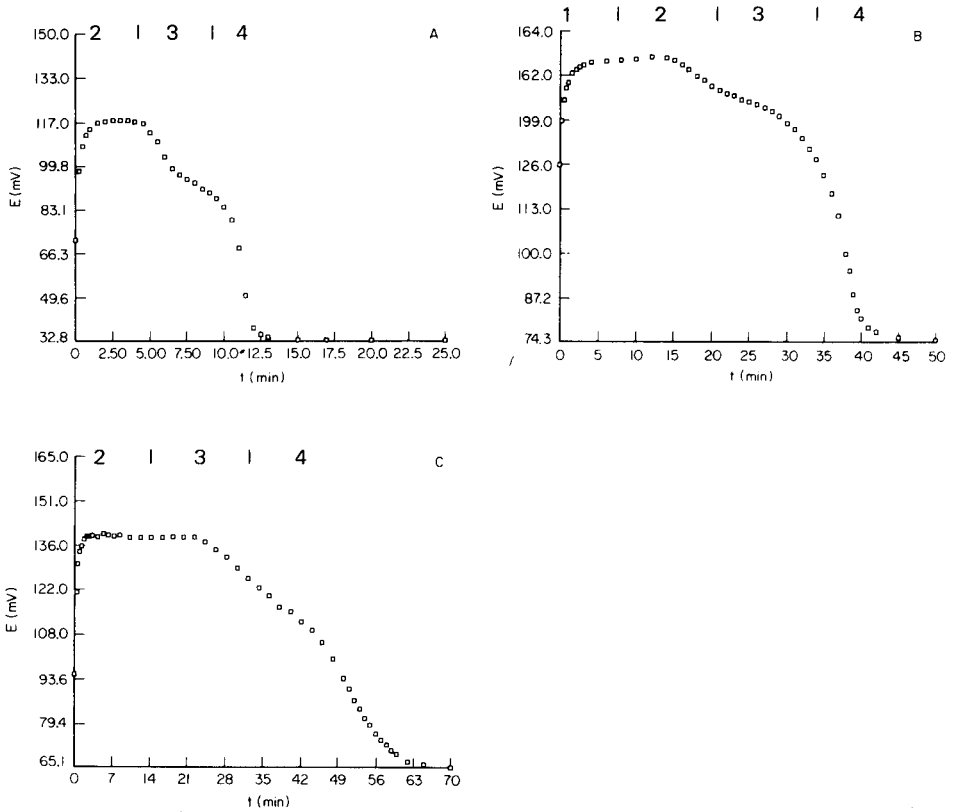

Fig. 1. Potential—time transients resulting for activity step from the baseline solution to solutions with different initial halide concentrations: (A) to 4.43 × 10^{-4} M in KBr and 1.47 × 10^{-3} M in KCl (electrode thickness 1.2 × 10^{-4} cm); (B) to 1.47 × 10^{-4} M in KBr and 1.57 × 10^{-4} M in KCl (electrode thickness 1.2 × 10^{-4} cm); (C) to 2.96 × 10^{-4} M in KBr and 2.96 × 10^{-4} M in KCl (electrode thickness 2.4 × 10^{-4} cm). Initial potentials (not shown) are given in Table 1. Regions are identified.

The Orion bromide electrode can be used to follow the depletion of bromide activity in the bulk solution during bromide attack on the AgCl test electrode. From previous studies in the rotating disk configuration, the diffusion time from bulk solution to electrode surface, $\delta^2/2D_i$, was known to be about 0.05 s. Thus it can be assumed that bromide activities in the bulk solution and on the surface are equal. Assuming that bromide decay in the bulk solution is a true reflection of bromide incorporation into the electrode with equivalent chloride release, it is possible to obtain bromide activity and AgCl decay curves and chloride activity and AgBr growth curves. Typical examples are shown in Figs. 2 and 3. It is immediately obvious that not only is the surface of the electrode being metathesized to AgBr, but also a minimum of approximately 60% of the electrode is converted to AgBr. This result indicates anionic diffusion of bromide into and chloride out of the electrode interior. This process is already fairly well known in solid state

TABLE 1

Potential—time characteristics of bromide interference[a]

δ (cm)	Br_0 (10^{-4} M)	Br_f (10^{-4} M)	Cl_0 (10^{-4} M)	Cl_f (10^{-4} M)	ϕ_1 (mV)	ϕ_2 (mV)	ϕ_3 (mV)	t_1 (min)	ϕ_4 (mV)	t_2 (min)	ϕ_5 (mV)	t_3 (min)
6×10^{-5}	0.74	0.37	0.22	0.55	218.4	130	184.6	8.0	150.8	28.0	88.7	55.0
	2.22	1.85	0.22	0.54	215.9	125	161.4	2.5	133.9	9.5	54.9	20.0
	0.74	0.32	0.83	1.24	219.2	129	177.0	8.0	157.2	32.0	91.8	55.0
	2.22	1.83	0.83	1.21	208.3	98	149.1	3.0	114.7	8.0	48.5	20.0
	0.74	0.36	7.39	7.77	209.1	122	133.2	5.0	117.8	26.0	88.9	55.0
	2.22	1.81	7.39	7.79	210.2	102	125.9	2.0	100.9	8.0	48.7	20.0
1.2×10^{-4}	1.48	0.69	0.38	1.02	205.0	126	167.1	15.0	143.0	32.0	81.3	50.0
	4.43	3.44	0.28	1.23	196.5	134	144.6	2.5	94.1	9.5	35.8	20.0
	1.48	0.66	1.56	2.37	203.1	126	156.8	13.0	140.8	28.0	74.3	50.0
	4.43	3.42	1.56	2.57	206.4	106	144.8	4.0	104.0	12.0	35.0	20.0
	1.48	0.67	14.8	15.6	200.8	101	119.0	6.0	108.3	28.0	74.4	60.0
	4.43	3.38	14.8	15.8	200.4	71	117.2	3.0	89.4	9.0	32.8	25.0
2.4×10^{-4}	2.96	1.07	0.41	2.26	199.4	121	148.5	5.0	—	—	65.1	75.0
	8.87	6.76	0.41	2.48	195.9	90	123.6	1.5	72.0	13.5	16.1	25.0
	2.96	1.20	2.96	4.72	207.8	95	140.1	5.0	105.0	46.0	65.1	70.0
	8.87	6.35	2.96	5.47	198.8	75	123.2	1.5	72.1	13.0	17.5	25.0
	2.96	1.27	29.5	31.2	210.2	70	107.5	3.0	96.9	18.0	65.9	80.0
	8.87	6.37	29.5	32.1	208.2	60	95.6	1.5	—	—	16.6	30.0

[a] $Br_{0,f}$ = initial and final bulk solution bromide activity; $Cl_{0,f}$ = initial and final bulk solution chloride activity; δ = electrode thickness; ϕ_1 = baseline potential; ϕ_2 = initial transient potential; ϕ_3 = plateau potential; ϕ_4 = breakdown potential; ϕ_5 = final potential; t_1 = plateau time; t_2 = breakdown time; t_3 = final time.

physics [11] and solid solutions of all proportions of AgCl—AgBr mixtures have been reported [12]. Percent electrode conversion increased with increased initial bromide activity and was independent of initial chloride activity.

There are two ways in which surface coverages of the respective salts can be calculated from potential data. In the first, the electrode potential is assumed equal at all points on or in the surface and may be defined as

$$E = E^0_{Ag^+/Ag} + (RT\,F^{-1}) \ln \bar{a}_{Ag^+} \tag{3}$$

where $\bar{a}_{Ag^+}$ is the average surface activity. Since both silver halide salts respond to silver ion activity, this average may be defined by the solubility products and surface coverages of the respective salts and the bulk solution halide activities

$$2\bar{a}_{Ag^+} = (1 - s)\,K_{so}^{AgCl}/a_{Cl^-} + (s)\,K_{so}^{AgBr}/a_{Br^-} \tag{4}$$

Since the halide concentrations and electrode potential are known, the surface coverage is defined as

$$s = 2[(\bar{a}_{Ag^+})(a_{Br^-})(a_{Cl^-}) - (K_{so}^{AgCl})(a_{Br^-})]/[K_{so}^{AgBr})(a_{Cl^-}) - (K_{so}^{AgCl})(a_{Br^-})] \tag{5}$$

In the second method a mixed potential is assumed at the surface due to the average potential of the two salts

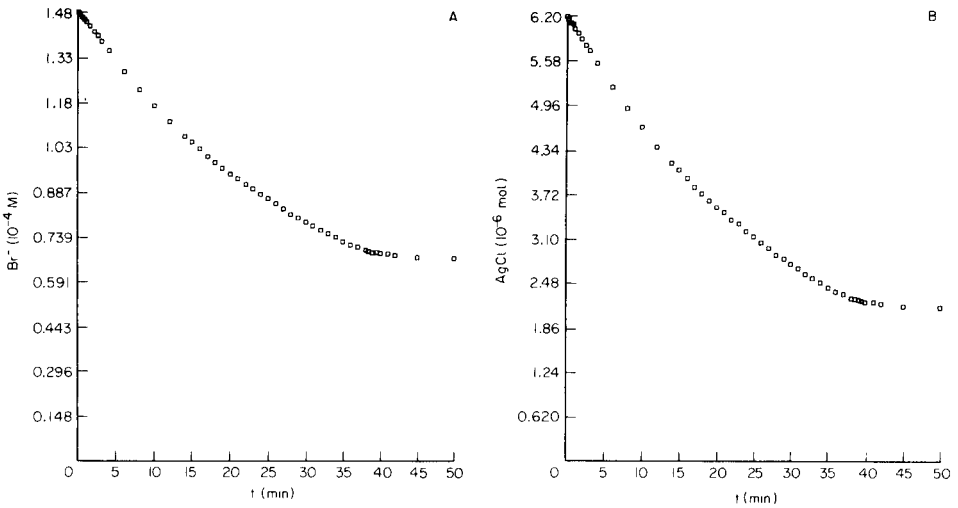

Fig. 2. (A) Bromide activity decay in solution versus time and (B) silver chloride depletion versus time, for a 1.2 × 10^{-4} cm thick electrode in solution initially 1.47 × 10^{-4} M in KBr and 1.57 × 10^{-4} M in KCl.

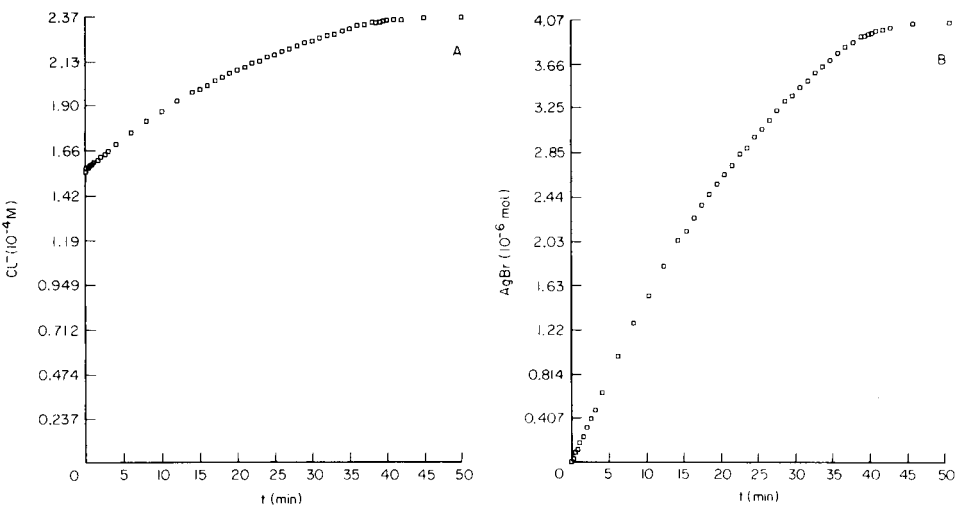

Fig. 3. (A) Chloride activity enhancement in solution versus time and (B) silver bromide formation versus time, for a 1.2 × 10^{-4} cm thick electrode in solution initially 1.47 × 10^{-4} M in KBr and 1.57 × 10^{-4} M in KCl.

$$E_{obs} = (1 - s)\ E_{AgCl/Cl^-} + (s)\ E_{AgBr/Br^-} \tag{6}$$

or

$$s = (E_{obs} - E_{AgCl/Cl^-})/(E_{AgBr/Br^-} - E_{AgCl/Cl^-}) \tag{7}$$

TABLE 2

Surface coverage, selectivity coefficients and percentage interconversion characteristics for the bromide interference on anodized silver/silver chloride electrodes[a]

δ (cm)	s_{1pt}	s_{2pt}	K^{pot}_{pt}	s_{1bd}	s_{2bd}	K^{pot}_{bd}	s_{1f}	s_{2f}	K^{pot}_{f}	% IC
6×10^{-5}	0.91	0.37	5.6	0.97	0.56	15.1	1.00	0.99	464	60.0
	0.97	0.45	4.4	0.98	0.56	14.5	1.00	1.00	352	58.8
	0.82	0.30	6.7	0.90	0.44	26.1	1.00	0.99	462	66.8
	0.94	0.40	6.9	0.98	0.59	31.1	1.00	0.99	458	62.2
	0.76	0.36	32.1	0.89	0.57	10.5	1.00	0.95	450	61.2
	0.82	0.33	14.7	0.93	0.54	51.2	1.00	0.97	455	64.8
1.2×10^{-4}	0.92	0.38	6.4	0.96	0.52	23.5	1.00	0.96	331	63.5
	0.97	0.44	4.3	0.99	0.67	37.6	1.00	0.99	404	79.9
	0.84	0.32	4.1	0.90	0.44	24.0	1.00	0.98	452	65.6
	0.90	0.34	4.0	0.98	0.57	25.4	1.00	1.00	419	81.9
	0.73	0.33	28.6	0.83	0.49	74.4	1.00	0.96	422	64.6
	0.73	0.37	9.7	0.91	0.50	41.0	1.00	1.00	467	90.2
2.4×10^{-4}	0.91	0.39	6.1	—	—	—	1.00	0.98	404	75.9
	0.97	0.44	4.9	0.99	0.69	47.3	1.00	1.00	453	87.6
	0.83	0.33	7.2	0.96	0.62	63.9	1.00	0.98	360	71.0
	0.92	0.36	4.7	0.99	0.65	48.2	1.00	1.00	451	100.0
	0.65	0.26	18.5	0.78	0.40	44.6	0.97	0.88	308	68.0
	0.78	0.30	11.6	—	—	—	1.00	1.00	462	100.0

[a] δ = electrode thickness; s_1 = model 1 fractional surface coverage; s_2 = model 2 fractional surface coverage; K^{pot} = selectivity coefficient; % IC = percent electrode interconversion. Initial and final halide activities are the same as in Table 1. pt = plateau region; bd = breakdown region; f = final region.

Table 2 reports the results for the two models of surface coverage for the plateau region, the breakdown potential region and the final coverage. The first model forces a minimum AgBr coverage of 65% at all times and averages 80—85% in the plateau region, 90% in the breakdown region and 99.8% or more at the final potential. The second model allows minimum coverages of 25—30% and averages about 35% in the plateau region, 55% in the breakdown region and 96—98% at the final potential. The real test for the validity of these two models come from later fitting to the ion-exchange kinetic data.

Implicit in the concept of concentration-dependent surface coverages is the possibility of selectivity coefficients dependent on concentration and time. Values for this coefficient are empirically calculated from the Nicolsky equation. Figure 4 shows a typical plot of selectivity coefficient value versus time. Values range from 4 to 32 for all electrodes in the plateau region to the limiting value of 450 when the electrode surface is completely converted from AgCl to AgBr. These values are also included in Table 2. These final values are within ±10% of the theoretical ratio of the salt solubility products. For the standard Orion chloride electrode in these low levels

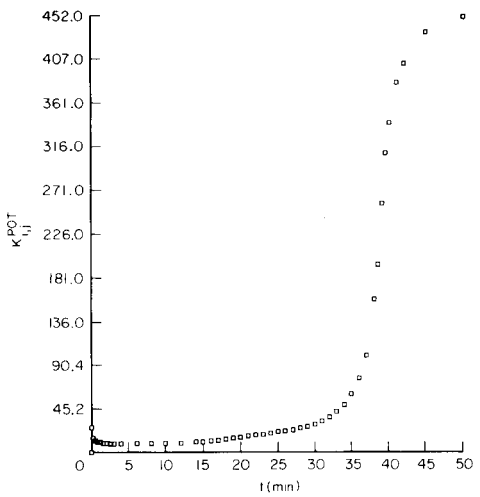

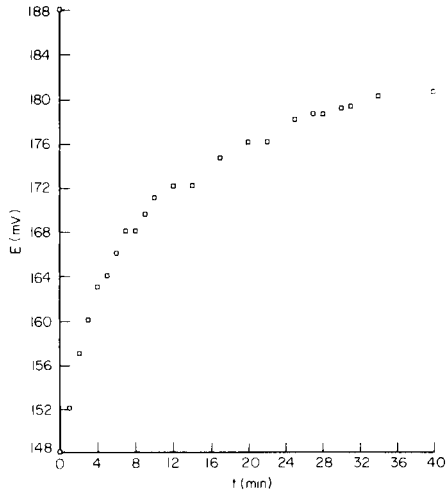

Fig. 4. Nicolsky equation selectivity coefficient versus time for a 1.2×10^{-4} cm thick electrode in solution initially 1.47×10^{-4} M in KBr and 1.57×10^{-4} M in KCl.

Fig. 5. Potential—time transient of the standard Orion chloride electrode resulting for activity step from baseline solution to solution initially 7.34×10^{-5} M in KBr and 7.63×10^{-5} M in KCl.

of bromide activity, the selectivity coefficient remained small (5—10) and relatively constant indicating a fairly constant surface coverage of silver bromide with time. This result seems reasonable since the silver bromide formed at the surface may always be partially depleted by diffusion into the electrode which is essentially an infinite sink. At sufficiently low bromide levels, it is possible for a commercial electrode completely to scavenge the interferent and almost return to the initial chloride-poised potential (Fig. 5). This experimental point has been considered and avoided in the studies reported here.

The potential interferent effect for these electrodes is metathesis controlled mainly by the ion-exchange metathesis reaction (eqn. 2). A possible complete rate expression has the form.

$$dx/dt = k_1(a - x)\ (1 - s) - k_2\,(b + x)\ (s) \tag{8}$$

where $(a - x)$ and $(b + x)$ are bromide and chloride activities, and $(1 - s)$ and (s) are fractional surface coverages of AgCl and AgBr. The steady state approximation requires

$$k_2 = k_1\ (a - x_f)\ (1 - s_f)/(b + x_f)\ (s_f) = k_1\ (\text{const.}) \tag{9}$$

or

$$dx/dt = k_1\ [(a - x)\ (1 - s) - (b + x)\ (s)\ (\text{const.})] \tag{10}$$

Bromide and chloride activities in solution are known directly or calculable at each time. Surface coverages can be computed by one of the trial functions in eqns. (5) and (7). The more appropriate model will give the more nearly constant "rate constants". Of course, a non-surface effect such as diffusion of attacking bromide into the AgCl lattice is expected to cause variability in computed rate constants as a function of time for the same run and as a function of electrode thickness for differing runs.

The rate expression may then be simplified to

$$\int_0^x dx/(Ax + B) = \int_0^t k_1 dt \tag{11}$$

where

$$A = (1 - s) + (\text{const.})\,(s) \text{ and } B = (b)\,(\text{const.})\,(s) - (a)\,(1 - s) \tag{12}$$

integrated to give

$$\ln\,[B/(Ax + B)]\,/At = k_1 \tag{13}$$

and solved numerically for k_1 to test the two models. Fig. 6 shows a typical plot of ln k_1 versus time for the two models and Table 3 reports the "rate constants" for both models as functions of electrode thickness and solution activities in both the plateau and breakdown regions. Solution-independent rate constants are better produced by the mixed-potential surface coverage (model 2). An average value of $5.18 \pm 0.80 \times 10^{-4}$ s^{-1} is found for the forward rate constant in the plateau region. This value appears to increase systematically with increased electrode layer thickness. Values at the longest times and greatest surface coverages also increase dramatically because of the uncertainty in the surface coverage. These apparent "rate constants" are in fact extensive in nature because of the volume dependence of solution activity changes, the dependence of bromide decay on electrode area and porosity, and the normalization of total active surface sites to unity. The uncertainty in the reverse rate is large. All that can be said is that the reverse rate is at least 200 times smaller than the forward rate. The result is of a similar order to the theoretical salt solubility product ratio of 450.

To verify the suggested response mechanism of the metathesized electrodes, impedance measurements are made. A comparison of electrode impedance in 10^{-4} M KCl before and after addition of bromide interferent is shown in Fig. 7. In pure chloride solutions, the bulk electrode and solution diffusional impedance properties are similar to those previously reported [13]. The metathesized electrodes show the higher bulk conductivities expected for a silver bromide surface layer and solution diffusion controlled by bulk bromide activity. This again indicates an ion-exchange mechanism with high surface coverage of silver bromide.

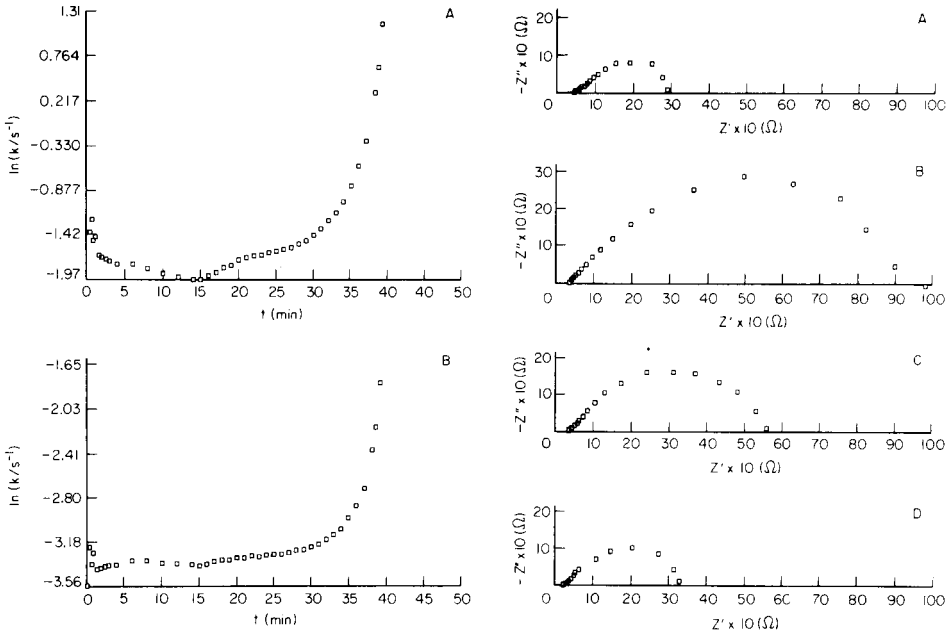

Fig. 6. ln k_1 versus time for a 1.2 × 10^{-4} cm thick electrode in solution initially 1.47 × 10^{-4} M in KBr and 1.57 × 10^{-4} M in KCl. Surface coverage calculated (A) from equipotential surface and (B) from mixed-potential surface.

Fig. 7. Impedance plane plots for 1.2 × 10^{-4} cm thick electrode in solution initially (A) 1 × 10^{-4} M KCl; (B) 1 × 10^{-4} KCl plus 1 × 10^{-4} M KBr; (C) 1 × 10^{-4} M KCl plus 2 × 10^{-4} M KBr; (D) 1 × 10^{-4} M KCl plus 1 × 10^{-3} KBr.

DISCUSSION AND CONCLUSIONS

The potential–time transient observed upon addition of an interferent halide solution is a combination of two effects. The first behaves like an internal lattice diffusion potential caused by the movement of bromide into and chloride out of the internal electrode lattice. This process is experimentally dominant as a negative overshoot prior to the plateau potential. The development of the plateau regions means that internal concentration gradients are smaller and the diffusion potential decreases in absolute magnitude to zero. The second effect is interfacial and is interpreted as a mixed-potential response, governed by the respective salt surface coverages, solubility products and bulk solution halide activities. With subtraction of the first effect, the steady replacement of chloride by bromide on the surface results in a monotonic negative transient to the plateau region. Initially there is a limiting constant, but incomplete, surface coverage of bromide. However, as the experiment progresses, the inward diffusion of

TABLE 3

Ion-exchange kinetics for bromide metathesis of anodized silver/silver chloride electrodes[a]

δ (cm)	$K_{s1,pt}$ ($\times 10^{-3}$ s^{-1})	$K_{s2,pt}$ ($\times 10^{-4}s^{-1}$)	$K_{s1,bd}$ ($\times 10^{-3}s^{-1}$)	$K_{s2,bd}$ ($\times 10^{-4}s^{-1}$)	$K_{s2\ (av.)}$ ($\times 10^{-4}$ s^{-1})
6×10^{-5}	4.03	5.43	10.8	7.90	6.06 ± 0.83
	8.11	4.38	7.24	5.66	4.85 ± 0.49
	1.80	4.55	3.42	6.04	5.00 ± 0.30
	4.43	4.37	17.2	7.27	5.68 ± 1.00
	1.17	4.37	3.02	8.00	6.14 ± 1.19
	1.31	3.67	4.81	6.94	4.70 ± 1.74
1.2×10^{-4}	4.18	5.51	7.34	6.68	5.97 ± 0.40
	13.4	6.06	50.6	10.4	7.65 ± 1.42
	2.34	5.67	3.67	6.38	5.98 ± 0.23
	2.98	4.48	12.3	7.00	5.39 ± 0.82
	1.50	6.14	2.04	6.64	6.11 ± 0.31
	1.41	5.12	4.36	7.60	6.23 ± 0.93
2.4×10^{-4}	9.55	6.62	—	—	—
	21.5	6.18	48.1	9.61	6.91 ± 1.24
	2.68	5.77	6.71	7.77	5.81 ± 0.71
	4.43	5.10	25.4	10.1	7.01 ± 1.30
	1.05	5.10	0.15	5.63	5.27 ± 0.16
	1.51	4.80	—	—	—
All runs	—	5.18 ± 0.80	—	7.47 ± 1.47	5.92 ± 0.80

[a] δ = electrode thickness; $k_{s1,pt}$ = apparent rate constant surface coverage model 1 (plateau region); $k_{s2,pt}$ = apparent rate constant surface coverage model 2 (plateau region); $k_{s1,bd}$ = apparent rate constant surface coverage model 1 (breakdown region); $k_{s2,bd}$ = apparent rate constant surface coverage model 2 (breakdown region); $k_{s2(av.)}$ = apparent rate constant surface coverage model 2 (average through both regions). Initial and final halide activities are the same as in Table 1.

the surface layers slows down and the percentage surface coverage by bromide increases (region 3) until the entire surface is covered (region 4) and the electrode then is in the bromide form.

Buildup—depletion curves for the electrode materials show nearly complete conversion of the electrode from chloride to bromide. Selectivity coefficients vary with surface coverages and therefore vary with time. Thin electrodes reach the upper limiting value of the ratio of salt solubility products (ca. 500) very quickly while very thick electrodes retain a selectivity coefficient of less than 10 for bromide less than 10^{-3} M.

Surface coverage is best modeled by a mixed rather than constant potential surface and the kinetics of the forward reaction rate averages 5.18 ± 0.80 × 10^{-4} s^{-1}. The reverse reaction is at least 200 times slower. Impedances verify the ion-exchange mechanism and the degree of electrode interconversion from AgCl to AgBr.

This work was supported by National Science Foundation Grant CHE77-20491.

REFERENCES

1 B. P. Nicolsky, Zh. Fiz. Khim., 10 (1937) 495.
2 F. Conti and G. Eisenman, Biophys. J., 5 (1965) 247.
3 R. P. Buck, Anal. Chim. Acta, 73 (1974) 321.
4 R. P. Buck, Anal. Chem., 40 (1968) 1432.
5 E. Pungor and K. Toth, Anal. Chim. Acta, 47 (1969) 291.
6 J. R. Sandifer, private communication (1976).
7 A. Hulanicki and A. Lewenstam, in E. Pungor and I. Buzas (Eds.), Conference on Ion-Selective Electrodes, Budapest, 1977, Akademia Kiado, Budapest, 1978.
8 A. Hulanicki and A. Lewenstam, private communication (1979).
9 D. E. Mathis and R. P. Buck, Anal. Chem., 48 (1976) 2033.
10 R. K. Rhodes and R. P. Buck, Anal. Chim. Acta, 110 (1979) 185.
11 A. P. Batra and L. Slifkin, J. Phys. Chem. Solids, 30 (1969) 1315.
12 L. S. Cain, H. Manning and L. M. Slifkin, Abstracts of International Conf. on Defects in Insulating Crystals, 9—14 October 1977, 58 (1977).
13 R. K. Rhodes and R. P. Buck, Anal. Chim. Acta, 113 (1980) 55.

Analytica Chimica Acta, 113 (1980) 79—90

STRIPPING POLAROGRAPHY AND THE REDUCTION OF COPPER(II) IN SEA WATER AT THE HANGING MERCURY DROP ELECTRODE

ALBERTO ZIRINO* and S. P. KOUNAVES

Chemistry and Environmental Sciences Group, Naval Ocean Systems Center, Code 5132 San Diego, California 92152 (U.S.A.)

(Received 18th July 1979)

SUMMARY

An approximate but general theoretical treatment for reversible and irreversible stripping polarographic systems is presented. The treatment is based on the development of an average current (i), which at plating times exceeding 15 s, is analogous to the instantaneous current in d.c. polarography. Plots of i vs. $(E - E^0)$ are generated for reversible and irreversible waves and are discussed for the reduction of copper(II) in sea water as an example. From stripping polarography and anodic stripping voltammetry, this work indicates that the overall reduction of copper(II) at the natural pH is kinetically hindered and thus is "irreversible". The reversibility and the determination of copper in sea water by a.s.v. can be improved by acidification and/or by the addition of ethylenediamine.

In recent years much of the work concerned with the speciation of trace metals in natural waters has been done using anodic stripping voltammetry (a.s.v.). This work has primarily progressed in two directions: studies of the shift in trace metal peak potentials with changing concentrations of ligands [1—5] and studies of changes in metal peak height or peak area under differing experimental conditions. Variants of the second approach include pH titrations [5—7] and complexiметric titrations [8] in which natural or added ligands are quantitatively titrated with metal ions or, alternatively, metal ions are titrated with ligands [8—10]. In this technique, the electrolysis potential is set at a value which presumably discriminates between the "free" (i.e., rapidly reducible) metal and the complexed metal, which is reduced at a much slower rate. This approach has been used extensively to estimate the "complexation capacity" of natural waters.

Techniques based on the shift of the peak potential depend on the degree of reactivity of the oxidized metal with the ligand of interest in the reaction layer. They can describe the species undergoing reduction, i.e., the speciation in the natural medium, only indirectly and by assuming reversibility. Thus, they are more suitable for model studies [1, 11] and for the determination of stability constants in known media [2, 3, 12] than for direct determination of natural speciation. On the other hand, methods dependent on peak height or peak area can give direct information on the natural species as long as a

direct proportionality exists between the quantity of metal reduced during electrolysis and the metal oxidized from the amalgam. One relatively novel form of a.s.v. which gives information about the species undergoing reduction is stripping polarography, sometimes called pseudopolarography [13, 14].

In stripping polarography, peak heights or peak areas obtained by a.s.v. are plotted against the applied electrolysis potential. These plots have the sigmoidal shape of ordinary d.c. polarograms but without the residual current component, and present the possibility of extending existing polarographic methodology to trace metals at the part per billion (ppb) level. The shapes of the plots indicate the degree of reversibility of the species undergoing reduction and may be useful for their identification. The reduction of copper in sea water provides a good example of the usefulness of stripping polarography for these purposes. Figure 1 shows three plots of 6 ppb copper added to unfiltered sea water from San Diego Bay and analyzed under varying conditions. Each of the experimental points represents the copper peak current obtained by a.s.v. after a 5-min electrolysis at a hanging mercury drop electrode (HMDE). The plots obtained for copper at pH 8 (Fig. 1, curves a and b) feature broadly curving slopes, and no distinct limiting plateau is reached, even at the highest applied potential. The shapes of these "waves" indicate an irreversible reduction. On the other hand, the reduction of copper at pH 3 is quasi-reversible (Fig. 1c) with $E^*_{3/4} - E^*_{1/4} = 42$ mV. These plots may be compared with the reduction of cadmium in sea water, which proceeds reversibly both at pH 3 and 8 as discussed by Zirino and Kounaves [14] and Kounaves and Zirino [15]. This paper presents a more general treatment for reversible and irreversible systems and examines some of the analytical implications of irrevers-

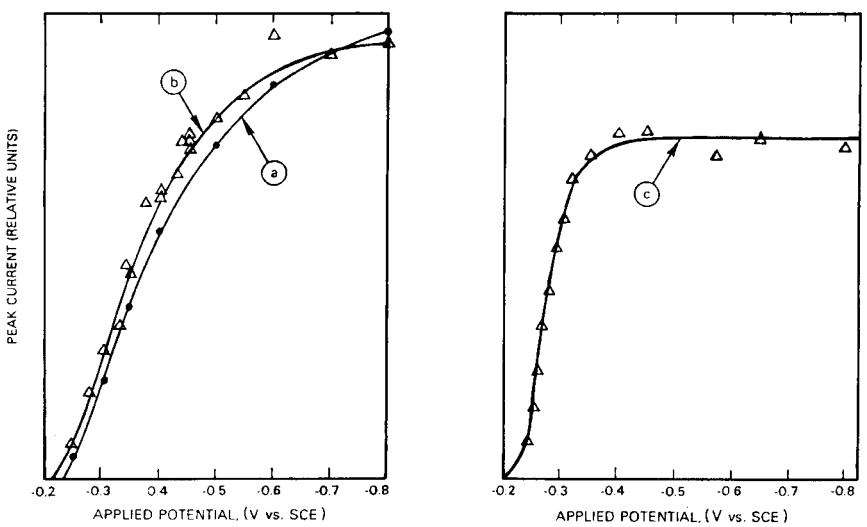

Fig. 1. Stripping polarographic plots of 6 ppb Cu in sea water (not to scale). (a) Raw sea water, pH 8; (b) u.v.-oxidized sea water, pH 8; (c) raw sea water, pH 3.

ibility. The reduction of copper in sea water is used to illustrate some of these points.

THEORY

The general equation for the instantaneous current resulting from the reduction of a simple metal ion to a metal which in turn forms an amalgam with the HMDE is [16]

$$i = nFAk\{C_s^0 \exp[-\alpha nF(RT)^{-1}(E - E^0)] - C_a^0 \exp[1 - \alpha nF(RT)^{-1}(E - E^0)]\} \quad (1)$$

where k is the formal rate constant for the reaction, E is the electrode potential, E^0 is the standard potential for the amalgam electrode, C_s^0 and C_a^0 are the concentrations of simple metal ion and reduced (amalgamated) metal, A is the area of the electrode, α is the transfer coefficient, and n, F, R and T have their usual meanings.

For a prolonged electrolysis time t, integration of expression (1) over the interval $0 \leqslant X \leqslant t$ will yield q, the charged passed in the accumulation of reduced metal in the HMDE. If, for the moment, it is assumed that there are no losses in the electrode, then q will equal q', the charge obtained from the integration of the a.s.v. peak. Rigorous integration of eqn. (1) is difficult, however, and will not be attempted here. Nevertheless, an analytically useful expression may be obtained in terms of the average current $\bar{i}$ which flows over the same time interval. From the mean value theorem, it can be shown that $\bar{i}t = \int_0^t i\,dt = q$. Now, the peak current electrolysis potential relationship can be derived in terms of an average flux $\bar{F}_s$ to the electrode since $\bar{i} = nFA\bar{F}_s$. For a stirred solution, and assuming that the concentration of the simple ion does not change appreciably with time, the relationship between F_s and the concentration of the simple ion in the bulk of solution can be given by the Nernst diffusion layer equation $\bar{F}_s = [C_s - \bar{C}_s^0]\, D_s/\delta_s$, where D_s is the diffusion coefficient of the simple metal ion, δ_s is the average thickness of the diffusion layer, C_s is the concentration of the simple metal ion in the bulk solution.

Similarly, Zirino and Kounaves [14] have shown experimentally that the average concentration of the reduced metal at the surface of the electrode can be approximated by

$$\bar{C}_a^0 = 3\bar{i}t/8\pi\, nFr^3 \quad (2)$$

where r is radius of the HMDE. Although a strict interpretation of eqn. (2) yields a physical impossibility, $\bar{C}_a^0$ becomes a satisfactory approximation for C_a^0 for electrolysis times longer than about 15 s [14]. Expression (1) can now be rewritten in terms of the average quantities $\bar{i}$, $\bar{C}_s^0$, and $\bar{C}_a^0$, yielding

$$\bar{i} = k\{[C_s - (\bar{i}(\delta_s/D_s)/nFA)] \exp[-\alpha nF(RT)^{-1}(E - E^0)] - (3\bar{i}t/2r) \exp[(1 - \alpha)nF(RT)^{-1}(E - E^0)]\} \quad (3)$$

Expression (3) can also be rearranged to obtain an equation which relates the average peak current directly to the concentration of the reactant species:

$$\bar{i} = C_s nFA \Big/ \left\{ \frac{\delta_s}{D_s} + \frac{1}{k \exp\left[-\alpha nF(RT)^{-1}(E-E^0)\right]} + \frac{3t}{2r} \exp\left[nF(RT)^{-1}(E-E^0)\right] \right\} \tag{4}$$

Figure 2 plots the average current occurring over the interval $0 \leqslant t \leqslant 1000$, versus $E - E^0$ for various values of k. It can be seen that $\bar{i}$ behaves analogously to i in d.c. polarography and that stripping polarograms can be expected to broaden out and reach the limiting plateau less rapidly as the rate constant for the reaction diminishes. It is also evident from expression (4) that for any given E and t, the proportionality between $\bar{i}$ and C_s is maintained regardless of whether the reaction is reversible or irreversible. Stirring ($\delta_s \to 0$) will yield increasingly larger currents, while $\bar{i}$ will decrease with smaller values of k. At large overpotentials the second and third terms in the denominator will tend to zero and $\bar{i} \to nFA(D_s/\delta_s)C_s$ the limiting current at the experimentally chosen cell conditions.

In a manner similar to the above, the relationship between $\bar{i}$ and C_0^* for a reversible reaction is

$$\bar{i} = C_s nFA \Big/ \left\{ \frac{\delta_s}{D_s} + \frac{3t}{2r} \exp\left[nF(RT)^{-1}(E-E^0)\right] \right\} \tag{5}$$

This is the expression originally derived by Zirino and Kounaves [14], and it describes the familiar sigmoidal form of a reversible polarographic wave. As pointed out earlier [14], $E_{1/2}^*$ for this function is a log-linear function of the electrolysis time t and will vary as $-(\ln t)\, RT/nF$. ($E_{1/2}^*$ is used for the half-wave potential of a stripping polarographic wave while $E_{1/2}$ refers to the half-wave potential of a d.c. polarogram.)

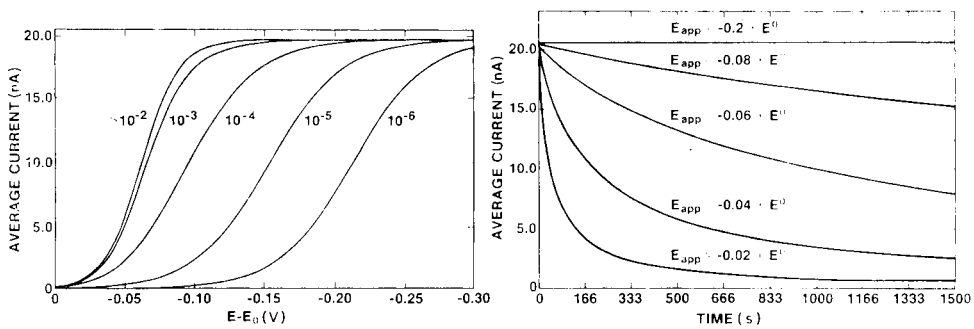

Fig. 2. $\bar{i}$ plotted as a function of $E - E_0$ for various values of k and $C_s = 1 \times 10^{-6}$ M, $\alpha = 0.5$, $t = 1000$ s, $\delta_s/D_s = 2.64 \times 10^2$ cm s^{-1}, $r = 0.046$ cm.

Fig. 3. $\bar{i}$ plotted as a function of t at various over-potentials. Conditions: $k > 10^{-2}$; $C_s = 1 \times 10^{-6}$ M, $\alpha = 0.5$, $\delta_s/D_s = 2.64 \times 10^2$ cm s^{-1}, $r = 0.046$ cm.

For the totally irreversible reduction of the simple metal ion to an amalgamated metal, eqn. (3) yields

$$\bar{i} = C_s nFA \Big/ \left\{ \frac{\delta_s}{D_s} + \frac{1}{k \exp\left[-\alpha nF(RT)^{-1}(E - E^0)\right]} \right\} \quad (6)$$

Now, because the back-reaction occurs at a negligible rate, $\bar{i}$ is no longer dependent on the electrolysis time t, even at very low overvoltages. This dependence of $E^*_{1/2}$ on electrolysis time may also be useful to characterize the degree of reversibility of the reduction. The slope of $E^*_{1/2}$ vs. ln t will always be RT/nF for a reversible reaction and something less than that for an irreversible reaction, and it will approach zero as the reaction approaches total irreversibility.

The average current $\bar{i}$ is also useful for calculating q, the charge passed in the reduction and amalgamation of the metal in the mercury drop, since $q = \bar{i}t$. This quantity can then be compared to q', the charge obtained by integrating the area under the experimentally obtained a.s.v. peak. It also follows that when q is proportional to the peak current (i_p), then $\bar{i} \propto i_p$.

EXPERIMENTAL

Instrumentation and solutions

All current—voltage measurements were made with a Princeton Applied Research Corporation (PAR) Model 174 Polarographic Analyzer in conjunction with a Hewlett-Packard Model 7034A x-y recorder. A PAR Model 315 Automated Electroanalysis Controller was used to automate the Model 174. pH was measured with a Corning No. 476055 combination microelectrode connected to an Orion Model 801 Research pH Meter. Stripping polarograms of copper—ethylenediamine, $Cu(en)_2$, in sea water were generated with a specially programmed Hewlett-Packard 21 MX minicomputer interfaced with a PAR 174 polarographic analyzer and a PAR electrolysis cell [15].

The electrolysis cell consisted of a PAR No. 9323 HMDE fitted into a PAR No. 9300 polarographic cell top. A PAR No. 3343 borosilicate glass polarographic cell bottom completed the cell. A vessel corresponding to the PAR cell bottom but machined from acrylic plastic was also used. Solutions were stirred with a 1.1-cm teflon-covered stirring bar coupled to a Sargent-Welch 600-rpm synchronous speed magnetic stirrer. A Beckman fiber-junction saturated calomel electrode (SCE) was placed in a PAR K65 reference electrode bridge tube with vycor tip to form a double-junction reference electrode. The outer junction was filled with sea water. A bare platinum wire served as the auxiliary electrode. All experiments were done at room temperature.

Solutions were made with reagent-grade salts. Pre-purified nitrogen and pre-purified nitrogen containing 300 ppm CO_2 were used to remove oxygen from all solutions. Additions of ethylenediamine (en) were made from a stock solution of 3×10^{-2} M en in distilled, de-ionized water. The pH of this solution was adjusted to 6.3 with hydrochloric acid; (Ultrex Grade, J. T. Baker and Co.).

Procedure

Electrodes of suitable size were produced by turning the micrometer capillary four divisions. Drops formed in this manner have a diameter of approximately 0.093 cm [14]. New drops were used for each plating stripping cycle. An electrolysis potential of −1.0 V vs. SCE was selected for individual determinations by a.s.v. For stripping polarography, the electrolysis potentials were selected randomly from a list of those bracketing E^0. In both cases, the electrolysis potential was applied for a preselected time t, during which the solution was stirred. Afterwards, stirring was ceased, the solution was allowed to come to rest for 30 s while maintaining the applied potential and then the metal was stripped out of the drop. Stripping was carried out at 5 mV s^{-1} either in the linear sweep (l.s.a.s.v.) or in the differential pulse (d.p.a.s.v.) mode; a 50-mV pulse was used in the latter case.

RESULTS AND DISCUSSION

Stripping polarography

Inspection of Fig. 1 shows that the shapes of the stripping polarograms of copper in San Diego Bay water are approximately comparable to the plots (Fig. 2) generated from the theory (eqns. 4—6) developed above. At pH 3 (Fig. 1, curve c) copper(II) is reduced quasi-reversibly and reaches a distinct limiting current plateau within 0.2 V of $E^*_{1/2}$. However, at the natural pH (Fig. 1, curve a) no well-defined limiting current plateau is reached within the range of applied potentials, indicating less reversibility and possible complexation by the natural organic ligands. Removal of the dissolved organic matter in the sample by oxidation with a high-energy mercury vapor lamp [17] does not alter markedly the shape of the curve (Fig. 1, curve b) strongly suggesting that the reduction of copper(II) at pH 8 is hindered by the inorganic constituents of sea water. A more careful comparison of Fig. 1, curve a and Fig. 2 also shows that the experimental data do not fit the "theoretical" irreversible curve very well. This is because the theory has been developed for electron transfer reactions only, while the irreversibility of the copper(II) reductions is probably caused by a more complex series of chemical steps occurring at the electrode surface. The magnitudes of the respective peak currents obtained at each potential also contain information about the reduction. Highest currents occur at pH 3, where the reaction is most reversible and there is the least adsorption. On the other hand, the u.v.-oxidized sea water yields the smallest currents because the opportunity for adsorption of copper on hydrated iron and manganese oxides is the greatest in the organic-free matrix [18].

$E^*_{1/2}$ for the reduction of copper in sea water at pH 3 and t = 300 s is −0.275 V. If, for the moment, reversibility is assumed and the potential is corrected to t = 0, then $E^*_{1/2}$ = −0.20. Heyrovsky and Kuta [19] list $E_{1/2}$ for the reduction of Cu(I) to Cu(Hg) in 1 M KCl as −0.23 V. Within the assumptions made, these two values can be considered the same. Thus, the

reduction of copper in acidified sea water may proceed in a manner similar to that in 1 M KCl. The chlorocuprate ion $(CuCl_x)^{2-x}$ is reduced in two steps: Cu(II) → Cu(I) proceeds easily at any potential more negative than 0.00 V, while Cu(I) → Cu(Hg) occurs at approximately −0.2 V. However, it should be noted that the experimental value of $E^*_{3/4} - E^*_{1/4}$ = 42 mV lies between a single and double electron transfer. The irreversibility of the reduction of copper in sea water at pH 8 strongly suggests some mechanistic hindrance, either associated with the predominant form of copper in sea water, presumably a hydroxide or a carbonate [11, 20], or with the chemical composition of the electrical double layer, or both. The above observations are also in agreement with the findings of Odier and Plichon [26] who used a.c. polarography to study the speciation of copper in sea water. They found that the reduction of copper at the DME produced only one peak, corresponding to $CuCl_2^-$ → Cu(Hg) + 2 Cl^-. In a similar manner these workers also found evidence for the existence in sea water of a $[Cu(HCO_3)_2OH]^-$ complex.

Equations (4—6) also predict that at limiting potentials $\bar{i}/C_s = k_1$, where k_1 is a constant, and that $i_p/C_s = k_2 t$, where k_2 is also a constant and t is the electrolysis time. This is the basis for the use of a.s.v. in quantitative analysis, and the validity of the relationship for a.s.v.-measurable metals in many media is well established. Deviations from linearity have, in general, been ascribed to the presence of complexing agents in natural media [4, 7, 10].

Equations (4) and (5) also predict that at low overvoltages, $\bar{i}$ and thus i_p vary markedly with electrolysis time and the degree of reversibility of the reaction. Figure 3 shows the effect of the electrolysis time on $\bar{i}$ for a reversible reaction at a HMDE at low overpotentials. It can be seen that the influence of t on $\bar{i}$ becomes vanishingly small in all cases when the applied potential is 0.2 V more negative than E^0. This situation includes most analytical applications, and thus experimental plots of i_p vs. t are generally shown to be linear.

The reduction of copper in sea water at pH 8

From the analytical point of view, the irreversibility of the reduction of copper at pH 8 in sea water implies a loss of sensitivity. Moreover, the analysis by standard addition is further complicated by adsorption of the standard on the cell walls and on surface-active particulates and colloids present in natural samples. For these reasons, copper in sea water is measured in acidic solutions almost universally. Nevertheless, the measurement of copper under natural conditions is important because any metal so determined represents the copper fraction in solution which is most available to marine organisms and is most toxic to marine algae [21]. The behaviour of copper peak currents in filtered (0.22 μm), organic-free [17] sea water was studied at pH 8 and 2 by making successive copper additions to sea-water samples followed by analysis of d.p.a.s.v. Figure 4 shows the results of several such sets of standard additions. At pH 8 and at low copper concentration, standard addition plots show a considerable degree of curvature, particularly just after the cell surface has

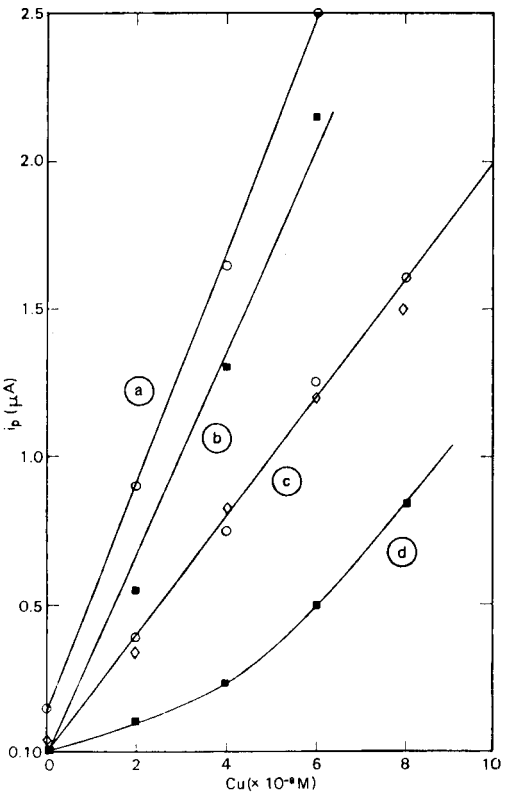

Fig. 4. Additions of copper to filtered, organic-free sea water. (a) pH 2; (b) pH 8 and 3×10^{-5} M in en; (c) pH 8 cell equilibrated with sea water; (d) pH 8, cell acid-cleaned, not equilibrated with sea water. Conditions: d.p.a.s.v., t = 900 s, current at instrument for value.

been brought to pH 8 after a thorough acid cleaning (Fig. 4, curve d). This is caused by the adsorption of copper on the cell walls. Copper additions give linearly changing peak currents after the cell has been equilibrated for several hours with a subsample of sea water at pH 8 (Fig. 4, curve c). This effect was observed for both the acrylic and borosilicate cell bottoms. The slopes of the standard addition plots were reproducible, and the slope at pH 8 was 51 ± 1% of the slope at pH 2. This diminution in the current can be attributed to the irreversibility of the overall Cu(II) → Cu(Hg) reaction. Such an explanation does not exclude the possibility that the oxidation of copper from the amalgam may also be hindered in sea-water media and may contribute to the overall process as determined by a.s.v. This aspect was studied as follows: samples of 0.5 M NaCl and filtered (0.22 μm) organic-free sea water were made 2×10^{-7} M and 5×10^{-8} M in copper and cadmium respectively, and analyzed at pH 8.3 and pH 2 by l.s.a.s.v. A third analysis was done by first carrying out the electrolysis at pH 8 as customary. Then, during the quiescent

period, acid was added to bring the pH to 2, stirring was briefly resumed, the solution was allowed to come to rest once more and the amalgam was stripped as previously. This procedure is essentially one of medium exchange [22, 23] where the reduction is carried out at pH 8 and the stripping occurs at pH 2. The number of coulombs transferred in the stripping step were calculated from the peak areas. The results of this experiment are shown in Table 1, which gives the sea-water data along with the values obtained in the NaCl medium; q', the charge obtained by plating and stripping cadmium in NaCl, is 0.85 ± 0.05 μC. Assuming that $q' = q$, the charge transferred during plating, a value for δ_0/D_0 of 2.77×10^2 cm s^{-1} can be calculated. This value can be compared to 2.64×10^2 cm s^{-1} obtained earlier for cadmium in 1 M KCl, using a cell with similar geometry and stirring conditions [14]. Under the same experimental conditions, q' for 2×10^{-7} M copper is only 1.00 ± 0.04 μC, despite the fact that copper is four times more concentrated than cadmium in solution. Because cadmium is known not to interfere with copper [24], this poor recovery can be attributed to the irreversibility of copper reduction, to possible losses of copper within the drop, and to the fact that Cu(Hg) is oxidized primarily to copper(I) in chloride media [25].

The charges obtained for cadmium and copper in the sea-water samples at pH 8 are slightly lower than those obtained in NaCl. The loss is greater for copper than for cadmium, confirming that the reduction of copper is hindered more in sea water at the natural pH than in NaCl. Electrolysis at pH 8 and stripping at pH 2 produces no significant difference over electrolysis and stripping at pH 8. This supports the stripping polarographic data suggesting that the slow step in the a.s.v. analysis of copper occurs on reduction. A complete a.s.v. operation at pH 2 does not increase the yield of cadmium significantly but increases copper by 58%. This is in reasonable agreement with the results obtained earlier from the standard addition plots.

TABLE 1

Peak potentials (E_p) and peak charge (q') for 2.0×10^{-7} M Cd and 5.0×10^{-8} M Cu in 0.7 M NaCl and sea water by l.s.a.s.v.

Solution	pH		E_p Cd (mV)	E_p Cu (mV)	q' Cd (μC)	q' Cu (μC)
	Plate	Strip				
0.7 M NaCl	8.2	8.2	−0.630	−0.150	0.85	0.96
	8.2	8.2	−0.625	−0.150	0.89	1.03
	8.2	8.2	−0.620	−0.150	0.85	0.96
	6.3	6.3	−0.625	−0.150	0.89	1.04
	6.3	6.3	−0.625	−0.150	0.75	1.01
	8.3	8.3	−0.610	−0.125	0.72	0.76
Organic-free sea water	8.3	2.0	−0.605	−0.115	0.74	0.82
	2.0	2.0	−0.610	−0.125	0.74	1.20

Improving the reversibility of the reduction of copper in sea water

In general, previous workers have chosen to improve the reversibility of the a.s.v. determination of copper in sea water by lowering the pH and by adding substantial quantities of an additional electrolyte, usually sodium acetate. The latter carries the risk of contaminating natural samples with copper in the electrolyte. Thus the use of ethylenediamine (en) as a reagent was explored to facilitate the reduction of copper in sea water. The addition of en during analysis has two virtues: $Cu(en)_2^{2+}$ is reduced reversibly in some media [7] and en effectively scavenges copper(II) off the cell walls and off particulates. From stripping polarographic plots, the reduction of $Cu(en)_2^{2+}$ in sea water was found to be irreversible at small concentrations of en but that a distinct limiting plateau was reached within 0.2 V of $E^*_{1/2}$. Thus, en was effective in improving the reduction of copper in sea water. This can be seen in Fig. 4 (curve b), which shows a standard addition plot of copper in sea water at pH 8 made 3×10^{-5} M in en. Similarly, the use of en was also explored as a method for determining ultra-trace levels of copper at the normal pH of sea water: 100 μl of 3×10^{-2} M en was added to 100 ml of raw sea water and allowed to equilibrate for 1 h, and the sample was then analyzed as usual by d.p.a.s.v.; standard additions were then made, each of which increased the concentration of copper(II) in the sample by 1.8×10^{-9} M. The resulting

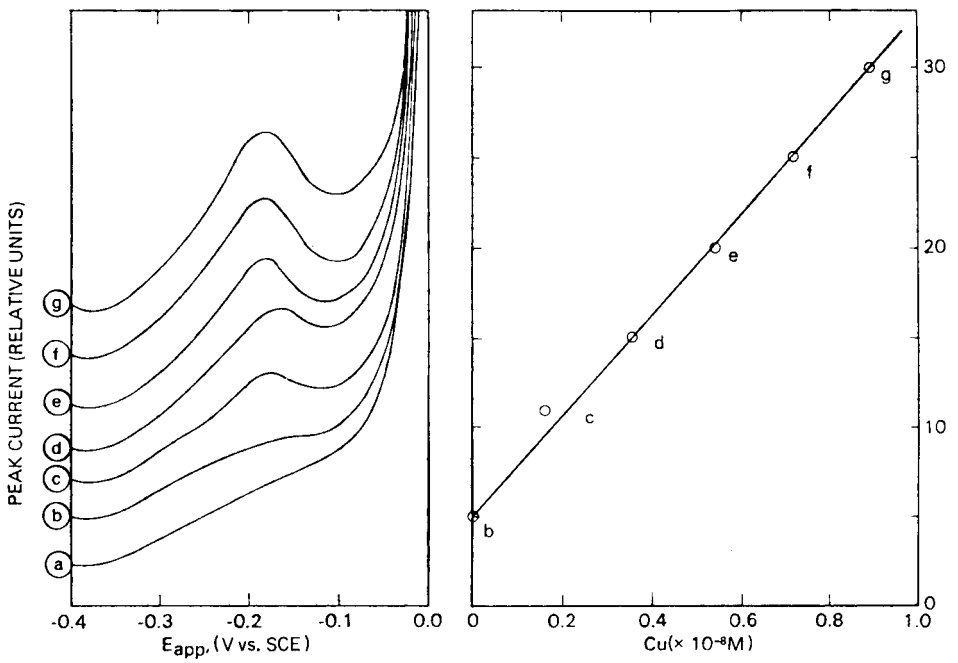

Fig. 5. D.p.a.s.v. measurement of copper additions to sea water. Conditions: t = 900 s, sweep 5 mV s^{-1}, pulse 50 mV. (a) raw sea water, pH 8; (b) raw sea water, pH 8, made 3×10^{-5} M in en; (c—g) plus successive additions of copper.

current—voltage plots are reproduced in Fig. 5. With en, the standard addition plot was linear at a concentration level where copper(II) would have been readily adsorbed by the cell and sample surfaces. This experiment also suggests than en may be used in analyses of sea water for natural copper which is readily complexed by this reagent.

Conclusion

Stripping polarography is a useful complement to a.s.v. because it gives information about the substance undergoing reduction as well as about the mechanism of the reduction. This information can then be applied directly to the study of electroactive species in natural media which are measurable by a.s.v. This work indicates that the reduction of copper(II) in sea water at the HMDE at natural pH is irreversible and that the irreversibility can be lessened by acidification or by complexation with ethylenediamine. These treatments also prevent the adsorption of copper(II) on cell walls and natural particulate matter and improve the analytical sensitivity of the a.s.v. analysis for copper. Current speciation models suggest that the overall reduction of copper(II) in sea water at pH 8 at the HMDE is kinetically hindered because (1) copper(II) at pH 8 forms a hydroxide or carbonate or hydroxycarbonate complex, or (2) hydrogencarbonate and carbonate in the reaction layer impede the reduction, or (3) both occur.

We wish to thank S. Yamamoto and E. P. Cooper for their continuing support of this effort. We are also indebted to Jacques Buffle for many constructive suggestions. Work was funded by the Naval Ocean Systems Center IR/IED program and by the Office of Naval Research under contract NR 083-301.

REFERENCES

1 A. Zirino and M. L. Healy, Limnol. Oceanogr., 15 (1970) 956.
2 W. L. Bradford, Limnol. Oceanogr., 18 (1973) 757.
3 H. Bilinski, R. Huston and W. Stumm, Anal. Chim. Acta, 84 (1976) 157.
4 T. A. O'Shea and K. H. Mancy, Anal. Chem., 48 (1976) 1603.
5 J. C. Duinker and C. J. M. Kramer, Mar. Chem., 5 (1977) 207.
6 A. Piro, M. Bernhard, M. Branica and M. Verzi, in Radioactive Contamination of the Marine Environment, Proc. Symp., Seattle, July 1972, IAEA edn., IAEA, Vienna, pp. 287—304.
7 R. Ernst, H. E. Allen and K. H. Mancy, Water Res., 9 (1975) 969.
8 M. S. Shuman and G. P. Woodward, Anal. Chem., 45 (1973) 2032.
9 Y. K. Chau and K. Lum-Shue-Chau, Water Res., 8 (1974) 383.
10 T. M. Florence and G. B. Batley, J. Electroanal. Chem., 75 (1977) 791.
11 A. Zirino and S. Yamamoto, Limnol. Oceanogr., 17 (1972) 661.
12 W. Stumm and H. Bilinski, in Advances in Water Pollution Research, 6th International Conference, Jerusalem, June 8—23, 1972, Pergamon, Oxford, 1973, p. 39.
13 S. Bubic and M. Branica, Thalassia Jugosl., 9 (1973) 47.
14 A. Zirino and S. P. Kounaves, Anal. Chem., 49 (1977) 56 (correction, 51 (1979) 592).
15 S. P. Kounaves and A. Zirino, Anal. Chim. Acta, 109 (1979) 327.

16 P. Delahay, New Instrumental Methods in Electrochemistry, Interscience, New York, 1954, p. 437.
17 F. A. J. Armstrong, P. M. Williams and J. D. H. Strickland, Nature, 211 (1966) 481.
18 J. Vuceta and J. J. Morgan, Environ. Sci. Technol., in press.
19 J. Heyrovsky and J. Kuta, Principles of Polarography, Academic Press, New York, 1966, p. 581.
20 D. R. Kester, personal communication.
21 W. Sunda and R. R. L. Guillard, J. Mar. Res., 34 (1976) 511.
22 M. Ariel, V. Eisner and S. Gottesfeld, J. Electroanal. Chem., 5 (1963) 362.
23 L. Zieglerova, K. Stulik and J. Dolezal, Talanta, 18 (1971) 603.
24 J. D. Smith and J. D. Redmond, J. Electroanal. Chem., 33 (1972) 169.
25 M. J. Pinchin and J. Newham, Anal. Chim. Acta, 90 (1977) 91.
26 M. Odier and V. Plichon, Anal. Chim. Acta, 55 (1971) 209.
27 L. Meites, Polarographic Techniques, 2nd edn., Interscience, New York, 1965.

Analytica Chimica Acta, 113 (1980) 91—96

DIFFERENTIAL PULSE POLAROGRAPHIC STUDY OF THE DEGRADATION OF AMPICILLIN

A. G. FOGG* and N. M. FAYAD

Department of Chemistry, Loughborough University of Technology, Loughborough, Leicestershire (Gt. Britain)

(Received 24th May 1979)

SUMMARY

Ampicillin (α-aminobenzylpenicillin) degrades in pH 2.5 buffer at 37°C or 80°C to form penicillamine and 2-hydroxy-3-phenyl-6-methylpyrazine which can be identified and measured by differential pulse polarography. The relationships between the peak potentials and pH are described. The yields of the degradation products are significantly affected by the presence of molecular oxygen.

Optimum solution conditions for the determination of cephalosporins were reported previously [1] together with initial results of degradation studies of cephalothin, cephaloridine and cephalexin which indicated the potentialities of differential pulse polarography (d.p.p.) for studying such degradations. In a further study [2] the degradation of cephalexin was studied in more detail: in particular the large proportion of hydrogen sulphide evolved in degradations in neutral buffers was determined and the peaks of several degradation products were identified.

Cephalosporins that do not have the α-aminobenzyl group substituted at C-7 were shown not to give hydrogen sulphide [2]. In the case of cephalexin (I) the evolution of hydrogen sulphide is clearly associated with the formation of the diketopiperazine derivative (II) by intramolecular aminolysis involving attack by the α-aminobenzyl group on the β-lactam ring of cephalexin. Degradation of compound II probably via a thiolactone [2] gives hydrogen sulphide. The sulphur atom in the diketopiperazine derivative is clearly more labile than that in the degradation products of cephalosporins that do not undergo the intramolecular aminolysis.

The purpose of the present work was to investigate by means of differential pulse polarography the degradation of the related α-aminobenzylpenicillin, ampicillin (III), and in particular to ascertain whether intramolecular aminolysis and/or the evolution of hydrogen sulphide features largely in its degradation.

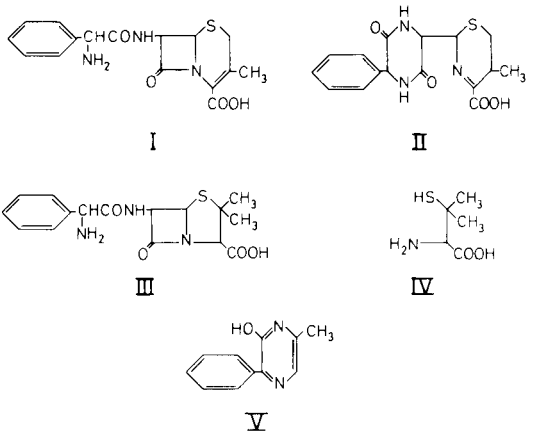

EXPERIMENTAL

Equipment, reagents and samples

Measurements were made with a PAR 174 polarographic analyser (Princeton Applied Research Corp.). For d.p.p. operation, a forced drop time of 0.5 s, a scan rate of 5 mV s^{-1} and a pulse height of 50 mV were used. Three-electrode operation was employed with a dropping mercury electrode, a platinum counter electrode and a saturated calomel reference electrode (all potentials are expressed against this electrode). The water-jacketted polarographic cell was maintained at 25°C. Solutions for polarography were deoxygenated with nitrogen which had previously been passed through a vanadium(II) scrubber. Polarography was carried out in the buffer solutions used for the degradation studies: aliquots of degraded sample solutions were polarographed directly at 25°C after adequate deoxygenation.

Samples of ampicillin trihydrate (III), penicillamine (IV) and 2-hydroxy-3-phenyl-6-methylpyrazine (V) were kindly provided by Beecham Pharmaceuticals Ltd., Glaxo Ltd. and Fisons Pharmaceuticals Ltd., respectively.

Methods

Degradation studies were carried out as described previously [2]. Degradation solutions were contained in a suitable wash container in a water bath at the required temperature. Nitrogen, presaturated with water, was passed through the solution throughout the degradation and the evolution of hydrogen sulphide was tested for by passing the effluent nitrogen through cadmium nitrate solution. In studies of the effect of molecular oxygen on the degradation, nitrogen was replaced by air.

Degradation studies were carried out in 0.5 M phosphate buffer (pH 7.4) at 37°C, in citrate—phosphate buffer of pH 2.5 (0.1 M in citric acid and 0.2 M in disodium hydrogenphosphate adjusted to pH 2.5) at 37°C, 60°C and 80°C, and in citrate—phosphate buffer of pH 8.5 at 80°C.

The amounts of penicillamine and 2-hydroxy-3-phenyl-6-methylpyrazine formed were determined by comparing the heights of d.p.p. peaks with those of standards. Polarography was done at the degradation pH except where otherwise stated.

RESULTS

The initial study was done at the 100 μg ml^{-1} ampicillin level at 37°C in pH 7.4 phosphate buffer. Ampicillin itself did not give a polarographic wave in the available potential range (0 to −1.6 V), but after 1 h an anodic wave at −0.1 V appeared and continued to increase in height with time. Hydrogen sulphide was not formed during the degradation.

The degradation pattern at pH 2.5 was different. Two major peaks were obtained: the anodic peak at −0.14 V and the cathodic peak at −0.64 V were subsequently shown to be due to penicillamine and 2-hydroxy-3-phenyl-6-methylpyrazine, respectively. The rate of degradation was found to increase with temperature in the range 37–80°C. Dissolved oxygen significantly decreased the yield of penicillamine. Typical results and polarograms from these studies are given in Table 1 and Fig. 1. In addition to the peaks arising

TABLE 1

Data obtained for degradation of ampicillin trihydrate solutions (100 μg ml^{-1}; amount 2.45 × 10^{-5} mol) at pH 2.5

Time (h)	Penicillamine		2-Hydroxy-3-phenyl-6-methylpyrazine		Peak at −0.45 V	Peak at −0.8 V
	i_p (μA)	Amount (× 10^{-7} mol)	i_p (μA)	Amount (× 10^{-7} mol)	i_p (μA)	i_p (μA)
(i) 37°C in presence of air						
4.3	0.0	0.0	0.0	0.0	0.0	0.0
19.5	0.55	1.5	0.55	0.46	0.3	0.02
22.8	0.80	2.7	1.10	0.86	1.3	0.05
45.7	1.90	7.8	3.80	2.8	0.0	0.25
97.1	2.70	11.5	9.55	7.8	0.0	0.75
(ii) 60°C in presence of air						
1.2	0.1	0.6	0.05	0.09	—	0.0
6.7	2.9	12.4	5.3	3.91	—	0.25
30.4	2.0	8.2	16.3	13.5	—	1.2
60°C in absence of air						
1.2	0.1	0.6	0.05	0.01	—	0.0
6.7	4.4	19.3	5.7	4.2	—	0.1
30.4	13.8	48.3	16.0	13.24	—	0.2
(iii) 80°C in absence of air						
0.5	0.45	1.1	0.2	0.2	—	0.0
1.1	3.0	12.8	4.4	3.25	—	0.02
6.3	14.9	52.1	16.3	13.5	—	0.03

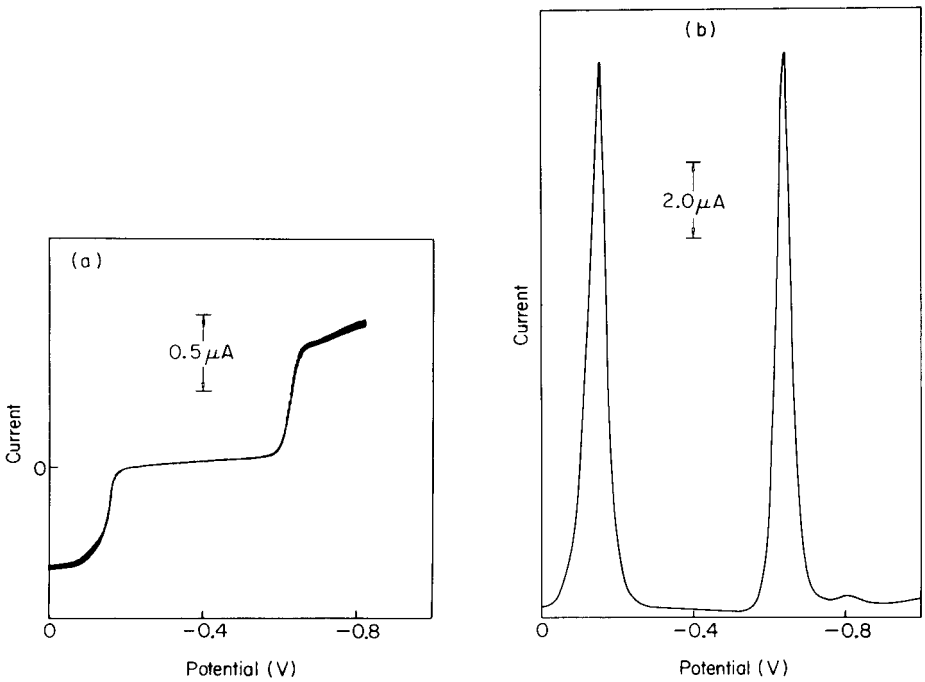

Fig. 1. Polarograms of an ampicillin solution (100 μg ml^{-1}) after degradation at pH 2.5 for 3.5 h at 80°C. (a) D.c. polarogram, natural drop time, scan rate 1 mV s^{-1}, low pass filter 3, (b) D.p. polarogram, drop time 0.5 s, scan rate 5 mV s^{-1}, modulation amplitude 50 mV.

from penicillamine and 2-hydroxy-3-phenyl-6-methylpyrazine, an unidentified peak at —0.8 V (pH 2.5) was observed in all degradation solutions at a later stage. In the presence of molecular oxygen, a further transient peak appeared at —0.45 V (pH 2.5), the compound responsible for this peak apparently degrading rapidly itself. The peak at —0.8 V was much larger in the presence of oxygen.

Degradation of ampicillin at pH 8.5 again followed a different pattern. The anodic peak first formed at —0.16 V decreased in height as a broad cathodic peak appeared at —1.16 V. The anodic peak is thought to be due to a thiol compound formed from the opening of the thiazolidine ring and the peak at —1.16 V to a carbonyl compound formed as this thiol is hydrolysed.

The polarographic behaviour of penicillamine was investigated with a pure sample. The anodic polarographic wave was shown by mercury height and temperature studies to be diffusion-controlled; a rectilinear calibration plot was obtained in citrate—phosphate buffer of pH 2.5 over the range 0.1—5.0 × 10^{-6} M. The peak potential varied rectilinearly over the pH range 2—8 (E_p(V) = —0.030—0.059 pH). The peak current varied with pH, a plot of peak current against pH showing maximum values at pH 3 and 10 (4.7 and

3.8 μA, respectively) with a minimum value (3.2 μA) at pH 7. The peak at —0.45 V formed in the degradation of ampicillin at pH 2.5 was shown not to be formed by degradation of penicillamine. The degradation of penicillamine in the presence of molecular oxygen at pH 2.5 is illustrated by the polarograms in Fig. 2: the broad peak which appears at —1.0 V is probably due to a carbonyl compound.

The polarographic behaviour of 2-hydroxy-3-phenyl-6-methylpyrazine was also studied with a pure sample. The cathodic polarographic wave was shown to be diffusion-controlled (mercury height and temperature studies): a rectilinear calibration plot was obtained in pH 2.5 citrate—phosphate buffer over the range 0.1—1.2 $\times$ 10^{-6} M. The peak potential varied rectilinearly over the pH range 2—9 (E_p (V) = —0.49—0.067 pH). The peak current is highly dependent on pH, having a maximum value at pH 3 and becoming almost zero at pH 11.

DISCUSSION

The first study of the kinetics and mechanism of the degradation of ampicillin in solution appears to be that of Hou and Poole [3] who used the iodimetric method to monitor the intact ampicillin and u.v. absorption spectrophotometry to identify products. They stated that the amino side-chain group in ampicillin plays a significant role in the rate but not on the mechanism of the reaction. Subsequently, however, Indelicato et al. [4], Cohen et al. [5] and Bundgaard [6] isolated diketopiperazine products from the degradation solutions of α-aminobenzylcephalosporins: these are formed

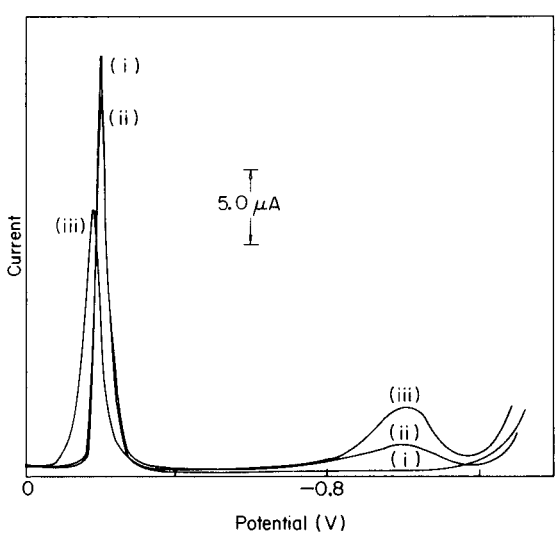

Fig. 2. Polarograms showing the degradation pattern for a penicillamine solution (100 μg ml^{-1}) at pH 2.5 and 60°C in the presence of air. Time: (i) 0, (ii) 3.0 h., (iii) 18.5 h.

by intramolecular aminolysis of the β-lactam ring and directly involve the α-amino group.

Barbhaiya et al. [7] isolated a fluorescent alkaline degradation product formed from several α-aminobenzylcephalosporins, including cephalexin and cephradine, and also from ampicillin; in all cases the product was shown by unambiguous synthesis to be 2-hydroxy-3-phenyl-6-methylpyrazine. This reaction also illustrates the possibility of intramolecular aminolysis in the case of ampicillin. The present authors [2] studied the d.p.p. of 2-hydroxy-3-phenyl-6-methylpyrazine and showed that it is formed in high yield in the degradation of cephalexin solutions at pH 8.5. Formation of this compound was observed only in acidic solutions of ampicillin.

In the present study, two major products, 2-hydroxy-3-phenyl-6-methylpyrazine and penicillamine, were observed at pH 2.5. The yields of the two compounds obtained at 80°C after 30 h in the absence of oxygen were 5% and 20%, respectively. Other non-reducible products must also be formed, including various polymeric species containing up to nine ampicillin units [8, 9].

Compound II is the initial product observed in the degradation of cephalexin. The analogous compound which might be expected to be formed from ampicillin was not observed: this compound would be expected to give a d.p. peak near −0.9 V at pH 7 as does compound II. Indelicato et al. [4] were unable to obtain this compound from ampicillin trichloroethyl ester under the same conditions in which they obtained compound II. Instead, in the degradation of ampicillin, penicillamine and 2-hydroxy-3-phenyl-6-methylpyrazine are formed in a ratio of approximately 4:1. If it is assumed that the penicillamine is formed by simple hydrolysis from the ampicillin molecule, the formation of 2-hydroxy-3-phenyl-6-methylpyrazine involves a reduction process. This presumably means that the fragment of the ampicillin molecule left when the penicillamine is formed undergoes a disproportionation reaction in forming the 2-hydroxy-3-phenyl-6-methylpyrazine.

REFERENCES

1 A. G. Fogg, N. M. Fayad, C. Burgess and A. McGlynn, Anal. Chim. Acta, 108 (1979) 205.
2 A. G. Fogg, N. M. Fayad and C. Burgess, Anal. Chim. Acta, 110 (1979) 107.
3 J. P. Hou and J. W. Poole, J. Pharm. Sci., 58 (1969) 447.
4 J. M. Indelicato, T. T. Norvilas and W. J. Wheeler, J. Chem. Soc. Chem. Commun., (1972) 1162.
5 A. I. Cohen, P. T. Funke and M. S. Puar, J. Pharm. Sci., 62 (1973) 1559.
6 H. Bundgaard, Arch. Pharm. Chem. Sci., 5 (1977) 149.
7 R. H. Barbhaiya, R. C. Brown, D. W. Payling and P. Turner, J. Pharm. Pharmacol., 30 (1978) 224.
8 E. J. Kuchinskas and G. N. Levy, J. Pharm. Sci., 61 (1972) 727.
9 M. K. Stanfield, B. T. Butcher and G. T. Stewart, Anal. Biochem., 89 (1978) 1.

Analytica Chimica Acta, 113 (1980) 97—106

X-RAY FLUORESCENCE ANALYSIS WITH A SEEMANN SPECTROMETER, IMPROVED PULSE ANALYSIS AND CRYSTAL DISPERSION

E. BRUNINX

Philips Research Laboratories, Eindhoven (The Netherlands)

(Received 13th August, 1979)

SUMMARY

The use of the pulse rise-time method for position determination in a position-sensitive proportional detector and the influence of crystal dispersion on the performance of a Seemann spectrometer are discussed. The advantages and disadvantages are compared with those of other x-ray fluorescence analysis spectrometers.

Earlier work on the Seeman spectrometer combined with a position-sensitive proportional detector (PSPD) showed that the asymmetric peak shapes obtained were due to the associated electronics [1, 2]. In the present work these asymmetries have been eliminated by using a different electronic pulse analysis system. The peak/background ratio has been further improved by means of selected diffraction crystals. Some minor modifications have been introduced into the geometry previously described.

INSTRUMENTATION

Electronics

In both previous publications [1, 2], the point of impact on the anode wire in the PSPD was determined by means of the charge division technique, i.e., by measuring the quantity of charge flowing to the left and right sides of the PSPD. This technique has been abandoned and the position of a pulse is now measured by means of the rise-time method [3] (see Fig. 1). The rise-time of the output pulse of the preamplifier (Ortec-127) will be shorter the closer is the point of impact on the anode wire to that particular preamplifier (Fig. 1a). Both preamplifier signals are processed in the main amplifiers (Ortec-472 A) in order to give a doubly-differentiated pulse.

A steep rise time after the preamplifier is translated into an early cross-over time (t_L) (see Fig. 1b), while the other pulse (with a slower rise time) will have a longer cross-over time (t_R). At these cross-over times, a pulse is generated by means of the timing single-channel analyzers (Ortec-455). Both pulses are fed into the time-to-pulse height converter (TPHC; Ortec-467).

The electronic section associated with the right-hand side of the PSPD is

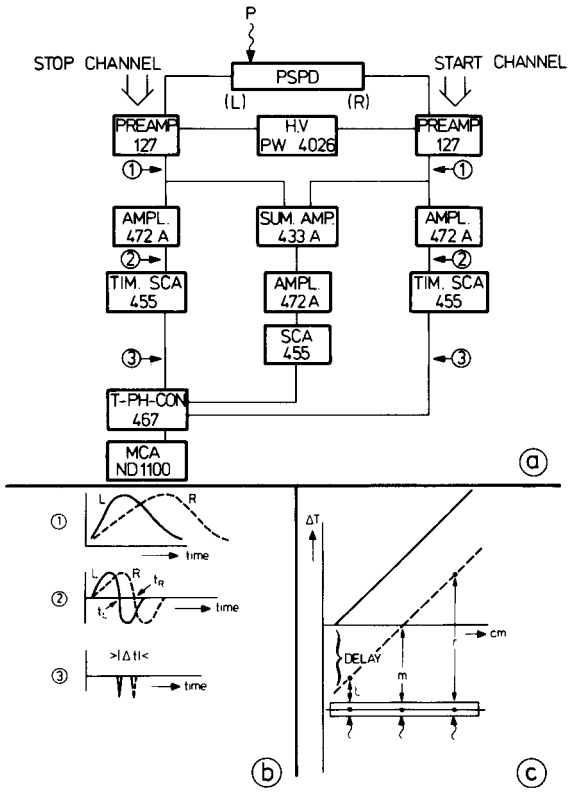

Fig. 1(a) block diagram of the electronics; (b) pulse shapes at different stages; (c) time difference between start and stop pulse as a function of point of incidence on the PSPD. The numbers refer to Ortec type numbers; ND100 is a Nuclear Data multi-channel analyzer; PW means Philips.

arbitrarily designated as the start channel while the other side is labelled the stop channel. Upon arrival of a pulse from the start channel, the time-to-pulse height converter generates a voltage whose magnitude increases until a pulse from the stop channel is received. A photon arriving exactly at the centre m of the detector (Fig. 1c) results in a time difference $\Delta t=0$, while a photon arriving at l triggers the stop channel earlier than the start channel, resulting in a negative time difference. In order to avoid these negative times the stop channel is delayed by, say, 200 ns, the effect of which is a parallel upward shift of the line in Fig. 1c. This shift does not influence in any way the generated voltage in the TPHC since only time differences are being considered.

A drawback of this electronic method is its insensitivity to pulse-height variations. In other words, two collimated beams of, for example, 20 and 4 keV will both produce the same peak in the spectrum when incident at

the same position in front of the PSPD. It is nevertheless possible to use some kind of energy discrimination as follows. The output pulses from both preamplifiers are added in a sum amplifier (Ortec 433 A) and amplified. The amplified pulse, whose height is a measure of the incident energy, is then passed through a single-channel analyzer. The lower and upper levels are set in such a way that they encompass the desired energy range in which the detector is used. The coincidence circuit in the TPHC is used to reject all pulses lying outside this range. In the present experiments the lower and upper levels were set at 4 and 14 keV. This is a rather wide energy band compared to those used in pulse-height analysis but it must be remembered that the element identification is made through the position of a line, not its energy.

Detector

The detector is made of brass; the internal dimensions are 20 × 4 × 4 cm. The anode wire (quartz coated with pyrolytic graphite, 25 μm diam.) is glued to the connector plugs with Leit-C cement (colloidal carbon in an organic solvent; Neubauer Chemikalien, D-4400, Münster, W. Germany). Both preamplifiers are attached directly to the connector plugs, outside the detector. The window height is 2 cm and the window material is aluminized mylar (thickness 6 μm).

In the earlier experiments, a mixture of Ar : CH_4 (90 : 10) was employed. This resulted in deterioration of the wire and detector characteristics. Seen under the microscope, the carbon layer appeared to be pockmarked. In all further experiments Ar : CO_2 (90 : 10) was employed, which yielded no visible deterioration of the carbon layer.

The detector was operated in the flow mode with a slight-overpressure of 10 mbar. A constant pressure regulator was included in the gas circuit.

The total peak area was determined by means of a program analogous to that described by Verheijke [4]. In this program the limits of peak integration (on the left and right of the peak) are set at the point where the peak becomes indistinguishable from the background.

The resolution of the detector was measured with a collimated ^{55}Fe source in the central portion of the detector. The results (Table 1) are the average of three measurements.

For x-ray fluorescence measurements only the central part over a distance of 60 mm was employed. The overall linearity of the whole detection system was measured by moving the collimated ^{55}Fe source (0.3 mm width) on a micrometer support in front of the detector. The results are given in Table 2. The deviation represents the difference between the experimental points and the line calculated by least squares. The data indicate the excellent resistance uniformity of the $SiO_2(C)$ wire and the stability of the pulse processing system.

The slope of the plot of channel number vs. distance (in mm) for this experiment was 8.782 ± 0.012 channel mm^{-1} (± one standard deviation).

TABLE 1

Full-width at half maximum (FWHM) and peak/background ratio(P/BG) for collimated ^{55}Fe source

Collimated source width[a] (mm)	P/BG[b] ± 1s[c]	$FWHM$ ± 1s[c] (mm)
0.1	60.5 ± 2.5	0.39 ± 0.01
0.2	65.9 ± 4.6	0.46 ± 0.08
0.3	67.8 ± 0.6	0.50 ± 0.03

[a]Length of collimated beam, 30 mm; height, 10 mm.
[b]The count rate was low, around 160 s^{-1}.
[c]Uncertainty is one standard deviation.

TABLE 2

Overall linearity of PSPD and electronics

Source position (mm)	Deviation (%)	Source position (mm)	Deviation (%)	Source position (mm)	Deviation (%)
5	−2.2	25	−0.3	45	0
10	+0.9	30	−0.1	50	−0.1
15	+0.3	35	+0.4	55	0
20	0	40	−0.1		

The value changed little from one day to another; the standard deviation measured over a period of several months was 0.03.

Excitation conditions

In all experiments the excitation conditions were: tungsten tube, 20 kV, 5 mA; 100 μm aluminium on x-ray tube window; distance from slit to PSPD, 235 mm; thick copper sample; K_α line measured in central part of detector; counting time, 1000 s; total count rate incident upon detector, 500 s^{-1}.

Geometry

The same geometry G-3 as described earlier [2] was used with only minor changes (Fig. 2a, b). One of the modifications tried was the introduction of a small collimator between sample and slit. The first type (Fig. 2c) consisted of horizontal foils, spaced 2 mm apart, and placed as shown in Fig. 2a (i.e. the foils are parallel to the plane of the drawing). The P/BG ratio improved by 5—10% while the count rates for Cu K_α radiation and background decreased. A wedge-shaped collimator (Fig. 2d) was also tried. It yielded a somewhat greater improvement than the horizontal foil, the advantage being that there was no reduction in diffracted intensity.

The replacement of the air path between the slit and the PSPD by vacuum or a helium atmosphere gave no improvement in the P/BG ratio.

In the selection of a gap width, it is necessary to take into consideration the following points. For a given gap width, g, the diameter of the diffracted

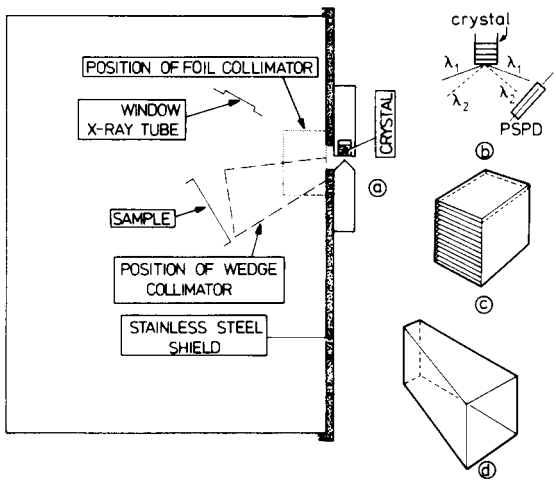

Fig. 2(a, b) Geometry of assembly; (c) spaced-foil collimator; (d) wedge collimator.

beam increases for decreasing diffraction angle θ. Based on purely geometric considerations, omitting mosaic spread of the crystal and penetration of the incident beam into the crystal, it is easy to deduce that for $5° < \theta < 50°$, the fractional increase is given by $D/g = 2 \cos \theta$, where D is the width of the diffracted beam. The value of this ratio is plotted in Fig. 3. It can be seen that small diffraction angles yield broadened beams in the PSPD. The gap width also determines the width, w, of the crystal necessary to intercept the incident beam of characteristic radiation. Again, on a geometrical basis this total width, w, is given by $w = 2g/\tan \theta$, and is shown in Fig. 4. Measurements with LiF crystals having widths of 5, 3 and 1 mm (gap width 0.1 mm,

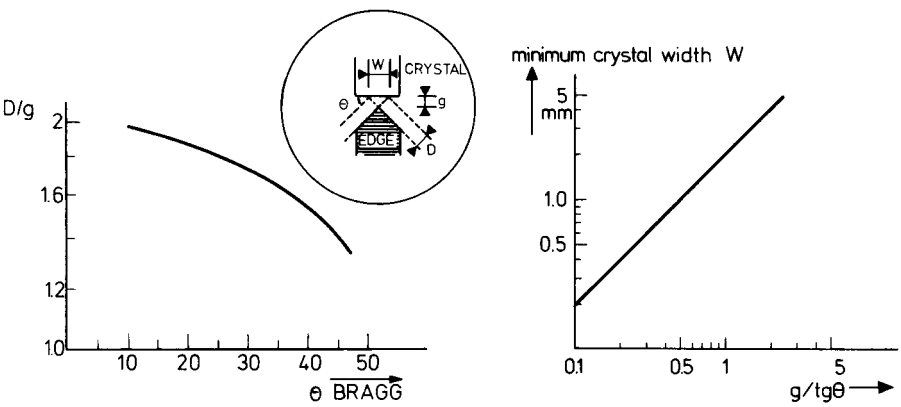

Fig. 3. Variation in diffracted beam width as a function of diffraction angle.

Fig. 4. Minimum crystal width as a function of slit width and angle of diffraction.

tan θ/g = 0.24) indicated, as expected, no change in diffracted intensity. For the 1-mm crystal, however, the background was considerably higher; this is probably due to increased scatter from the surrounding aluminium holder.

INVESTIGATION OF DIFFERENT CRYSTALS

It has already been mentioned that the Seemann geometry "sees" only a fraction of the total sample area [1, 2]. It is thus necessary to maximize the reflected intensity and resolution and to minimize the background. The following crystals were tested: topaz 303 ($2d$ = 2.712 Å), GaAs 220 ($2d$ = 3.9974 Å), four specimens of LiF 200 ($2d$ = 4.028 Å), GaAs 111 ($2d$ = 6.5278 Å), quartz 1011 ($2d$ = 6.687 Å). The width of all crystals was 5mm and the height 20 mm, except for the gallium arsenide crystals which were 16 mm high. The slit width in all measurements was 0.2 mm. Table 3 summarizes the Cu K_α peak and background intensities, *P/BG* ratio and full width at half maximum (*FWHM*).

Topaz and GaAs 220 can be ruled out immediately by their low reflected intensities and unfavourable *P/BG* ratios. LiF 200 shows a large variation in reflected intensity depending strongly on the surface treatment of the crystal. The first lithium fluoride crystal was not further used as its rocking curve for Cu K_α radiation, as measured with a double crystal spectrometer, was very broad.

The other three lithium fluoride crystals had been given various surface treatments. Although no details were given by the manufacturer, it appeared that the amount of surface treatment decreased from LiF/1 up to LiF/3. The rocking curve for LiF/3 had a *FWHM* of 50 s. Quartz yielded fairly good results, albeit with a lower resolution and a somewhat lower reflected Cu K_α intensity than lithium fluoride. GaAs 111 gave extremely good resolution (the rocking curve had a *FWHM* of 10 s), a good *P/BG* ratio and an acceptable intensity of reflected Cu K_α radiation.

TABLE 3

Peak characteristics for different crystals

Crystal	Peak (s^{-1})	*BG* (s^{-1})	*P/BG*	*FWHM* (mm)
Topaz	14.8	4.4	3.4	0.84
GaAs 220	34.4	2.7	12.5	0.70
LiF 200	637.7	45.1	14.1	0.77
LiF/1	462.8	23.3	19.8	0.87
LiF/2	235.0	9.2	25.5	0.81
LiF/3	158.5	7.2	22.1	0.65
GaAs 111	162.2	4.6	35.5	0.58
quartz	131.6	5.7	23.0	0.68

From the data in Table 3, it follows that LiF/3 (with the least surface treatment) and GaAs 111 yield comparable values of reflected intensities and *FWHM*. The *P/BG* ratio is better for GaAs 111. The angle of diffraction for a given element, however, is smaller than for LiF; this is a small disadvantage.

Improving the quality of the crystal hardly seems feasible, and any improvement in the *P/BG* ratio would have to come either from a reduction of the background or from an increase in the diffracted intensity. In 1937, Fankuchen proposed [5] the interesting possibility of using a crystal with a surface at a slight angle τ to the diffracting planes. It can easily be shown that the width of the diffracted beam is reduced by a value f (compared to the incident beam width) given by $f = \sin(\theta + \tau)/\sin(\theta - \tau)$ (see Fig. 5). This reduction is not constant for all diffracted wavelengths, as is shown in Fig. 5, where f vs.θ. is plotted. Physically it means that a larger width (i) from the sample is analysed (and compressed) into a smaller width (o) after diffraction. Measurements with the LiF 200 crystal showed that the use of such a crystal ($\tau = 10°$) gave an increase in diffracted intensity. This treatment caused quite considerable deterioration of the crystal surface since the *FWHM* increased. It is not impossible, however, that better surface treatment could improve the results. Furthermore, because of the various components of background radiation, it is not easy to predict the influence of this "concentration" on the diffracted background intensity.

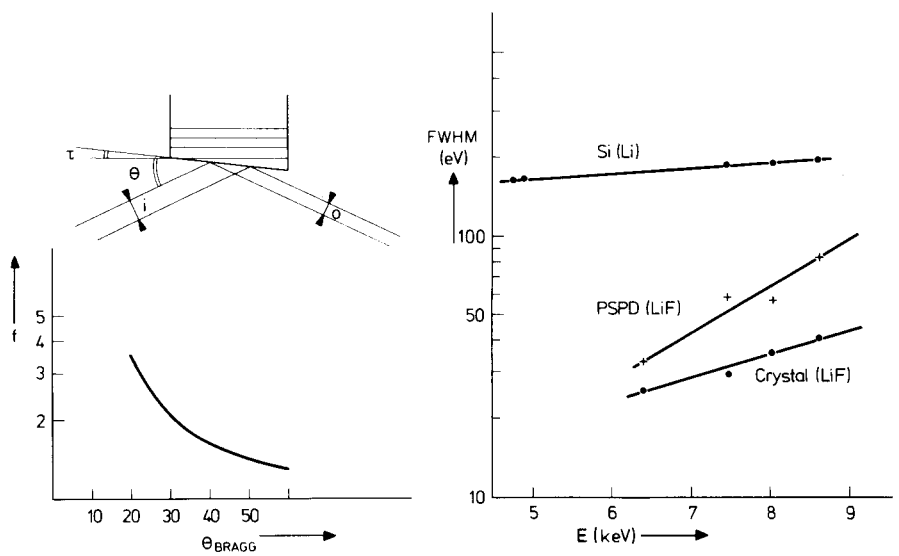

Fig. 5. Principle of Fankuchen crystal and increase of analysed surface as a function of diffraction angle ($\tau = 10°$).

Fig. 6. *FWHM* (in eV) for Si(Li), Seemann and wavelength-dispersive spectrometers. For conversion of *FWHM* (mm) of PSPD into *FWHM* (eV) see [2].

In view of the results obtained with quartz, LiF/3 and GaAs 111, these crystals were examined in more detail.

Lithium fluoride, gallium arsenide and quartz crystals

Two series of measurements were made. In the first the slit width was varied and a copper sample was used. The results are given in Table 4. In the second series the slit width was fixed at 0.2 mm and various elements (thick samples) were measured. Since a linear PSPD was used, these measurements required repositioning of the detector for each element. The results of these measurements are summarized in Table 5. In both sets of measurements the wedge-shaped collimator was in place.

The results show that the peak and background count rates and the *FWHM* increase continually with increasing slit widths. However, beyond a slit width of 0.2 mm, the background increases faster; this is reflected in the *P/BG* ratio, which tends to decrease. The slit width, therefore, was fixed at 0.2 mm for the measurements with different elements.

The increase followed by a decrease of the peak count rate in going from chromium to germanium is simply due to the 20-keV excitation condition. Unfortunately, on average, the *FWHM* increases from chromium to germanium according to $D/g = 2 \cos \theta$. There is no simple explanation for the apparent random variation of the *FWHM*: the standard deviation of these measurements was 0.02 mm.

TABLE 4

Peak characteristics with varying slit width[a]

	Slit width (mm)				
	0	0.1	0.2	0.3	0.4
Lithium fluoride					
P (s^{-1})	84.3	199.5	241.4	349.9	503.2
BG (s^{-1})	3.6	7.3	9.1	13.8	19.3
P/BG	23.6	27.2	26.5	25.4	26.0
FWHM (mm)	0.60	0.62	0.71	0.84	0.94
Gallium arsenide					
P (s^{-1})	23.3	97.0	162.2	230.7	283.1
BG (s^{-1})	0.8	2.9	4.6	6.8	8.6
P/BG	28.4	33.7	35.5	34.1	32.8
FWHM (mm)	0.45	0.49	0.58	0.76	0.88
Quartz					
P (s^{-1})	27.0	205.1	391.9	581.8	719.0
BG (s^{-1})	1.3	9.2	17.5	27.5	34.2
P/BG	21.6	22.4	22.4	21.2	21.0
FWHM (mm)	0.61	0.62	0.66	0.76	0.83

[a] P = count rate of Cu K_α line; BG = background count rate under the Cu K_α line.

TABLE 5

Peak characteristics with fixed slit width for different elements[a]

	Cr	Fe	Ni	Cu	Zn	Ge
Lithium fluoride						
P (s^{-1})	8.5	52.4	290.7	202.3	304.2	211.6
BG (s^{-1})	0.8	2.6	11.1	8.1	12.0	13.8
P/BG	11.3	20.0	26.2	24.9	25.4	15.3
FWHM (mm)	0.64	0.67	0.84	0.69	0.86	0.81
Gallium arsenide						
P (s^{-1})	14.1	66.9	141.1	117.0	93.7	42.2
BG (s^{-1})	1.1	2.5	3.8	3.0	3.3	4.7
P/BG	13.3	26.7	37.7	38.4	28.6	9.0
FWHM (mm)	0.55	0.56	0.66	0.54	0.68	0.68
Quartz						
P (s^{-1})	40.1	169.0	257.8	205.1	198.8	102.9
BG (s^{-1})	2.5	8.4	11.7	9.2	10.5	6.8
P/BG	16.1	20.2	22.1	22.4	18.9	15.2
FWHM (mm)	0.51	0.50	0.80	0.62	0.58	0.67

[a] P and BG as in Table 4.

The best P/BG ratios and the lowest *FWHM* are obtained with gallium arsenide. Unfortunately, the count rate is lower than with lithium fluoride or quartz. Since gallium arsenide and quartz have virtually the same $2d$ value, the former is to be preferred because of its better P/BG and *FWHM* values. To make a definite choice between lithium fluoride and gallium arsenide is not easy and will probably have to await an overall comparison with a curved detector.

COMPARISON WITH OTHER X-RAY FLUORESCENCE SYSTEMS

For general purposes, the Seemann spectrometer equipped with a PSPD will never be able to compete with the classical wavelength-dispersive spectrometer owing to the inherent fact that only a fraction of the irradiated surface is analysed. The wavelength-dispersive spectrometer has a very high P/BG ratio; for example, at 20 keV copper had a P/BG value of 500 with a LiF 200 crystal and a 160-μm spaced collimator. In an energy-dispersive spectrometer, the P/BG was 60 (also measured at 20 keV, with tungsten as the secondary fluorescer) as against 35 in the Seemann spectrometer (GaAs crystal). It is quite possible that further developments may improve this situation.

The main advantage of the Seemann spectrometer, however, lies in its very good resolution. This can be seen in Fig. 6, where the resolution (in eV) is given for the three types of spectrometer for iron, nickel, copper and

zinc. Furthermore the Seemann spectrometer equipped with a PSPD does not require any moving parts or liquid nitrogen cooling.

To measure simultaneously over a wide range of energies, a curved detector is necessary because the incident characteristic radiation must be perpendicular to the anode wire [2] (see also Fig. 2b).

No curved detector with a SiO_2(C) anode has yet been built. It is quite likely that technical problems in accurately suspending such a thin wire will not be easy to solve. A much more elegant solution would be to use a multi-wire detector with the single anode replaced by a set of parallel wires, i.e., the set of wires is perpendicular to the plane of Fig. 2(a, b) and thus parallel to the slit. Such a detector would allow an enormous increase in count rate, something which is not feasible with the slow electronics at present in use. However, this is not the only possible solution. Progress being made in position-sensitive detectors of all kinds (as developed in high-energy physics) will doubtless allow other approaches [6]. Recently [6], a simple single-wire PSPD has been described, where the anode is held in place by a magnetic field. The position determination is somewhat different from that described above, but allows a higher count rate.

REFERENCES

1 E. Bruninx, Spectrochim. Acta, Part B, 31 (1976) 221.
2 E. Bruninx, Phil. Res. Repts., 32 (1977) 253.
3 C. Borkowski and M. Kopp, Rev. Sci. Instrum., 39 (1968) 1515.
4 M. L. Verheijke, J. Radioanal. Chem., 10 (1972) 299.
5 I. Fankuchen, Nature, 139 (1937) 193.
6 See, e.g., Proc. Wire Chamber Conference, Vienna, 1978, Nucl. Instrum. Methods, 156 (1978) 1—354.

Analytica Chimica Acta, 113 (1980) 107—112

BIOTIN-BESTIMMUNG IN LEBERGEWEBE NACH DEM PRINZIP DER ISOTOPEN-VERDÜNNUNGSANALYSE

R. RETTENMAIER

Abteilung für Vitamin- und Ernährungsforschung, F. Hoffmann-La Roche & Co. AG, Basel (Schweiz)

(Eingegangen am 9. Juli 1979)

SUMMARY

Radioligand assay for biotin in liver tissues

A radioligand assay for biotin in liver tissue is described. ^{3}H-biotin is used as tracer and avidin as binder. The biotin-loaded avidin is separated from free biotin on dextran-coated charcoal, which leaves the avidin—biotin complex in the supernatant liquid. Thus, the avidin—biotin complex can easily be utilized for determination of the radioactivity. Calibration with known additions of biotin in the range 0.25—8.0 ng per assay sample yields a linear logit-log plot. The biotin is extracted from liver tissues by enzymatic proteolysis with papain. This treatment is optimized to liberate the bound forms of the vitamin. Microbiological parallel assays with *Lactobacillus plantarum* were in good agreement with the radioligand assay giving a regression coefficient of 0.974 (n = 44). The coefficient of variation was found to be 4.2% in the range 500—1200 ng of biotin per g of liver tissue (n = 46). The method is simple and reliable and allows the simultaneous analysis of a considerable number of samples.

ZUSAMMENFASSUNG

In der beschriebenen Methode werden ^{3}H-Biotin als Tracer und Avidin als Binder verwendet. Das im Probenmaterial gebunden vorliegende Biotin wird enzymatisch mit Papain freigesetzt. Die Methode, deren Anwendungsbereich sich auf Lebern beschränkt, ist einfach und zuverlässig und ermöglicht einen erheblichen Probendurchsatz.

Die gebräuchlichsten Biotin-Bestimmungsmethoden sind mikrobiologischer Art [1–5]. In den letzten Jahren wurden jedoch verschiedene Analysenmethoden für Biotin beschrieben, die von der Bindung an Avidin Gebrauch machen [6–9]. Die hier beschriebene Methode zur Biotin-Bestimmung in Lebern beruht auf dem Prinzip der Isotopen-Verdünnungsanalyse unter Ausnützung der starken Bindung von Biotin an Avidin ($K_d = 10^{-15}$ bei pH 7 [10]).

Für diese Biotin-Bestimmung in Lebern muss ebenso wie für die mikrobiologische Bestimmung eine Freisetzung des Biotins, das im Gewebe hauptsächlich gebunden vorliegt [11, 12], erfolgen. Ein Säureaufschluss mit 1 M [5, 8] bzw. 4 M [6] Schwefelsäure im Autoklaven ist unbefriedigend, da keine Reproduzierbarkeit erreicht wird. Dies wurde von unserem mikro-

biologischen Labor bestätigt. Eine mögliche Erklärung hierfür wäre, dass zwar Biotin bei pH 4—9 im Kochprozess stabil ist, doch durch starke Säuren und Laugen zerstört wird [3, 12]. Eine proteolytische Hydrolyse kann bei Lebergewebe mit Papain erreicht werden [12], doch muss eine optimale Papainmenge in bezug zur Lebermenge gefunden werden. Baker und Frank [12] schlagen 100 mg Papain für 5 mg Leberlyophilisat vor. In einer zusammen mit unserem mikrobiologischen Labor durchgeführten Versuchsreihe wurde festgestellt, dass eine Proteolyse mit 50 mg Papain pro 1 g Frischleber eine optimale Biotin-Freisetzung gewährleistet.

Soll nun mittels Radiobiotin und Avidin das Biotin in der Probe ermittelt werden, so ist das an Avidin gebundene Biotin von dem nicht gebundenen abzutrennen.

Vorbehandeltes Bentonit, das grosse Moleküle wie den Avidin—Biotin-Komplex adsorbiert [6, 7], ist hierfür verwendbar. Die erzielten Werte variieren jedoch sehr stark. Eine Proteinfällung mit Zinksulfat—Natronlauge [8] ist pH-abhängig. Auch hier konnte keine zufriedenstellende Reproduzierbarkeit in Serien erreicht werden.

Daraufhin wurde versucht, in Anlehnung an gewisse Radioimmunoassays, die Abtrennung des freien Biotins vom Avidin—Biotin-Komplex mit Dextranbeschichteter Aktivkohle zu erreichen. Vorteilhaft ist hier, dass die so behandelte Kohle nur kleine Moleküle adsorbiert. Der Avidin—Biotin-Komplex bleibt somit im Ueberstand, welcher direkt zur Radioaktivitätsmessung im Flüssigkeitsszintillationszähler verwendet werden kann. Die erzielten Resultate sind gut.

EXPERIMENTELLES

Reagenzien

Zur Herstellung wässriger Lösungen wurde generell doppelt destilliertes Wasser verwendet.

Avidinlösungen. Avidin (Serva; ca. 12 Einheiten mg^{-1}). Für die Stammlösung wird 1 mg Avidin mit 12 Einheiten in 100 ml NaCl (0,9% G/V) gelöst. Dies entspricht 0,12 Einheiten ml^{-1} (bei 4°C lichtgeschützt aufbewahrt, ist diese Lösung 2 Wochen haltbar). Die Arbeitsverdünnung von 0,024 Einheiten ml^{-1} wird vor Gebrauch frisch hergestellt, indem 5 ml der Stammlösung auf 25 ml mit NaCl (0,9% G/V) verdünnt werden.

Biotinlösungen. Zur Herstellung der Stammlösung wird 1 mg ^{3}H-Biotin mit einer spezifischen Aktivität von 13,4 mCi mg^{-1} in 0,5 ml 1%iger Ammoniaklösung vorgelöst und das Volumen mit NaCl (0,9% G/V) und 0,2 ml 1 M HCl auf 100 ml ergänzt. Dies entspricht einer Konzentration von 10 μg ^{3}H-Biotin ml^{-1}. Davon wird eine Arbeitsverdünnung von 3,9 ng ml^{-1} hergestellt, indem man (a) 3,9 ml der Stammlösung auf 100 ml mit NaCl (0,9% G/V) und (b) 1 ml von Lösung (a) auf 100 ml mit NaCl (0,9% G/V) verdünnt.

Für die Stammlösung von d(+)-Biotin werden 10 mg d(+)-Biotin reinst in 1 ml 1%iger Ammoniaklösung vorgelöst und das Volumen mit NaCl (0,9% G/V)

HCl und 0,4 ml 1 M HCl auf 100 ml gebracht. Diese Lösung enthält 100 μg d(+)-Biotin ml^{-1}. Davon werden die Arbeitsverdünnungen (a) von 2,5 ng ml^{-1} und (b) von 20 ng ml^{-1} durch eine Verdünnungsreihe mit NaCl (0,9% G/V) hergestellt.

Dextran-beschichtete Aktivkohle. Gelatine (600 mg; Rousselot A.2.P. Bloom 200) werden in 65 ml Wasser durch leichtes Erwärmen gelöst; 300 mg Dextran T70 [M_w (light scattering) 70 000; Pharmacia] zu der wieder teilweise abgekühlten Gelatinelösung gegeben und gut gemischt, 6 g Aktivkohle (p.a., Merck) unter Rühren zugegeben und das Volumen auf 100 ml mit Wasser ergänzt. Während 1 Std wird die Suspension gerührt. Die Dextran-beschichtete Aktivkohle-Suspension ist 1 Tag vor dem ersten Gebrauch herzustellen. Bei 4°C aufbewahrt, kann sie einen Monat verwendet werden.

Enzymatische Freisetzung des Biotins im Lebergewebe

Frisches oder bis zum Zeitpunkt der Analyse bei −20°C gelagertes und schonend aufgetautes Lebergewebe oder eine grössere Stichprobe aus einer ganzen Leber wird mittels eines Homogenisators zu einem Brei verarbeitet. Zu 1 g homogenem Probenmaterial in einem 20-ml Messkolben werden 10 ml Papainlösung (0,5% G/V) in Citratpuffer pH 5,9 (440 ml 0,01 M Citronensäure + 560 ml 0,021 M Dinatriumhydrogenphosphat) pipettiert und sorgfältig gemischt. Nach Zugabe einiger Tropfen flüchtigen Konservierungsmittels (1 + 1 + 2) Aethylenchlorid—Chlorobenzol—Chlorbutan) werden die verschlossenen Proben während 18 Std bei 37°C inkubiert. Danach ist das Enzym durch Autoklavieren während 10 Min bei 118°C und 1 atm zu desaktivieren. Nach Abkühlen wird das Volumen auf 20 ml mit Wasser ergänzt und durch Faltenfilter (Nr. 597 1/2, Schleicher und Schüll) filtriert.

Zur Ermittlung der Eichkurve wird eine Papain-Aufschlusslösung verwendet. Hierfür wird das Lebergewebe durch Puffer ersetzt.

Für Leberproben mit einem Biotingehalt zwischen 100 und 800 ng Biotin g^{-1} Leber wird das Filtrat direkt für die Isotopen-Verdünnungsanalyse verwendet. Werden höhere Biotinwerte erwartet, so muss das Filtrat 1 + 1 mit NaCl-Lösung (0,9% G/V) verdünnt werden.

Avidin-Bindungsreaktion und Radioaktivitätsmessung

Die Reaktion ist in Plastikröhrchen (11 mm Durchmesser und 50 mm Höhe) nach dem Pipettierschema (dargestellt in Tabelle 1) unter Beachtung der angegebenen Reihenfolge und Wartezeiten durchzuführen. Das verwendete ^{3}H-Biotin muss im geringen Ueberschuss zu dem verwendeten Avidin sein. Die Dextran-beschichtete Aktivkohle ist durch Rühren im Eisbad in Suspension zu halten. Unmittelbar nach Zugabe der Kohlensuspension werden die Proben während 10 Sek auf dem Vortex gut durchgemischt. Anschliessend sind die Proben während 10 Min auf dem Minishaker zu schütteln, um die Kohle in Suspension zu halten. Zur Abtrennung der Kohle zentrifugiert man sodann bei 4°C und 2000 G. Vom Ueberstand wird 1 ml in 10 ml Ria Luma Szintillator (Fakola AG) gegeben und die Radioaktivität während 10 Min im Flüssigkeitsszintillationszähler gemessen.

TABELLE 1

Pipettierschema für die Biotin-Isotopen-Verdünnungsanalyse[a]
(TC = Total Counts; NSB = Unspezifische Bindung (nonspecific binding); MB = Maximale Bindung; E_{1-7} = Eichpunkte; L_1, $L_2 \ldots L_n$ = Leberextrakt 1, 2 ... n, L_1 Rec. = Wiedergewinnung bekannten Zusatzes)

Probe	In n-facher Ausführung	d(+)-Biotin µl	Verd.	ng	NaCl 0,9% (µl)	Papainlösung (µl)	Leberextrakt (µl)	Avidin 0,024 E ml^{-1} (µl)
TC	3	—		—	650	100	—	100
NSB_{E_1}	1	100	a	0,25	400	100	—	—
NSB_{L_1}	1	—		—	500	—	100	—
NSB_{L_n}	1	—		—	500	—	100	—
MB	3	—		—	400	100	—	100
E_1	2	100	a	0,25	300	↓	—	↓
E_2	2	200	↓	0,50	200	↓	—	↓
E_3	2	400	↓	1,00	—	↓	—	↓
E_4	2	100	b	2,00	300	↓	—	↓
E_5	2	200	↓	4,00	200	↓	—	↓
E_6	2	300	↓	6,00	100	↓	—	↓
E_7	2	400	↓	8,00	—	↓	—	↓
L_1	2	—		—	400	—	100	↓
L_1 Rec.	2	100	b	2,00	300	—	100	↓

[a] Vor der Avidinzugabe gibt man zu allen Proben 650 µl der ^{3}H-Biotinlösung (3,9 ng ml^{-1}). Nach Zugabe des Avidins und kurzem mischen auf dem Vortex lässt man die Proben 20 Min bei Zimmertemperatur auf dem Minishaker bei mittlerer Schüttelfrequenz reagieren. Danach gibt man zu allen Proben, ausser den TC-Proben, 250 µl Dextran-beschichtete Aktivkohle und mischt dieselben 10 Sek auf dem Vortex. Nach einer 10-Min Mischperiode auf dem Minishaker werden die Proben 10 Min bei 2000 G und 4°C zentrifugiert. 1 ml des Ueberstandes wird in 10 ml Ria Luma Szintillator gegeben.

Berechnung

Die Auswertung kann über den cpm-Wert der Doppelbestimmung erfolgen, da das "sample channels ratio" (SCR) im allgemeinen konstant ausfällt. Von jeder gemessenen Zählrate wird die durchschnittliche unspezifische Bindung (NSB) abgezogen; diese wird an drei Proben ohne Avidin-Zusatz ermittelt: Unspezifische Bindung der Eichprobe 1 (NSB_{E_1}), unspezifische Bindung der Leberprobe 1 (NSB_{L_1}), unspezifische Bindung der Leberprobe n (NSB_{L_n}).

Die Bestimmung der maximalen Bindefähigkeit (MB) erfolgt dreifach. Die ermittelten cpm-Werte ergeben nach Abzug der NSB die Zählrate B_0, die in Prozent der Gesamtaktivität (TC) ausgedrückt zwischen 80 und 50% liegen sollte.

Die Eichung erfolgt über die bekannten Biotin-Zusätze E_1—E_7, welche im Doppel angesetzt sind. Ihre für NSB korrigierten Zählraten B werden in Prozent der MB ausgedrückt: $B/B_0 \times 100$. Diese Werte liefern im Logit-log-Diagramm eingetragen eine Eichgerade (Ordinate = Logit B/B_0, Abszisse = log Biotinmenge per Probe [13]). Von den unbekannten Proben wird nach Abzug

der NSB die prozentuale Bindung im Verhältnis zur MB (Zählrate B_0) errechnet und der Biotingehalt der Probe von der Logit-log Eichgeraden abgelesen. Ueber die Verdünnung der Aufschlusslösung und die eingesetzte Lebermenge errechnet man den Biotingehalt pro g Leber.

RESULTATE UND DISKUSSION

Bekannte Mengen Biotin werden zu einigen Leber-Aufschlussproben zupipettiert. Die angereicherten Proben werden wie unbekannte Proben gemessen. Eine Wiedergewinnungsrate um 100% lässt auf Abwesenheit von Störfaktoren im Leberextrakt schliessen.

Nach dem von Dörffel [14] beschriebenen Verfahren für Mehrfachbestimmungen wurde die Standardabweichung ermittelt. Sie ergab im Bereich von 500—1200 ng g^{-1} bei 14 Leberproben und 46 Bestimmungen ein s = 42,90 und ein s_r = 4,17.

Der Vorteil der beschriebenen Biotin-Analysenmethode liegt in der Möglichkeit der direkten Radioaktivitätsmessung des an Avidin gebundenen Biotins im Ueberstand, da der Biotin—Avidin-Komplex nicht von der behandelten Kohle adsorbiert wird. Geringfügige Verunreinigungen des Radiobiotins stören die Analyse nicht. Auch die absolute Bindefähigkeit des Avidins muss nicht ermittelt werden, da die ^{3}H-Biotin-Konzentration und die Avidin-Konzentration nicht in die Auswertung miteinbezogen werden.

Sehr wichtig ist dagegen, dass eine gute Reproduzierbarkeit aller Pipettierungen im Analysengang gewährleistet ist. Ferner muss bei der Herstellung der Dextran-beschichteten Aktivkohle der Beschreibung genauestens Folge geleistet werden. Wird dem nicht Rechnung getragen, so kann die Selektivität der Kohle stark verändert sein. Bei neuen Kohlechargen muss eventuell die Kohlenmenge nach oben oder unten angepasst werden, damit man die gleiche Trennleistung erhält.

Eine Kontrolle der Analysengüte stellt die auf TC bezogene MB dar. Diese Grösse sollte nicht unter 50% liegen. Ist die MB $<$ 50%, so hat entweder die Avidinlösung durch Alterung nicht mehr die notwendige Bindefähigkeit, oder das ^{3}H-Biotin ist durch radioaktive Zerfallsprodukte so stark verunreinigt, dass der notwendige geringe Ueberschuss von ^{3}H-Biotin gegenüber Avidin nicht mehr besteht.

Die NSB sollte, bezogen auf TC, $\leqslant$ 4% und innerhalb einer Probenserie etwa gleich gross sein. Die optimale Papainmenge für den Aufschluss ist 50 mg g^{-1} Frischleber. Bei grösseren Mengen Papain wird die NSB $>$ 4% und variabel. Bei 1000 mg Papain g^{-1} Leber ist eine Auswertung nicht mehr möglich. Bei kleineren Papainmengen sinken die Bestimmungswerte (Tabelle 2).

Mit der beschriebenen Biotin-Bestimmungsmethode wurde die von der Mikrobiologie vorgeschlagene optimale Menge Papain von 50 mg zur Hydrolyse von 1 g Frischleber bestätigt (Tabelle 2).

Parallel mit der Mikrobiologie durchgeführte Biotin-Bestimmungen in Lebern ergaben eine gute Uebereinstimmung der Methoden. Die Berechnung

TABELLE 2

Ermittelter Biotingehalt bei Verwendung verschiedener Mengen Papain zur Leberproteolyse

mg Papain/g Leber	*n* Proben	ng Biotin/g Leber Isotopen-Verdünnungsmethode	*n* Proben	ng Biotin/g Leber *L. plantarum*
0	2	527 (515—540)	4	482 (429—599)
5	3	1070 (1060—1140)	5	1081 (901—1280)
25	1	1180	4	1125 (1073—1150)
50	11	1198 (1080—1380)	7	1180 (1045—1346)
100	3	1150 (1140—1160)	5	1108 (903—1312)
200	2	1050 (1000—1100)	3	979 (873—1126)
300	4	1000 (870—1080)	4	914 (707—1025)
500	4	953 (764—1300)	8	778 (568—944)
1000	—	— nicht auswertbar	3	647 (625—659)

der Regression, y = Werte aus der Isotopenverdünnungsanalyse, x = Werte aus mikrobiologischen Bestimmungen, ergab die Beziehung $y = 92{,}44 + 0{,}96x$ mit dem Regressionskoeffizienten von 0,974 bei 44 Bestimmungen im Bereich von 500—1300 ng g^{-1} Lebergewebe.

Für die Herstellung von ^{3}H-Biotin mit hoher spezifischer Aktivität möchte ich Herrn Dr. Würsch, Abt. Zentrale Forschungseinheit und für die Durchführung der mikrobiologischen Biotin-Bestimmungen Frl. Engler, Abt. für Vitamin- und Ernährungsforschung der F. Hoffmann-La Roche danken.

LITERATUR

1 E. E. Snell, R. E. Eakin und R. J. Williams, J. Am. Chem. Soc., 62 (1940) 175.
2 D. S. Genghof, C. W. H. Partridge und F. H. Carpenter, Arch. Biochem., 17 (1948) 413.
3 G. Semenza, L. S. Prestige, D. Menard-Jeker und M. Bettex-Galland, Helv. Chim. Acta, 42 (1959) 669.
4 C. M. Baugh, J. H. Malone und C. E. Butterworth, Am. J. Clin. Nutr., 21 (1968) 173.
5 H. N. Bhagavan und D. B. Coursin, Am. J. Clin. Nutr., 20 (1967) 903.
6 K. Dakshinamurti, A. D. Landman, L. Ramamurti und R. J. Constable, Anal. Biochem., 61 (1974) 225.
7 A. D. Landman, Int. J. Vit. Nutr. Res., 46 (1976) 310.
8 R. L. Hood, J. Sci. Food Agric., 26 (1975) 1847.
9 H. R. Schroeder, P. O. Vogelhut, R. J. Carrico, R. C. Boguslaski und R. T. Buckler, Anal. Chem., 48 (1976) 1933.
10 N. M. Green, Biochem. J., 89 (1963) 599.
11 J. Pispa, Ann. Med. Exptl. Biol. Fenn., 43, Suppl. 5 (1965) 6.
12 H. Baker und O. Frank, Clinical Vitaminology, Methods and Interpretations, Interscience-Wiley, New York, 1968, p. 22.
13 H. Feldman und D. Rodbard, aus W. D. Odell und W. H. Daughaday (Eds.), in Principles of Competitive Protein-Binding Assay, Lippincott, Philadelphia, Toronto, 1971, p. 158.
14 K. Dörffel, Fresenius Z. Anal. Chem., 185 (1962) 1.

Analytica Chimica Acta, 113 (1980) 113—122

SPECTROPHOTOMETRIC DETERMINATION OF TRACE AMOUNTS OF THALLIUM(III) AND GOLD(III) BY QUANTITATIVE OXIDATION OF 3-CARBOXYMETHYLTHIO-1,5-DIPHENYLFORMAZAN

ALAN T. HUTTON* and HARRY M. N. H. IRVING

Department of Analytical Science, University of Cape Town, Rondebosch 7700 (South Africa)

(Received 10th July 1979)

SUMMARY

The carboxylic proton of 3-carboxymethylthio-1,5-diphenylformazan is so strongly internally hydrogen-bonded that metal complexes cannot be prepared even under forcing conditions. In contrast, the orange-red reagent (ϵ_{max} = 2790 m^2 mol^{-1} at 420 nm) is oxidized stoicheiometrically by one equivalent of thallium(III) or gold(III) to the water-soluble 5-carboxymethylthio-2,3-diphenyltetrazolium salt which does not absorb in the visible region. A sensitive spectrophotometric method for the determination of Tl^{3+} or Au^{3+} in the range 0.1—5.0 ppm is proposed. Interferences are discussed and attempts to adapt the procedure to quantitative chromatography on solid supports are briefly reported.

3-Carboxymethylthio-1,5-diphenylformazan (I; HL) is a deeply coloured red compound (ϵ_{max} = 2790 m^2 mol^{-1} at 420 nm) originally prepared as a potential terdentate ligand coordinating through oxygen, nitrogen, and sulphur [1]. It proved to have most unexpected properties [2]. The presence of a novel type of internal hydrogen bond involving the carboxylic proton and the quasi-aromatic formazan ring (as in II) has been shown [3, 4] to account for the exceptionally low basicity for which $pK_1 = -\log([H^+][HL]/[H_2L^+]) = -0.43 \pm 0.04$ and the unusually low acidity for which $pK_2 = -\log([H^+][L^-]/[HL]) = 12.48 \pm 0.05$ at an ionic strength of 1.0 M (NaCl). These data explain why the formazan (I) exists effectively in the formally neutral form, HL, at least to 90% over the pH range 1—11 and is only extractable from a solution in an organic solvent such as chloroform by very strong acid or very strong alkali. Since the carboxyl group remains undissociated over such a wide pH range, it is scarcely surprising that only small, and analytically unserviceable, changes in absorption spectrum take place when an aqueous solution of the formazan (I) is mixed with excess of most metal ions. Although the biggest changes are obtained with Cu^{2+}, Ag^+, and Pt^{2+}, where the peak at 420 nm gives way to a broad absorption at ca. 500 nm, no solid metal complexes could be isolated either from aqueous solutions or from solutions in ethanol, acetone, or dimethylsulphoxide, even when attempts were made to break the intramolecular

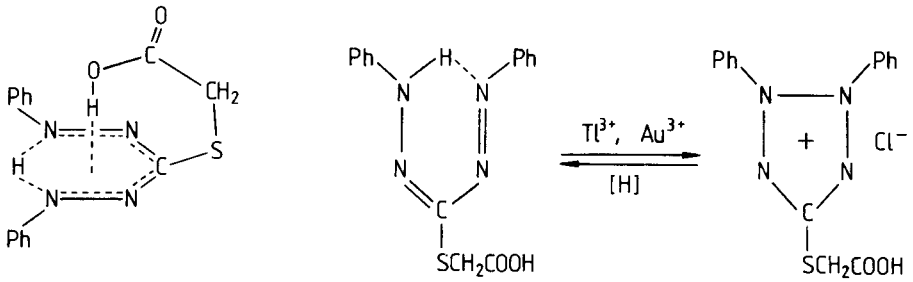

(II) (I) (III)

hydrogen bond by the addition of such bases as pyridine, triethylamine, or sodium ethoxide.

Reactions of a yellow ethanolic solution of the formazan (I; ca. 4×10^{-4} M) towards some 30 metal cations at concentration levels of 0.01, 0.1, and 1.0 M were studied in neutral, acidic, and alkaline solutions. No detectable colour changes were noted with K^+, Be^{2+}, Mg^{2+}, Ca^{2+}, Ba^{2+}, Fe^{2+}, Co^{2+}, Ni^{2+}, Zn^{2+}, Cd^{2+}, Pb^{2+}, Al^{3+}, Ga^{3+}, In^{3+}, Cr^{3+}, Ru^{3+}, Sb^{3+}, Bi^{3+}, and La^{3+}, whereas slight changes were detected with Cu^{2+} (brown), Ag^+ (pink), Pt^{2+} (orange), Pd^{2+} (pink), Hg^{2+} (orange), and Sn^{4+} (orange). No complexes extractable into chloroform were formed under any conditions [1].

However, Tl^{3+} and Au^{3+} behaved exceptionally in that they completely bleached the yellow colour of the formazan (I) either to give colourless metal complexes or to give a colourless oxidation product of the formazan or perhaps a colourless metal complex derived from it. It was shown that the colourless solution produced by excess of Tl^{3+} contained the 5-carboxymethylthio-2,3-diphenyltetrazolium chloride (III) previously prepared by Ogilvie and Corwin [5] : this has a single absorption band at 260 nm (ϵ_{max} = 800 m^2 mol^{-1}).

Although reducing agents such as sulphite and hydroxylamine have no effect on the tetrazolium salt (III), an alkaline solution of dextrose regenerates the coloured formazan (I). Subsequent experiments showed the process to be substantially stoicheiometric since after a known amount of (I) had been oxidized with an excess of Tl^{3+}, reduction by alkaline dextrose regenerated over 96% of the original 3-carboxymethylthio-1,5-diphenylformazan (I). Spectrophotometric measurements established that the tetrazolium cation (as III) did not form complexes with either thallium(I) or thallium(III) in 30-fold excess unless these are very weak. It was similarly shown that the formazan (I) did not give a complex in solution with even an 8-fold excess of thallium(I).

Spectrophotometric determination of thallium(III)

The stoicheiometry of the reaction between the formazan (I) and thallium-(III) was established by a photometric titration (Fig. 1). The absorption of

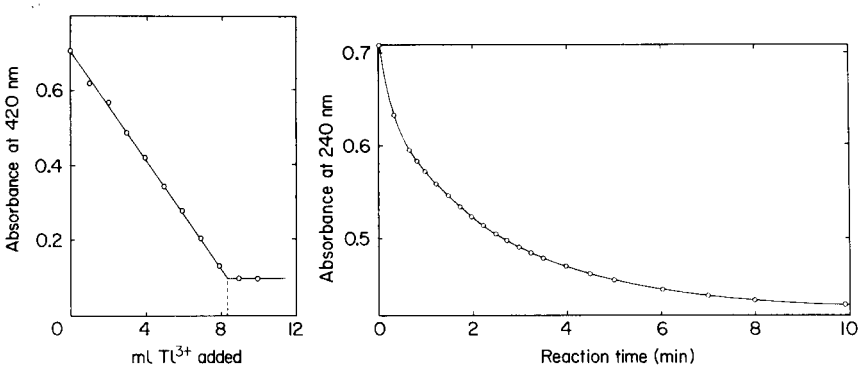

Fig. 1. Photometric titration at 420 nm of the formazan (I) (0.5 cm^3 of 4.391×10^{-4} M) with varying amounts of 3.034×10^{-5} M thallium(III). The total volume of the medium (5% ethanol—95% water) was maintained at 10 cm^3. At the end-point 8.40 cm^3 had been added corresponding to the ratio [formazan]: [thallium(III)] = 1.0 : 1.1.

Fig. 2. The progress of the oxidation of a mixture of the formazan (I) (0.5 cm^3 of 4.391×10^{-4} M) and thallium(III) (9.5 cm^3 of 3.034×10^{-5} M) in neutral aqueous solution. Photometric measurements were made at 420 nm in 1-cm cells.

the formazan at 420 nm decreased monotonically in proportion to the amount of thallium(III) added until one equivalent had reacted, whereafter the absorbance remained constant. Simultaneous measurement of the absorption spectra showed only the decrease in the absorption at 420 nm: no new bands appeared. These results point to the reaction

$$Tl^{3+} + \text{formazan (I)} + Cl^- \rightarrow Tl^+ + \text{tetrazolium chloride (III)} + H^+ \qquad (1)$$

However, this reaction does not take place rapidly and it appears from Fig. 2 that 10 min should be allowed for oxidation to be completed.

For the determination of thallium(III) in the range 0—5 ppm, a standard curve was constructed by using 0.5 cm^3 of standard formazan (4.414×10^{-4} M) made up to 10.0 cm^3 with water in the reference cell (placed in the sample beam of the spectrophotometer) and 0.5 cm^3 of standard formazan, x cm^3 of thallium(III) (3.175×10^{-5} M), and $(9.5 - x)$ cm^3 of water in the sample cell (placed in the instrument reference beam). In this way, as x increased, the net absorbance at 420 nm (1-cm cells) increased from zero to a maximum (when $x \approx 8$ cm^3) and thereafter remained constant. The calibration curve passed through the origin and was linear up to at least $x = 7.5$ cm^3, equivalent to 5 ppm thallium(III). This procedure also compensates for any coloured impurities in the formazan reagent which might not be oxidized by the thallium(III).

Concentrations of thallium(III) may then readily be determined down to 0.2 ppm, which represents a considerable improvement on a recent and less selective determination of thallium(III) as the ternary complex $[Tl(SCN)_2(\text{pyridine})_2]^+$ which is recommended for the range 20—300 ppm [6].

Oxidation by the couple Tl^{3+}/Tl^{+} ($E^0 = +1.25$ V) is involved in this reaction. A survey of a table of standard oxidation—reduction potentials [7] shows that a very similar reaction would certainly occur with gold(III) [$E^0(Au^{3+}/Au^{+}) = +1.29$ V] and presumably with more powerful oxidants such as Ce^{4+}, Ag^{2+}, and $S_2O_8^{2-}$ and possibly even with couples of lower oxidizing potential such as Fe^{3+}/Fe^{2+}, for which $E^0 = +0.77$ V.

A study of interferences (Table 1) shows that 30-fold amounts of Na^+, K^+, NH_4^+, Tl^+, Mg^{2+}, Ca^{2+}, Sr^{2+}, Ba^{2+}, Mn^{2+}, Fe^{2+}, Co^{2+}, Ni^{2+}, Zn^{2+}, Cd^{2+}, Sn^{2+}, Pb^{2+}, Al^{3+}, Ga^{3+}, In^{3+}, La^{3+}, Gd^{3+}, Sb^{3+}, and Bi^{3+} do not interfere. Interference through oxidation of the formazan increases in the order VO^{2+}, Ce^{4+}, UO_2^{2+}, Fe^{3+}, Au^{3+}, and Sn^{4+}, whereas interferences caused possibly by complexation increase in the order Hg^{2+}, Pt^{2+}, Ag^{+}, Pd^{2+}, and Cu^{2+}. Among anions, Cl^-, Br^-, NO_3^-, SO_4^{2-}, CO_3^{2-}, PO_4^{3-}, and acetate do not interfere, whereas the interferences of I^-, CN^-, and EDTA are serious as expected, as are those of oxidizing anions such as MnO_4^-, CrO_4^{2-}, $Cr_2O_7^{2-}$, and $S_2O_8^{2-}$.

Spectrophotometric determination of gold(III)

That gold(III) might be determined selectively and in low concentrations

TABLE 1

Effect of diverse ions on the spectrophotometric determination of 2.92 ppm Tl^{3+} by oxidation of the formazan (I)
(Unless otherwise indicated, 100 ppm of the added ion was present[a]. Details are given in the Experimental section.)

Ion added	Tl^{3+} found (ppm)	Ion added	Tl^{3+} found (ppm)	Ion added	Tl^{3+} found (ppm)
—	2.91	Cd^{2+}	2.81	VO^{2+}	3.21
—	2.87	Hg^{2+}	2.12	VO^{2+c}	3.18
Na^+	2.91	Hg^{2+c}	2.37	UO_2^{2+}	3.72
K^+	2.84	Sn^{2+}	3.00	Cl^-	2.87
NH_4^+	2.92	Pb^{2+}	2.83	Br^-	2.77
Ag^+	1.04	Pd^{2+}	0.93	I^-	1.93
Tl^+	2.83	Pt^{2+}	1.30	I^{-c}	2.38
Tl^{+b}	2.76	Fe^{3+}	3.86	NO_3^-	2.91
Mg^{2+}	2.92	Au^{3+}	4.14	SO_4^{2-}	2.85
Ca^{2+}	2.88	Al^{3+}	2.92	CO_3^{2-}	2.88
Sr^{2+}	2.96	Ga^{3+}	2.74	PO_4^{3-}	2.81
Ba^{2+}	2.90	In^{3+}	2.84	CH_3COO^-	2.84
Mn^{2+}	2.84	Sb^{3+}	2.78	CN^{-b}	2.37
Fe^{2+}	2.83	Bi^{3+}	2.81	CN^-	2.63
Co^{2+}	2.82	La^{3+}	2.97	CN^{-c}	2.91
Ni^{2+}	2.76	Gd^{3+}	2.85	$EDTA^b$	1.34
Cu^{2+}	0.84	Sn^{4+}	4.19	EDTA	1.54
Zn^{2+}	2.84	Ce^{4+}	3.66	$EDTA^c$	2.17

[a]Trace amounts of MnO_4^-, CrO_4^{2-}, $Cr_2O_7^{2-}$, and $S_2O_8^{2-}$ interfered seriously. [b]10^3 ppm added ion present. [c]10 ppm added ion present.

in the same way as thallium(III) was next examined in some detail. A spectrophotometric titration resembled that with thallium(III) (cf. Fig. 1) and indicated a reacting ratio [formazan]: [gold(III)] = 1.0:0.9. When a known amount of formazan was first oxidized with gold(III) in slight excess to the tetrazolium salt (III), reduction with alkaline glucose gave only an 89% recovery. Nevertheless, simultaneous measurement of absorption spectra (Fig. 3) showed definite isosbestic points and no other coloured by-products would appear to have been formed. Reference to standard oxidation—reduction potentials [7] indicates that the couple Au^{3+}/Au ($E^0 = +1.50$ V) is a more powerful oxidant than Au^{3+}/Au^{+} ($E^0 = +1.29$ V) whereas the couple $AuCl_4^-/Au$, $4Cl^-$ is less powerful ($E^0 = +1.00$ V). If the reaction with the formazan proceeded exclusively with reduction to elementary gold (rather than to Au^+) the equation would be

$$\tfrac{2}{3}Au^{3+} + \text{formazan (I)} + Cl^- \rightarrow \tfrac{2}{3}Au + \text{tetrazolium chloride (III)} + H^+ \qquad (2)$$

Comparison with the stoicheiometry proposed in eqn. (1) indicates that any contribution by this reaction would lead to a molar ratio [formazan] : [gold(III)] $> 1:1$. The actual ratio found was 1.0:0.85.

The oxidation of the formazan by gold(III) was noticeably slower (30 min for complete reaction) than with thallium(III) under the same conditions but it was greatly accelerated by adding hydrochloric acid (Fig. 4). The optimum concentration was found to be between 0.02 and 0.05 M HCl wherein the reaction was complete after 1 min. However, acidity (or chloride ion concentration) is not critical and 3 min suffices if hydrochloric acid is present in the range 10^{-5}—2.5×10^{-1} M. Moreover, in the presence of hydrochloric acid the reaction appears to be less complex, for the stoicheiometry [formazan] :

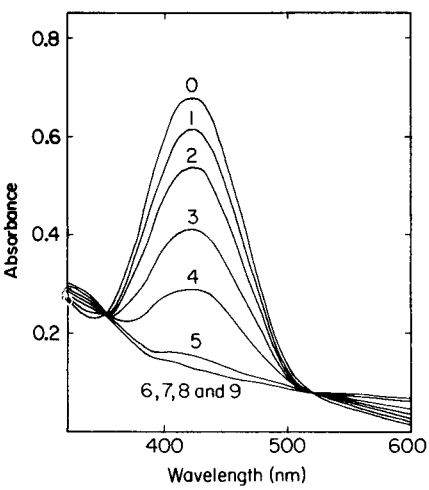

Fig. 3. Absorption spectra of mixtures of x cm^3 of 3.668×10^{-5} M gold(III), 0.5 cm^3 of 4.391×10^{-4} M formazan (I), and $(9.5 - x)$ cm^3 water. The value of x is given for each curve.

[gold(III)] now becomes 1.0 : 0.94. The standard curve is linear and passes through the origin and is suitable for the spectrophotometric determination of gold in the range 0.1—4.0 ppm. A typical calibration curve, similar to that described for thallium(III), is shown in Fig. 5.

Applications

Since In^{3+} does not oxidize the formazan (I), the determination of trace thallium (10^{-5}—10^{-6}%) in indium prepared for semiconductor purposes could be carried out by the present method, thus avoiding the need for separation from the major constituent indium by liquid—liquid extraction prior to a spectrophotometric determination with Brilliant Green. Marczenko et al. [8] removed interference by gold by a preliminary reduction with metallic copper before extracting the thallium as $TlCl_4^-$ into di-isopropyl ether from 6 M HCl. This method of eliminating gold (by adding copper wire and 6 M HCl and taking to dryness followed by reoxidation of thallium(I) with bromine water and destroying excess with phenol) can be used in the present procedure. However, cyanide ions in moderate concentration do not interfere with the determination of thallium(III) by the present method (Table 1) although they completely inhibit interference by Au^{3+}, which forms the very stable complex $Au(CN)_4^-$ ($\log \beta_4 \approx 56$), and interference by Hg^{2+} is masked at the same time by the formation of $Hg(CN)_4^{2-}$ ($\log \beta_4 \approx 41$), despite the fact that the thallium complex is also very stable ($\log \beta_4$ for $Tl(CN)_4^- \approx 35$) [9].

A good deal of effort has recently been devoted to procedures in which an analytical reagent is supported on a permeable matrix as a chromato-

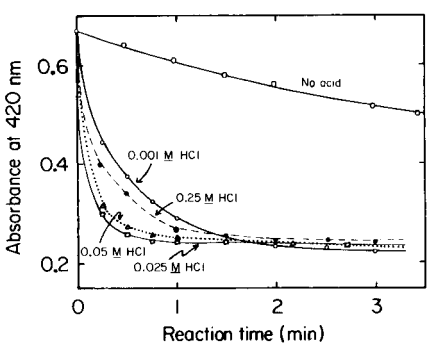

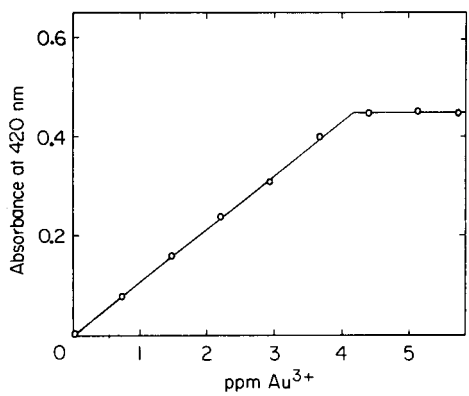

Fig. 4. Curves showing the rate of oxidation of 0.5 cm^3 of 4.391×10^{-4} M formazan by 9.5 cm^3 of 3.668×10^{-5} M gold(III) in hydrochloric acid of various concentrations.

Fig. 5. Standard curve for the reaction of 2.195×10^{-5} M aqueous formazan (I) with aqueous gold (III) solutions. The reference cell contained 2.195×10^{-5} M formazan and measurements were made in 1-cm cells at 420 nm.

graphic column. Passage of a suitable ion would then produce a differently coloured reaction zone of length proportional to the concentration of the analyte. For example, a column packed with gel beads impregnated with zinc dithizonate changes from pink to green when an acidic solution passes down it, but to orange if this contains mercury(II) [10]. Various types and grades of Merckogels, silica gels, Biogels, and Sephadex gels were tried as supports for the formazan (I) but when used as column material the reagent washed out too readily. Braun and Farag [11—13] have achieved striking results with "Chromofoams" [11], prepared by immobilizing a chromogenic organic reagent in a plasticized open-cell polyurethane foam which, when packed into columns, can be used for the determination of cations at ppm levels by passing sample solutions at flow rates as high as 10—15 cm^3 min^{-1}.

Although a highly coloured and stable Chromofoam was eventually prepared by using a 20% solution of tri-n-butyl phosphate in chloroform saturated with the formazan (I) [14], the concentration of reagent was too high to use in trace metal analysis for either trivalent thallium or gold.

EXPERIMENTAL

Preparation of 3-carboxymethylthio-1,5-diphenylformazan (I)

Sodium metal (0.12 g) was dissolved in dry ethanol (60 cm^3) and dithizone (3-thiol-1,5-diphenylformazan, 1.0 g) was added to give a bright orange solution. Chloroethanoic acid (0.3 g) was added and the solution was boiled under reflux (3 h). Additional chloroethanoic acid (0.2 g) was then added and after heating for a further 1 h the formazan (I) was isolated by pouring the reaction mixture slowly into 300 cm^3 of dilute sulphuric acid (ca. pH 5) with stirring. The fine brown suspension of (I) was extracted with chloroform and the solvent evaporated. The residual oil was taken up in benzene and chromatographed on alumina with benzene—methanol to remove (finally with methanol) an orange-brown band. The remaining stationary brown band was leached out with water, filtered, and just acidified (pH 5) with dilute sulphuric acid. The flocculent brown precipitate was taken up in chloroform, dried over sodium sulphate, and the solvent allowed to evaporate at room temperature. The formazan (I) which remained was recrystallized from aqueous ethanol or (better) benzene—n-hexane as fine brown needles (0.41 g, 33% yield; m.p. 143—145°C decomp.). (Found: C, 57.4; H, 4.5; N, 17.7%. Calc. for $C_{15}H_{14}N_4O_2S$: C, 57.3; H, 4.5; N, 17.8%.)

This procedure is more convenient than that of Ogilvie and Corwin [5] who oxidized dithizone to "dehydrodithizone" (2,3-diphenyl-2*H*-tetrazolium-5-thiolate), reacted this with chloroethanoic acid and reduced the ensuing 5-carboxymethylthio-2,3-diphenyltetrazolium chloride (III) with alkaline dextrose to give the formazan (I) in approximately the same overall yield.

Preparation of 5-carboxymethylthio-2,3-diphenyltetrazolium chloride (III)

Dehydrodithizone (0.95 g), prepared by oxidation of dithizone with

potassium hexacyanoferrate(III) as described by Ogilvie and Corwin [5], was heated under gentle reflux with chloroethanoic acid (0.47 g) and trichloromethane (60 cm^3) for 1 h during which the colour changed from red to violet-green. After treatment with animal charcoal, the solution deposited white crystals of (III) on cooling. These were collected, washed with chloroform and recrystallized from ethanol—diethyl ether (3 + 1) and 1-propanol —diethyl ether (3 + 1) and dried in vacuo over silica gel (1.21 g, 90% yield; m.p. 197—201°C decomp.). (Found: C, 51.45; H, 3.7; N, 16.0%. Calc. for $C_{15}H_{13}N_4O_2SCl$: C, 51.6; H, 3.8; N, 16.1%.)

Preparation of stock solutions of thallium(III) and gold(III)

Solutions of thallium(III) were prepared by adding bromine water to thallium(I) chloride (7.277 mg) dissolved in glass-distilled water (500 cm^3) until faintly coloured and then removing the excess of bromine by adding a crystal of phenol. Dilution to 1 l gave a 3.034×10^{-5} M Tl^{3+} solution. Similar solutions were prepared freshly as required.

Sodium tetrachloroaurate(III) dihydrate (14.591 mg) dissolved in 1 l of glass-distilled water gave a 3.668×10^{-5} M solution of gold(III).

Oxidation of the formazan (I) by thallium(III) or gold(III) and the reduction of the resulting tetrazolium salt (III)

(a) The absorbance of a mixture of stock ethanolic 4.509×10^{-4} M formazan (I) solution (0.5 cm^3), 0.01 M hydrochloric acid (1 cm^3), and water (23.5 cm^3) was found to be 0.222 at 420 nm when 1-cm matched quartz cells were used with glass-distilled water as the reference.

(a) The absorbance of a mixture of stock ethanolic 4.509×10^{-4} M formazan hydrochloric acid (1 cm^3), water (13.5 cm^3), and 3.034×10^{-5} M thallium-(III) (10.0 cm^3) was found to be 0.036 under the same conditions.

(c) Stock formazan solution (0.5 cm^3) and hydrochloric acid (1 cm^3) was first oxidized by thallium(III) solution (10.0 cm^3) and the product reduced by adding excess (5 cm^3) of dextrose in 0.01 M NaOH and the volume made up to 25 cm^3 with water. The absorbance, 0.214, corresponds to a recovery of 96%.

A similar sequence of reactions with 3.668×10^{-5} M gold(III) gave absorbance readings of 0.231, 0.039, and 0.206, corresponding to a recovery of 89%. The spectrum after reduction reproduced that before the oxidation stage.

Photometric titration of the formazan (I) with thallium(III) or gold(III)

The absorbances of mixtures of 0.5 cm^3 of 4.391×10^{-4} M formazan (I), x cm^3 of 3.034×10^{-5} M thallium(III) [or x cm^3 of 3.668×10^{-5} M gold(III)], and $(9.5 - x)$ cm^3 water were measured at 420 nm against water in 1-cm matched quartz cells. Typical results are shown in Fig. 1.

Interaction between the tetrazolium salt (III) and thallium(III) or thallium(I)

A mixture of 1 cm^3 of 8.6×10^{-4} M tetrazolium chloride (III) and x cm^3

of 3.034×10^{-5} M thallium(III) [or 2.0×10^{-4} M thallium(I)] was made up to 10 cm^3 with distilled water and the absorbances were read at 260 nm in 1-cm cells after 5 min and 60 min (in parentheses). The results were as follows:

x(cm^3)	0	4	4[a]	9
A(Tl^{3+} present)	0.818 (0.820)	0.802 (0.804)	0.811 (0.815)	0.807 (0.811)
A(Tl^{+} present)	0.818 (0.820)	0.801 (0.805)	0.805 (0.809)	0.806 (0.815)

[a]2 cm^3 of 0.5 M HCl replaced 2 cm^3 of the water added.

Reaction of the formazan (I) with thallium(I)

The absorbances of mixtures of 0.5 cm^3 of 4.591×10^{-4} M formazan, x cm^3 of 2.0×10^{-4} M thallium(I), and $(9.5 - x)$ cm^3 of water were measured at 420 nm. The results were as follows:

x(cm^3)	0	4	4[a]	9
A after 5 min	0.714	0.709	0.718	0.704
A after 60 min	0.719	0.711	0.720	0.705

[a]2 cm^3 of 0.5 M HCl replaced 2 cm^3 of the water added.

Interference study

Solutions comprising 0.5 cm^3 of 4.414×10^{-4} M formazan, 5 cm^3 of the ion solution to be tested, and 4.5 cm^3 of 3.175×10^{-5} M thallium(III) were made up in this order; the reference solution contained 0.5 cm^3 of the formazan, 5 cm^3 of the ion solution to be tested, and 4.5 cm^3 of distilled water; absorbances were measured at 420 nm. Cations were generally added as their nitrate, sulphate, or chloride salts and anions as their sodium or potassium salts. The apparent concentration of thallium was read off from a calibration curve prepared as described above.

Standard curve for gold(III)

The reference cell (placed in the sample beam) contained 4.391×10^{-4} M formazan (0.5 cm^3), 0.5 M HCl (0.5 cm^3), and water (9.0 cm^3). The sample cell (placed in the reference beam in place of the usual solvent "blank") contained 4.391×10^{-4} M formazan (0.5 cm^3), 0.5 M HCl (0.5 cm^3), x cm^3 of 3.668×10^{-5} M gold(III) solution, and $(9.0 - x)$ cm^3 water. Readings of absorbance at 420 nm (1-cm cells) were taken after 10 min. The results were as shown in Fig. 5. At the equivalence point, 2.195×10^{-7} mol of the formazan (I) had reacted with 2.054×10^{-7} mol of Au^{3+}, the combining ratio being 1 : 0.94.

We are indebted to Dr. A. H. Nabilsi for his preliminary measurements [1] and to Dr. T. Braun (L. Eötvös University, Budapest) for his interest and help in attempts to adapt the new reaction to a chromatographic procedure [14]. The S. A. Council for Scientific and Industrial Research and the University of Cape Town are thanked for research grants.

REFERENCES

1 A. H. Nabilsi, Ph. D. Thesis, Leeds (1972).
2 A. T. Hutton, M. Sc. Thesis, Cape Town (1978).
3 A. T. Hutton, H. M. N. H. Irving, K. R. Koch, L. R. Nassimbeni and G. Gafner, J. Chem. Soc. Chem. Commun., (1979) 57.
4 A. T. Hutton and H. M. N. H. Irving, J. Chem. Soc. Perkin Trans. 2, (1979) in press.
5 J. W. Ogilvie and A. H. Corwin, J. Am. Chem. Soc., 83 (1961) 5023.
6 R. S. Ramakrishna and M. E. Fernandopulle, Anal. Chim. Acta, 60 (1972) 87.
7 R. C. Weast (Ed.), Handbook of Chemistry and Physics, 55th edn., Chemical Rubber Co., Cleveland, Ohio, 1975.
8 Z. Marczenko, H. Kalowska and M. Mojski, Talanta, 21 (1974) 93.
9 L. G. Sillén and A. E. Martell (Eds.), Stability Constants of Metal-Ion Complexes, Spec. Publ. No. 17 (1964) and Suppl. No. 1, Spec. Publ. No. 25 (1971), The Chemical Society, London.
10 Y. K. Lee, K. J. Whang and K. Ueno, Talanta, 22 (1975) 535.
11 T. Braun and A. B. Farag, Anal. Chim. Acta, 73 (1974) 301.
12 T. Braun and A. B. Farag, Talanta, 22 (1975) 669.
13 T. Braun and A. B. Farag, Anal. Chim. Acta, 99 (1978) 1.
14 T. Braun, L. Eötvös University, Budapest, personal communication, 1978.

Analytica Chimica Acta, 113 (1980) 123–130

DETERMINATION OF TRACE VANADIUM IN PETROLEUM OILS BY OXYGEN FLASK COMBUSTION AND A CATALYTIC METHOD**

TSUTOMU FUKASAWA* and TAKESHI YAMANE

Department of Applied Chemistry, Faculty of Engineering, Yamanashi University, Takeda-4, Kofu-shi, 400 (Japan)

(Received 25th June 1979)

SUMMARY

The petroleum oil sample is combusted in an improved oxygen flask and vanadium (≥0.1 ppm) is then determined by a catalytic method based on spectrophotometric monitoring of the gallic acid—bromate reaction. For most samples, there is no interference from other elements normally present, but an ion-exchange separation prior to catalytic determination is recommended in order to achieve reliable analyses of a wide variety of real petroleum samples.

The need for the determination of trace metals in petroleum oils is well known; several methods have been reported for the determination of vanadium, most of which do not provide satisfactory results. Conventional spectrophotometric [1—8] and spectrographic [9—13] methods are not adequately sensitive, so that large samples must be used, leading to inconvenience of sampling and sample treatment and to increased blank values owing to possible contamination. Dry ashing or wet ashing of the sample is usually employed prior to the determination of metals. Dry ashing frequently leads to volatilization losses of analytes and to contamination by interfering substances. In contrast, wet ashing is considered not to cause loss of metals but often introduces contamination owing to the large amounts of digesting reagents required, and it is time-consuming and laborious.

Recently, atomic absorption methods have been reported by some workers [14—19]; these include dilution of the sample with an organic solvent and direct introduction into a flame or flameless atomization system. Many problems, however, have arisen owing to the complex matrix and the dependence of the vanadium signal on the type of vanadium compound. Neutron activation analyses have also been reported [20, 21], but they require special facilities which are not universally available.

Oxygen flask combustion should prevent losses of metals and the introduction of contamination because burning occurs in a closed system, but it usually has the disadvantage of a limited sample size (<0.1 g). If an

**Presented at the ACS/CSJ Chemical Congress, Honolulu, Hawaii, April 1979.

extremely sensitive method for determining trace metals is available, the flask combustion technique may conveniently be used for trace metal analysis of oil samples.

An extremely sensitive catalytic method for the determination of vanadium is possible using the gallic acid—bromate reaction [22]. The present paper describes an investigation of the oxygen flask combustion of petroleum samples followed by the determination of vanadium by this catalytic method. Many of the problems encountered in direct atomic absorption analysis and other existing methods do not occur in the method proposed here. The method, which requires only a small sample, is simple, sensitive and free from interferences from coexisting elements and matrix, in addition to the advantages of good precision and the use of only an inexpensive spectrophotometer.

EXPERIMENTAL

Reagents and apparatus

All chemicals used were of analytical grade, unless otherwise specified. A standard vanadium solution (500 μg V ml^{-1}) was prepared by dissolving ammonium metavanadate in water. More dilute solutions were prepared from this standard solution by appropriate dilution with water. Acetate buffer solution (pH 3.8) was prepared by mixing 10 M acetic acid and 2 M sodium acetate solution in the ratio of 1.6 : 1.0.

Sulfuric acid (98.0%), hydrochloric acid (20%, 36%), acetic acid (99—100%) and ammonia liquor (25%) were Super Special Grade (Wako Pure Chemical Industries Ltd.).

The resins used were Diaion SK-1 strongly acidic cation-exchange resin (8% DVB, 100—200 mesh) and Diaion SA-100 strongly basic anion-exchange resin (8% DVB, 100—200 mesh).

All spectrophotometric measurements were done with a Hitachi Model 100-10 spectrophotometer with 10-mm glass cells. The temperature in the cell chamber was maintained at 30 ± 0.5°C by circulating water from an external thermostatted water bath. A Daiiti Riko Model FHO 1A modified combustion flask [23] was used; this is made of borosilicate glass, except for the wire, basket and coil which are made of platinum. A schematic diagram of the combustion apparatus is shown in Fig. 1.

Ion-exchange columns

A cation-exchange and an anion-exchange column, each with resin beds 3 cm high and 1.6 cm diameter, were prepared and used in series in that order. Before use, the columns were washed successively with 50 ml of 1 M HCl—0.1% H_2O_2 solution, 30 ml of water and 20 ml of 0.05 M HCl—0.1% H_2O_2 solution [24].

Procedure for determination of vanadium in oils

The oil sample is weighed after painting it onto a piece of filter paper with

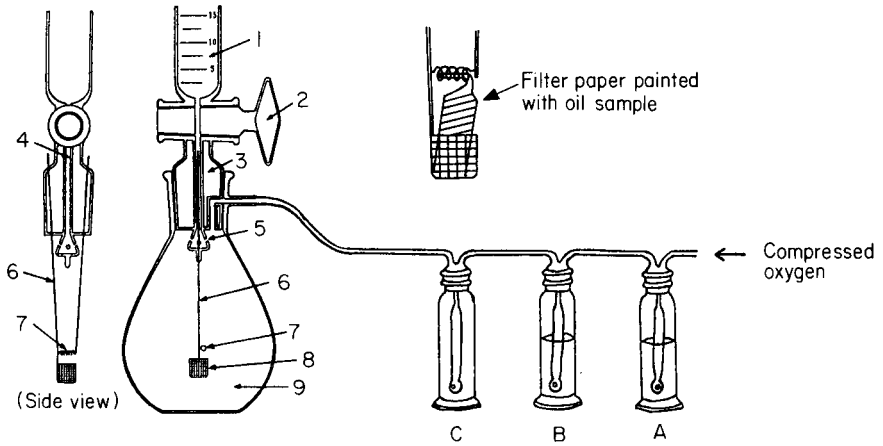

Fig. 1. Schematic diagram of combustion apparatus. (1) Absorbing solution; (2) stopcock; (3) ground-glass stopper; (4) path of absorbing solution; (5) holes for spouting absorbing solution; (6) platinum suspension wire; (7) platinum coil; (8) platinum basket; (9) flask (300 ml). (A) 3 M H_2SO_4—5% H_2O_2 solution; (B) distilled water; (C) empty.

a glass capillary. The paper with the sample is placed in the platinum basket and the upper end of the paper is inserted into the platinum coil (see Fig. 1). After the apparatus has been set up, the air in the flask is replaced with oxygen bubbled through three wash bottles, the first containing 3 M H_2SO_4—5% H_2O_2 solution, the second distilled water and the third empty. The ground-glass stopcock and the stopper are then closed. On passing a small current through the platinum wires the platinum coil glows and the filter paper with the sample is ignited. A plastic safety shield is used when the sample is burned. After the flask has cooled in an ice-bath for 5 min, 10 ml of 0.3 M HCl—0.1% H_2O_2 absorbing solution is introduced into the flask by turning the stopcock. The flask is shaken and the resulting solution is transferred to a glass beaker (100 ml) with small portions of 0.1% hydrogen peroxide solution. The solution is diluted to ca. 50 ml with 0.1% hydrogen peroxide to give a concentration of ca. 0.06 M HCl—0.1% H_2O_2.

The solution is then passed through the ion-exchange columns. Vanadium is selectively eluted by passing 25 ml of 1 M HCl—0.1% H_2O_2 solution through the anion-exchange column [24]. All the effluent is collected in a glass beaker (50 ml), and, after the addition of 2 ml of 1.5 M sulfuric acid, it is heated on a hot plate to expel HCl and H_2O_2 until white fumes of sulfur trioxide begin to appear. After cooling, the solution is transferred to a graduated test tube (25 ml) with a ground-glass stopper, using a little water and adjusted to pH 3.8 with 2 M ammonia solution; 1.3 ml of the buffer solution and 3 ml of 1% (w/v) gallic acid solution are then added and the solution is diluted to 18 ml with water. The oxidation of gallic acid is initiated by the addition of 2 ml of 2% (w/v) bromate solution. The reaction is followed spectrophotometrically at 420 nm. The rate is obtained

graphically from the slope of the linear plot of absorbance vs. time in the range 15—40 min. Vanadium is determined by use of a calibration curve previously prepared by plotting the reaction rate vs. known amounts of vanadium, which is rectilinear in the range of 0—100 ng of vanadium.

When the ion-exchange separation is omitted, the sample solution is transferred from the combustion flask to a beaker (50 ml) and heated with 2 ml of 1.5 M sulfuric acid, and vanadium is determined as described above.

RESULTS AND DISCUSSION

Combustion of petroleum oils in the oxygen flask

Preliminary tests showed that the success of the combustion of an oil sample in the oxygen flask depends mainly on sample size, the geometry of the filter paper sample carrier and the extent of spreading of the sample on the paper. The combustion of the oil sample painted on a limited area on the paper as shown in Fig. 2(c) generated considerable amounts of soot and dispersed part of the sample inside the flask. These defects are due to temporary deficiencies of oxygen during the rapid combustion of the sample. To avoid these it is recommended that the oil sample should be distributed over the whole surface of the paper, as shown in Figs. 2(a) and (b). The sample size leading to successful combustion was 20—30 mg with the 300-ml capacity flask used in this study. No significant interference was observed in vanadium determination from the presence of only small amounts of soot. Much soot, however, cannot be tolerated because it affects the column separation (or interferes with the determination if ion-exchange separation is not used).

The choice of a suitable reagent and its concentration is very important to ensure complete absorption of vanadium after combustion of the sample. In consideration of the subsequent ion-exchange separation, 0.05, 0.1, 0.3 and 0.5 M hydrochloric acid solutions containing 0.1% hydrogen peroxide were examined as the absorbing solution for the determination of vanadium

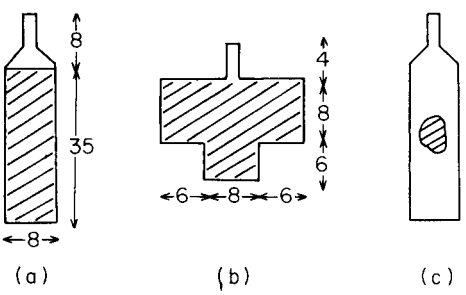

Fig. 2. Different shapes of filter paper used as sample carrier and loading distributions of oil sample. Weight of filter paper, 20 mg. All dimensions in mm. The shading shows the distribution of the oil samples.

in the J.P.I. (Japan Petroleum Institute) standard residual fuel oils. Results showed that hydrochloric acid concentrations ranging from 0.05 to 0.5 M did not cause significant differences between the vanadium values determined. Thus, 10 ml of 0.3 M hydrochloric acid solution containing 0.1% hydrogen peroxide was preferred for absorbing vanadium, because the dilution of this solution to ca. 50 ml with 0.1% hydrogen peroxide results in final concentrations of ca. 0.06 M HCl—0.1% H_2O_2, which are suitable for the subsequent ion-exchange separation. The combustion flask used is designed so that effective washing of the inner wall and effective absorption of vanadium may be achieved by using a sprinkler for passing the solution into the flask. Possible transference of metals to the inner wall of the flask during combustion, which was suggested by Mizuike et al. [25], was eliminated in the present study by washing with 0.1% hydrogen peroxide.

The fumes appearing in the flask with combustion of oil samples gradually disappeared on cooling the flask in an ice-bath. In order to establish a suitable cooling period, vanadium determinations were carried out with the J.P.I. standard residual fuel oils. There were no differences in the measured values of vanadium for cooling periods in the range 1—60 min. Therefore, cooling for 5 min is recommended.

The time required for combustion was less than 30 s.

Determination of vanadium in petroleum oils

Table 1 shows the results of recovery tests by the complete recommended procedure. In these experiments, known amounts of standard vanadium solution were previously added to the paper carriers, the papers were air-dried, and vanadium determinations were then carried out by using these papers with or without an oil sample. The recovery in the presence of oil was

TABLE 1

Recovery of vanadium added to the filter paper with and without addition of J.P.I. standard residual fuel oil B

Sample	Oil taken (mg)	Vanadium		
		Added (ng)	Found (ng)	Recovery (%)
No oil[a]		50	52	104
		50	50	100
		50	49	98
		50	48	96
Oil added	5.28	40	67	98[b]
	4.15	40	61	98[b]

[a]Vanadium found in the filter paper and the blank value of the complete procedure were almost negligible.

[b]Calculated on the basis of 5.3 ppm vanadium previously determined in this laboratory.

calculated on the basis of the vanadium content previously determined in this laboratory. As shown in Table 1, satisfactory recoveries were obtained in both cases.

Results of analyses by the proposed method are shown in Tables 2 and 3, for three J.P.I. standard residual fuel oils, and for three commercially available residual fuel oils and a crude oil, respectively. There were some samples with relatively high vanadium contents as shown in Table 3. An extremely small sample was needed for the analysis of such high vanadium samples in order that the vanadium to be determined fell into the linear range of the calibration curve (0—100 ng). In this study, a sample greater than 3 mg was burned in order to avoid errors in handling very small samples, and the analysis was continued by use of an appropriate aliquot of the resulting solutions containing vanadium.

TABLE 2

Analytical results for J.P.I. standard residual fuel oils by the proposed method

Sample	Sample wt. (mg)	No. of detns.	V found[a] (ppm)	V certified[b] (ppm)	Coexisting elements (ppm)[b]
A	3.36—6.63	5 (3)	15.3 ± 0.3 (15.4 ± 0.2)	14	Ni 4; S 2.03 (%) Na 35; Fe 7
B	5.28—12.01	6 (3)	5.3 ± 0.2 (5.4 ± 0.2)	6	Ni 21; S 0.43 (%) Na 5; Fe 10
C	5.23—11.93	9 (6)	7.2 ± 0.1 (7.2 ± 0.3)	7	Ni 2; S 1.05 (%) Na 24; Fe 4

[a]Mean ± standard deviation. Values in parentheses were obtained without ion-exchange separation.
[b]Values certified by the Japan Petroleum Institute.

TABLE 3

Analytical results for some petroleum oil samples by the proposed method

Sample	Sample wt. (mg)	Aliquot	No. of detns.	V found[a] (ppm)
Crude oil (Iranian heavy)	4.79—6.52	1/10	6 (6)	82 ± 3 (85 ± 10)
Residual fuel oil (D)	33.8—57.2		4	0.1 ± 0.01
Residual fuel oil (E)	7.55—9.50	1/5	3 (3)	39 ± 1 (42 ± 2)
Residual fuel oil (F)	6.20—14.5	1/5—1/10	4 (4)	47 ± 2 (47 ± 1)

[a]Mean ± standard deviation. Values in parentheses were obtained without ion-exchange separation.

Table 2 shows that the values of vanadium obtained by the proposed method for J.P.I. samples are in reasonably good agreement with the certified values; the relative standard deviations are within 4%. The values in parentheses in these tables indicate the results obtained without the ion-exchange separation. For individual samples, there is no significant difference between the values of vanadium and the standard deviation obtained by the methods with and without separation, except for the crude oil sample. In the separation procedure employed, most cations are adsorbed on the cation-exchange resin in the first column, whereas vanadium, tungsten and molybdenum are adsorbed on the anion-exchange resin in the second column. Vanadium is eluted from the second column selectively with a 1 M HCl—0.1% H_2O_2 solution [24]. The good agreement between the results by the two methods suggests that there is no interference from other elements in the sample, even when the separation is omitted, owing to the small content of interfering elements such as iron and the small sample sizes. There is no reason to expect any interference from a few per cent level of sulfur in the sample because this is converted to sulfate in the procedure.

In the analysis of the crude oil, somewhat higher vanadium values with significantly lower precision were observed as the result of omitting the separation procedure. The reason for this is not clear, but the effect may be attributed to other elements in the sample. Therefore, the method with ion-exchange separation is recommended for the reliable analysis of a wide variety of real samples.

It should be noted that in the early stages of this study, high blank values, equivalent to 10—50 ng of vanadium, were observed by using compressed oxygen directly from a cylinder. Washing the oxygen with a mixture of sulfuric acid and hydrogen peroxide solutions was found to be very effective in reducing the blank value. Experiments showed that the blank value through the whole procedure, including the combustion of the filter paper sample carrier, was almost negligible. However, the blank value should be checked every time the reagent solution, batch of filter paper or ion-exchange columns are changed.

This work was supported in part by the Asahi Glass Foundation for the Contribution to Industrial Technology.

REFERENCES

1 R. J. Nadalin and W. B. Brozda, Anal. Chem., 32 (1960) 1141.
2 E. J. Agazzi, D. C. Burtner, D. J. Crittenden and D. R. Patterson, Anal. Chem., 35 (1963) 332.
3 O. I. Milner, J. R. Glass, J. P. Kirchner and A. N. Yurick, Anal. Chem., 24 (1952) 1728.
4 J. S. Forrester and J. L. Jones, Anal. Chem., 32 (1960) 1443.
5 T. Yotsuyanagi, J. Itoh and K. Aomura, Jpn. Anal., 18 (1969) 1498.
6 S. Banerjee, B. P. Sinha and R. K. Dutta, Talanta, 22 (1975) 689.
7 G. E. Janauer and J. Korkisch, Fresenius Z. Anal. Chem., 179 (1961) 241.

8 W. M. Wise and W. W. Brandt, Anal. Chem., 27 (1955) 1392.
9 J. E. McEvoy, T. H. Milliken and A. L. Juliad, Anal. Chem., 27 (1955) 1869.
10 J. G. Bergman, C. H. Ehrhardt, L. Granatelli and J. L. Jamik, Anal. Chem., 39 (1967) 1258.
11 C. W. Key and G. D. Hoggan, Anal. Chem., 25 (1953) 1673.
12 J. A. Kanehann, Anal. Chem., 27 (1955) 1873.
13 A. P. Kuznetsova, Z. I. Otmakhova and G. D. Ktaev, Zavod. Lab., 39 (1973) 957.
14 S. H. Omang, Anal. Chim. Acta, 56 (1971) 470.
15 K. G. Brodie and J. P. Matousek, Anal. Chem., 43 (1971) 1557.
16 G. Šebor, I. Lang, P. Vavrecka, V. Sychra and O. Weisser, Anal. Chim. Acta, 78 (1975) 99.
17 G. Šebor and I. Lang, Anal. Chim. Acta, 89 (1977) 221.
18 M. Kashiki and S. Oshima, Jpn. Anal., 20 (1971) 1398.
19 J. Rofass, Analusis, 2 (1973) 119.
20 A. Arroy and D. Brume, Mikrochim. Acta, (1972) 239.
21 S. M. Al-Jobori, S. Szegedi and J. Csikai, Radiochem. Radioanal. Lett., 25 (1976) 87.
22 T. Yamane and T. Fukasawa, Bunseki Kagaku, 25 (1976) 454.
23 S. Ohta, Jpn. Anal., 17 (1968) 1322.
24 T. Fukasawa and T. Yamane, Anal. Chim. Acta, 88 (1977) 147.
25 A. Mizuike, Y. Iida, Y. Ujihira and Y. Takada, in E. Minami, S. Hirano, S. Araki and S. Fujiwara (Eds.), Instrumental Analysis of High Polymers, Vol. II, Hirokawa, Tokyo, 1964, p. 169.

Analytica Chimica Acta, 113 (1980) 131—137

PRECONCENTRATION AND SPECTROPHOTOMETRIC DETERMINATION OF CHROMIUM(VI) IN NATURAL WATERS BY COPRECIPITATION WITH BARIUM SULFATE

HIDEO YAMAZAKI

Department of Chemistry, Faculty of Science and Technology, Kinki University, 3-4-1, Kowakae, Higashi-Osaka, Osaka (Japan)

(Received 26th June 1979)

SUMMARY

A selective preconcentration of chromium(VI) is proposed for analysis of natural waters. Chromium(VI) is quantitatively separated from chromium(III) by coprecipitation with barium sulfate; salicylic acid is used as a masking agent for iron(III), aluminum(III) and chromium(III). The precipitate is fused with alkali carbonate, and the chromium(VI) in the melt is isolated with hot water and determined spectrophotometrically with diphenylcarbazide. The detection limit is 0.02 $\mu g\ l^{-1}$; the relative standard deviation for chromium(VI) in river water is less than 5%.

An understanding of the chemical state and behavior of trace elements in natural waters is important from both environmental and geochemical viewpoints. In natural waters, it is well known that chromium exists in the trivalent and hexavalent states [1, 2], and accurate and selective analytical methods are required in order to distinguish and determine these oxidation states. Accordingly, various techniques, such as coprecipitation with metal hydroxides [3—6], solvent extraction [7, 8] and ion-exchange [9, 10] have been widely used for the preconcentration and separation of mixtures of the two oxidation states, spectrophotometric or atomic absorption methods subsequently being applied for the quantitative analyses.

This paper describes a selective and accurate procedure for the preconcentration of chromium(VI), in which chromate ion is selectively coprecipitated with barium sulfate prior to a spectrophotometric determination. The method utilizes the fact that the solubility product of barium sulfate is similar to that of barium chromate (pK_{so} ($BaSO_4$) 10.0; pK_{so} ($BaCrO_4$) 9.9) [11], and is suitable for the determination of chromium(VI) in natural waters.

EXPERIMENTAL

Reagents

Chromium(VI) stock solution (1000 $\mu g\ ml^{-1}$) was prepared by dissolving potassium dichromate in redistilled water. Working chromium(VI) solutions

were prepared as needed by dilution with redistilled water. Solutions containing $^{51}Cr(III)$ and $^{51}Cr(VI)$ were prepared from $Na_2{}^{51}CrO_4$ (ca. 0.03 μg Cr/μCi; Japan Atomic Energy Research Institute) by treating the solution with hydrogen peroxide in acidic and alkaline media, respectively. Barium(II) solution (0.5 M) was prepared from reagent-grade barium chloride: the solution was purified by precipitating part of the barium(II) as barium sulfate at pH 10, before the final dilution with redistilled water to make 0.5 M barium(II) solution. A solution containing 0.5 M sulfate was prepared from sodium sulfate, and 2% (w/v) salicylic acid solution was prepared daily by dissolving *o*-hydroxybenzoic acid in dilute alkaline solution.

Apparatus

Absorption measurements were made with a Hitachi spectrophotometer model 556 with 1-cm cells. The radioactivity measurements were made with a Fuji Electric well-type scintillation probe NDP 22 [2 × 2 in. NaI (Tl)] and a scaler model NHS 2.

Coprecipitation of chromium with barium sulfate

The coprecipitation behavior of chromium with barium sulfate was studied by using the radioactive tracer, ^{51}Cr. To about 180 ml of water, were added a known amount of barium(II) and $^{51}Cr(III)$ or $^{51}Cr(VI)$, which contained 2 μg of chromium(III) or chromium(VI) carrier, were added. The pH of the solution was adjusted to the desired value (3—5) with dilute hydrochloric acid and/or sodium hydroxide solution, and a known amount of sulfate solution was added with vigorous stirring. The resulting solution was allowed to stand overnight and filtered through a membrane filter (Toyo filter TM 100, pore size 1 μm). Subsequently a constant volume of the filtrate was pipetted into a test tube and the γ-activity of the solution was measured. The extent of coprecipitation (%) was calculated by comparing the γ-activity with that of the original tracer solution.

Spectrophotometric determination of chromium(VI) with diphenylcarbazide

The barium sulfate precipitate containing chromium(VI) was ignited in a platinum crucible, the residue was fused with 2 g of potassium sodium carbonate, and the melt was dissolved with 10 ml of hot water. The solution was filtered through a glass-fiber filter (Toyo filter GC 90, pore size 0.5 μm), the pH was adjusted to 2 with sulfuric acid, and 0.5 ml of 0.01 M potassium permanganate was added. The solution was warmed in boiling water for 40 min to oxidize chromium completely to chromium(VI). After cooling, a few drops of 4% sodium azide were added and the solution warmed again at 60°C for 3 min to reduce excess of permanganate ion. After cooling in ice water, 2 ml of a 0.25% (w/v) solution of diphenylcarbazide in acetone was added, and the mixture was made up to 20 ml. The absorbance was measured at 540 nm against the reagent blank.

Analysis of fresh waters

Immediately after collection, the water sample was filtered through a membrane filter (Millipore filter HA type, pore size 0.45 μm) to remove suspended matter, and its pH was adjusted to 3.5—4.0 with hydrochloric acid. To each 2.5 l of the sample, 100 ml of 0.5 M barium(II) solution and 15 ml of 2% salicylic acid solution were added. After the pH had been adjusted to 3.7, 5 ml of 0.5 M sodium sulfate solution was added with vigorous stirring. After standing overnight, the barium sulfate precipitate was filtered off on a membrane filter (HA type) and washed with redistilled water. The filter and precipitate containing chromium(VI) were ashed, and fused with 2 g of potassium sodium carbonate. The melt was dissolved with 10 ml of hot water, and the chromium(VI) was determined as described above.

In order to prevent contamination, the membrane filter, the sample bottles and other vessels were carefully precleaned with concentrated hydrochloric acid and redistilled water. The coprecipitation step for chromium(VI) was carried out as soon as possible after sampling to minimize the sample storage problem.

RESULTS AND DISCUSSION

Effect of pH

The coprecipitation behavior of chromium(III) and chromium(VI) is shown in Fig. 1. The coprecipitation of chromium was strongly pH-dependent. When 5 ml of 0.5 M sodium sulfate solution was added to about 180 ml of sample solution containing 0.0125 M barium(II) ion, chromium(VI) was quantitatively coprecipitated with barium sulfate above pH 3. But coprecipitation of chromium(III) began at pH 5 owing to hydrolysis. For the separation of chromium(VI) from chromium(III) the optimum pH region was 3—5.

Effects of $[Ba^{2+}]/[SO_4^{2-}]$ *ratio and of the amount of barium sulfate*

The coprecipitation behavior of chromium(VI) in solutions containing various mole ratios of $[Ba^{2+}]/[SO_4^{2-}]$ is shown in Fig. 2. The coprecipitation of chromium(VI) was affected by the initial mole ratio and decreased as $[Ba^{2+}]/[SO_4^{2-}]$ decreased, but chromium(VI) was quantitatively coprecipitated with barium sulfate from solutions containing an excess of barium(II) ion over sulfate ion.

The effect of the amount of barium sulfate was studied by precipitating different amounts of barium sulfate from 1-l samples containing various excess concentrations of barium(II) ion. The results are presented in Fig. 3. Quantitative recovery of chromium(VI) could be achieved by precipitation of 0.2 g of barium sulfate per liter of sample, provided that the mole ratio of $[Ba^{2+}]/[SO_4^{2-}]$ was over 10: when the ratio $[Ba^{2+}]/[SO_4^{2-}]$ was only 1.25, ca. 2 g of barium sulfate per liter was needed for complete recovery.

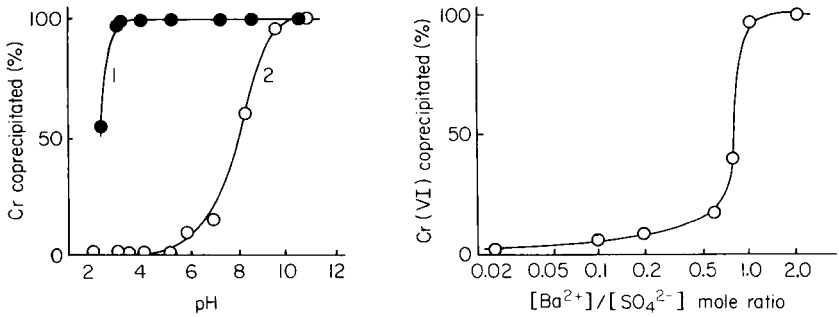

Fig. 1. Effect of pH on the coprecipitation of chromium with barium sulfate. [Cr] = 2×10^{-7} M; $[Ba^{2+}] = 0.0125$ M; $[SO_4^{2-}] = 0.0125$ M. Curve (1) chromium(VI); curve (2) chromium(III).

Fig. 2. Effect of mole ratio of barium(II) to sulfate ion on the coprecipitation of chromium(VI) with barium sulfate. $[Cr(VI)] = 2 \times 10^{-7}$ M; $[SO_4^{2-}] = 0.0125$ M; pH 3.0 ± 0.1.

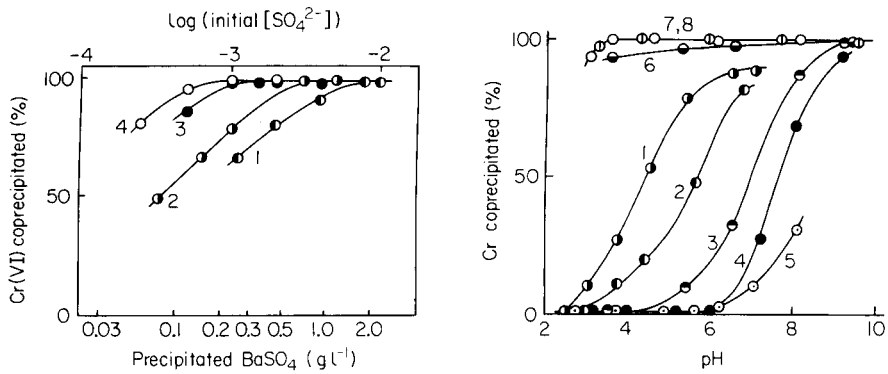

Fig. 3. Effect of amount of barium sulfate on the coprecipitation of chromium(VI) at various $[Ba^{2+}]/[SO_4^{2-}]$ ratios. $[Cr(VI)] = 2 \times 10^{-8}$ M; pH 3.7 ± 0.2; $[Ba^{2+}]/[SO_4^{2-}]$ mole ratios: (1) 1.25, (2) 2.0, (3) 10, (4) 20.

Fig. 4. Effect of masking agents on the coprecipitation of chromium with barium sulfate in the presence of iron(III) or aluminum(III). [Cr] = 10^{-7} M; $[Ba^{2+}] = 0.025$ M; $[SO_4^{2-}] = 0.005$ M; $[Fe^{3+}] = 0.2$ ppm; $[Al^{3+}] = 0.2$ ppm. Curves: (1) Cr(III), Fe(III); (2) Cr(III), Al(III); (3) Cr(III), Fe(III), 10^{-3} M 1, 10-phen; (4) Cr(III), Fe(III), 10^{-3} M salicylic acid; (5) Cr(III), Al(III), 10^{-3} M salicylic acid; (6) Cr(VI), Fe(III), 10^{-3} M 1,10-phen; (7) Cr(VI), Fe(III), 10^{-3} M salicylic acid; (8) Cr(VI), Al(III), 10^{-3} M salicylic acid.

Effect of masking agents for Fe(III), Al(III) and Cr(III)

When sample solutions contained iron(III) or aluminum(III), chromium-(III) was coprecipitated with barium sulfate at pH values below 5 (see curves 1 and 2, Fig. 4), probably because chromium(III) was readily adsorbed onto iron(III) and/or aluminum(III) hydroxide (cf. Shigematsu et al. [3]). The effect of iron(III) concentration on the coprecipitation of 10^{-7} M

chromium(III) was studied at pH 3.7 with 0.025 M barium(II) and 0.005 M sulfate solutions. The coprecipitation of chromium(III) was negligible when 0.02 ppm iron(III) was present but increased as the concentration of iron(III) increased, becoming about 25% at iron(III) levels of 0.2 ppm and approaching 50% at iron(III) levels of 0.5 ppm.

To prevent the interference of iron(III), salicylic acid, 1,10-phenanthroline, citric acid, ethylenediamine and PAR [4-(2-pyridylazo)-resorcinol] were studied as masking agents for iron(III), aluminum(III) and chromium(III); the effects of these reagents are summarized in Table 1. Ethylenediamine and (particularly) PAR were not effective, because their chromium(III) chelates seemed to be adsorbed onto barium sulfate precipitates. In addition, in the presence of citric acid or PAR, chromium(VI) was probably partially reduced during the aging of the precipitate so that its recovery was not quantitative. Salicylic acid and 1,10-phenanthroline were more suitable masking agents and the coprecipitation behavior of chromium in the presence of iron(III) or aluminum(III) and of these reagents was thus further studied. As shown in Fig. 4, 1,10-phenanthroline might cause the reduction of chromium(VI) at low pH, and so salicylic acid was the most suitable masking agent.

Concentrations of iron(III) of 0.2—2.5 ppm could be effectively masked by adding 0.7×10^{-3} M or more salicylic acid; more than 99% of chromium-(VI), and less than 0.5% of chromium(III) were recovered in these conditions.

Accuracy and precision

To examine the accuracy of the proposed procedure, known amounts of chromium(III) and chromium(VI) were added to water samples, and the entire procedure for the determination of chromium(VI) was performed. The results of these analyses are shown in Table 2. Chromium(VI) could be selectively determined by using salicylic acid as a masking agent and the relative standard deviation was estimated to be less than 1.0%. The detection limit of the procedure, defined as twice the standard deviation of the blank value, was ca. 0.02 $\mu g\ l^{-1}$.

Application to river water

Three river-water samples were collected and the chromium(VI) contents were determined by the proposed procedure. The results are listed in Table 3, with standard deviation values of triplicate runs. When known amounts of chromium(VI) and/or chromium(III) were added to these samples, the chromium(VI) could be quantitatively recovered. The results obtained with samples 1 and 2 by this method were in good agreement with the results obtained by an aluminum hydroxide coprecipitation method [3]. The relative standard deviation for the determination of chromium(VI) in river water was estimated to be less than 5.1%.

From the results, it can be considered that the recommended procedure is an accurate and selective technique for the determination of chromium(VI) in fresh waters.

TABLE 1

Effects of masking agents for iron(III) and chromium(VI)

Sample and volume (l)	Cr added[a]	Fe(III) added (mg)	Masking agent[b]	Amount added (M)	Cr copptd.[c] (%)
Distilled water (0.2)	(III)	—	PAR	2.3×10^{-5}	78.0
	(VI)	—	PAR	2.3×10^{-5}	94.7
	(III)	—	en	0.15	12.5
	(VI)	—	en	0.15	100
	(III)	—	cit.	5.0×10^{-4}	0.2
	(VI)	—	cit.	5.0×10^{-4}	93.8
	(III)	—	phen	10^{-3}	0.5
	(VI)	—	phen	10^{-3}	99.1
Distilled water (1.0)	(III)	—	sal.	1.5×10^{-3}	0.4
	(III)	0.2	sal.	1.5×10^{-4}	1.9
	(III)	0.2	sal.	0.7×10^{-3}	0.2
	(III)	1.0	sal.	1.5×10^{-3}	0.3
	(III)	2.5	sal.	1.5×10^{-3}	0.2
	(III)	0.2	none		47.6
	(VI)	—	sal.	1.5×10^{-3}	99.7
	(VI)	0.2	sal.	1.5×10^{-3}	99.5
	(VI)	0.2	none		99.0
River water (1.0)	(III)	—	sal.	1.5×10^{-3}	0.7
	(III)	1.0	sal.	1.5×10^{-3}	1.3
	(III)	1.0	none		27.8
	(VI)	1.0	sal.	1.5×10^{-3}	99.2

[a]Radioactive tracer (containing 1.0 μg Cr carrier) was used. [b]en, ethylenediamine; cit., citric acid; phen, 1,10-phenanthroline; sal., salicylic acid. [c]Coprecipitated at pH 3.7 ± 0.2. 3.7 ± 0.2

TABLE 2

Precision and recovery for spiked samples of distilled water

Sample volume (l)	Fe(III) added (mg)	2% Salicylic acid added (ml)	Cr added (μg)		Cr found (μg)	*n*	R.s.d. (%)
1.0	—	5	Cr(VI)	2.0	1.99 ± 0.01	4	0.5
3.0	—	15	Cr(VI)	2.0	2.00 ± 0.02	3	1.0
1.0	—	—	Cr(VI)	1.0	0.97 ± 0.03	3	3.1
3.0	—	—	Cr(III)	5.0	0.45 ± 0.24	3	—
2.5	—	15	Cr(III)	5.0	0.01	1	—
2.5	0.25	15	Cr(III)	5.0	0.02	1	—
2.5	0.50	15	Cr(III)	10.0	0.08	1	—

The author expresses his sincere thanks to Dr. Shiro Gohda and Dr. Yasuharu Nishikawa, Faculty of Science and Technology, Kinki University, and Dr. Masayuki Tabushi, College of Medical Technology of Hirosaki University, for their kind advice and suggestions.

TABLE 3

Results of analyses for chromium(VI) in river water

Sample volume	Volume (l)	Cr added (μg)	This method		Other method[a]
			Cr(VI) found (μg)	Cr(VI) content ($\mu g\ l^{-1}$)	Cr(VI) content ($\mu g\ l^{-1}$)
(1) Yamato river, Osaka pref.[b]	2.0	—	0.20 ± 0.02	0.10 ± 0.02[c]	0.09 ± 0.01
(2) Nunobiki river, Hyogo pref.[d]	2.5	—	0.50 ± 0.02	0.20 ± 0.01	0.19 ± 0.02
	2.5	Cr(VI) 2.0	2.47 ± 0.04	0.19 ± 0.01	
(3) Nunobiki river, Hyogo pref.[e]	2.5	—	0.57 ± 0.02	0.23 ± 0.01[c]	
	2.5	—	0.53 ± 0.003	0.21 ± 0.001	
	2.5	Cr(III) 2.0	0.71 ± 0.11	0.28 ± 0.04[c]	
	2.5	Cr(III) 2.0	0.56 ± 0.01	0.22 ± 0.003	
	2.5	Cr(III) 2.0 Cr(VI) 2.0	2.68 ± 0.03	0.27 ± 0.02[c]	
	2.5	Cr(III) 2.0 Cr(VI) 2.0	2.52 ± 0.01	0.21 ± 0.004	

[a]Aluminum hydroxide coprecipitation method [3]. [b]Iron content, 13 $\mu g\ l^{-1}$; pH 6.50. [c]Masking agent was not used. [d]Iron content, 40 $\mu g\ l^{-1}$; pH 6.60. [e]Iron content 33 $\mu g\ l^{-1}$; pH 6.82.

REFERENCES

1 P. G. Brewer, in J. P. Riley and G. Skirrow (Eds.), Chemical Oceanography, 2nd edn., Vol. 1, Academic Press, London, 1975, p. 463.
2 H. Elderfield, Earth Planet. Sci. Lett., 9 (1970) 10.
3 T. Shigematsu, S. Gohda, H. Yamazaki and Y. Nishikawa, Bull. Inst. Chem. Res., Kyoto Univ., 55 (1977) 429.
4 L. Chuecas and J. P. Riley, Anal. Chim. Acta, 35 (1966) 240.
5 R. Fukai and D. Vas, J. Oceanogr. Soc. Jpn., 23 (1967) 298.
6 R. E. Cranston and J. W. Murray, Anal. Chim. Acta, 99 (1978) 275.
7 G. J. de Jong and U. A. Th. Brinkman, Anal. Chim. Acta, 98 (1978) 243.
8 T. R. Gilbert and A. M. Clay, Anal. Chim. Acta, 67 (1973) 287.
9 J. F. Pankow and G. W. Janauer, Anal. Chim. Acta, 69 (1974) 97.
10 M. S. Cresser and R. Hargitt, Anal. Chim. Acta, 81 (1976) 196.
11 L. G. Sillén and A. E. Martell, Stability Constants of Metal-Ion Complexes, Chem. Soc., Spec. Publ., No. 17 (1964).

Analytica Chimica Acta, 113 (1980) 139—147

PREPARATION OF DITHIOCARBAMATECELLULOSE DERIVATIVES AND THEIR ADSORPTION PROPERTIES FOR TRACE ELEMENTS

SAKINGO IMAI*, MOTOHO MUROI and AKIRA HAMAGUCHI

Public Health Research Institute of Kobe City, 1-5, Kano-Cho, Ikuta-Ku, Kobe-Shi, Hyogo 650 (Japan)

ROKUJI MATSUSHITA and MUTSUO KOYAMA

Research Reactor Institute, Kyoto University, Kumatori-Cho, Sennan-Gun, Osaka (590-04) (Japan)

(Received 10th July 1979)

SUMMARY

Tosylcellulose was treated separately with aniline, benzylamine, n-butylamine and piperazine to give four different aminocelluloses which were further treated with carbon disulfide to furnish four dithiocarbamatecelluloses (AND, BZD, BUD and PID). A comparative study was made of their performance as adsorbents for several kinds of metal ions. PID, which has the highest degree of substitution of the dithiocarbamate group of the four derivatives obtained, was investigated for its adsorption behavior towards Ag^{+}, As^{5+}, Cd^{2+}, Co^{2+}, Cr^{3+}, Cr^{6+}, Cu^{2+}, Fe^{3+}, Hg^{2+}, Mn^{2+}, Pb^{2+}, Sb^{5+}, Se^{4+}, Te^{4+} and Zn^{2+}. PID showed good adsorption characteristics with relatively large capacities for Ag^{+}, Cr^{6+}, Cu^{2+}, Hg^{2+}, Pb^{2+} and Se^{4+} ranging from 9.5 to 370 mg g^{-1} of resin.

The separation and concentration of metal ions from aqueous samples can often be speeded up and simplified by the application of a chelating polymer. Some attempts have been made to synthesize cellulose-based polymers containing the dithiocarbamate group which forms chelates with a relatively wide variety of metal ions. Dingman et al. [1] reported a polymer with dithiocarbamate groups obtained by treating a polyamine-polyurea resin with carbon disulfide. More recently, Hayashi et al. [2] synthesized cellulose derivatives containing the dithiocarboxyaminoethylcarbamoyl group.

Dithiocarbamate derivatives of cellulose are synthesized by introduction of the amino group into cellulose followed by reaction of the amino derivative with carbon disulfide. Several known methods of substituting the hydroxyl group of cellulose with the amino group [3, 4] tend to cause side reactions and often give low degrees of substitution. Rogovin [5] prepared a series of substituted cellulose derivatives by tosylation of cellulose followed by reaction of the tosylcellulose with a variety of reagents.

According to the method of Rogovin [5], tosylcellulose has been treated separately with aniline, benzylamine, n-butylamine and piperazine to obtain aminocelluloses, abbreviated respectively as ANA, BZA, BUA and PIA. These

aminocelluloses were then treated with carbon disulfide to furnish the corresponding dithiocarbamatecelluloses, AND, BZD, BUD and PID. Of these, BUD was studied earlier [6].

This paper reports a comparative study of the uptake of metal ions by these four dithiocarbamatecelluloses. Particular attention was given to the adsorption characteristics of PID, the most highly substituted dithiocarbamate derivative.

EXPERIMENTAL

Apparatus

Radioactive tracers (see Table 1) with the exception of ^{74}As, $^{51}Cr(III)$, ^{59}Fe and ^{54}Mn (see below) were prepared by KUR (5 MW) at the Research Reactor Institute, Kyoto University. The radioactivity was measured by a well-type NaI(Tl) scintillation counter (Aloka, SC-6, Japan).

Cadmium and lead were determined with an atomic absorption spectrometer (Hitachi Ltd., Type 518, Japan); mercury(II) was determined with a cold-vapor atomic absorption spectrometer (Hiranuma Machinery, Japan). A pH meter (Hitachi-Horiba Ltd., Type F-5ss, Japan) was used.

Materials

Reagents for synthesis. Microcrystalline cellulose was used as a starting material. Pyridine was dehydrated by NaOH and *N,N*-dimethylformamide (DMF) was dehydrated by molecular sieve (5A, 1/16) before use. The amines used were benzylamine, aniline, n-butylamine and piperazine; except for piperazine, they were purified by drying over NaOH followed by distillation. Other reagents used were *p*-toluenesulfonyl chloride, carbon disulfide, aqueous ammonia, methanol and acetone. All the reagents were of special

TABLE 1

Radioactive tracers used

Nuclide	Target materials	Half-life (days)	Specific activity (Ci g^{-1})
^{110m}Ag	Ag metal	253	3.6×10^{-5}
^{74}As	H_3AsO_4	17.9	Carrier-free
^{58}Co	Ni metal	71.3	Carrier-free
$^{51}Cr(VI)$	Cr_2O_3	27.8	1.9×10^{-2}
$^{51}Cr(III)$	$CrCl_3.6H_2O$	27.8	9.9×10
^{67}Cu	Zn metal	58.5	Carrier-free
^{59}Fe	$FeCl_3$	45.1	8.1
^{54}Mn	$MnCl_2$	303	Carrier-free
^{124}Sb	Sb_2O_5	60.4	6.5×10^{-2}
^{75}Se	Se metal	120	1.1×10^{-2}
^{123m}Te	Te metal	117	6.1×10^{-3}
^{65}Zn	Zn metal	245	1.9×10^{-2}

grade. Pure water was prepared by double distillation of deionized water in a quartz apparatus.

Radioactive tracers. The nuclides (Table 1) except for $^{74}As(V)$, $^{51}Cr(III)$, $^{59}Fe(III)$ and $^{54}Mn(II)$ (obtained from Japan Isotope Association) were prepared by sealing about 10 mg of a suitable metal, 99.999% in purity, or its oxide (of special reagent grade) in a fine quartz tube, placing the quartz tube in an aluminum capsule and submitting the capsule to neutron irradiation for 10 h in a KUR hydraulic exposure tube system with a thermal neutron flux of 8.15×10^{13} n cm^{-2} s^{-1}. For the preparation of ^{67}Cu and ^{58}Co, the nuclides formed by the ^{67}Zn (n,p) ^{67}Cu and ^{58}Ni (n,p) ^{58}Co reactions, respectively, were separated by ion exchange. Table 1 lists the radionuclides used in the tracer experiment, the target materials and the specific activity.

Carrier solutions: For the elements tested, except for As, Cr(III), Fe, Mn and Te for which carriers were not used, the 1000-ppm standard solutions commercially available for a.a.s. were used as carriers. The standard solution of tellurium was prepared by dissolving the metal of 99.999% purity in hydrochloric acid to a concentration of 1000-ppm.

Procedures

Synthesis of tosylcellulose. A suspension of 64 g of cellulose (glucose unit, 0.4 mol) in 1 l of pyridine was prepared and a solution of 762 g of *p*-toluenesulfonyl chloride in 500 ml of pyridine was added dropwise to the suspension with stirring. The mixture was stirred at room temperature for 7 days and 1.5 l of acetone containing 150 ml of pure water was added, again with stirring, while cooling the mixture with ice. The resulting mixture was poured into a large quantity of pure water and the solid matter was filtered, washed thoroughly with pure water and methanol in that order and dried. (Yield: 172 g).

Synthesis of aminocelluloses. To a suspension of 43 g (0.1 mol) of tosylcellulose in 400 ml of DMF was added the required amount (0.2 mol) of amine: (I) aniline, 19 g; (II) benzylamine, 21 g; (III) n-butylamine, 15 g; (IV) piperazine, 17 g. Stirring was continued for 5 h for (I), 2 h for (II) and (III) and 4 h for (IV). The reaction mixture was then cooled in acetone–dry ice and poured into cold aqueous 5% ammonia. The solid matter was filtered, washed with pure water repeatedly until the filtrate became neutral to phenolphthalein and finally extracted with methanol for 8 h in a Soxhlet extractor. The amino derivatives were obtained in the following yields: 22 g from (I), 12 g from (II), 8 g from (III) and 18 g from (IV).

Synthesis of dithiocarbamatecelluloses. A mixture of 0.035 mol of aminocellulose (10.4 g of ANA, 8.4 g of BZA, 7.8 g of BUA or 8.4 g of PIA), 18 ml of carbon disulfide, 36 ml of aqueous 28% ammonia and 200 ml of methanol was stirred at room temperature for 7 days. Upon completion of the reaction, the solid matter was filtered, washed thoroughly with pure water and methanol in that order, dried, and stored in a stoppered bottle in an atmosphere of ammonia gas. The dithiocarbamatecelluloses thus obtained have the following structures:

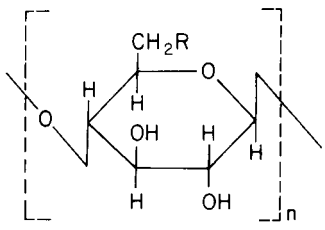

(I) AND; R=$-N(CS_2NH_4)-C_6H_5$

(II) BZD; R=$-N(CS_2NH_4)-CH_2C_6H_5$

(III) BUD; R=$-N(CS_2NH_4)-C_4H_9$

(IV) PID; R=$-N(CH_2CH_2)_2N-CS_2NH_4$

Measurement of metal ion uptake. The adsorption behavior of the 12 metal ions, except Cd^{2+}, Pb^{2+} and Hg^{2+}, was studied by the radioactive tracer technique as follows. Pure water (50 ml) was placed in a beaker, the carrier (100 μg) was added from its standard solution and a given quantity of the radioactive tracer was further added. After the addition of 50 mg of the resin to this solution, stirring was started and the pH was adjusted with 0.1 M or 0.01 M sodium hydrogencarbonate or carbonate solution and hydrochloric acid (or nitric acid in the case of Ag^{+} and Pb^{2+}). Stirring was continued for 15 min for silver(I) and 30 min for other elements. Immediately thereafter, the resin was filtered through a membrane filter (Millipore Filter RAWP-047). The resin collected on the filter was transferred, together with the filter, to a polyethylene capsule (15 mm diameter, 85 mm high, equipped with a screw cap); 1 ml of 18 M sulfuric acid was added to dissolve the resin and water was added slowly to make the total volume 5 ml. The activity of the samples prepared in this manner and the control standard samples prepared separately was counted for 1 min, and the adsorption rate of each metal ion was computed, taking the count of the control standard sample as 100.

The adsorption rates of cadmium and lead ions were determined by a.a.s. as follows. The ion in question (100 μg) was added to 50 ml of water and the pH was adjusted as described above. After stirring for 30 min, the resin was filtered off, the filtrate was concentrated or diluted to a specified volume, the ion was determined in the usual manner and the adsorption rate was calculated for each resin. The cold-vapor a.a.s. method was applied to determine the adsorption rate of mercury(II). In all cases, blanks were done with the raw cellulose material as a control.

RESULTS

Composition of synthesized polymers

The contents of nitrogen and sulfur and the composition calculated therefrom are shown in Table 2 for the aminocelluloses obtained from tosylcellulose (content of sulfur, 11.4%; degree of substitution, 1.28) and the dithiocarbamatecelluloses derived from the aminocelluloses. As is apparent

TABLE 2

Components of aminocellulose and dithiocarbamatecellulose derivatives

	Amine	Contents (%)		Components
		S	N	
ANA	$C_6H_5NH_2$	8.41	0.91	$(OTs)_{0.78}$ $(C_6H_5NH)_{0.19}$
BZA	$C_6H_5CH_2NH_2$	4.51	2.04	$(OTs)_{0.35}$ $(C_6H_5CH_2NH)_{0.36}$
BUA	$C_4H_9NH_2$	4.15	1.75	$(OTs)_{0.29}$ $(C_4H_9NH)_{0.27}$
PIA	$(C_2H_4NH)_2$	4.48	4.74	$(OTs)_{0.34}$ $(C_4H_{10}N_2)_{0.41}$
AND		9.30	0.82	$(C_6H_5NH)_{0.14}$ $(CS_2NH_4)_{0.05}$
BZD		6.52	1.83	$(C_6H_5CH_2NH)_{0.27}$ $(CS_2NH_4)_{0.09}$
BUD		5.67	1.83	$(C_4H_9NH)_{0.21}$ $(CS_2NH_4)_{0.06}$
PID		8.24	5.14	$(C_4H_{10}N_2)_{0.25}$ $(CS_2NH_4)_{0.16}$

from Table 2, PID has the largest proportion of the amino and dithiocarbamate groups. In the light of the high content of the residual tosyl group in ANA, it seemed possible to increase the amino group content in ANA by extending the reaction time and raising the reaction temperature.

pH dependency

The pH dependency of the adsorption of various metal ions by the four dithiocarbamatecelluloses was investigated. The results obtained are presented in Fig. 1. With Cu^{2+}, Cd^{2+} and Pb^{2+}, any one of the four dithiocarbamatecelluloses showed a maximum adsorption in the neutral region. The adsorption occurred most markedly for PID; AND behaved similarly to the cellulose used as the control. With Ag^{+}, BUD, BZD and AND behaved similarly, but PID showed a maximum at pH 7—8 and adsorbed more Ag^{+} than the others.

With Cr^{6+} and As^{5+}, BUD, BZD and PID all showed a maximum adsorption in the acidic region. Both BUD and PID adsorbed Hg^{2+} sufficiently over a wide range of pH.

Compared with other metal ions, Fe^{3+}, Mn^{2+} and Zn^{2+} started to form precipitates at relatively low concentrations at pH 7 or above. For this reason, they were studied under conditions which were carrier-free or nearly so. Both BUD and PID showed maximum adsorption of Fe^{3+} in the alkaline region. In contrast, cellulose as a control showed maximum adsorption of Fe^{3+} in the neutral region but an abrupt drop in adsorption in the alkaline region, which suggested no formation of precipitates. The adsorption of Mn^{2+} by BUD and PID was less than that of Fe^{3+} in the neutral region, but increased sharply in the alkaline region. The adsorption of Mn^{2+} by cellulose showed a maximum in the neutral region, as in the case of Fe^{3+}. Differing markedly from Cr^{6+} which was adsorbed well in the acidic region, Cr^{3+} was adsorbed more in the alkaline region by BUD and PID, as were Fe^{3+} and Mn^{2+}. The adsorption of Zn^{2+} by PID increased in the alkaline region; however, some precipitates are likely to form at pH 8 or more and the occurrence of

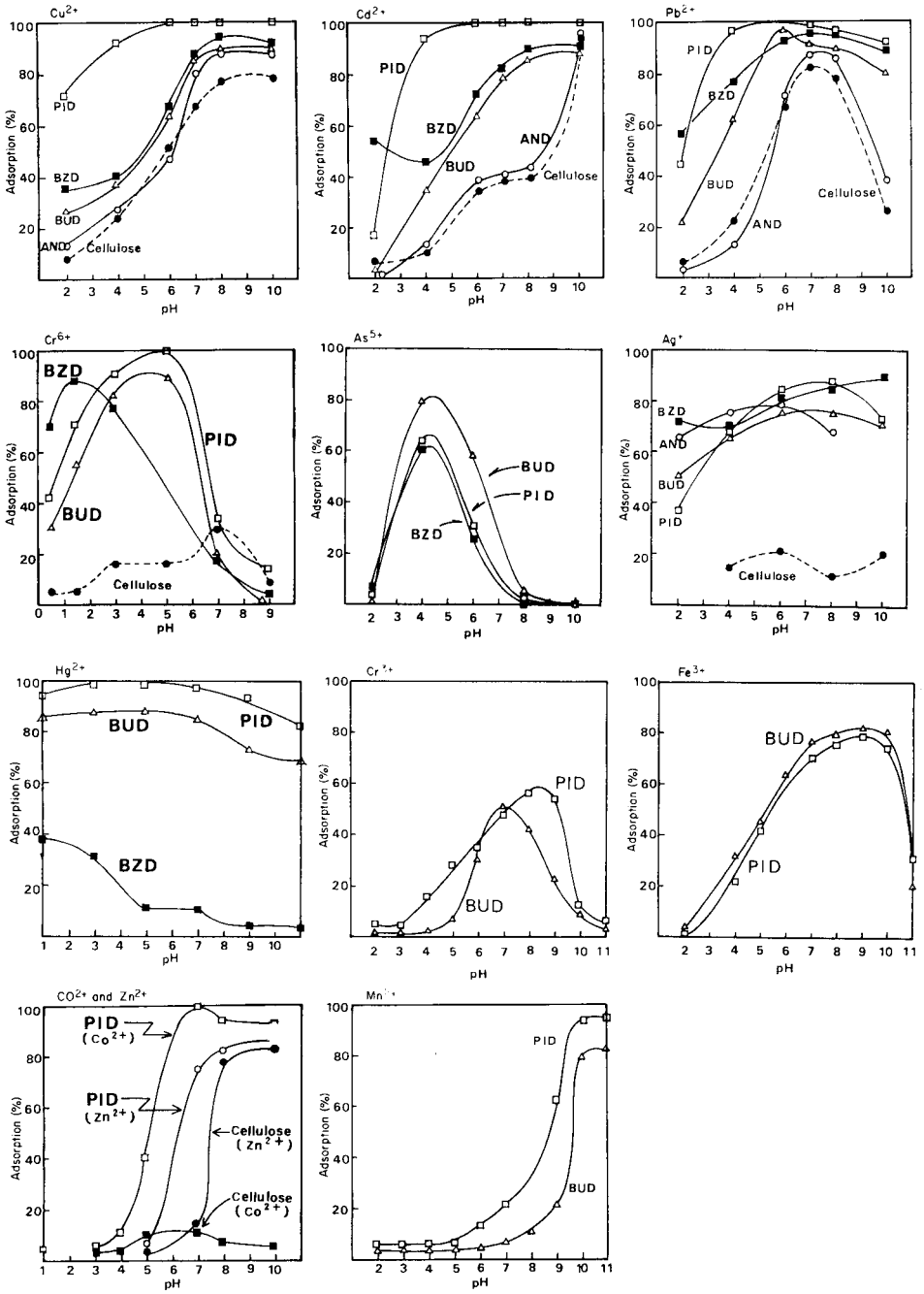

Fig. 1. Adsorption behavior of the ions studied by the batch method on 50 mg of resin in 50 ml of water with equilibration for 30 min (unless noted otherwise). Amount of carrier added: Cu^{2+}, 200 μg; Cd^{2+}, Pb^{2+}, Co^{2+}, Zn^{2+}, 100 μg; As^{5+}, Cr^{3+}, Fe^{3+}, Mn^{2+}, none; Hg^{2+}, 1000 μg. For Ag^{+}, only 10 mg of resin was used, with 15-min equilibration; the amount of carrier was 500 μg for PID and 100 μg for AND, BZD and BUD. For Cr^{6+}, the amount of carrier was 1000 μg for PID and 500 μg for BZD and BUD with 100 mg of resin.

adsorption above pH 8 was not confirmed. In the case of Sb^{5+}, Se^{4+} and Te^{4+}, PID showed a maximum adsorption in the acidic region, roughly equal to that of BUD. PID was also similar to BUD in that it adsorbed Co^{2+} well in the alkaline region.

Effects of the amino group of metal ion uptake

Of the metal ions showing maximum adsorption on the acid side, some seem to be adsorbed on the amino group remaining in the resin rather than on the dithiocarbamate group. The earlier study [6] of the adsorption behaviors of As^{5+}, Cr^{6+} and Hg^{2+} on BUA (an aminocellulose) and on BUD (a dithiocarbamatecellulose) showed that the amino group is involved in the adsorption of As^{5+} or Cr^{6+}.

Consequently, a further study was conducted on the adsorption behavior of As^{5+}, Se^{4+}, Te^{4+} and Sb^{5+} on PIA and PID. These ions had shown a maximum in the acidic region in their adsorption by PID. The results are given in Fig. 2. Both Se^{4+} and Te^{4+} are adsorbed only slightly on PIA and it is likely that the adsorption on PID occurs mainly via the dithiocarbamate group. However, As^{5+} and Sb^{5+} are also adsorbed on PIA and some contribution from the amino group is conceivable here.

Capacities of BUD and PID

The capacities of BUD and PID for metal ions were determined as breakthrough capacities as follows. BUD or PID (1 g) was packed in a column (10 mm i.d.) and a 1000 ppm standard solution of Ag^{+} ($AgNO_3$) or Hg^{2+} ($HgCl_2$) or 100 ppm standard solution of Cu^{2+} ($CuSO_4$), Pb^{2+}[$Pb(CH_3COO)_2$], Se^{4+}(SeO_2) or Cr^{6+}($K_2Cr_2O_7$) was passed through the column at a given pH and at a flow rate of 0.5 ml min^{-1}. The results (Table 3) show that the capacities of both BUD and PID decreased in the order Hg^{2+}>Cr^{6+}>Ag^{+}>Se^{4+}>-Cu^{2+}>Pb^{2+}.

The capacity for Cr^{6+} is greater than those for Cu^{2+} and Pb^{2+} and the

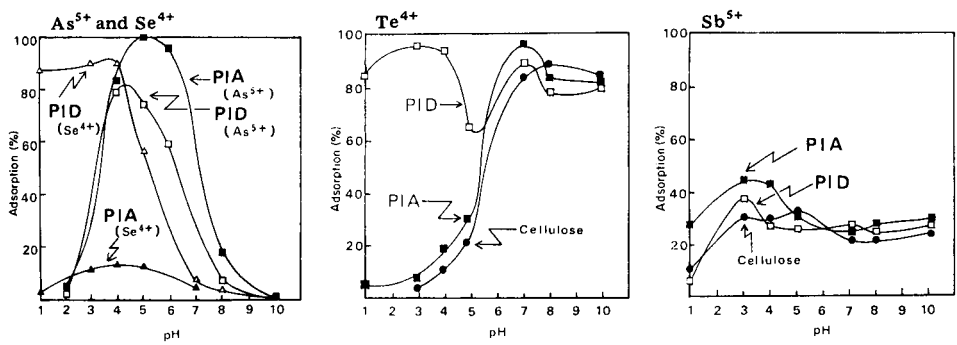

Fig. 2. Adsorption behavior of As^{5+}, Se^{4+}, Te^{4+} and Sb^{5+} on PIA and PID on 50 mg of resin with equilibration for 30 min. The amount of carrier was 100 μg, except for As^{5+} which was carrier-free.

TABLE 3

Break-through capacity for BUD and PID

Metal ion	Resin	pH	Capacity (mg M^{n+} g^{-1} resin)	Metal ion	Resin	pH	Capacity (mg M^{n+} g^{-1} resin)
Hg^{2+}	BUD	4.3	220	Se^{4+}	BUD	3.2	41
	PID	4.3	370		PID	3.2	86
Cr^{6+}	BUD	2.6	72	Cu^{2+}	BUD	5.4	7.3
	PID	2.6	155		PID	5.4	15
Ag^{+}	BUD	5.2	67	Pb^{2+}	BUD	5.9	6.9
	PID	5.2	120		PID	5.9	9.5

plausible explanation is that Cr^{6+}, in addition to sorption by the dithiocarbamate group, is adsorbed by the amino group remaining in the resin and also adsorbed as Cr^{3+} which results from oxidation of the resin with Cr^{6+}.

In the case of Hg^{2+}, contributions to the adsorption are apparently made not only by the dithiocarbamate group but also by the functional groups containing S and N.

Stability of BUD and PID to acid and heat

The stability of BUD and PID to acid and heat was examined. Portions (1 g) of the resin were immersed in 0.1, 0.5 and 2.0 M hydrochloric acid for 1 h, and washed with water, and the resin was packed in a column. A 100-ppm standard solution of Cu^{2+}(pH 5.4) was passed through the column, the amount of Cu^{2+} adsorbed was determined and the adsorption rate was calculated, taking the amount of Cu^{2+} adsorbed on the untreated resin as 100.

Next, 1 g of the resin heated at 110°C for 1 h or 20 h was packed in a column and the adsorption rate of Cu^{2+} was determined as above. The results (Table 4) show that the acid treatment reduces the capacity of BUD or PID to 25% or less. The heat treatment reduces the capacity to ca. 75% after 1 h and to ca. 50% after 20 h.

TABLE 4

Stability of resin

Immersion in HCl			Heating at 110°C		
HCl (M)	Cu^{2+} Adsorption (%)		Time (h)	Cu^{2+} Adsorption (%)	
	BUD	PID		BUD	PID
0.1	25	7	1	73	87
0.5	19	7	20	48	50
2.0	16	7			

Immersion time; 1 h.

Conclusions

Four kinds of dithiocarbamatecelluloses were synthesized and their adsorption of metal ions was investigated. The pH-dependence of the adsorption of Ag^{+}, Cd^{2+} and Pb^{2+} by the four resins was similar although some differences were found in the amount of the ions adsorbed. BZD, BUD and PID showed a relatively similar pH-dependence in the adsorption of Cr^{6+}, as did BUD and PID in the adsorption of Hg^{2+}.

BUD and PID showed a maximum in the acidic region in the adsorption of As^{5+}, Sb^{5+}, Se^{4+} and Te^{4+} and a maximum in the alkaline region in the adsorption of Cr^{3+}, Fe^{3+} and Mn^{2+}. Moreover, it is likely that the residual amino group participates in the adsorption of As^{5+} and Sb^{5+} by BUD and PID. The capacities of BUD for Hg^{2+}, Cr^{6+}, Ag^{+}, Se^{4+}, Cu^{2+} and Pb^{2+} range from 6.9 to 220 mg g^{-1} of resin while those of PID for the same metal ions range from 9.5 to 370 mg g^{-1} of resin. Both BUD and PID are relatively stable to heat but not to acid.

Of the four resins, AND and BZD adsorb various metal ions to a relatively small extent, but BUD and PID generally have satisfactory capacities for practical use. BUD does not take up Na^{+} as was reported previously; it contains very little metal ions as impurities and offers an advantage for the neutron activation analysis of trace elements in natural water. In addition, BUD can be readily decomposed by low-temperature plasma ashing and this facilitates application of the sample after uptake of metal ions to atomic absorption spectrometry and emission spectrometry.

The authors express their appreciation to Professor Yuzuru Kusaka and Assistant Professor Haruo Tsuji, Faculty of Science, Konan University, for their guidance and advice and thank research members of the Hot Laboratory, Research Reactor Institute, Kyoto University, for their cooperation.

REFERENCES

1 J. F. Dingman Jr., K. M. Gloss, E. A. Milano and S. Siggia, Anal. Chem., 46 (1974) 774.
2 K. Hayashi, K. Sakai, K. Usami and K. Kotsuji, Jpn. Anal. (Bunseki Kagaku), 27 (1978) 579.
3 R. A. A. Muzzarelli, Natural Chelating Polymers, Pergamon Press, 1973.
4 M. Okawara, Sen-i Gakkaishi, 30 (1974) 245.
5 Z. A. Rogovin, Vysokomol. Soyedin., 13 (1971) 437.
6 S. Imai, M. Muroi, A. Hamaguchi, R. Matsushita and M. Koyama, Jpn. Anal. (Bunseki Kagaku), 28 (1979) 415.

Analytica Chimica Acta, 113 (1980) 149—158

THE SEPARATION OF LANTHANIDES ON ANION-EXCHANGE RESIN IN ANHYDROUS ACETIC ACID MEDIUM

P. VAN ACKER*

Institute for Nuclear Sciences, Rijksuniversiteit Gent, Proeftuinstraat 86, 9000 Gent (Belgium)

(Received 16th July 1979)

SUMMARY

The suitability of anhydrous acetic acid as a medium for the separation of some lanthanides (neodymium, samarium, terbium and thulium) on anion-exchange resins was investigated; the results indicated that although transfer to the anhydrous solvent does not influence the distribution coefficients of these elements in this medium, the addition of anions drastically changes their adsorption behaviour so that separations become possible.

Many theoretical investigations [1—5] have dealt with the anion-exchange behaviour of elements in organic and in mixed organic—inorganic solutions of very low water content. The importance of such media for practical separations has however rarely been mentioned. In addition to earlier work [6—8] on the influence of low water contents on the anion-exchange behaviour of elements in anhydrous acetic acid, it was interesting to investigate the suitability of this solvent for some difficult separations, e.g. those of the different rare earth elements. Previous studies indicated that at very low water contents (<0.5%) a solvation-hydration transition of the metal complexes in both the solvent and the resin phase takes place; the transition differs for different elements.

In this study, the adsorption behaviour of Nd(III), Tb(III), Sm(III) and Tm(III) was investigated in acetic acid on an anion-exchange resin in the chloride form as a function of the water content. No adsorption was found over the concentration range studied.

A comparison of these results with those of Van de Winkel et al. [6] indicated the possible importance of the effect of nitrate ions on the adsorption behaviour of these elements; this was confirmed by a comparative study of the influence of chloride and nitrate on their adsorption on an anion-exchanger in acetic acid. From these data, a separation procedure was worked out for some rare earth elements.

*Present address: Vrije Universiteit Brussel, Pleinlaan 2, 1050 Brussel, Belgium.

EXPERIMENTAL

Apparatus

A dry atmosphere glove-box (ca. 20 mg H_2O m^{-3}) was used to avoid absorption of moisture by the dried reagents, working at acetic acid water contents below 5%.

Radioactivity measurements were performed with a Ge(Li)-detector coupled to a 4000-channel analyser. The radioactivity of the mono-energetic radiotracer ^{170}Tm was measured by discriminative counting in a NaI(Tl) well-type detector, coupled to a single-channel analyser.

Reagents and radioactive tracers

The strong base anion exchanger Dowex 1-X8 (100—200 mesh) and (200—400 mesh) was used in the chloride and nitrate forms after purification by a column-conditioning procedure with sodium hydroxide and hydrochloric acid. The resin was dried and stored as described earlier [9]. For conversion to the nitrate form, an RCl-resin column, was purified and washed with several bed volumes of 1 M nitric acid until the eluent was free of chloride ions and then rinsed with water till the eluent was free of nitrate ions.

After drying for 14 days, the water content of the resin was 0.3—0.8% water per g of dry resin. The total exchange capacity of the exchanger in the chloride form was 3.8 meq Cl^- g^{-1} of dried resin.

Acetic acid with various water contents was prepared and stored as reported previously [9]. The minimum water content, determined by Karl Fischer titration, was 33 μg H_2O ml^{-1}.

Chloride was added to the anhydrous acetic acid solvent with HCl—acetic acid mixtures and solutions of lithium chloride in acetic acid. The HCl—acetic acid mixtures were made with an HCl generator. Figure 1 gives the maximum hydrogen chloride uptake as a function of the water content of the acetic acid solvent.

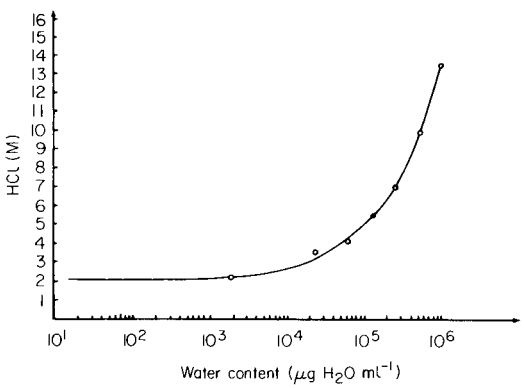

Fig. 1. Maximum HCl uptake as a function of the acetic acid water content.

Nd(III), Sm(III), Tb(III) and Tm(III) stock solutions were prepared by dissolving appropriate amounts of the neutron-irradiated and dehydrated metal acetates in acetic acid of known water content. The water contents of the metal acetates themselves varied between 1.8 and 4.0%.

The distribution coefficients were determined with the radiotracers ^{147}Nd ($t_{1/2}$ 10.99 d; γ, 91 keV, 5.31 keV); ^{153}Sm ($t_{1/2}$ 47 h; γ 103.1 keV); ^{160}Tb ($t_{1/2}$ 73.3 d; γ 879.3 keV); and ^{170}Tm ($t_{1/2}$ 128 d; γ 84.1 keV). The radiotracers were obtained by irradiation of the dehydrated acetates in the Thetis reactor of the I.N.W. at a neutron flux of 1.5×10^{12} n cm^{-2} s^{-1}.

Determination of distribution coefficients, K_d

The weight distribution coefficients (ratio of the amount of metal per g of dry resin to the amount of metal per ml of solvent) were determined by batch experiments and column elution experiments at 25°C, unless otherwise mentioned.

For the batch experiments, the weights of the resin and the volume of the solvent varied in the ranges 25—100 mg and 25—50 ml, respectively [8]. The standard deviations for the distribution coefficients were determined as described elsewhere [10].

For measurements of small distribution coefficients (K_d<100), elution chromatography was used. The quantities of resin and solvent are discussed below (Table 1). The values of the specific volume of the resin and the interstitial fraction were taken from the literature [11].

RESULTS

Batch equilibration

The distribution coefficients (K_d values) of the four rare earth elements were determined by batch equilibration experiments as a function of the resin loading in acetic acid containing 37 μg H_2O ml^{-1} and 8.87% H_2O. At resin loadings smaller than 0.5% mmol meq^{-1}, the K_d values were studied

TABLE 1

Conditions for the column experiments

Expt.	LiCl, ($\times 10^{-3}$ M)	Elution speed (drops s^{-1})	Resin beads mesh-size	Weight of resin (mg)	Column diameter (mm)
1	0.971	1/17	100—200	191.4	6
2	1.94	1/17	100—200	196.6	6
3	1.94	1/17	200—400	292.6	4
4	2.22	1/17	200—400	294.1	4
5	2.72	1/5	200—400	298.0	4
6	3.88	1/17	200—400	292.4	4
7	9.71	1/17	100—200	290.6	6

as a function of the water content of acetic acid (37, 210, 860, 3200 μg H_2O ml^{-1}).

No adsorption was found on the RCl resin (K_d<1), contrary to a report [6] of K_d values exceeding 100 under supposedly similar conditions. As the distribution coefficients were determined as described previously [6], except for the preparation of the tracer elements, the different behaviour can probably be attributed to the presence of nitrate ions arising from the nitric acid—acetic acid solution used earlier [6] for the dissolution of the metal oxides. This indicates the important influence of small amounts of anions on the adsorption behaviour of the elements under study.

Additional experiments were therefore carried out to obtain more information about the effect of anions on the adsorption; chloride and nitrate were chosen because the anion exchanger was in the chloride form and the previous results indicated possible interference from nitrate.

The influence of chloride on the anion exchange behaviour of the rare earth elements in anhydrous acetic acid was studied. The adsorption isotherms of Nd(III) and Tm(III) were determined on RCl resin in anhydrous acetic acid (water content 38 μg H_2O ml^{-1}) as a function of the chloride content added to the solvent as HCl and LiCl. The resin loading was below 0.5% mmol meq^{-1}.

For Tm(III) the results (Fig. 2A) indicate a steep increase in adsorption with increasing chloride content. With HCl the adsorption starts at lower chloride concentrations than with LiCl but the shapes of the curves are nearly identical. The shift in the position of both curves is probably due to the second cation effect and indicates a possible formation of ternary complexes with the HCl—acetic acid mixture. Because of the easier mani-

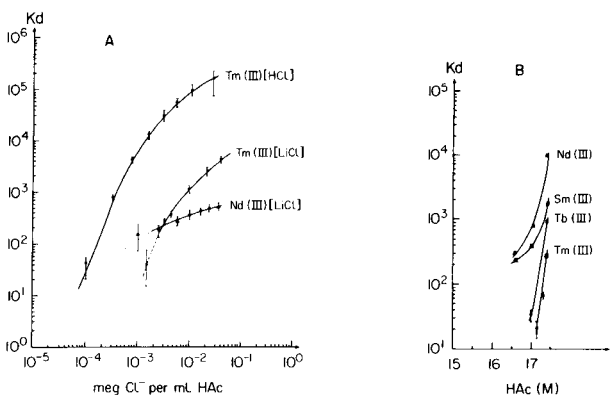

Fig. 2(A). Adsorption isotherms for Tm(III) and Nd(III) on RCl resin in acetic acid (38 μg H_2O ml^{-1}) as a function of the chloride content. (B) Adsorption isotherms for Nd(III), Sm(III), Tb(III) and Tm(III) on RNO_3 resin as a function of the acetic acid molarity.

pulation and preparation of the chloride solution, LiCl—acetic acid mixtures were preferred.

At chloride concentrations above 2.5×10^{-3} M, the adsorptions of the elements Nd(III) and Tm(III) diverge clearly but were too high for practical use (K_d>100). Below 2.5×10^{-3} M chloride, the situation is not so clear and more detailed information on the position of both isotherms could only be obtained by using column elution experiments.

The influence of nitrate anions on the adsorption behaviour was determined by batch experiments with RNO_3 resin as a function of the acetic acid concentration. The resulting adsorption isotherms (Fig. 2B) show an increase in adsorption going from the lower to the higher molarity. Over the entire interval the adsorption sequence was: Nd>Sm>Tb>Tm. The differences in adsorption indicate the possibility of separating these four rare earth elements, two by two, or individually. As for the RCl—LiCl—acetic acid medium, a determination of the distribution coefficients in the region K_d<100 by column experiments was necessary.

Column experiments

Distribution coefficient determination in acetic acid—LiCl medium on RCl resin. For the determination of small distribution coefficients, the column elution technique was used under different experimental conditions, summarized in Table 1. The ratio of the column height to diameter was always greater than 20. Before the column was made, the resin was equilibrated overnight in acetic acid of identical LiCl content to that used for the elution experiments, then 25 μl of a tracer solution (prepared by dissolving the metal acetate after irradiation in an identical solution) was adsorbed on the top of a RCl resin column, keeping the resin loading below 0.05% mmol meq^{-1}. The temperature of the column was 25°C. Figure 3 gives a typical elution curve: from its form, it is obvious that no distribution constant could be calculated. A fraction of the loaded metal elutes immediately, while the rest of the metal elutes slowly with the solvent. For each of the experimental conditions mentioned in Table 1, the elution data for Tm(III) are summarized in Table 2, which indicates that changing the experimental conditions, e.g. resin bead size, column dimensions, and elution speed, did not improve the characteristics of the elution curve. The fraction of the elements eluted at the peak maximum decreased with increasing chloride content. At relatively high chloride concentrations (3.88×10^{-3} M and 9.71×10^{-3} M), the maximum disappeared completely and it was only possible to elute small quantities of metal even after elution with many column volumes of solvent. Only slow kinetics of the complex formation or adsorption of the complex on the resin can explain this kind of behaviour.

Distribution coefficients in acetic acid on RNO_3 resin. Similar column experiments were carried out with the selected rare earth elements in acetic acid medium on RNO_3 resin. The acetic acid concentration varied between 16.7 and 17.4 M. The resulting curves were identical to those in Fig. 3, indicating a similarly slow complex formation or adsorption step.

TABLE 2

Results for Tm(III) in column experiments under the conditions given in Table 1

Expt.	Eluted volume LiCl—HAc—solvent (ml)	Percentage eluted (%)	Results
1	1.5	83	max. after 0.19 ml
2	34.9	84	max. after 0.63 ml
3	51.9	93	max. after 0.87 ml
4	37.4	56	max. after 0.88 ml
5	41.1	56	max. after 0.31 ml
6	75.1	30	max. not found
7	50.0	<10	max. not found

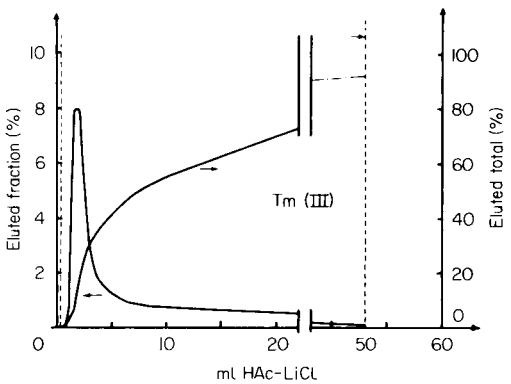

Fig. 3. Elution curve for Tm(III) on RCl resin (Dowex 1-X8, 100—200 mesh) in acetic acid—LiCl medium.

Influence of temperature

In the system RCl—LiCl—acetic acid with thulium acetate, the influence of the temperature on K_d was studied by batch experiments at different temperatures for different agitation times. The water content of the solvent was 38 μg H_2O ml^{-1}; the LiCl concentration was 3.8×10^{-3} M. The experiments done as a function of the agitation time at 25°C (Fig. 4) indicate slow equilibration (equilibrium reached after 1000 min). The experiments at 75°C, however, indicated that the equilibrium was reached within 1 h although the adsorption had decreased. As a consequence, it seemed interesting to do column experiments at 75°C on RCl resin in a LiCl—acetic acid solvent with Nd(III) and Tm(III). (The LiCl concentrations were 3.6×10^{-3} M and 3.8×10^{-3} M).

Figure 5A shows the total elution curve for Tm(III) under these conditions. It is obvious that raising the temperature of the experiments drastically changes the shape of the elution curve (compared with Fig. 3). The first elution peak, corresponding to the slow equilibration, decreases and a

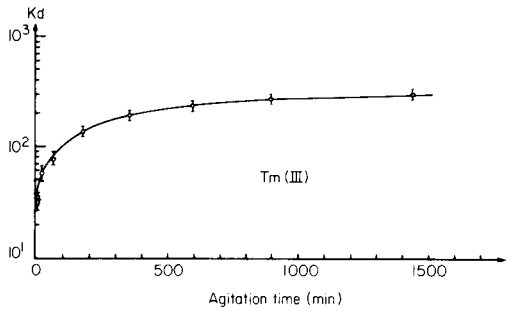

Fig. 4. Distribution coefficients for Tm(III) on RCl resin (Dowex 1-X8, 100—200 mesh) as a function of the agitation time at 25°C.

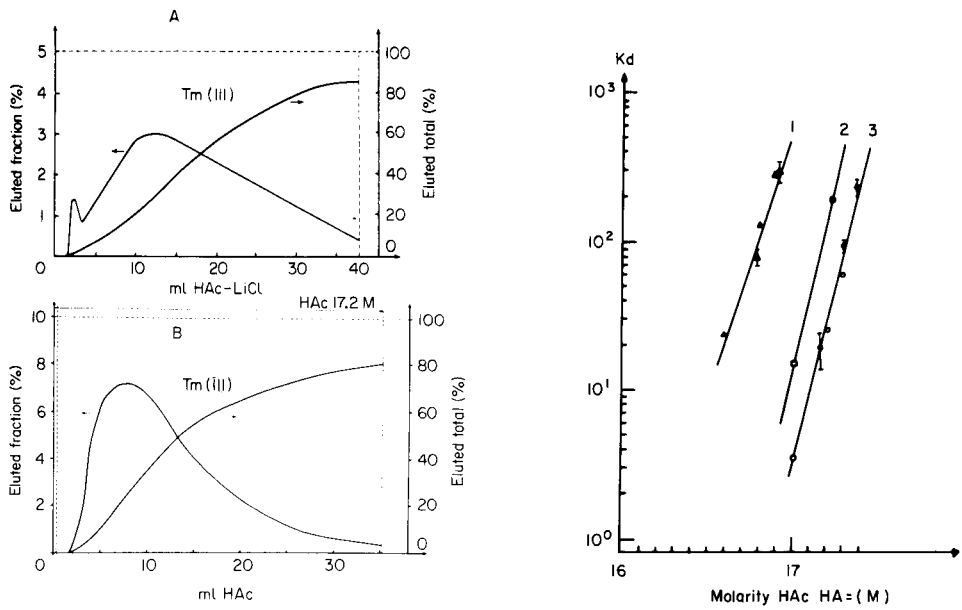

Fig. 5(A). Elution curve for Tm(III) on RCl resin (Dowex 1-X8, 100—200 mesh) in acetic acid—LiCl medium (38 μg H_2O ml^{-1}; 3.6×10^{-3} M LiCl) at 75°C. (B) Elution curve for Tm(III) in acetic acid (17.16 M) on RNO_3 resin proceeding from $Tm(NO_3)_3$.

Fig. 6. Adsorption isotherms for (1) Nd(III), (2) Tb(III), (3) Tm(III) on RNO_3 resin as a function of the acetic acid molarities, proceeding from the elements in the nitrate form. Open symbols indicate column experiments and filled symbols batch experiments.

broad second maximum appears. Unfortunately, however, the position of this maximum in the elution curves of both elements Nd and Tm was identical, which made it impossible to separate the rare earth elements in a RCl—acetic acid—LiCl medium.

From these experiments it is clear that a separation procedure is impossible because of the slow kinetics of complex formation or the adsorp-

tion step. Therefore improvements were to be expected by activating the equilibration, starting from the element in the same ionic form as that adsorbed on the resin, i.e. with the rare earth elements in the chloride form for separation in anhydrous acetic acid—LiCl on RCl resin, and in the nitrate form for separations in acetic acid on RNO_3 resin.

Separation on RNO_3 resin in acetic acid medium

From batch equilibration experiments, starting from the metal nitrate instead of the metal acetate for Nd(III) and for Tm(III), the distribution coefficients were calculated as a function of the acetic acid concentration on RNO_3 resin. These results are shown in Fig. 6. From comparison with the results in Fig. 2B, it is clear that the nitrate ions introduced with the tracer do not drastically change the position of the adsorption isotherms.

Column experiments were also carried out to determine low distribution coefficients on RNO_3 resin in acetic acid solvent. As an example of such an elution curve the results for Tm(III) on RNO_3 resin in 17.16 M acetic acid, starting from $Tm(NO_3)_3$ as tracer element, are shown in Fig. 5B. Under these conditions, no element was eluted below a certain volume that differed for each element and acetic acid concentration. The curves showed an appreciable amount of tailing. From the position of the maximum, however, it was possible to calculate distribution constants. These values, calculated for Nd(III), Tb(III) and Tm(III) as a function of the water content of the acetic acid solvent, are indicated in Fig. 6; good agreement was found between the distribution coefficients determined by both methods. It can be concluded that it is possible to separate the rare earth elements, although contamination of the fractions due to tailing is to be expected; tailing results from slow equilibration which could not be improved by using smaller beads or by increasing the temperature. This slow equilibration can be ascribed to instability of the adsorbed metal complexes, difficult equilibration between the metal complex and the exchanger, interference of acetate anions, etc.

As an example, Nd(III) and Tm(III) were separated on the RNO_3 resin in acetic acid. The concentration of the acetic acid was chosen so that the elements could be eluted with a small volume of solvent. Therefore, the initial acetic acid concentration for the adsorption of the metal nitrates on the top of the column was 17.03 M. (Before making the column, the resin was equilibrated overnight in acetic acid of identical concentration.) The elution was started with 17.03 M acetic acid. Because the distribution constants of Tm(III) and Nd(III) were 4 and >700, respectively, under these conditions, Tm(III) was obtained in a pure form. After the quantitative elution of Tm(III) from the column (the fraction left behind on the resin was smaller than 0.5% of the initial amount), the acetic acid concentration was reduced to 15 M for the elution of Nd(III). The elution curves are shown in Fig. 7; 88% of the Tm(III) was eluted in the first 10 ml of solvent, while the other 12% needed a further 40 ml of acetic acid.

These results show that a separation of Tm(III) and Nd(III) is readily

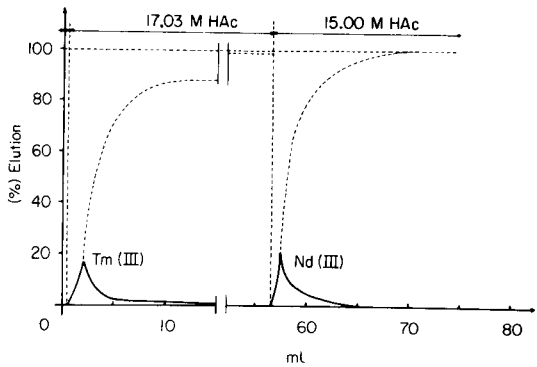

Fig. 7. Separation of Tm(III) and Nd(III) on RNO_3 resin (Dowex 1-X8, 100—200 mesh) in acetic acid medium.

possible because of the large difference in distribution coefficients, but tailing will always complicate the separation of a mixture of rare earth elements in spite of the favourable position of the adsorption isotherms. It is always possible to obtain a pure fraction of the first eluted element and to separate a mixture of elements by repeated elutions. An added advantage of this separation procedure is the easier solubility of the rare earth elements in nitric acid.

Elution curves on RCl resin in acetic acid—LiCl solutions

Elution experiments were carried out, starting from metal chloride instead of metal acetate, to determine the distribution coefficients of the elements on RCl resin in acetic acid—LiCl medium. The water content of the solvent was 38 μg H_2O ml^{-1} and the LiCl concentration was 1.37×10^{-3} N. The shape of the elution curves was similar to those in Fig. 5b. However the very small differences in K_d values calculated from the elution curves (K_d = 3.2 for Nd(III) and K_d = 1.6 for Tm(III)) made this medium unsuitable for separations.

Conclusions

It is clear that anhydrous acetic acid is not as interesting for practical purposes as expected. The results, together with those of previous theoretical studies on the influence of water on the anion-exchange behaviour of elements in acetic acid medium, indicate that the use of anhydrous solvent is restricted to separations where the distribution coefficients of the hydrated and the solvated complexes differ greatly. The transition solvation-hydration must be considered as a marginal effect, which hardly influences K_d.

The results further indicate that small amounts of anions have a far larger effect on the adsorption behaviour of the rare earth elements on the

anion-exchange resin in acetic acid medium than do very low water concentrations.

Tailing of the elution curves was difficult to minimize under classical experimental conditions, e.g. an increase in the theoretical plates (smaller resin beads, other column dimensions), and an increase in the temperature. A fundamental investigation into the kinetics of complex formation and adsorption under these conditions could give more insight into these problems and perhaps reveal the practical possibilities of anhydrous media.

Thanks are due to Prof. Dr. J. Hoste for his interest and helpful suggestions during the work and to T. DeWispelaere for technical assistance. The financial support of the Interuniversitair Instituut voor Kernwetenschappen is gratefully acknowledged.

REFERENCES

1 Y. Marcus and E. Eyal, J. Inorg. Nucl. Chem., 32 (1970) 2045.
2 J. Kennedy and R. V. Davies, J. Inorg. Nucl. Chem., 12 (1959) 193.
3 D. H. Wilkins and G. E. Smith, Talanta, 8 (1961) 138.
4 J. Penciner, I. Eliezer and Y. Marcus, J. Phys. Chem., 69 (1965) 2955.
5 L. W. Marple, J. Inorg. Nucl. Chem., 26 (1964) 859.
6 P. Van de Winkel, F. De Corte and J. Hoste, Anal. Chim. Acta, 56 (1971) 241.
7 F. De Corte, P. Van Acker and J. Hoste, Anal. Chim. Acta, 64 (1973) 177.
8 P. Van Acker, F. De Corte and J. Hoste, J. Inorg. Nucl. Chem., 37 (1975) 2549.
9 P. Van Acker, F. De Corte and J. Hoste, Anal. Chim. Acta, 73 (1974) 198.
10 F. De Corte, P. Van Acker and J. Hoste, Anal. Chim. Acta, 75 (1975) 246.
11 F. De Corte, J. Inorg. Nucl. Chem., 37 (1975) 2546.

Analytica Chimica Acta, 113 (1980) 159—164

Short Communication

A SYSTEMATIC ERROR FROM COUNT RATES IN NEUTRON ACTIVATION ANALYSIS OF ARCHAEOLOGICAL MATERIALS

JOSEPH YELLIN*

Institute of Geophysics and Planetary Physics, University of California, Los Angeles, California 90024 (U.S.A.)

(Received 16th May 1979)

Summary. Errors of the order of a few per cent may occur in trace element measurements because of changes in the Ge(Li) detector resolution caused by count rate; errors appear when photopeak intensities are measured by summing a fixed number of data channels. A simple correction method based on a gaussian approximation is proposed. The problem is discussed in the context of trace element measurements in archaeological material.

The determination of the provenance of archaeological material by instrumental neutron activation analysis (i.n.a.a.) generally involves measurement of large numbers, sometimes hundreds, of archaeological specimens such as pottery shards or obsidians. Automation is therefore necessary in the measuring process as well as in the data reduction. A strict irradiation and analysis schedule must be maintained in order to maximize both the capacity of the system and the precision of measurements. It may also be necessary to operate the equipment for long periods without human attendance.

When automatic transport mechanisms are employed to position samples on the γ-ray detector, a fixed detector—sample geometry is employed. This fixed geometry can lead to a systematic bias in the measurements because of count-rate differences between the standards and samples. The reason for the systematic bias is that the resolution of the radiation counter degrades with count rate. In a given batch of irradiated samples some will be more active than the standards and some less active. Hence for any given sample γ-ray, the detector resolution will be worse or better than the resolution of the same γ-ray in the standard. There are other effects connected with count rate but here only the loss of resolution with count rate is considered.

Two approaches are commonly employed to measure the area of photopeaks. In one, line-shape fitting computer routines are used to measure the area and the peak widths are duly accounted for [1]; this is complicated, expensive and of dubious advantage in dealing with complex spectra. In the other, γ-ray intensities are measured by summing a fixed number of channels

*Present address. Institute of Archaeology and Department of Physics, Hebrew University of Jerusalem, Israel.

on each photopeak [2]. So long as the same proportion of the true peak area is measured for both the standard and sample γ-rays the fact that the summation is truncated at some arbitrary point is of little consequence since the ratio of the sample to standard photopeak area is ultimately used. The precision of measurement depends on the choice of the peak boundaries [3, 4]. The problem addressed here is that caused by differences in the peak width between standard and sample γ-rays: the method of summing a fixed number of channels on a photopeak, as opposed to summing a constant fraction of the peak width, results in different proportions of the area measured for the standard and sample γ-rays.

The way in which differences in detector resolution can affect a measurement is illustrated in Fig. 1. The two curves shown each have the same area, arbitrarily taken as 10,000 counts, but different widths. For curve A the full-width at half maximum (FWHM) is 3 channels whereas for curve B the FWHM is 4 channels. Consider the sum of curves A and B over a fixed number of channels, say 3 channels above and below the peak channel. Suppose that

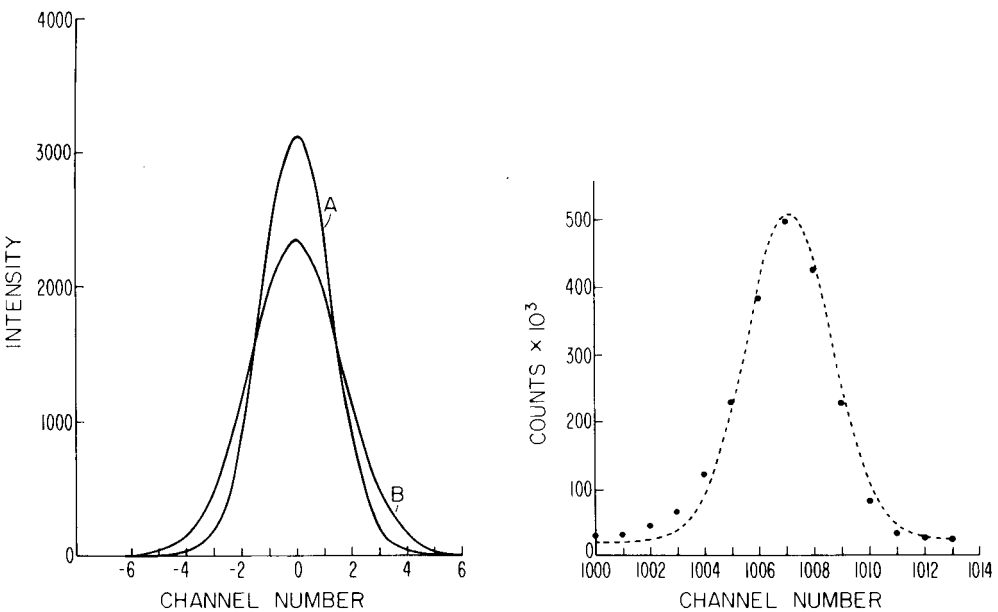

Fig. 1. Two simulated gaussian γ-ray photopeaks with the same area but different widths. For A, *FWHM* = 3 and for B, *FWHM* = 4. The tabulated results are:

$n - n_0$	−6	−5	−4	−3	−2	−1	0	1	2	3	4	5	6	Σ	Σ_{-3}^{3}
$I_A(W = 3)$	0	1	23	196	913	2301	3131	2301	913	196	23	1	0	9999	9951
$I_B(W = 4)$	5	31	147	494	1174	1975	2349	1975	1174	494	147	31	5	10001	9635

Fig. 2. ^{46}Sc 889-keV photopeak measured with a 42-cm^3 Ge(Li) detector. The dashed curve is a gaussian fit to the experimental points, showing the degree to which the photopeak can be approximated.

curve A is a standard γ-ray while curve B is the same γ-ray in a pottery shard and has been broadened by high-intensity γ-rays in a different portion of the spectrum of which B is a component. Because the peak areas are the same, the elemental abundances corresponding to peaks B and A are the same, but the partial sum for A yields 9951 while the partial sum for B yields 9635, i.e. a ratio of 0.97. Thus a 3% error results if allowance is not made for the fact that curve B has been broadened.

In actual experiments, the errors associated with differences between the standard and sample peak widths may vary from 0.1% to 5% or even occasionally 10%. Since pottery groups usually have compositional spreads on the order of 10—20%, the errors associated with the γ-ray photopeak are of little consequence when they are ca. 1%; however, some pottery groups and obsidians are very homogeneous and may show compositional spreads on the order of 5% or less [5]. Thus for unknown specimens, it is prudent to make corrections for sample/standard peak-width differences whenever a γ-ray intensity is measured by summing a fixed number of channels on the photopeaks and the summation does not cover the whole peak.

Photopeaks measured by Ge(Li) detectors are approximately gaussian and this suggests a simple way of offsetting errors resulting from peak width differences, namely, by normalizing the intensity of a sample γ-ray to the standard peak width. In the gaussian approximation, the normalization factor can be shown to be

$$f = [W_x \sum \exp(-2.7726(n - n_0)^2/W_s^2]/[W_s \sum \exp(-2.7726(n - n_0)^2/W_x^2]$$

where W_x is the FWHM of the sample photopeak, W_s is the *FWHM* of the standard photopeak, n_0 is the peak channel, and the sum extends over the channels n summed on the photopeak. The factor 2.7726 arises from the relationship between the variance, σ^2, of the gaussian curve and the FWHM, i.e. $\sigma^2 = (FWHM)^2/(8 \ln 2)$.

For the case shown in Fig. 1, the normalization factor f can be obtained from the values in the legend, giving $f = 1.033$. Multiplication of the partial sum of curve B by f gives $1.033 \times 9635 = 9952$ in agreement with partial area A.

Results

An illustration of how the gaussian correction works in practice is shown in Table 1, which summarizes measurements of scandium-46 in U.S.G.S. BCR-1 basalt standard, relative to the Perlman and Asaro Standard Pottery (SP) [2]. These measurements were made with a 42-cm^3 Ge(Li) detector at the Archaeometry Laboratory, Hebrew University. The ^{46}Sc γ-ray is free of interferences and can be measured with great precision; the true area of the photopeak can be measured by summing enough channels to ensure that peak-width differences are of no consequence. The BCR-1/SP scandium ratio is then re-evaluated by summing fewer channels on the photopeaks so as to indicate the error resulting from peak-width differences, and this result,

TABLE 1

Partial area of the 889-keV ^{46}Sc photopeak and ratios for BCR-1/Standard Pottery (SP). The areas are expressed in counts per minute normalized to the end of irradiation and corrected for weight differences. PWC is the factor which normalizes the BCR-1 partial area to the standard width.

No. of channels used	Peak areas (cpm)				
	SP	BCR-1	BCR-1/SP ratio[a]	*PWC*	(BCR-1/SP) *PWC*
14	23156 ± 18	38560 ± 33	1.665 ± 0.002	1.000	1.665
10	23001 ± 17	38185 ± 32	1.660 ± 0.002	1.001	1.662
8	22762 ± 17	37602 ± 31	1.652 ± 0.002	1.006	1.662
6	21801 ± 16	35577 ± 29	1.632 ± 0.002	1.021	1.666
4	23100 ± 17	29429 ± 26	1.601 ± 0.002	1.047	1.676

[a]Errors shown are due to counting statistics only and are negligible for the present purpose.

corrected for peak-width differences, is then compared with the first truer measurement, etc. Fourteen channels corresponding to ca. 12 keV were first summed on the photopeak shown for BCR-1 in Fig. 2. The *FWHM* is 3.7 channels (3.12 keV) for the BCR-1 and 3.4 channels (2.86 keV) for the SP, i.e. a 9% difference. The partial areas of the photopeaks determined by summing 10, 8, 6 and 4 channels are shown in Table 1. The peak-area ratios (column 4) vary from 1.665 to 1.601, the difference being 3.8% for these extremes. The ratio 1.665 ± 0.002 leads to a scandium value of 34.22 ± 0.04 ppm for BCR-1. The gaussian peak-width corrections (*PWC*) necessary for the area ratios are shown in column 5 and the corrected ratios in column 6. For the 10, 8, 6 and 4-channel summations, the uncorrected ratios cause negative errors of 0.3%, 0.8%, 2.0% and 3.8%, respectively; after the peak width corrections have been applied, the errors are —0.2%, —0.2%, 0.06% and 0.66%, respectively. Thus, serious errors arising from sample-standard peak-width differences can be largely offset by the simple gaussian approximation. For the example shown, enough channels can usually be summed so that peak-width corrections are unnecessary. However, in many instances the γ-rays of interest suffer interferences, and it is desirable to truncate the area measurements to minimize interference corrections which may lead to greater uncertainties than are introduced by peak-width differences.

Discussion

An alternative approach which is sometimes employed to correct for peak broadening is to measure the counts lost under a photopeak as a function of count rate. Empirical calibration curves are developed for each mode of summing the peak by artificially broadening a photopeak with a γ-source. For example, the intensity of the 60-keV peak of an ^{241}Am source is measured by summing a fixed number of channels on the photopeak. The measurement, at constant live time, is then repeated for different degrees of broadening

induced by a ^{57}Co source, the quantities measured being the area of the ^{241}Am photopeak and the count rate. The variation of peak area is then developed as a power series in count rate by least-squares analysis. The process is repeated for each mode of summing the peak and for each detector. A serious drawback to this procedure is that the count rate is not the only parameter affecting the peak width. The degree to which the detector performance degrades with count rate depends also on the energy of the γ-rays, high-energy γ-rays giving greater broadening. The degree of broadening therefore depends on the spectrum profile and significant deviations from the calibration curves can therefore be expected for some spectra. In contrast, the gaussian approximation is based directly on a measure of the peak width and is therefore independent of the spectrum profile.

Table 2 compares some trace element measurements corrected for peak broadening by a count rate correction (CRC) and by the gaussian approximation (PWC). This example relates to a slag in which the photopeaks were very much broader than in the standard. The ^{169}Yb and ^{182}Ta photopeaks were 50% broader in the specimen than in the standard while the ^{153}Sm and ^{177}Lu photopeaks were respectively 37% and 16% broader. The results in Table 2 show that for moderate peak-width differences (Sm, Lu) both methods give substantially the same results while for extreme broadening (Yb, Ta) substantial differences occur. The count rates involved in these measurements were not excessive and lead to only minor corrections, but the peaks were very much broadened. The point is that the spectrum profile responsible for the broadening was very different from that used to calibrate the CRC. The CRC can be improved by developing it as functions of the dominant γ-ray in a given spectrum and of the γ-ray analyzed, but such refinements would greatly complicate the measuring process and are unlikely to result in improvements over the peak-width correction method.

Application of the peak-width correction outlined above requires that the width of every γ-ray analyzed be known. For many peaks, a good measure of

TABLE 2

Measurements corrected for peak broadening by a gaussian approximation (*PWC*) and by a count-rate correction (*CRC*). *G*(corr.) is the gaussian correction expression as a percentage of the uncorrected composition.

Nuclide	Peak (keV)	Content found (ppm)[a]		*G* corr. (%)
		PWC	*CRC*	
^{153}Sm	103	4.42 ± 0.02	4.42 ± 0.02	2.3
^{177}Lu	208	0.422 ± 0.013	0.416 ± 0.013	2.4
^{169}Yb	63	2.74 ± 0.07	2.59 ± 0.07	6.9
^{182}Ta	68	0.58 ± 0.02	0.54 ± 0.02	10.6

[a]See footnote to Table 1.

the width cannot be obtained, because of poor statistics or interferences; however, it is generally possible to find two or more interference-free peaks which are intense enough to permit accurate measurements of widths without resort to line-shape fitting. The widths of other photopeaks can then be determined by interpolation. Such a procedure can be easily incorporated into data-processing programs.

Conclusion

Archaeological provenance studies require that trace elements be determined with a precision of 1—2% wherever possible in order that the compositional spread of an assembly of specimens not be dominated by random measuring errors [6—8]. Errors associated with standard—sample peak-width differences are systematic but they differ from one photopeak to another and from one specimen to another. Even for an assembly of materials of similar composition, these errors would be different for any given element unless all specimens were analyzed at approximately the same time, i.e., unless the activities were similar at the time of measurement. Thus these errors introduce additional dispersions into group averages which, for some elements, may exceed natural dispersions unless care is taken to correct for standard—sample peak-width differences. The method of correction proposed can be easily incorporated into computer routines in which photopeak areas are measured by summing a fixed number of channels.

The author thanks Professor John T. Wasson of the U.C.L.A. Chemistry Department for his hospitality and for the use of computing facilities. Special thanks are due to Professor I. Perlman, Hebrew University, for his interest. This work was supported in part by NASA grant NGL-05-007-367.

REFERENCES

1 C. Michael Lederer, Lawrence Radiation Laboratory Report, UCRL-18948 (September 1969).
2 I. Perlman and F. Asaro, Archaeometry, 11 (1969) 21.
3 D. F. Covell, Anal. Chem., 31 (1959) 1785.
4 K. Heydorn and W. Lada, Anal. Chem., 44 (1972) 2313.
5 H. R. Bowman, F. Asaro and I. Perlman, J. Geol., 81 (1973) 312.
6 J. Yellin, I. Perlman, F. Asaro, H. V. Michel and D. F. Mosier, Archaeometry, 20 (1978) 95.
7 A. L. Wilson, J. Arch. Sci., 5 (1978) 219.
8 A. M. Bieber, D. V. Brooks, G. Harbottle and E. V. Sayre, Archaeometry, 18 (1976) 59.

Analytica Chimica Acta, 113 (1980) 165—169

Short Communication

ION-SELECTIVE ELECTRODES BASED ON TETRAPHENYLPHOSPHONIUM 12-TUNGSTOSILICATE AND ON CRYSTAL VIOLET TETRAPHENYLBORATE IN THE POTENTIOMETRIC TITRATION OF ACID AND BASIC DYES

A. G. FOGG* and K. S. YOO

Chemistry Department, Loughborough University of Technology, Loughborough, Leicestershire (Gt. Britain)

(Received 6th April 1979)

Summary. Poly(vinyl chloride) membrane electrodes containing the specified substances are suitable as indicator electrodes in titrations of basic dyes with sodium tetraphenylborate solution and of acidic dyes with crystal violet solution. Useful curves are obtained even at the 10^{-3} M level.

The response of liquid-state ion-selective electrodes based on the water-insoluble salts of crystal violet with PAR or solochrome violet RS, to acidic and basic dyes has already been described [1]. These electrodes were used as indicator electrodes in titrations of several acid dyes with a solution of crystal violet, but because the salts formed on mixing acid and basic dyes are significantly soluble, the end-points were not sharp. Preliminary work on liquid-state electrodes based on crystal violet tetraphenylborate and crystal violet 12-tungstosilicate showed that sharper potential jumps can be obtained in titrations of basic dyes with sodium tetraphenylborate [2].

The present communication describes a further search for a satisfactory PVC electrode for use in potentiometric titrations of acidic and basic dyes. Electrodes based on tetraphenylphosphonium 12-tungstosilicate and on crystal violet tetraphenylborate were found to give useful titration curves.

Electrodes based on tetraphenylphosphonium 12-tungstosilicate

Preparation of tetraphenylphosphonium 12-tungstosilicate. Tetraphenylphosphonium chloride (1.5 g) was dissolved in 50 ml of water and 30 g of 12-tungstosilicic acid in a further 50 ml of water was added. The tetraphenylphosphonium 12-tungstosilicate precipitated was digested by adding 50 ml of acetone and heating the mixture on a water bath at 50—60°C for 1 h after which the supernatant layer was decanted off and discarded. The precipitate was digested in the same way with two further 50-ml portions of acetone, filtered off and then dried at 50°C in a vacuum oven (yield 5 g).

Preparation of PVC membrane and electrode. A paste was made from 0.15 g of tetraphenylphosphonium 12-tungstosilicate and 0.2 ml of 2-nitrophenyl

n-butyrate (solvent mediator); 0.2 ml of diiso-octyl phthalate (plasticiser) was then mixed in to give a homogeneous paste. This was mixed well with a solution of 0.15 g of PVC powder in 6 ml of tetrahydrofuran. The master membrane was cast in a glass ring (3.6 cm i.d.) as described by Craggs et al. [3]. The thickness of the membrane after drying was 0.4—0.45 mm. PVC electrodes were assembled as indicated by Craggs et al. [3]. A solution 10^{-1} M in potassium chloride and 10^{-3} M in tetraphenylphosphonium chloride was used as internal reference solution.

Membranes prepared with 2-nitrotoluene as solvent mediator, and dinonyl phthalate or di-n-butyl phthalate as plasticiser were less satisfactory.

Response to tetraphenylphosphonium ion. After conditioning overnight in 10^{-3} M tetraphenylphosphonium chloride solution, the electrode gave full Nernstian response to the tetraphenylphosphonium ion (as chloride) in the 10^{-6}—10^{-2} M range. After electrode storage in 10^{-3} M tetraphenylphosphonium chloride solution for 37 days, the response fell to 35 mV per decade. The electrode also gave full Nernstian response initially to the tetraphenylborate ion: a saturated sodium sulphate salt bridge was used with the calomel reference electrode in order to prevent formation of potassium tetraphenylborate at the junction.

The response decreased with time; thus a curve for the potentiometric titration of 10^{-2} M tetraphenylphosphonium chloride with 10^{-3} M sodium tetraphenylborate showed a potential jump of about 200 mV with a new electrode but only about 50 mV with an electrode which had been used for several weeks. The electrode was also useful for the standardization of sodium tetraphenylborate solutions with silver(I) solutions. In this titration a newly-cleaned Orion silver sulphide electrode gave a potential jump of about 300 mV at the end-point with 10^{-3} M solutions, whereas the proposed electrode gave a jump of only 100 mV; but in both cases, the inflexions were very sharp and so were equally useful.

Response to basic dyes and titration of basic dyes with tetraphenylborate. The response of new, conditioned membranes to basic dyes was less than Nernstian: the response to crystal violet, for example, was 25—30 mV per decade in the range 10^{-5}—10^{-3} M. Nevertheless, satisfactory titration curves were obtained for several basic dyes when they were titrated with standard sodium tetraphenylborate solution. The purities of the dye samples calculated from these titration curves are given in Table 1, and are compared with the nominal strengths (based on elemental analyses) provided by the supplier. In three cases the agreement is good but in the case of Basic Blue 141 a marked difference is observed. Titrations of Basic Red 14 and Basic Blue 3 gave unsatisfactory titration curves and these dyes are not included in Table 1. The sodium tetraphenylborate solutions were standardised with silver nitrate. A representative titration curve (for the titration of Basic Blue 141) is given in Fig. 1; the curves obtained even with an old membrane, indicate that good end-points can be obtained.

During these and other titrations of dyes, the membrane frequently

TABLE 1

Assay values obtained by potentiometric titration of basic dyes with sodium tetraphenylborate and of acid dyes with crystal violet

Dye	Potentiometric result (%)	Nominal strength of dye sample[a]	Dye	Potentiometric result (%)	Nominal strength of dye sample[a]
Basic Yellow 59	22	20	Acid Yellow 199	103	96.2
Basic Yellow 28	24	20	Acid Blue 62 (CI 62045)	91	79.6
Basic Orange 30:1	89	85	Acid Red 151 (CI 26900)	74	92.7
Basic Blue 141	32	20	Acid Red 114 (CI 23635)[b]	80	98.2
			H 87034[c]	99	99

[a]Based on elemental analysis (values provided by Imperial Chemical Industries Ltd.). [b]Dibasic acid. [c]Structure:

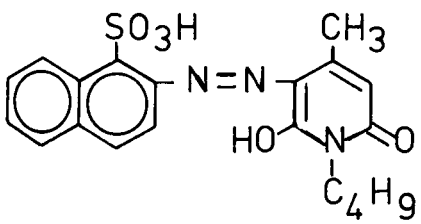

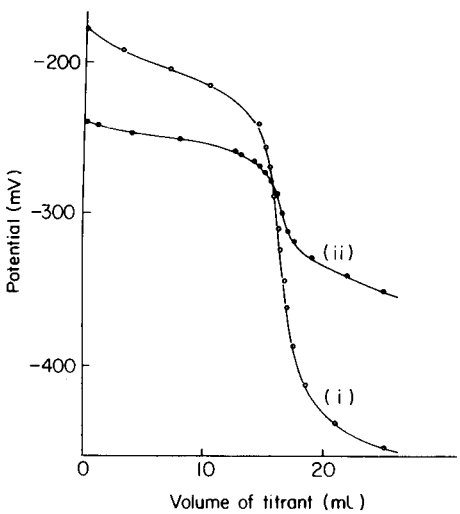

Fig. 1. Potentiometric titration curves of Basic Blue 141 with 10^{-3} M sodium tetraphenylborate using a tetraphenylphosphonium 12-tungstosilicate electrode. (i) New membrane, (ii) membrane used several times.

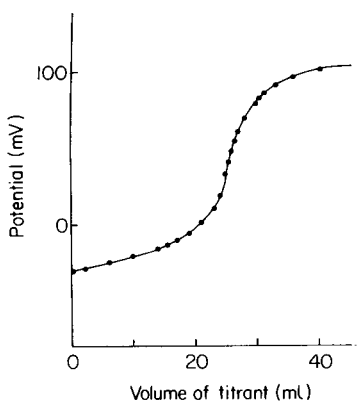

Fig. 2. Potentiometric titration curve of Acid Red 114 with 10^{-3} M crystal violet solution using a tetraphenylphosphonium 12-tungstosilicate electrode.

became covered with the precipitate formed. As far as possible this was removed by washing with water and by careful cleaning with a paper tissue. Occasionally however, precipitate had to be removed by dissolving it in a small amount of ethanol or methanol. As this process was likely to deplete the membrane of active material, the treatment was carried out as quickly as possible and the membrane was washed immediately with water and then reconditioned.

Titration of acid dyes with crystal violet. Acid dyes were titrated with a standard solution of crystal violet using the tetraphenylphosphonium 12-tungstosilicate electrode as indicator electrode. The crystal violet used (British Pharmacopoeia grade) contains a minimum of 96% of crystal violet based on titanium(III) titration [4]; by titration with sodium tetraphenylborate the sample used was found to contain 96.7% of crystal violet.

As was expected from the higher water-solubility of the crystal violet–acid dye salts, the potential jumps were smaller than those obtained for the tetraphenylborate titration of basic dyes, and the end-points were less sharp. The purities of the acid dye samples calculated from these titration curves are also given in Table 1 along with the nominal strengths provided by the supplier. In some cases the agreement is good but in others a marked difference is apparent. A representative titration curve for Acid Red 114 is shown in Fig. 2.

Electrodes based on crystal violet tetraphenylborate

Preparation of crystal violet tetraphenylborate. Sodium tetraphenylborate solution (300 ml, 10^{-2} M) at 70°C was added slowly with continuous stirring to 250 ml of 10^{-2} M crystal violet solution (containing 10 ml of concentrated hydrochloric acid) also at 70°C. The precipitate was washed with water by decantation over a period of several hours and was filtered finally onto a No. 4 glass sinter and washed with water until the filtrate was colourless. The precipitate was dried in a vacuum oven at 70°C (yield 1.7 g).

Preparation of PVC membrane and electrode. Crystal violet tetraphenylborate (0.2 g) was dissolved in 0.2 ml of 2-nitrophenyl n-butyrate (solvent mediator). To this was added a solution of 0.15 g of PVC powder in 3 ml of tetrahydrofuran, and then 0.2 ml of dinonyl phthalate. Even after thorough mixing this mixture tended to separate. For this reason, after addition to the glass ring, tetrahydrofuran was allowed to evaporate freely and the mixture was stirred occasionally during the first 30 min, until the mixture had become more viscous. The ring was then covered and the remaining tetrahydrofuran allowed to evaporate in a controlled manner in the usual way. The electrode was assembled as indicated by Craggs et al. [3].

Membranes prepared from 2-nitrotoluene (solvent mediator) and di-iso-octyl phthalate and di-n-butyl phthalate (plasticiser) were slightly inferior.

Titration of acid and basic dyes. The use of the crystal violet tetraphenylborate electrode in titrations of acid and basic dyes with crystal violet and with sodium tetraphenylborate was investigated. The dyes studied were those which had been used previously with the tetraphenylphosphonium

12-tungstosilicate electrode: the titration curves were very similar to those shown in Figs. 1 and 2. The values obtained for the purities of the dye samples were the same as those obtained with the tetraphenylphosphonium 12-tungstosilicate electrode (see Table 1) within experimental error.

The response of the crystal violet tetraphenylborate electrode to crystal violet (50 mV/decade within the range 10^{-6}—10^{-3} M) is more nearly Nernstian than is that of the tetraphenylphosphonium 12-tungstosilicate electrode: the response to tetraphenylborate was usually Nernstian but occasionally a super-Nernstian response was obtained. The liquid-state electrodes based on crystal violet tetraphenylborate studied previously gave responses of 30—40 mV/decade and 64—67 mV/ decade to crystal violet and tetraphenylborate, respectively.

Discussion

The two PVC electrodes described above provide a means of determining acid and basic dyes by potentiometric titration. Sharp end-points are obtained for the titration of basic dyes with tetraphenylborate but the end-points obtained for the titration of acid dyes with crystal violet are less sharp owing to the higher water-solubility of the salts formed.

Both PVC electrodes gave good results but membranes based on crystal violet tetraphenylborate responded marginally more slowly than those based on tetraphenylphosphonium 12-tungstosilicate: both membranes, however, generally gave a steady response well within 30 s. The crystal violet tetraphenylborate electrodes had a slightly longer effective life (8 weeks compared with 6 weeks) and were less prone to physical deterioration.

A major difficulty in assessing the accuracy of dye assay procedures is that pure dye samples are seldom available. Different analytical methods when applied to impure dye samples frequently give different assay values [4], as different parameters are being measured. The present titration methods determine the large cation or anion contents of the dye sample. The reason for the large difference, in the case of some dyes, between the assay values obtained by these titration methods and by elemental analysis is not known. Further studies are being made to assess the accuracy of the titration methods described here and the reliability of dye assay procedures.

The authors thank staff of Imperial Chemical Industries (Organics Division) Ltd. for providing samples and for helpful discussion.

REFERENCES

1 A. G. Fogg, A. A. Al-Sibaai and K. S. Yoo, Anal. Lett., 10 (1977) 173.
2 A. G. Fogg and K. S. Yoo, Proc. Conf. on Ion-Selective Electrodes, Budapest, Hungary, September 1977, Akadémiai Kiado, Budapest, p. 369.
3 A. Craggs, G. J. Moody and J. D. R. Thomas, J. Chem. Educ., 51 (1974) 541.
4 C. Burgess, A. G. Fogg and D. T. Burns, Lab. Pract., 22 (1973) 472.

Analytica Chimica Acta, 113 (1980) 171—173

Short Communication

DIFFERENTIAL PULSE POLAROGRAPHIC DETERMINATION OF TRACES OF ARSENIC IN SEMICONDUCTOR SILICON

PIER LUIGI BULDINI*

C.N.R. — LAMEL Laboratory, Via de'Castagnoli 1, 40126 Bologna (Italy)

DONATELLA FERRI and PIETRO LANZA

Chemical Institute 'G. Ciamician', University of Bologna, 40126 Bologna (Italy)

(Received 14th June 1979)

Summary. The method is based on silicon dissolution with hydrofluoric and nitric acids; losses of arsenic through volatilization along with hexafluorosilicic acid are avoided by oxidation with permanganate. Arsenic(III) is formed on addition of sulphite in 2 M hydrochloric acid. Differential pulse polarography of this solution provides a precision of ±1.5%, a limit of determination of ca. 1 $\mu g\ g^{-1}$, and linear calibration graphs up to 10 μg As ml^{-1}.

Traces of arsenic have severe effects on the electrical properties of silicon used in semiconductor devices, hence much interest has been shown in sensitive and reliable methods for their determination. Arsenic in silicon is usually determined by neutron activation analysis [1—4]. Among chemical methods of analysis, only spectrophotometry has been used [5—7], although techniques such as atomic absorption [8] or emission [9] spectrometry and voltammetry [10] are currently applied in silicate analysis. Chemical methods cannot attain the high sensitivity of the more sophisticated physical methods such as neutron activation analysis, but they can be accurate and reliable as well as relatively cheap.

A previous study [11] suggested that it would be useful to apply differential pulse polarography (d.p.p.) to the determination of arsenic in semiconductor silicon. For this purpose, the traces of arsenic are converted to involatile arsenic(V) during the matrix dissolution. After volatilization of silicon, arsenic(V) is reduced to the trivalent form with sodium sulphite in acidic medium, and this medium serves as the supporting electrolyte for polarography.

Experimental

Reagents. Analytical-grade chemicals were used and normal precautions for trace analysis were taken throughout. All glassware and PTFE vessels were filled with concentrated sulphuric acid, left overnight and rinsed thoroughly before use.

Working standards were prepared daily by diluting stock As(V) or As(III) solutions (1000 $\mu g\ ml^{-1}$) obtained from $Na_2HAsO_4 \cdot 7H_2O$ or As_2O_3 (dissolved

in the minimum quantity of 1 M NaOH, and neutralized with 1 M HCl), respectively.

Apparatus. The silicon samples were dissolved in PTFE test tubes (25 mm i.d., 100 mm long).

An AMEL (Milan) Model 472 Multipolarograph equipped with a Model 460 stand was used. The working electrode was a common mercury dropping electrode ($m^{2/3}$ = 1.73), the reference electrode was an Ingold Model 303/NS saturated calomel electrode and the counter electrode was an Ingold Model Pt-805/NS platinum ring. Instrumental conditions were: pulse height 100 mV, drop time 2 s and scan 2 mV s^{-1}. A 5-ml microcell was normally used. Solutions were carefully deaerated with pure nitrogen for 20 min before analysis, and thermostated at 25.0 ± 0.1°C.

Procedure. A general preliminary sample treatment based on matrix elimination has been reported [12]. Clean the samples (usually slices) carefully by ultrasonic washing and degreasing with trichloroethylene—acetone—methanol [13]. After etching with hydrofluoric—nitric acids (1 + 1), powder the samples finely in an agate mortar.

Place 10—100 mg of sample in a PTFE test tube; add 2 ml of 65% HNO_3, 10—30 mg of $KMnO_4$ and 5 ml of 12 M HF. The reaction starts spontaneously. To complete the dissolution, place the covered tube in a glycerol bath at 60°C for about 1 h. Then fit the tube with a PTFE plug, adapted for passing filtered air, and eliminate silicon as hexafluorosilicic acid by heating at 110°C; after 2 h, only a brown residue remains. Then add 2 ml of 5 M HCl and 1 ml of twice-distilled water. Add 0.3 g of anhydrous sodium sulphite and heat the covered tube at 90°C for at least 1 h, cool and dilute to 5 ml.

Transfer the solution to a polarographic cell, deaerate and record the polarogram from −0.2 to −1.0 V (vs. SCE). Measure the peak height at −0.43 to −0.46 V and compare it with a calibration curve. The typical polarogram shown in Fig. 1 illustrates the method of peak measurement.

The calibration curve obtained under the recommended conditions is quite reproducible and linear up to at least 10 μg As ml^{-1}.

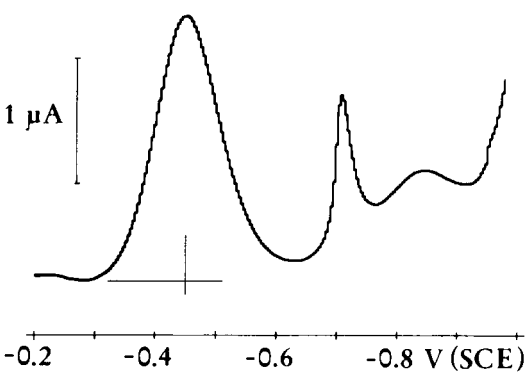

Fig. 1. A typical polarogram for arsenic(III) (1 μg g^{-1}) showing the method of peak measurement. Polarographic conditions as in text.

Results and discussion

The effects of heating time, acidity and excess of sulphite on the arsenic(V) reduction have been described [11]. As reported by Feldman [9], arsenic was not lost when permanganate was present provided that the temperature for sample dissolution did not exceed 70°C. When suitable quantities of As(III) and/or As(V) standard solutions were added to pure semiconductor silicon before dissolution, the values obtained were in good agreement with those obtained by direct addition of equivalent arsenic(III) aliquots to 2 M HCl solutions.

The working conditions reported above permit an average recovery of 98—99%. The excesses of nitric acid and potassium permanganate added are not critical for ensuring complete conversion of arsenic to the involatile pentavalent form.

The proposed method permits determinations as low as 20 ng As ml^{-1}, i.e. 1 μg As g^{-1} for a 100-mg silicon sample; the relative standard deviation is better than ±3%.

Table 1 shows the results obtained for some silicon samples, with a comparison of results obtained by neutron activation analysis.

The authors thank Prof. Dario Nobili and the MOS Development Labs. of SGS-ATES (Agrate Brianza, Italy) for continuing support and discussions.

TABLE 1

Determination of arsenic in samples of semiconductor silicon

Sample	As found (μg g^{-1})		No. of detns.	s	s_r (%)
	N.a.a.	Proposed method			
SGS 79/1	1700 ± 100	1670	8	±10	0.6
SGS 79/2	800 ± 40	805	4	±5	0.6
SGS 79/3	190 ± 10	196	4	±2	1.0

REFERENCES

1 G. Lunde, Solid-State Technol., 13 (1970) 61.
2 J. A. Keenan and G. B. Larrabee, Chem. Instrum., 3 (1971) 125.
3 F. De Corte, A. Speecke and J. Hoste, J. Radioanal. Chem., 9 (1971) 9.
4 N. I. Marunina, A. E. Chernova and B. F. Bogatikov, Zh. Anal. Khim., 31 (1976) 1146.
5 C. L. Luke and M. E. Campbell, Anal. Chem., 25 (1953) 1588.
6 A. A. Tumanov, A. N. Sidorenko and F. S. Taradenkova, Zav. Lab., 30 (1964) 652.
7 V. A. Nazarenko, G. V. Flyantikova and N. V. Lebedeva, Zav. Lab., 23 (1957) 891.
8 S. Terashima, Anal. Chim. Acta, 86 (1976) 43.
9 C. Feldman, Anal. Chem., 49 (1977) 825.
10 P. L. Buldini and D. Ferri, Chem. Geol., in press.
11 P. L. Buldini, D. Ferri and P. Lanza, Anal. Chim. Acta, 106 (1979) 137.
12 P. Lanza and M. T. Lippolis, Anal. Chim. Acta, 87 (1976) 27.
13 P. Lanza and P. L. Buldini, Anal. Chim. Acta, 85 (1976) 69.

Analytica Chimica Acta, 113 (1980) 175—178

Short Communication

SOLVENT SYSTEMS FOR THE DIRECT ATOMIC ABSORPTION SPECTROMETRIC DETERMINATION OF IRON IN VEGETABLE OILS WITH AQUEOUS INORGANIC STANDARDS

P. K. HON*, O. W. LAU, S. F. LUK and C. S. MOK

Department of Chemistry, Chinese University of Hong Kong, Shatin, N.T. (Hong Kong)

(Received May 29th 1979)

Summary. Two solvent systems, 4-methyl-2-pentanone—ethanol (8 + 3) and propionic acid are satisfactory for the determination of iron in vegetable oils directly by atomic absorption spectrometry with aqueous inorganic standards. Iron present at the ppm level can be determined with a relative error of less than 5%.

The determination of trace metals in vegetable oils by atomic absorption spectrometry has proved problematic because with vegetable oils the common ashing technique causes serious errors by spattering, foaming and volatilization of the sample. The problem can be overcome by measuring solutions of oil in kerosene or other suitable organic solvents without prior ashing of the sample [1]; however, with this method organometallic compounds are normally used as standards and these compounds are not always readily available and may be expensive.

Holding and Matthews [2] developed a mixed-solvent system that permits the use of inorganic compounds as standards for the determination of calcium and zinc present in used lubricating oils and automatic transmission fluids at the g kg^{-1} level by the atomic absorption method. The purpose of the present work was to devise similar solvent systems which enable aqueous inorganic standards to be used for the direct atomic absorption determination of trace metals in vegetable oils; iron is used as an example.

Experimental

Apparatus and reagents. A Perkin-Elmer atomic absorption spectrometer Model 360 was used with a 10-cm single-slot burner, an acetylene flow rate of 0.7 l min^{-1} and an air flow rate of 7.4 l min^{-1}. The 248.3-nm line from an iron hollow-cathode lamp operated at a current of 5.5 mA and a spectral band pass of 0.7 nm were employed.

All reagents used were of analytical-reagent grade. Stock iron solution (200 ppm) was prepared by dissolving 0.2000 g of iron in 10 ml of concentrated nitric acid and diluting to 1000 ml in a volumetric flask. Standard solutions of iron (0—200 ppm) were then prepared by appropriate dilution of the stock solution with approximately 1.5 M nitric acid.

Synthetic unknowns used for the recovery tests were made up from iron(III) caprate prepared and analysed as described by Hearn et al [3].

Procedure. Solutions of the oil samples (15—20% w/v) were prepared by weighing the appropriate amounts of oil into volumetric flasks and diluting to the mark with either propionic acid or the mixed solvent MIBK—ethanol (8 + 3).

The technique of standard addition was employed for the determination of the iron content in vegetable oils. The solutions for analysis were made up by pipetting into 10 ml of the oil solution contained in 10-ml volumetric flasks, 0.2 ml (for MIBK—ethanol as diluent) or 0.50 ml (for propionic acid as diluent) of distilled water or the aqueous iron standards of appropriate concentrations. The instrument zero was set with the solvent blank between samples. For each measurement at least five readings were recorded and averaged; care was taken to shake the solutions thoroughly before measurements.

Results and discussion

Choice of solvents. Four types of common vegetable oils (peanut, corn, salad and sesame oils) were found to form a homogeneous mixture with 4-methyl-2-pentanone (MIBK), water and ethanol or acetone. The MIBK—ethanol mixture was chosen as the diluent for subsequent experiments since ethanol is less volatile than acetone and gave a more stable flame. After a number of simple compatibility tests, a mixture consisting of MIBK—ethanol (8 + 3) was selected; this forms a homogeneous solution with up to 2.5 ml of an aqueous solution of an inorganic salt together with up to 20 g of vegetable oil per 100 ml of solution.

Kabanova et al. [4] found that propionic acid, which has a low viscosity compared to other fatty acids, mixes well with lubricating oils so that it could be used as a diluent for viscous petroleum products and in the preparation of standard solutions for the atomic absorption determination of impurities in lubricating oils. This acid also mixes well with the vegetable oils under study and is completely miscible with 5 ml of an aqueous inorganic standard solution together with up to 20 g of vegetable oil per 100 ml of solution.

It is noteworthy that up to 20% (w/v) oil solutions can be prepared with either solvent system so that the oil samples need not be excessively diluted, and metal ions present at the ppm level can be determined by this technique.

Effect of oil concentration on absorption. Figure 1 shows typical curves for the absorbance of iron (2.5 ppm) in the MIBK—ethanol mixture and in propionic acid containing different quantities of oil and 2.4% and 4.8% (v/v) of water, respectively. A similar curve with MIBK as diluent and containing no water was included for comparison. It can be seen that in all cases the absorbance decreases with increasing amounts of oil though to different extents, and becomes nearly constant once the oil concentration reaches about 12% (w/v). The observed depression of the absorption was

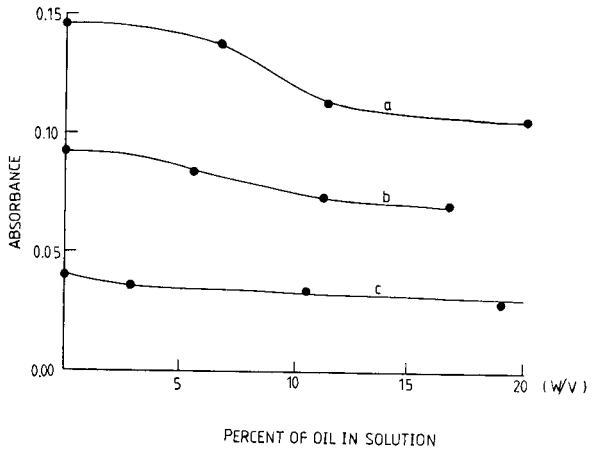

Fig. 1. The effect of oil concentration on the absorbance of iron (2.5 ppm) in (a) MIBK, (b) MIBK—ethanol and (c) propionic acid, measured against a blank without added iron.

probably due to the lowering in efficiency of the nebulization with increasing viscosity and apparently there was little or no significant enhancement of the metal absorption caused by the oil sample present. It can also be deduced from Fig. 1 that the sensitivity for the determination of iron in vegetable oils with the three diluents decreases in the order MIBK, MIBK—ethanol and propionic acid for the same concentration of oil. Again this trend is caused presumably by the difference in viscosity of the diluents.

Analysis of oil samples. Recovery tests on four oil samples to which known concentrations of iron were added showed 95—103% (mean 99%) recovery from MIBK—ethanol and 96—105% (mean 100%) from propionic acid. The solutions analysed contained 15% (w/v) of oil. Table 1 shows the standard deviations of ten replicate determinations on several oil samples for both solvent systems. The analyte solutions contained 15% (w/v) of oil. There is no significant difference between the diluents in this respect.

Application of the procedure to the determination of the iron content of the four vegetable oils gave the results shown in Table 2. Results obtained by an established method (direct dilution with MIBK and iron(III) caprate as standard) are included for comparison. Considering the relatively low iron content in these oils, the agreement between these techniques is quite good.

Conclusion. It is possible to use aqueous inorganic standards for the direct atomic absorption determination of iron in vegetable oils which have simply been diluted with either propionic acid or MIBK—ethanol mixture. The results obtained with either solvent are of comparable precision and accuracy. However, propionic acid is considered to be inferior to the MIBK—ethanol mixture because of its pungent smell and corrosive character, and

TABLE 1

Precision data for determination of iron in various oils

Diluent	Oil	Fe in soln. (ppm)	R.s.d. (%)[a]
MIBK—ethanol	Corn	2.5	3.3
	Peanut	2.0	2.2
	Salad	2.3	4.4
Propionic acid	Corn	4.8	2.4
	Peanut	4.5	2.4
	Salad	4.8	4.7

[a]10 measurements.

TABLE 2

Determination of iron (in ppm) in vegetable oils by a.a.s.

Sample	By an established method	MIBK—ethanol dilution	Propionic acid dilution
Corn oil	1.50	1.43	1.55
Peanut oil	1.43	1.45	1.36
Salad oil	0.59	0.58	0.64
Vegetable oil	1.86	1.89	1.90

because its higher viscosity causes lower sensitivity. This dilution technique should be applicable to the determination of other metals in vegetable oils at the ppm level.

The authors thank M. C. Wong and W. H. Yu for experimental assistance.

REFERENCES

1 Iron in Vegetable Oil, Analytical Methods for Flame Spectroscopy, Varian Techtron, Springvale, Victoria, Australia, 1972.
2 S. T. Holding and P. H. D. Matthews, Analyst, 97 (1972) 189.
3 W. E. Hearn, R. A. Mostyn and B. Bedford, Anal. Chem., 43 (1971) 1822.
4 M. A. Kabanova, D. A. Loseva and Y. I. Turkin, Zh. Prikl. Spektrosk., 18 (1973) 378.

Analytica Chimica Acta, 113 (1980) 179—184

Short Communication

THE SPECTROFLUORIMETRIC DETERMINATION OF EUROPIUM(III) IN SOLID DIKETONATE COMPLEXES

SWAGATA BHATTACHARYA and SAMUEL J. LYLE*

The Chemical Laboratories, University of Kent at Canterbury, Kent CT2 7NH (Gt. Britain)

(Received 13th July 1979)

Summary. Modification of a technique previously described for the determination of europium(III) in lanthanides allows samarium interference to be overcome. Provided that cerium is first removed and the sample contains <0.2 mg of neodymium, lanthanides do not interfere in the determination of ≥10 μg europium. Some applications are described.

Europium(III) can be coprecipitated by isomorphous replacement with yttrium or another trivalent lanthanide as a tetrakis diketonate complex of the form $MLn(Eu)L_4$. When M^+ is the piperidinium cation (pip), Ln is yttrium, lanthanum, gadolinium or terbium(III), L is the anion derived from acid dissociation of 1,1,1-trifluoro-4-phenylbutane-2,4-dione (Hbta) and the Ln:Eu ratio is large (about 10^3—10^6), irradiation of the solid with near u.v. light produces strong fluorescence from the europium(III). This phenomenon is probably due to an exciton process in the mixed crystal [1] and can be made the basis of a sensitive spectrofluorimetric determination of europium [2, 3]. In the presence of other trivalent lanthanides and yttrium ions, cerium(III), neodymium(III) and samarium(III) interfere when present at moderate levels relative to europium [2, 3]. Potential interferences from lanthanides have been investigated further in an attempt to overcome them. The results and some applications of the methods evolved are described here.

Experimental

Reagents and samples. The reagents and solutions prepared from them have been described previously [2]. Oxides of the lanthanides were of 99.9% purity (Koch-Light Ltd., Colnbrook, or Rare Earth Products Ltd., Widnes, England).

Binary crystalline mixtures of europium(III) fluoride with LiF, CaF_2 and LaF_3 were prepared by grinding the solids together. Single crystals of these fluorides doped with europium were prepared by using an induction furnace. These samples, the weight depending on the europium content, were dissolved by heating with roughly (4 + 1) mixtures of concentrated nitric acid and a saturated solution of boric acid in water. Prolonged heating of CaF_2 and LaF_3 with topping up of solvent may be required to effect dissolution; this could be aided by first grinding up large crystals. The

measured quantity of matrix-forming element, if required, was then added and its hydroxide with that of europium precipitated with concentrated aqueous ammonia. The precipitate was separated, washed with water by centrifugation and taken up in the minimum of nitric acid from which the nitrate mixture was recovered by solvent evaporation.

Preparation of the mixed metal diketonate complex, [pip][Ln(Eu)(bta)$_4$] has been described [2]. Generally 200 mg of the matrix-forming lanthanide were added to each sample.

Equipment. Most of the quantitative measurements were made with an Aminco-Bowman spectrophotofluorimeter and the sample cell and cell-holder described previously [2]. Excitation was at 366 nm and slit widths of 2 mm were normally used on both the excitation and emission sides of the sample. A Perkin-Elmer MPF3 spectrophotofluorimeter with a cell holder modified to fit its sample compartment was occasionally used; this instrument was preferable for obtaining emission spectral scans (Figs. 1 and 3) of samples for which purpose slit settings of 8 nm (excitation) and 2 nm (emission) were employed with excitation at 366 nm. The Aminco-Bowman instrument was fitted with a 100-W Wotan Super-Pressure mercury lamp.

Unless otherwise stated, where europium or samarium contents are given in ppm, they are relative to the main matrix-forming metallic element.

Results and discussion

It was found that yttrium, lanthanum, gadolinium and terbium were equally satisfactory as matrix-forming elements when europium(III) emission at 611 nm was measured. However, yttrium and lanthanum are preferable on economic grounds and because they are readily obtained free of europium. (Lanthanides, other than those mentioned above and in the account to follow, were not tested.) Previous tests [2, 3], confirmed in the present work, had shown that, of the remaining lanthanides, only cerium, neodymium and samarium interfere seriously. Although erroneously stated [2] to be without serious interference, samarium is now known to interfere when present at $\geqslant$500 ppm with respect to yttrium. Cerium is readily separated from lanthanide mixtures [4] and therefore does not present a serious problem.

An emission spectral scan from 500 to 700 nm of [pip][Sm(bta)$_4$] revealed lines related to samarium at 564, 576, 600 and 608 nm with lines related to europium impurity at 586, 592 and 611 nm (Fig. 1). It seems likely that in addition to quenching of europium(III) emission at 611 nm there is some background enhancement from the neighbouring samarium lines. When [pip][Y(Eu)(bta)$_4$] containing a fixed ratio of europium to yttrium was doped with increasing amounts of samarium, the emission intensity at 611 nm fell away at first but became nearly constant and independent of samarium content when the samarium to yttrium weight ratio exceeded ca. 2×10^{-3} (Fig. 2). The emission scan of [pip][Y(Eu, Sm)(bta)$_4$] containing 100 ppm of europium and 3000 ppm of samarium

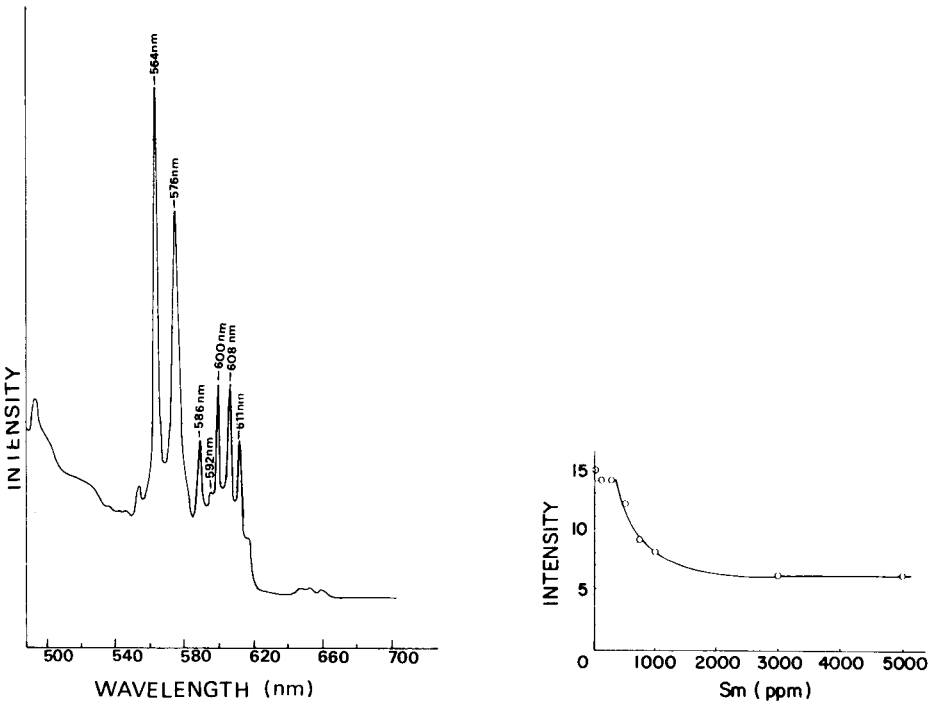

Fig. 1. Emission spectrum of [pip][Sm(bta)$_4$] containing traces of europium present in the samarium used to prepare the complex.

Fig. 2. Relative emission intensity at 611 nm from [pip][(Y + Sm)(bta)$_4$] containing 100 ppm of europium plotted against samarium content of the matrix.

relative to yttrium (Fig. 3) suggests that enhancement of the line at 611 nm by samarium is not excessive. When the matrix was [pip] [(Y + 3000 ppm Sm)(bta)$_4$], within which was incorporated varying amounts of europium, emission intensity plotted against europium content assumed the form evident from Fig. 4. The sensitivity to changing europium content fell away particularly above 2000 ppm of europium. The most satisfactory range for quantitative work with this mixed matrix is 50—1000 ppm of europium. An emission scan clearly showed that the positive instrumental response in the absence of europium (Fig. 4) was due to a combination of traces of europium in the samarium used and to background enhancement by samarium emission. Instrumental response to europium was reduced by a factor of about 7 relative to a yttrium matrix in which samarium was absent. Interference tests on the yttrium + 3000 ppm samarium matrix showed that only cerium and neodymium interfered below 10,000 ppm of the lanthanide being tested. Very large amounts (at least 50,000 ppm) of samarium could be tolerated. Neodymium began to interfere if present at >1000 ppm with respect to yttrium. When neodymium was made the matrix element in

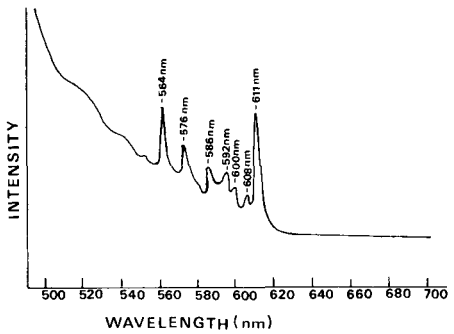

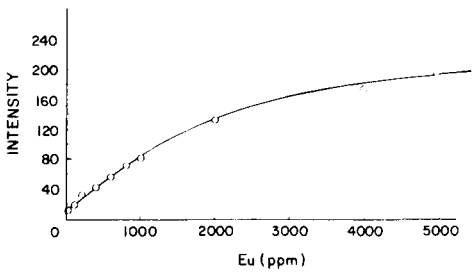

Fig. 3. Emission spectrum of [pip][(Y + 3000 ppm Sm)(bta)$_4$] with 100 ppm of europium added.

Fig. 4. Relative emission intensity at 611 nm from [pip][(Y + 3000 ppm Sm)(bta)$_4$] plotted as a function of added europium.

[pip][Nd(Eu)(bta)$_4$], 100 ppm of europium did not give a signal above background at 611 nm and the emission spectrum of the mixed complex was 'featureless' from 500 to 700 nm. Provided that cerium is separated, it may be concluded that neodymium is the only lanthanide which would interfere with europium determinations in the yttrium +3000 ppm samarium matrix. If 200 mg of yttrium is used to prepare the complex, then the neodymium in the sample should be $\leqslant$0.2 mg and the europium content $\geqslant$0.01 mg. Thus, while limiting the sample composition, the presence of neodymium does not prohibit europium determination.

Applications. Some applications to the determination of europium are summarized in Table 1. In the determinations of trace amounts in the oxide samples, the metal (gadolinium or terbium in the table) was used as matrix element. The europium present gives a positive europium(III) emission at 611 nm in the diketonate complex. If known additions of europium are made to further samples of the same oxide, the emission intensity is proportional to the sum of the indigenous and added europium. A plot of total emission intensity against europium added is rectilinear and extrapolation back to the latter axis gives the original europium content as the distance between the intersection on the axis and the origin. This may be done more objectively by a least-squares treatment from which the standard deviation of the mean can be obtained by calculation. Three or at most four individual samples from each 'population' had additions of europium made to them in these measurements. The errors ranged from 6 to 18% on the values quoted (Table 1) but could, of course, be reduced by taking more samples. Alternatively, a calibration curve prepared from europium-free yttrium or lanthanum could be used provided that the molar quantity of the chosen matrix element was kept the same as that of the gadolinium or terbium used to prepare the diketonate complex. Then the europium content could be read directly from the calibration curve. (Europium-free gadolinium

TABLE 1

Some applications to the determination of europium

Substance	Approximate sample size	Matrix used	Europium	
			Found[a]	Expected[b]
Gd_2O_3[c]	230 mg	[pip][Gd(bta)$_4$]	225 ± 23 ppm	210 ppm
Gd_2O_3[c]	230 mg		51 ± 9 ppm	55 ppm
Gd_2O_3[c]	230 mg		69 ± 4 ppm	70 ppm
'Tb_4O_7'[c]	240 mg	[pip][Tb(bta)$_4$]	49 ± 6 ppm	50 ppm
'Oxide concentrate'[d]	2 mg	[pip][(Y + 3000 ppm Sm)(bta)$_4$]	3.1 ± 0.5%	3.61%
Li(Eu)F	1.5 g	[pip][La(bta)$_4$]	(0.52 ± 0.03) mg g^{-1}	0.575 mg g^{-1}
	15 g		(0.049 ± 0.003) mg g^{-1}	0.057 mg g^{-1}
$Ca(Eu)F_2$	0.9 g		(1.00 ± 0.05) mg g^{-1}	1.06 mg g^{-1}
	9 g		(0.104 ± 0.005) mg g^{-1}	0.106 mg g^{-1}
$La(Eu)F_3$	280 mg		(1.41 ± 0.006) mg g^{-1}	1.41 mg g^{-1}
	280 mg		(0.14 ± 0.01) mg g^{-1}	0.14 mg g^{-1}

[a]Mean and standard error (n = 5). [b]See text. [c]Samples contained 99.9% of the specified oxide (Koch-Light, Ltd.). [d]Europium-enriched mixture derived from a monazite source (Rare Earth Products, Ltd.).

or terbium can also be used for calibration purposes but would add to the cost of the determination.) Comparison of the results with values obtained by a spectrophotometric modification [5] of the method of Foster and Kremers [6] (Table 1) shows that agreement is quite good.

When yttrium was used as matrix element in a measurement on the 'oxide concentrate' containing 3.6% europium by weight, a low result (around 2%) was obtained but with the mixed yttrium + samarium matrix-forming elements the value (Table 1) was in reasonable agreement with that obtained by the titrimetric method of Foster and Kremers [6]. In a sample of this kind it is necessary to have means of spotting interference from cerium, neodymium and samarium. If present, cerium can be identified by its colour and removed. An emission spectral scan of the [pip] [(Y + sample)(bta)$_4$] complex over the range 500—700 nm will reveal the presence of samarium (see Fig. 1) but not neodymium. A further check for possible interference from these two elements in mixtures of unknown composition can be obtained by taking two or more widely differing sample weights and comparing emission intensity at 611 nm.

The measurements on the europium-doped fluorides were checked by using synthetic mixtures of known composition and the expected results given in the Table refer to such mixtures. On the whole, agreement and precision are reasonably good; the tendency for results for lithium and calcium salts to be low may be due to small adsorption losses during the dissolution and subsequent chemical treatment.

The method discussed here is intended for determination of europium in yttrium and other lanthanides or their mixtures. After the lanthanide fraction has been separated, a single determination takes about 50 min but

several can be carried out together in a time only a little longer. Furthermore, when the matrix can be chosen independently of the sample, as in the measurements described for the oxide concentrate and the fluorides (Table 1), it is possible to make a series of standards, which, if stored in dark bottles or a cupboard, can be used for at least a year. Therefore measurements need not be as lengthy as the method might suggest initially.

The sensitivity attainable depends on the intensity of the excitation radiation at 366 nm. With a 100-W mercury lamp instrumental response was adequate for the detection and determination of >1 μg of europium per sample with yttrium or lanthanum as matrix-forming element. The europium content should exceed 10 μg when a mixed matrix like yttrium + 3000 ppm samarium is used. (These quantities may be compared with the 0.1—1 mg of europium required in the spectrophotometric method [5].) The sensitivity may be increased by the use of a more intense light source at 366 nm and by optimizing instrumental settings to a particular sample composition.

REFERENCES

1 J. S. Curran and T. M. Shepherd, J. Chem. Soc. Faraday Trans. 2, 69 (1973) 126.
2 S. J. Lyle and R. Maghzian, Anal. Chim. Acta, 80 (1975) 125.
3 S. J. Lyle and R. Maghzian, Proc. Anal. Div. Chem. Soc., 12 (1975) 292.
4 M. L. Salutsky, in C. L. Wilson and D. W. Wilson (Eds.), Comprehensive Analytical Chemistry, Elsevier, Amsterdam, 1962, Vol. 1C, p. 478.
5 S. Bhattacharya, S. J. Lyle and R. Maghzian, Talanta, in press.
6 D. C. Foster and H. E. Kremers, Anal. Chem., 25 (1953) 1921.

Analytica Chimica Acta, 113 (1980) 185—188

Short Communication

SPECTROPHOTOMETRIC DETERMINATION OF COBALT IN SEA WATER AND BRINES BY SOLVENT EXTRACTION WITH 2,2'-DIPYRIDYL-2'-PYRIDYLHYDRAZONE

TH. A. KOUIMTZIS*, C. APOSTOLOPOULOU and I. STAPHILAKIS

Laboratory of Analytical Chemistry, University of Thessaloniki, Thessaloniki (Greece)

(Received 9th July 1979)

Summary. Cobalt (⩾ 1 ppb) can be determined very selectively by extracting its 2,2'-dipyridyl-2-pyridylhydrazone complex into iso-amyl alcohol and back-extracting into dilute perchloric acid. For 500-ml samples of sea water the relative standard deviation is 5% for 2 ppb of cobalt. For brines (30 g NaCl l^{-1}), cobalt can be determined down to 5×10^{-7}% (5 ppb).

Various methods have been proposed for the determination of traces of cobalt in sea water and brines, most necessitating preconcentration. Solvent extraction followed by spectrophotometric measurements [1—8] is the most popular method but has many sources of errors; the big difference in the volumes of the two phases results in mixing difficulties, and the solubility of the organic solvent in the aqueous phase changes the volume of organic phase resulting in decreased reproducibility of the measurements. In many cases, excess of reagent and various metal complexes are co-extracted with cobalt and cause errors in determining the absorbance of the cobalt complex.

In the present communication, a new method is described for the determination of cobalt in sodium chloride and sea water, in which the cobalt is extracted with 2,2'-dipyridyl-2-pyridylhydrazone (DPPH) [9] and the cobalt complex is back-extracted into 20% perchloric acid. Many of the above sources of error are thus avoided.

Experimental

Reagents. 2,2'-Dipyridyl-2-pyridylhydrazone (DPPH) was prepared as described previously [9]; a 0.05 M solution was prepared in ethanol.

A 0.01 M solution of cobalt(II) was prepared from cobalt(II) chloride hexahydrate and standardized by EDTA titration. This solution was diluted accurately with 0.02 M hydrochloric acid solution to 10 and 0.5 ppm of cobalt.

Sodium chloride (350 g) was dissolved in distilled water and diluted to 1 l. Cobalt was removed by adding 5 ml of 0.05 M DPPH reagent and shaking with 100 ml of iso-amyl alcohol for 5 min. The aqueous phase, free of cobalt, was used to prepare solutions containing various amounts of sodium chloride.

Hydrochloric acid, perchloric acid and ammonia solution were BDH Aristar grade.

Procedure for sea water. Transfer 500 ml of the sample to a separatory funnel. Adjust the pH to 5—8 with dilute ammonia or hydrochloric acid solution. Add 1 ml of 0.05 M DPPH solution followed by 30 ml of iso-amyl alcohol. Shake the funnel vigorously for 3 min. Separate the two phases. Add another 30 ml of iso-amyl alcohol to the aqueous phase and shake for 2 min. Combine the two extracts in another funnel, and add 30 ml of cyclohexane and 10 ml of 20% perchloric acid. Shake for 2 min and separate the two phases. Measure the absorbance of the acid phase at 500 nm against a reagent blank (see below) using 10-mm or 40-mm cells. From the standard graph, calculate the amount of cobalt in the sample.

For calibration, transfer to six funnels containing 500 ml of 3.5% (w/v) sodium chloride solution, exactly 0, 0.5, 1, 2, 5 and 10 ml of cobalt solution (0.5 ppm). Add 1 ml of the DPPH solution to each and follow the above procedure. Plot absorbance against cobalt concentration.

Standard addition can be used for low cobalt concentrations. Extraction efficiency shows only small variations for different sea-water samples, so that the same calibration slope is valid for evaluation of many samples extracted on the same occasion. Transfer 500 ml of the sample to each of four separatory funnels. After pH adjustment, add 0.5, 1, 2 and 5 ml of cobalt solution (0.5 ppm) and proceed as described above. Use 40-mm cells.

Determination of cobalt in brines. Weigh 60 g of sodium chloride and dissolve in 500 ml of distilled water in a separatory funnel. Add 1 ml of 0.05 M DPPH followed by 30 ml of iso-amyl alcohol. Proceed as described for sea water. Determine the cobalt using the calibration graph obtained as follows.

For calibration, transfer to five 10-ml volumetric flasks 0, 0.2, 0.5, 1.0 and 2.0 ml of cobalt solution (10 ppm), followed by 2 ml of distilled water and one drop of concentrated ammonia solution. Add 1 ml of 0.05 M DPPH solution to each and mix. Add 3 ml of 70% perchloric acid and dilute to volume with distilled water. Measure the absorbance of the solutions at 500 nm against the reagent using 40-mm cells. Plot absorbance against cobalt concentration.

Results and discussion

In aqueous solution, pH 3—11, DPPH reacts instantly with cobalt(II) ions to form a water-soluble orange-yellow complex (λ_{max} = 480 nm). On adding a strong acid, the color changes to pink (λ_{max} = 500 nm, ϵ_{max} = 42 000 l mol^{-1} cm^{-1}). Other metal ions such as Zn^{2+}, Cu^{2+} and Ni^{2+} also form colored complexes but these are destroyed on adding the acid. Thus, DPPH can be made very selective for cobalt [9].

The orange-yellow cobalt complex is extracted from aqueous solution under appropriate conditions. This complex can also be back-extracted into a strongly acidic solution, forming the pink complex. Various solvents such

as butanol, cyclohexanol, octanol, iso-amyl alcohol and MIBK were tested for extraction of the cobalt complex from aqueous solution; only butanol, cyclohexanol and iso-amyl alcohol showed good extraction efficiency. The effect of pH on the extraction is not critical in the range 3—10, because the formation of the complex is independent of pH in that range [9]. The extraction efficiency was found to be constant from pH 5 to 8, so this range was used in the procedures described.

The presence of sodium chloride in the aqueous phase markedly increases the extraction of the cobalt complex, as is shown in Fig. 1. The complex is extracted quantitatively into iso-amyl alcohol when more than 10 g of NaCl per 100 ml is present. In the presence of 3.5 g of NaCl per 100 ml (the NaCl concentration in sea water) the extraction is about 80%. The same extraction percentage was found for sea water.

Back-extraction of the cobalt complex from butanol, cyclohexanol or iso-amyl alcohol into strongly acidic media was not quantitative. Maximum back-extraction was found for iso-amyl alcohol. Quantitative back-extraction was achieved by adding 30 ml of cyclohexane to 60 ml of iso-amyl alcohol to decrease the polarity of the solvent. The percentage back-extraction is constant for media containing 20—30% perchloric acid, so 20% perchloric acid is recommended for back-extraction.

The slope of the calibration graph prepared by using spiked solutions containing 3.5 g of NaCl per 100 ml was almost equal to the slope of the graph prepared by using spiked sea water. Cobalt can be determined down to 1 ppb in sea-water samples by the recommended procedure. The calibra-

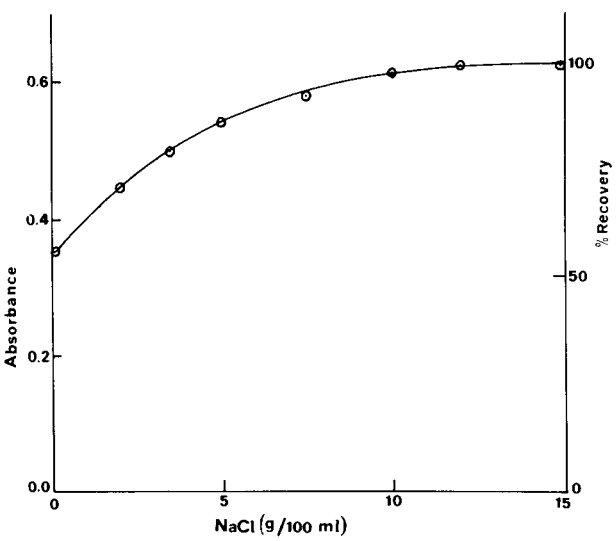

Fig. 1. Effect of sodium chloride on the extraction of cobalt from aqueous solution into iso-amyl alcohol. $[Co^{2+}]$ = 5 ppb, [DPPH] = 1×10^{-4} M. Absorbance measured against blank in 40-mm cells.

TABLE 1

Precision of determination of cobalt

Sample	Cobalt (ppb)	Mean absorbance[a]	R.s.d. (%)
Spiked sea water	2	0.208 ± 0.014	5
	5	0.505 ± 0.017	3
Spiked 12% NaCl solution	2	0.231 ± 0.012	4
	5	0.620 ± 0.015	2

[a]Eight determinations in 40-mm cells, with standard deviation.

tion graph used for the determination of cobalt in sodium chloride samples is prepared directly by using perchloric acid solution because the recovery of cobalt from solutions containing more than 10 g of sodium chloride per 100 ml as in this instance is 100%. This calibration graph was also used to determine the recoveries of cobalt by the procedures.

The precision of the method was evaluated with spiked sodium chloride solutions and sea water. Replicate analyses were carried out at the 2 and 5 ppb cobalt levels. The results of eight independent determinations at each level are summarized in Table 1.

REFERENCES

1 E. Kentner and H. Zeitlin, Anal. Chim. Acta, 49 (1970) 587.
2 S. Motomizu, Anal. Chim. Acta, 64 (1973) 217.
3 W. Forster and H. Zeitlin, Anal. Chim. Acta, 34 (1966) 211.
4 J. Riley and G. Topping, Anal. Chim. Acta, 44 (1969) 234.
5 B. Armitage and H. Zeitlin, Anal. Chim. Acta, 53 (1971) 47.
6 J. Going, G. Wesenberg and G. Andrejat, Anal. Chim. Acta 81 (1976) 349; 98 (1978) 47.
7 J. Korkisch and A. Sorio, Anal. Chim. Acta, 79 (1975) 207.
8 O. Gurtler, Fresenius Z. Anal. Chem., 284 (1977) 206.
9 G. Vasilikiotis, Th. Kouimtzis, C. Apostolopoulou and A. Voulgaropoulos, Anal. Chim. Acta, 70 (1974) 319.

Analytica Chimica Acta, 113 (1980) 189—194

Short Communication

SPECTROPHOTOMETRIC DETERMINATION OF TRACES OF FORMIC ACID AND FORMALDEHYDE IN EFFLUENT WATERS WITH OR WITHOUT PRECONCENTRATION

DONALD E. JORDAN*

Phelps Dodge Corporation, Extractive Metallurgy Research Laboratory, Morenci, Arizona 85540 (U.S.A.)

(Received 16th July 1979)

Summary. Formic acid plus formaldehyde are determined after reducing the acid with nascent hydrogen; formaldehyde alone is determined without reduction. The chromotropic acid method is used in 6—7.5 M sulfuric acid. The limit of determination is 0.05 $\mu g\ ml^{-1}$ without preconcentration and 0.05 $ng\ ml^{-1}$ with preconcentration by extraction with diethyl ether. Analysis time is 30 min by the direct method and 1 h with preconcentration.

The determination of formic acid in natural and effluent waters usually requires preconcentration. Various chromatographic techniques [1—3] and methods of determination [6—12] have been recommended. None of these is suitable for a fast precise direct determination of traces of formic acid with or without preconcentration. Rapid reliable colorimetric determinations of trace amounts of formaldehyde with 2, 7-dihydroxynaphthalene [13, 14] and chromotropic acid (1, 8-dihydroxynaphthalene-3, 6-disulfonic acid) [15] have been reported. If formic acid could be selectively reduced to formaldehyde, then its concentration could be readily determined with chromotropic acid. A rapid differentiation between formic acid and any formaldehyde already present in the sample would also be possible. The selective reduction of formic acid to formaldehyde with nascent hydrogen from powdered magnesium metal and hydrochloric acid has been described [16]. Preconcentration of formic acid with diethyl ether followed by determination with chromotropic acid has also been reported [17].

This communication describes rapid methods of determining formic acid and formaldehyde in waters with or without preconcentration. A lower limit of 0.05 $\mu g\ ml^{-1}$ is obtained without preconcentration by optimizing the variables described in the spot test [16]. Preconcentration by extraction with diethyl ether [17] readily extends the lower detection limit to 0.05 $ng\ ml^{-1}$ or less depending on sample volume. Briefly, the total

*Preliminary work done at Continental Oil Co., Research and Development Dept., Ponca City, Oklahoma 74601, U.S.A.

formic acid and formaldehyde is determined by reducing the formic acid to formaldehyde with magnesium metal and hydrochloric acid, acidifying further with sulfuric acid and applying the chromotropic acid method. Formaldehyde is determined separately in the same way without the reduction. Thus, formic acid can be determined by difference.

Experimental

Apparatus and reagents. An Hitachi 124 or Beckman DBG spectrophotometer was used with matched 50-mm or 40-mm silica cells.

Formic acid and chromotropic acid were of analytical-reagent grade.

Procedures. All water samples should be neutralized to pH 7 and filtered to remove suspended matter before analysis.

To determine total formaldehyde and formic acid add 25—30 mg of powdered magnesium metal to each dry 10-ml graduated mixing cylinder. Pipette 1.0 ml of sample into each cylinder. Carefully add 0.5 ml of 6 M HCl dropwise to dissolve the magnesium metal. Add 4 ml of 9 M sulfuric acid and 65—70 mg of chromotropic acid, stopper, and mix. Heat the cylinder and contents for 20 min at 80°C in a water bath. Remove, cool to near room temperature, dilute to 10.0 ml with distilled water, and mix. Read the absorbance at 562 nm using 4- or 5-cm matched cells against a reagent reference prepared in the same way as the sample. A midrange standard should be analyzed with each series of samples.

To determine formaldehyde pipette 1.0 ml of sample into a 10-ml graduated cylinder. Add 4 ml of 9 M sulfuric acid, 65—70 mg of chromotropic acid stopper, and mix. Heat the cylinder and contents at 80°C for 20 min. Remove, cool to room temperature, dilute to 10.0 ml, and mix. Read the absorbance as described above.

For preconcentration, extract up to 1 l of water twice with 30-ml portions of diethyl ether. Then acidify the water sample to pH 1.5—2.0 with hydrochloric acid and extract it again three times with 30-ml portions of diethyl ether. Neutralize the ether extract to pH 8—8.5 with 0.1 M NaOH. Evaporate the extract on a water bath with aeration to about 3 ml and then transfer it to a 10-ml graduated mixing cylinder with a few ml of ether. Then evaporate the extract to dryness, acidify with (1 + 1) HCl, remove CO_2 with air and adjust the volume to 1.0 ml. Continue with the procedure outlined for total formaldehyde and formic acid above.

For calibration of the direct method, prepare a series of formic acid and formaldehyde standards ranging from 0 to 36 μg ml^{-1}. Pipette 1 ml of each standard and treat in the same way as the samples. Plot an absorbance versus concentration curve.

For calibration of the preconcentration method, prepare standards containing 0—36 ng ml^{-1}. Extract each standard as described in the preconcentration section and prepare a standard curve with the extracted standards.

Discussion and results

The primary object of this investigation was to establish a direct, rapid method of determining formic acid in waters. Several techniques were studied, but all required separation or preconcentration, or were too time-consuming. The adaptation of the qualitative test for formic acid described by Feigl [16] showed the most promise, but the detection limit was not low enough. To avoid the lengthy preconcentration step of Stradomskaya and Goncharova [17], a study of procedural variables was initiated.

A critical evaluation of the reaction showed the sulfuric acid concentration in the reaction mixture to be the most important. West and Sen [15] found that to attain consistent color development in the reaction between chromotropic acid and formaldehyde the sulfuric acid must be between 86 and 96%. The present work showed consistent color development in 6—7.5 M sulfuric acid. Prior to sulfuric acid addition, reduction of formic acid to formaldehyde must be complete. The optimum amount of magnesium was 25 mg. The use of more simply added to the total volume before color development because of the additional hydrochloric acid required to dissolve it. If less than 25 mg was used inconsistent results were obtained. The reduction step was critical in that all the magnesium had to be dissolved to ensure complete reduction before sulfuric acid was added.

Addition of excess of chromotropic acid obscured the pink color; 65—75 mg sufficed for at least 36 μg of formic acid for formaldehyde. This contrasts significantly with earlier work [15] where 10—50 mg of chromotropic acid gave consistent color development with 100 μg of formaldehyde. Thus in the present work the reagent/formaldehyde ratios exceeded 2000:1 while in the previous work they were 100:1 to 500:1. The reason for such wide differences is not known although differences in purity of chromotropic acid, acid concentration, and temperature of color development are possible explanations. For reduction, the suggested temperature of 60°C [16] proved to be inadequate. Heating at 80°C for 20 min was adequate to achieve precise and accurate color development as long as the reaction mixture was fully immersed to ensure uniform heating; this proved to be nearly as critical as sulfuric acid concentration for consistent results. Magnesium salts precipitated in the cooled mixture and had to be dissolved prior to determining the absorbance of the chromophore. Dilution to 10.0 ml with water was convenient and enough to dissolve the magnesium salts. Occasionally, slight residues had to be separated by centrifugation.

By precisely following the procedural details, formic acid and formaldehyde could be determined accurately down to 0.05 μg ml^{-1} in the sample in 30 min without preconcentration. This level of detection compares favorably with the limits attained by Stradomskaya and Goncharova [17] after preconcentration.

It seemed logical to extend the basic method to include very low concentrations of formic acid and formaldehyde. Several organic extractants were studied: diethyl ether extracted formic acid and formaldehyde quickly and

and without difficulty, and was very readily vaporized. The formic acid–formaldehyde extract was reduced to ca. 3 ml and carefully transferred to a dry mixing cylinder; evaporation was then continued to dryness. After careful acidification of the residue and adjustment to 1.0 ml, the analysis was continued as described for samples without preconcentration. Transferring to a mixing cylinder eliminated the need to dilute the preconcentrate, thus effectively lowering the detection limit.

It can be seen from Fig. 1 that the preconcentration technique gives 82–85% extraction of formic acid. This poses no analytical problem since samples and standards are treated in exactly the same way. The formaldehyde preconcentration yields only 75–78% recovery, but again this poses no problem since standardization is done in exactly the same way. The extraction efficiency might be improved by salting or similar enhancers but this was not tested. The reduction of formic acid is stoichiometric. Curve 3 of Fig. 1 shows that the absorbance for 16.7 μg of formic acid is equivalent to 11 μg of formaldehyde (curve 3). Theoretically, 16.7 μg of formic acid is equivalent to 10.9 μg of formaldehyde.

The recovery of added formic acid and formaldehyde from various effluent water samples was tested and gave excellent results (Table 1). The results obtained for typical water samples are shown in Table 2. These and other samples were analyzed without apparent interference. Generally, formaldehyde is difficult to find in the presence of formic acid in effluent water. In fact, the samples shown are the only ones analyzed that did contain formaldehyde and formic acid. Sample E was analyzed by both techniques,

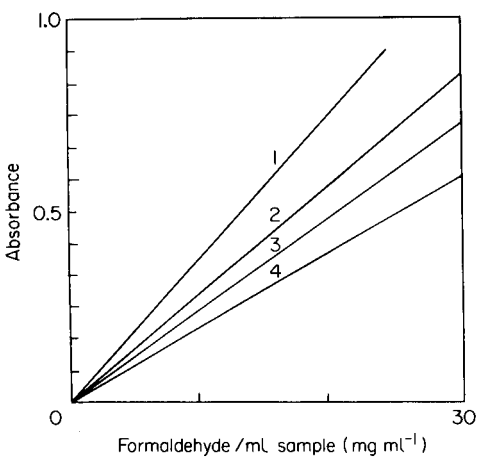

Fig. 1. Absorbance vs. concentration of formic acid or formaldehyde in the sample. Curves 1 and 2 correspond to formaldehyde, direct and preconcentrated; curves 3 and 4 correspond to formic acid, direct and preconcentrated, respectively. Determined at 560 nm in 40 mm matched cells and 1-ml samples in 10-ml total volumes.

TABLE 1

Recovery of formic acid and formaldehyde from effluent waters by the proposed direct procedure

Sample	No of detns.[a]	HCOOH (μg ml^{-1})				HCHO (μg ml^{-1})			
		Added	Range found	Av.	R.s.d. (%)	Added	Range found	Av.	R.s.d. (%)
A	—	0	—	0.1	—	0		0	—
	5	10	9.7—10.2	9.9	1.2	5.0	4.9—5.3	5.1	2.1
	—	20		20.2	—	10.0		9.7	
B	—	0	—	0.1	—	0	—	0	—
	5	10	9.7—10.2	9.8	1.9	5.0	4.7—5.4	5.1	3.6
C	—	0	—	0.5	—	0	—	0	—
	5	10	10.0—10.3	10.1	1.6	5.0	4.8—5.1	5.0	2.9
D	5	7	6.8—7.2	6.9	1.9	5.0	4.8—5.5	5.3	4.9
E	5	10	9.9—10.3	10.1	1.7	10.0	9.9—10.4	10.2	3.6
E[b]	5	0.01	0.009—0.011	0.01	4.8	0	—	—	—

[a]Single analyses except where mentioned. [b]Preconcentration.

TABLE 2

Typical samples analysed by the direct method (samples A—E) and by the preconcentration method (samples F—J)

Sample	HCOOH (μg ml^{-1})	HCHO (μg ml^{-1})	Sample	HCOOH (μg ml^{-1})	HCHO (μg ml^{-1})
A	0.1	0	F	0.0005	ND[a]
B	1.1	0	G	0.00006	ND
C	0.5	0	H	0.0009	0.0004
D	0.3	0	I	0.0006	0.00007
E	0	0	J	0.00007	0.00006

[a]None detected.

and after preconcentration, a very low concentration of formic acid and formaldehyde was found. When preconcentration is used, the utmost care and attention to detail must be taken to ensure that no contamination occurs during the analysis.

REFERENCES

1 L. A. Luré, L. A. Alferova and T. N. Bovdareva, Zavod. Lab., 30 (1964) 799.
2 H. F. Mueller, T. E. Larson and W. J. Lennarz, Anal. Chem., 30 (1958) 41.
3 N. I. Brodskaya and V. K. Tsyskovskii, Maslob. Zhir. Prom., 23 (1957) 28.
4 H. Salwin, J. Assoc. Off. Agric. Chem., 48 (1965) 628.

5 Y. Ueno, J. Biochem. (Tokyo), 48 (196) 161.
6 Fr. Muller, Helv. Chim. Acta, 33 (1950) 796.
7 L. G. Molnár, L. Szekeres and M. Zergényi-Balásfalvy, Fresenius Z. Anal. Chem., 159 (1958) 161.
8 E. R. Stephen, W. E. Scott, P. L. Hanst and R. C. Doerr, J. Air Pollut. Control Assoc., 6 (1956) 159.
9 M. Turowska, Chem. Anal. (Warsaw), 5 (1960) 815.
10 F. Hasegawa, Y. Tanizaki and N. Ando, Nippon Kagaku Zasshi, 88 (1967) 289.
11 S. A. Barker and P. J. Somers, Carbohydr. Res., 3 (1966) 220.
12 H. L. Polak, Fresenius Z. Anal. Chem., 176 (1960) 34.
13 C. E. Bricker and H. R. Johnson, Ind. Eng. Chem., Anal. Ed., 17 (1945) 400.
14 D. A. MacFayden, H. D. Watkins and P. R. Anderson, J. Biol. Chem., 158 (1945) 107.
15 P. W. West and B. Sen, Fresenius Z. Anal. Chem., 153 (1956) 12.
16 F. Feigl, Spot Tests in Organic Analysis, 5th edn., Elsevier, Amsterdam, 1956, p. 340.
17 A. G. Stradomskaya and I. A. Goncharova, Gidrokhim. Mater., 43 (1967) 57.

Analytica Chimica Acta, 113 (1980) 195—197

Short Communication

PRECIPITATION OF COPPER(I) THIOCYANATE FROM HOMOGENEOUS SOLUTION BY REDUCTION OF COPPER(II) WITH ASCORBIC ACID IN THE PRESENCE OF EDTA

K. N. UPADHYAYA*

Chemistry Department, University of Dar es Salaam, P.O. Box 35061, Dar es Salaam (Tanzania)

(Received 15th June 1979)

Summary. EDTA slows down the reduction of copper(II) by ascorbic acid and prevents interferences from many other metals. The method is applied to certified metal standards with good results.

The precipitation of copper(I) thiocyanate is the basis of a well known gravimetric method for copper, introduced by Rivot [1] and since widely studied [2, 3]. Most workers consider it necessary to age the precipitate before filtration. The use of ascorbic acid to reduce copper(II) ions in this procedure was reported by Stathis [4]. Whereas previous workers had recommended that oxidizing agents must be excluded, Stathis obtained quantitative precipitation of copper(I) thiocyanate from nitric acid solutions, with an ageing period of only 30 min. The main drawback of the procedure has been that the fine precipitate may creep up the sides of the container and clog or even pass through the filter.

Precipitation from homogeneous solution [5] often improves the granularity of a precipitate. Davis [6] precipitated copper(I) tetraphenylborate from homogeneous solution by adding ascorbic acid to acidic solutions containing copper(II) and tetraphenylborate ions; precipitation occurred after only about 30 s had elapsed. The same method was not applicable to copper(I) thiocyanate as immediate precipitation occurred when ascorbic acid was added to solutions containing copper(II) and thiocyanate ions under a wide range of temperature and acidity conditions. However, Newman [7] was able to add a solution of hydroxylammonium chloride to a solution containing copper(II) and thiocyanate ions with an acidity of about 0.2 M without precipitation occurring. When this solution was heated, precipitation of copper(I) thiocyanate began within a few minutes and was complete in 30 min. The precipitate was granular and had good filtration properties. The method, however, offered no advantage with respect to interferences caused by ions such as those of arsenic, antimony and bismuth.

If copper(II) ions are held as an EDTA complex in solution at an appro-

*On leave from Ramjas College, Delhi University, Delhi, India.

priate pH the reduction of copper(II) with ascorbic acid is considerably delayed, and the precipitation of copper(I) thiocyanate is effected from homogeneous solution. Interferences from some other metal ions are also avoided. This communication describes an investigation of this process.

Experimental

All chemicals used were of reagent-grade quality. Solutions of ascorbic acid, disodium EDTA and ammonium thiocyanate were made from purified samples in doubly distilled water. Copper was first determined on standardized solutions of copper(II) sulphate and the method was then applied to solutions prepared from electrolytic copper and copper-bearing alloys.

Procedures. Take 5—25 ml of copper sulphate solution (ca. 0.1 M) in a 400-ml beaker, add sufficient EDTA solution (0.2 M) to complex the copper (35 mg of copper are equivalent to 0.2 g of disodium EDTA) and any other metals present and 25 ml of ammonium thiocyanate solution (1% w/v), and dilute to 150 ml. Adjust the pH to 2—3 with ammonia or hydrochloric acid, add 5—25 ml of ascorbic acid solution (2% w/v) dropwise with constant stirring and heat on a steam bath for 1 h. Filter through a sintered-glass porosity G4 crucible, and wash 4 or 5 times with 0.1% ammonium thiocyanate solution and then with 20% ethanol. Dry at 110°C for 2 h, cool and weigh. The stoichiometric factor for Cu/CuSCN is 0.52253.

For the determination of copper in the metallic samples listed in Table 2 the sample weights indicated were dissolved in (1 + 1) nitric acid and the solutions were fumed with concentrated sulphuric acid in the conventional manner. After filtration (if necessary), the solutions were diluted to exactly 250 ml and 25-ml aliquots were used in the above procedure.

Notes. On addition of ascorbic acid the precipitation of copper(I) thiocyanate begins after 0.5 min. The pH is critical. If it is kept high ($\geqslant 5$) the rate of reduction of copper is much decreased and precipitation is not complete even after a long time. If the acidity increases above 0.2 M, precipitation occurs almost immediately and cannot be considered as precipitation from homogeneous solution.

Results and discussion

The results given in Table 1 show that the precipitation of copper(I) thiocyanate from homogeneous solution can be successfully carried out by the method described. Under normal conditions, reduction of copper(II) with ascorbic acid takes place immediately but it is considerably delayed in the presence of EDTA at pH 2—3. In addition, the EDTA keeps other metal ions complexed, thereby preventing their interference and allowing the method to be applied to a number of standard metallic samples (Table 2). Bismuth and antimony, which interfere in the usual copper(I) thiocyanate method, were found not to interfere in the proposed method in amounts up to 100 mg and 150 mg, respectively.

TABLE 1

Determination of copper in pure solution

Cu taken (mg)	31.75	50.70	69.75	97.85	123.25	158.25
Cu found (mg)	31.7	50.8	69.9	97.6	123.0	158.6
Difference (%)	−0.16	+0.19	+0.21	−0.25	−0.20	+0.22

TABLE 2

Determination of copper in metallic samples

Sample[a]	Wt. taken (g)	Cu found (%)[b]	Certified value (%)
Electrolytic copper	1.0430	100.0 ± 0.09	100.0
Brass[c]	1.4880	67.34 ± 0.10	67.4
Manganese bronze[d]	1.8426	61.0 ± 0.16	61.1
Cupronickel alloy[e]	1.7825	67.5 ± 0.15	67.6

[a]Bureau of Analysed Samples, Ltd.
[b]Average of 7 determinations of the same sample solution with standard deviation.
[c]Other constituents: 28.6% Zn, 1.09% Sn, 2.23% Pb, 0.32% Fe, 0.01% P, 0.33% Ni. Disodium EDTA added, 250 mg.
[d]Other constituents: 31.5% Zn, 0.15% Sn, 0.15% Pb, 1.38% Fe, 1.91% Mn, 0.11% Ni, 3.70% Al. The precipitated tin(IV) oxide was washed 10 times with (1 ± 9) nitric acid before the filtrate was evaporated and diluted to 250 ml.
[e]Other constituents: 30.3% Ni, 0.8% Fe, 0.82% Mn.

The precipitate obtained had excellent filtration properties; it was granular and showed no tendency to creep up, or stick to, the walls of the containers.

REFERENCES

1 L. E. Rivot, Compt. Rend., 38 (1854) 868.
2 I. M. Kolthoff and G. H. P. Van der Meene, Fresenius Z. Anal. Chem., 72 (1927) 337.
3 R. Belcher and T. S. West, Anal. Chim. Acta, 6 (1952) 337.
4 E. C. Stathis, Anal. Chim. Acta, 16 (1957) 21.
5 L. Gordon, M. L. Salutsky and H. H. Willard, Precipitation from Homogeneous Solution, J. Wiley, New York, 1959.
6 D. C. Davis, Anal. Chem., 32 (1960) 1321.
7 E. J. Newman, Analyst, 88 (1963) 500.

Analytica Chimica Acta, 113 (1980) 199—203

Book Reviews

M. S. Cresser, *Solvent Extraction in Flame Spectroscopic Analysis*, Butterworths, London, 1978, ix + 200 pp., price £15.00.

Solvent extraction is widely used in conjunction with flame spectroscopic and related techniques of analysis both for increasing sensitivity and for separating the analyte from concomitants. A detailed discussion of the subject, however, has not been forthcoming until the publication of this book, in contrast to the situation regarding solution spectrophotometry. The text contains a great deal of valuable and interesting information, in particular about the effects of the various solvents in nebulization and combustion, of the basics of liquid—liquid extraction processes, and of the practical aspects of extraction for flame spectroscopy. The second half of the book describes the applications of extraction to each element in turn.

The material is carefully presented in a well-written manner, is extensively referenced, and brings out very clearly the characteristics of solvent extraction which are particularly relevant to flame spectroscopy. It is often not appreciated that these have a different priority to other analytical applications of liquid—liquid extraction. The wealth of detail should help to clarify the applicability of different systems and enable analytical chemists to optimize these uses of solvent extraction.

A. Townshend

H. A. Laitinen and G. W. Ewing (Eds.), *History of Analytical Chemistry*, Division of Analytical Chemistry, American Chemical Society, Washington, 1977, xvi + 358 pp., price $7.00 (members), $10.00 (non-members).

The modern history of analytical chemistry has not been treated extensively in the literature. Ferenc Szabadvary's excellent book "History of Analytical Chemistry" barely touches on modern instrumental methods; indeed the origins of some of these methods appear to be so complex and the field is so wide that to place them all in a proper historical perspective would be beyond a single author, no matter how erudite.

Professors Herbert Laitinen and Galen Ewing invited 51 contributors to participate in this present history, which covers the broad areas of chemical, spectrochemical, electrochemical and separation methods in virtually all their analytical aspects. The book certainly achieves one of its editors' objects which was to dramatize the very wide scope of modern analytical sciences. There are sections on everything from the origins of the balance — "a false balance is an abomination to the Lord (Proverbs 11:1)" — to data manipulation by computer. Of particular interest are the personal reminiscences from several contributors closely associated with the development of particular techniques.

The History was prepared in the context of the centennial celebrations of the American Chemical Society and so emphasizes American contributions, though it is not entirely devoted to the chauvinistic view. It is a pity that ACS did not match the generosity of the contributors in donating their time and expertise by publishing the book in a more elegant format, for it is a book that should be widely read.

References are not given, and this was probably a wise decision. The interested reader will have to delve further for actual references and in the process may well find that everything was or is not precisely as stated here. The book provides interesting — sometimes fascinating — reading, however, not least in its broad modern view of what analytical chemistry comprehends. So long as it is not regarded as gospel, it should prove not only entertaining but valuable.

A. M. G. Macdonald

I. C. Smith, B. L. Carson and F. Hoffmeister, *Trace Metals in the Environment: Volume 5 — Indium*, Ann Arbor Science Publishers, Ann Arbor, 1978, xx + 000 pp., price £15.20.

This is the fifth in a series of volumes covering the chemistry of trace metals in the environment. The topic is one of the less well-studied elements, indium. The text includes an account of the physical properties and chemistry of the element and its compounds, and contains other sections dealing with geochemistry, industrial uses and potential sources of industrial pollution, as well as its physiological properties. Overall the book is well-written and provides a thorough coverage of those areas that have been researched. It is not meant to be a treatise on indium but gives the reader an overview of those aspects of indium chemistry that are important environmentally. Considerable effort has been made in this regard to produce a serviceable and useful volume. The bibliography is up-to-date and SI units are used extensively.

This book will be of considerable use to those engaged in the mining and smelting industry, or in environmental pollution control. It should also be a welcome addition to the shelves of most libraries.

D. A. Stiles

O. Mikes (Ed.), *Laboratory Handbook of Chromatographic and Allied Methods*, Ellis Horwood, Chichester, 1979, (ISBN 0-85312-080-3), 764 pp., price £38.50.

The present book is intended as a replacement for "Laboratory Handbook of Chromatographic Methods" published some thirteen years ago and which has now become out of date. The new book is bigger (747 pages versus 435): there are some 13 chapters, rather than 9 as in the earlier edition and the layout has been somewhat altered. As the title suggests, the book covers all chromatographic methods for all types of substances from simple cations and anions, through covalent volatile hydrocarbons to antibiotics and polymers.

The book opens without a Preface or Introduction but with a list of symbols. Chapter 1 is written by the Editor who discusses the fundamental types of chromatography; it is similar to the opening chapter of the 1966 book but now includes gel and bioaffinity chromatography. There then follows a concise but intelligible account of the theory of chromatography. The remaining chapters, each written by experts from the Czechoslovak Academy of Sciences, discuss the various chromatographic methods: paper, adsorption column, ion-exchange, gel, affinity, thin-layer and gas techniques all come under scrutiny. Counter-current distribution, electromigration methods, including electrophoresis, isotactophoresis, and isoelectric fractionation focusing are then described. The book closes with the literature citations, plus the United Kingdom sources of materials and equipment for chromatography. As is usual with all Czechoslovak publication/reviews in the chromatographic field, the book closes with a fully detailed subject index.

With such a large book, some of the treatment is of necessity uneven or, more accurately, uncritical being designed to teach as well as inform. Therefore certain sections are of historical importance rather than offering insight into the latest research techniques. The only major break is Chapter 8 which discusses the technology of the automation and mechanization of column operations in liquid chromatography.

The book is to be recommended; not only does it reflect the philosophy of the subject but it is a fairly complete review of this very important subject.

G. Nickless

E. Sawicki, J. D. Mulik and E. Wittgenstein (Eds.), *Ion Chromatographic Analysis of Environmental Pollutants*, Ann Arbor Science Publishers, Ann Arbor, 1978, vii + 210 pp., price £17.65.

The present book contains the proceedings of a symposium and is probably the first of several such books which will appear on this quickly growing subject. Methods for the analysis and determination of mixtures of relatively covalent molecules, especially these with chromophoric functional groups, has forged ahead in the last decade through the use of modern liquid chromatographic techniques. However, there still exists a need for a reliable and relatively simple method of analysis of mixtures of the more common water-soluble ions, especially anions, partly because of inadequate column materials and also the lack of suitable methods of determination. The discovery and exploitation of ion chromatography by Small and his co-workers at Dow should solve some of these problems.

The opening paper discusses the potential of the technique for analyses of a wide variety of ions in the environment and biological mixtures. The second paper, by Small, gives a brief account of the conception, development, as well as the scope and limitations of ion chromatography; this is a paper well worth studying carefully. The bulk of the book describes applications to the analysis

of atmospheric sulphur dioxide, ammonium ions in ambient aerosols, anions in filter catch samples, anions extracted from airborne particulate matter, anions in combustion products, applications to mobile source emissions, ammonia and alkylamines in automobile exhausts. An interesting possibility which is cogently presented is use of ion chromatography for organic elemental microanalysis; thus, methods for chlorine, bromine, phosphorus and sulphur in organic molecules are presented. Both accuracy and precision are quoted for all the elements. The final paper presents an analytical perspective of ion chromatography, where future developments are discussed relative to their possible impact on analytical problems particularly to quality control so returning us almost to Chapter 1.

An intriguing feature is that at the end of almost each chapter there is a number of questions and answers relevant to the paper being discussed. The book is a good collection of papers, is relatively free from errors, and has good diagrams. Because of its specialized interest, it will probably end up only on library bookshelves.

G. Nickless

A. Wiseman (Ed.), *Topics in Enzyme and Fermentation Biotechnology*, Vol. 3, Ellis Horwood, Chichester, 1979, 294 pp., price £19.50.

This third volume continues the policy of incorporating a wide selection of topics. In this instance the subjects covered are the use of oxyanions (mainly borate) in enzyme equilibrium displacement, microbial extracellular enzymes, "rennets" and cheese, the scale-up of fermentation processes, and new and modified invertases. None is of particular interest to analytical chemists, but the articles are well-written and extensively referenced; the book concludes with a subject index.

R. F. Hirsch (Ed.), *Statistics*, Franklin Institute Press, Philadelphia, 1978, viii + 308 pp., price $21.00.

This is one of a series of paperbacks based on the symposia presented at the Seventeenth Eastern Analytical Symposium, 1977. The authors have prepared extended versions of their talks, so that these papers are greatly superior to what usually appears in conference proceedings. The bare and rather forbidding title conceals an interesting collection of papers built around experimental design and data analysis. There are ten papers, which deal with experimental design (G. J. Hahn), method optimization (S. N. Deming), statistical analysis (J. Mandel), statistical inference (T. J. Killeen), quality control charts (J. J. Tsiakals), regression and correlation (J. Erjavec), factor analysis (D. G. Howery), pattern recognition and cluster analysis (P. C. Jurs), and storage and retrieval of mass spectral data (K. Biemann and J. E. Biller). The final paper on publication of analytical research (J. M. Petruzzi) is something of an anomaly, but is included because of its statistical evaluation

of where the analytical papers generally go; this is an extended version of the surveys which appeared recently in Analytical Chemistry. There are extensive reference lists for further reading.

The papers are written at an introductory level and the book can be recommended to general readers and to students who want a quick survey of what these topics are about without getting too involved in the mathematics. Essentially, this is very much a practical man's view of statistics.

(continued from outside of cover)

Short Communications

VOL. 113 No. 1 ANALYTICA CHIMICA ACTA JANUARY 1, 1980

CONTENTS

(continued on inside page of cover)

Printed in The Netherlands